

Enhancing the Practical Applicability of Smart Tuned Mass Dampers in High-Rise Civil Engineering Structures

Author: Demetris Demetriou

Supervisor: Dr. Nikolaos Nikitas

Co-supervisor: Dr. Konstantinos Daniel Tsavdaridis

Co-supervisor: Prof. John Forth

Submitted in accordance with the requirements for the degree of
Doctor of Philosophy in Civil Engineering

The University of Leeds
School of Civil Engineering

May, 2017

The candidate confirms that the work submitted is his own, except where work which has formed part of jointly-authored publications has been included. The contribution of the candidate and the other authors to this work has been explicitly indicated below. The candidate confirms that appropriate credit has been given within the thesis where reference has been made to the work of others.

The work in **Chapter 4** of the thesis has appeared in the following publications:

Demetriou, D. et al. 2014. Performance of Proportional-Integral-Derivative Controlled Variable Damping Tuned Mass Dampers. In: *6th International Conference of Structural Control, 15-17 July, Barcelona, Spain*.

Demetriou, D. et al. 2015. Performance of Fixed-Parameter Control Algorithms on High-Rise Structures Equipped With Semi-Active Tuned Mass Dampers. In: *8th International Conference on the Behavior of Steel Structures in Seismic Areas, July 1-3, Shanghai, China*.

Demetriou, D. et al. 2016. Performance of fixed-parameter control algorithms on high-rise structures equipped with semi-active tuned mass dampers. *The Structural Design of Tall and Special Buildings*. **25**(7), pp.340-354.

The work in **Chapter 5** of the thesis has appeared in the following publications:

Demetriou, D.; Nikitas, N.; Tsavdaridis, K.D. A Novel Hybrid Semi-active Tuned Mass Damper for Lightweight Steel Structural Applications. In Proceedings of the IJSSD Symposium on Progress in Structural Stability and Dynamics, Lisbon, Portugal, 21–24 July 2015.

Demetriou, D.; Nikitas, N. A Novel Hybrid Semi-Active Mass Damper Configuration for Structural Applications. *Appl. Sci.* **2016**, *6*, 397.

The work in **Chapter 6** of the thesis has appeared in the following publications:

Demetriou, D.; Nikitas, N. Hybrid Semi-Active Mass Dampers in Structures; Assessing and Optimising Their Damping Capacity. X International Conference on Structural Dynamics, EURO DYN 2017, Rome, September 2017. (Submitted)

This copy has been supplied on the understanding that it is copyright material and that no quotation from the thesis may be published without proper acknowledgement.

Acknowledgements

All I have achieved would not have been possible without the support, friendship and love of those close to me and I would like to take a moment to thank everyone who has helped me in this journey.

Firstly, I would like to express my gratitude to my supervisor and advisor, Dr. Nikolao Nikita for his priceless guidance throughout my research and academic life. He has guided, challenged and inspired me to get the most out of my work. He has given me opportunities and experience by getting me involved in other projects too. Thank you for helping me so much.

I would also like to thank my Co-supervisors Dr. Konstantino Tsavdaridi and Prof. John Forth for their support throughout my PhD.

I am also grateful to EPSRC and the department of Civil Engineering at the University of Leeds for financially supporting the project.

Most importantly, I would like to thank my family and friends for their love and support. Thank you for always being there. You always believed in me and for this and countless more reasons I would like to dedicate this work to you.

To my family

Abstract

The ability of bones to concentrate material where the body needs most of its strength and the ability of trees to spread roots in search of moisture rich locations are only a few amongst the many examples of nature's way of building adaptive "structures". Even though civil engineering structures often appear inefficient, static and cumbersome, a new era of structural design aims to alter the status quo by mimicking nature's way. This suggested adaptation process in civil structures often takes the form of passive, active and semi-active control. Through direct comparison of these methods, semi-active control is shown to combine the benefits of both active and passive systems and can be arguably considered the next step in improving dynamic structural performance; however the applicability of this exciting and novel for the structural engineering field technology, is not all-embracing. In order to enhance the development of this promising technology and contribute on the creation of a new era of "smart & thinking" structures that encompass an unconventional form of performance based design, this study aimed to develop enabling technologies and tools that enhance the selling strengths of semi-active and smart control using tuned-mass dampers.

The original contributions to knowledge in this work are divided in three aspects. Firstly, the investigation of the influence of control algorithms on smart tuned-mass damper equipped high-rise structures, for which practical limitations have been taken into account. Leading to conclusion on the conditions for which each algorithm exhibits superior performance over the other. Secondly, the development of a fail-safe novel semi-active hybrid device configuration that enables performance gains similar to the active mass damper at considerably lower actuation and power demands. Finally, the development of a simple and robust at all gains control algorithm based on the modification of one of the most widely used controller in the engineering industry, namely the proportional-integral-derivative controller.

Table of Contents

Acknowledgements	iii
Abstract	v
Table of Contents	vi
List of Tables	ix
List of Figures	x
Chapter 1 Introduction	1
1.1 Background and Motivation	1
1.2 Thesis Objectives	4
1.3 Readership and Organisation of the Thesis	6
Chapter 2 Literature Review	8
2.1 Problem Definition	8
2.2 The Civil Engineering Challenge	9
2.2.1 Passive Control	10
2.2.2 Active Vibration Control	14
2.2.3 Semi-Active Vibration Control.....	18
2.3 Principles of Structural Control	23
2.3.1 Structural control using semi-active and active dampers	27
2.4 Control Strategies.....	31
2.4.1 Evaluation of Control Strategy.....	32
2.5 Dynamics of High-Rise Structures.....	33
2.6 Control System Formulation	35
2.6.1 State Space Formulation.....	36
2.6.2 Transfer Function Formulation	38
2.7 Model Order Reduction	40
Chapter 3 Control Algorithms	43
3.1 Background	43
3.2 Fixed parameter controllers.....	44
3.2.1 On-off Controllers	45
3.2.1.1 Skyhook Control	45
3.2.1.2 Groundhook Control	48
3.2.2 PID controllers.....	51
3.2.3 Riccati Optimal Controllers.....	54
3.2.3.1 Optimal and suboptimal Bang-Bang control	56

3.2.4 Pole Placement Algorithms	57
3.2.5 Instantaneous optimal control:	59
3.2.6 Robust Controllers/ The H ₂ and H _∞ compensator	60
3.3 Adaptive controllers	60
Chapter 4 Control System Design-Influence of the control algorithm	62
4.1 Introduction	63
4.2 Numerical investigation	68
4.2.1 Frequency domain analysis of simplified SDOF system.....	69
4.2.2 Description of the SDOF and 2DOF (DVA equipped) system.....	69
4.2.3 Development of models/ state space representation.....	70
4.2.4 Optimisation of algorithms/ PID Gains and LQR control effort.....	72
4.2.4.1 Full state feedback controllers, LQR.	73
4.2.4.2 PID optimisation	76
4.2.5 Semi-active maximum damping optimisation	77
4.3 Effect of mass ratio and stiffness uncertainty	78
4.3.1 Frequency response comparison	81
4.4.1 Description of the benchmark structural system.....	83
4.4.2 The excitation	85
4.4.3 Sensor arrangement.....	86
4.4.4 Tuning and optimising the passive and semi-active devices	87
4.4.5 Evaluation criteria	92
4.5 Simulation results	94
4.5.1 Remarks	98
Chapter 5 A Novel Semi-Active Hybrid Configuration	101
5.1 Introduction	102
5.2 Modeling Principles	105
5.2.1 General Dynamic Vibration Absorbers Modeling Approach	105
5.2.1.1 Passive Tuned Mass Damper (TMD) Control.....	106
5.2.1.2 Active Mass Damper (AMD) Control and Hybrid Active-Tuned Mass Damper (ATMD) Control.....	107

5.2.1.3 Semi-Active Tuned Mass Damper (STMD) Control	108
5.2.2 Modeling the Semi-Active Hybrid Mass Damper	109
5.3 Control Methods	112
5.4 Numerical Investigation	113
5.4.1 Single Degree of Freedom (SDOF) Structural Configuration	113
5.4.1.1 Variable Damping Coefficient Configuration	113
5.4.1.2 Free vibration analysis	115
5.4.1.3 Forced vibration	116
5.4.2 Effect of mass and stiffness variation	119
5.4.2 High-Rise Structural Configuration	123
5.4.3 Evaluation Criteria	125
5.4.4 Simulation Results and Discussion	126
5.5 Conclusions	132
Chapter 6 In Search of a Suitable Method for SHMD Control	133
6.1 Introduction	134
6.2 Robust ATMD control design (a-ATMD)	136
6.3 Application of robust control to SHMD device (a-SHMD)	137
6.4 Modification of PID to aPID	143
6.4.1 Proof of stability at varying a and g parameters	144
6.4.2 Trial aPID controllers	149
6.5 Comparison with optimal LQR controllers	153
6.6 Conclusions	156
Chapter 7 Conclusions and Future Work Recommendations	158
7.1 Summary of contributions and impact	158
7.2 Future work recommendations	160
References	162
Appendix A	171

List of Tables

Table 1 . Summary of the advantages and disadvantages of each control method.....	22
Table 2. A simple Laplace transform table.....	39
Table 3. Groundhook Control Logic	49
Table 4. Summary of performance criteria.....	94
Table 5. Damping coefficients.....	125
Table 6. Summary of evaluation criteria.....	126

List of Figures

Figure 1. The various steps involved in control system design (Astrom and Hagglund, 1995).....	4
Figure 2. Organisation of thesis.....	7
Figure 3. Passively controlled structure.....	11
Figure 4. Schematic representation of active control, after Spencer and Soong (1999)	14
Figure 5 (a) Typical uniaxial AMD device (IHI Infrastructure Systems CO., 2013) (b) Model of SDOF structure equipped with AMD.....	16
Figure 6. Schematic representation of a semi-active control scheme (Soong and Spencer, 2002).....	19
Figure 7. Transmissibility of a SDOF at (a) Different values of supplemental damping, (b) and the addition of a PID calculated active force.....	26
Figure 8. Idealised n-DOF structural system equipped with a dynamic vibration absorber (DVA).....	28
Figure 9 Indicative power demand of an (a) Active device and (b) Semi-active device	30
Figure 10. Control strategies (a) Closed-loop system and (b) Open-loop system (Astrom and Murray, 2012).....	32
Figure 11. Classification of feedback controllers	44
Figure 12. Skyhook control of a variable damping device (a) Semi-active variable damping control model (b) Ideal configurations	47
Figure 13. Groundhook control of a variable damping device (a) Semi-active variable damping control model (b) Ideal configuration	49
Figure 14. Typical (a) Acceleration response and (b) Displacement response of a groundhook controlled STMD equipped structure	50
Figure 15. Second order system subjected to step input.....	52
Figure 16. Conventional 2-step control design approach for a) Selecting appropriate control algorithm and (b) Accounting for force and stroke saturation.....	66
Figure 17. Control system design procedure.....	68
Figure 18. Force-velocity relationship for the performance bands of a variable damping device	71
Figure 19. (a) Acceleration response, (b) Displacement response, (c) Damper stroke, (d) Relative phase, (e) Area under acceleration response curve (f) Peak acceleration response with varying controller effort r ranging from 0.1-10.....	74

Figure 20. (a) Acceleration response, (b) Displacement response, (c) Damper stroke, (d) Relative phase, (e) Area under acceleration response curve (f) Peak acceleration response with refined controller effort r ranging from $5e^{-5} - 0.01$	75
Figure 21. (a) Displacement response,(b) Extracted energy ,(c) Maximum stroke ,(d) Relative phase of the eleven trial PID and PD controllers and their comparison with the baseline DBG controller	76
Figure 22. Acceleration response of the different control configurations as a function of the damping ratio (ζ)	77
Figure 23. (a) Acceleration response, (b) Displacement response, (c) Maximum stroke, (d) Peak acceleration as a function of the mass ratio for the TMD case.....	79
Figure 24. (a) Acceleration response, (b) Displacement response, (c) Maximum stroke, (d) Peak acceleration as a function of the stiffness uncertainty for the TMD case	80
Figure 25. Acceleration response as a function of the mass ratio for the different control and algorithm configurationsError! Bookmark not defined.	
Figure 26. (a) Acceleration response, (b) Displacement response, (c) Maximum stroke, (d) Peak acceleration of different algorithms for 5% mass ratio and 1/1 stiffness uncertainty ratio.	82
Figure 27. Acceleration response as a function of stiffness uncertainty for the different control and algorithm configurations for 5% mass ratio	83
Figure 28. (a) Plan view and (b) elevation view of the 76-story benchmark structure (Yang et al., 2004).....	84
Figure 29. Mode shapes of the first six modes of the building.....	85
Figure 30. (a) Dynamic wind force time histories of last and first occupied floor, (b) frequency content of the wind excitation fluctuation.....	86
Figure 31. Ensemble of the structural configurations; left TMD equipped structure and right VD-STMD equipped structure	87
Figure 32. (a) Power spectral density of the acceleration of the 7th floor under harmonic loading and (b) rms acceleration response of different floors under the across wind loading derived from the static wind-tunnel tests.....	89
Figure 33. Numerical response optimisation using the Nelder-Mead simplex method; (a) damping band convergence and (b) rms response convergence	90
Figure 34. Optimal damping max-min ranges and damper strokes for the different VD-STMD control scenarios for the cases (top to bottom) of uncapped damper strokes, strokes capped at 95cm, 80cm and 75cm.....	91

Figure 35. Scaled (over the TMD performance) performance indices for uncapped damper strokes.....	95
Figure 36. Scaled (over the TMD performance) performance indices J_1 , ..., J_4 , J_7 , ..., J_{10} for damper strokes ≤ 95 cm.....	95
Figure 37. Scaled (over the TMD performance) performance indices J_1 , ..., J_4 , J_7 , ..., J_{10} for damper strokes ≤ 80 cm.....	96
Figure 38. Scaled (over the TMD performance) performance indices J_1 , ..., J_4 , J_7 , ..., J_{10} for damper strokes ≤ 70 cm.....	96
Figure 39. Structural configuration and mathematical models for (a) tuned mass damper (TMD); (b) semi-active tuned mass damper (STMD); (c) active mass damper (AMD); (d) active-tuned mass damper (ATMD); and (e) semi-active hybrid mass damper (SHMD) systems.....	105
Figure 40. Indicative example of the “power” scheme/demand practised in (a) Active; and (b) Semi-active control.	109
Figure 41. A schematic representation of the procedure followed for modeling the semi-active hybrid mass damper.	111
Figure 42. Control signals as a function of relative velocity for the (a) Purely active system; (b) Semi-active component; and (c) Active component of the hybrid configuration subjected to a white noise excitation.....	111
Figure 43. Acceleration response of (a) STMD; and (b) SHMD; and their (c) Difference at different damping ratios. (Units of acceleration response in $m^2 / s^3 / rad$).	114
Figure 44. Acceleration response at steady state for damping ratios of (a) 0.3; (b) 0.5; (c) 0.75; and (d) 1. Shaded area illustrates average system response.....	115
Figure 45. (a) Displacement response time history of different control configurations; (b) Control signal of active component and semi-active component of the hybrid configuration.....	116
Figure 46. Transient and steady-state response of the different control device configuration under harmonic loading at tuning frequency (excitation frequency 1 rad/s).....	117
Figure 47. Transient and steady-state Crms response of the different control device configuration under harmonic loading at tuning frequency (excitation frequency 1 rad/s).	118
Figure 48. (a) Steady-state; and (b) Peak frequency acceleration response of the different structural configurations.....	120
Figure 49. (a) Acceleration response, (b) Displacement response, (c) Maximum stroke, (d) Angular phase, (e) Control signal, and (f) Peak acceleration as a function of the mass ratio(μ) and frequency.	122

Figure 50. (a) Acceleration response, (b) Displacement response, (c) Maximum stroke, (d) Angular phase, (e) Control signal, and (f) Peak acceleration as a function of stiffness uncertainty percentage and frequency ($\mu = 0.05$).	122
Figure 51. Energy dissipation as a function of (a) Stiffness uncertainty and (b) Mass ratio for the different structural configurations	123
Figure 52. Ensemble of all the different control options (a) TMD; (b) STMD; (c) ATMD; (d) SHMD studied herein for the model 76-storey structure of Yang et al.(Yang et al., 2004).	124
Figure 53. Illustration of the performance of different control measures in terms of (a) rms acceleration; (b) rms displacement; (c) Absolute acceleration; and (d) Absolute displacement at different floor levels.	127
Figure 54. (a) Normalised; and (b) Non-normalised performance indices (lower index indicates better performance).	128
Figure 55. Power and its time integral (dotted line) energy for (a) ATMD; and (b) SHMD configuration. Positive stands for energy addition and negative for energy dissipation.	129
Figure 56. Power and its time integral (dotted line) energy of a purely active mass damper (AMD) system (no passive damping component) along with the corresponding performance indices. Positive stands for energy addition and negative for energy dissipation.	131
Figure 57. Root locus diagram of the ATMD-SDOF configuration described in Chapter 5	135
Figure 58. Root-locus diagram of the hybrid ATMD (left) and robust hybrid a-ATMD(right) configurations	138
Figure 59. Root-locus diagram of the SHMD (left) and a-SHMD (right) system.	139
Figure 60. (a) Acceleration response (b) Control energy and (c) Force/velocity relationship for the case of the capped a-SHMD configuration	142
Figure 61. (a) Acceleration response (b) Control energy and (c) Force/velocity relationship for the case of the uncapped a-SHMD configuration	142
Figure 62. aPID control system architecture	143
Figure 63. ATMD configuration	145
Figure 64. Values in the first column of the Routh matrix for $g \in [0; \infty] \leftrightarrow a \in [\omega_a; \omega_b]$	148
Figure 65. (a) Bode plot and (b) Nyquist plot for the aPID-SHMD system	148
Figure 66. aPID-SHMD configured system response as a function of gain	149

Figure 67. (a) Supplied maximum and rms force, (b) Total acceleration and displacement response reduction, and (c) Total control energy supplied by the aPID-SHMD system	151
Figure 68. (a) Acceleration response, (b) Displacement response, (c) Damper stroke, (d) Relative phase, (e) Control energy and (f) Peak acceleration response for the aPID-SHMD at low control gains.....	152
Figure 69. (a) Acceleration response (b) Control energy and (c) Force/velocity relationship for the case of the performance optimised LQR-SHMD system	153
Figure 70. (a) Acceleration response (b) Control energy and (c) Force/velocity relationship for the case of the a-SHMD system gains matching control effort of LQR-SHMD	154
Figure 71. (a) Acceleration response, (b) Displacement response, (c) Damper stroke, (d) Relative phase, (e) Control energy and (f) Peak acceleration response for the aPID-SHMD and LQR-SHMD systems.....	155

List of Common Symbols and Abbreviations

K_d	stiffness of auxiliary damper	PED	Passive Energy Dissipation
C_d	damping of auxiliary damper	TLD	Tuned liquid dampers
F_a	Actuator force	TMD	Tuned mass dampers
m	structural mass	AMD	Active mass driver/damper
c	damping coefficient	ATMD	Active tuned mass damper
k	linear elastic stiffness	STMD	Semi-active tuned mass damper
$x(t)$	Displacement	MDOF	multi-degree-of-freedom
$\dot{x}(t)$	Velocity	SDOF	Single-degree-of-freedom
$\ddot{x}(t)$	Acceleration	PID	Proportional Integral Derivative
$\ddot{x}_g(t)$	Ground acceleration	LQR	Linear Quadratic Regulator
ω_n	Natural circular frequency	LQG	Linear Quadratic Gaussian
ζ	Damping ratio	MR	Magnetorheological
P	Amplitude of sinusoidal excitation	ER	Electrorheological
θ	Circular frequency of sinusoidal excitation	VD	Variable Damping
\bar{m}	Mass of auxiliary device	VS	Variable Stiffness
Γ	Integrodifferential operator	OTE	Off-towards-equilibrium
\bar{c}	Damping coefficient of the control device	STFT	Short time Fourier transform
\bar{k}	Stiffness of the control device	FFT	fast Fourier transform
R	Restoring force	FRFs	frequency response functions

D	Damping force	HT	Hilbert Transform
I	Inertia force	RMS	Root-mean-square
β	Excitation to structural frequency ratio	LPM	Lumped Parameter Method
$H(s)$	Transfer function of the controller	FEM	Finite Element Method
$G(s)$	Transfer function of the plant	AMM	Assumed Modes Method
$y(t)$	Output signal	EMA	Experimental modal analysis
$r(t)$	Reference signal	FOS	full-order system
$e(t)$	Error	ROS	reduced-order system
$u(t)$	Input signal/control input (force)	SISO	single input – single output
$w(t)$	Wind excitation	MIMO	multiple input-multiple output
n	Number of DOFs	LTI	Linear-time-invariant
M	mass matrix	LTV	Linear-time-variant
C	damping matrix	MB	Model based
K	Stiffness matrix	DOFB	Direct output feedback
L	Actuator location matrix	ARE	Algebraic Riccati equation
α	number of actuators	IOC	Instantaneous optimal control
D	disturbance matrix	K_d	Derivative gain
X_1	State variable linked to the displacement	T_i	Integral time
X_2	State variable linked to the velocity	T_d	Derivative time
\dot{X}_1	Derivative of the first state variable	J	Performance index
\dot{X}_2	Derivative of the second state variable	Q,R	Weighting matrices

t	Time	\mathbb{R}	Set of real numbers
I	Identity matrix	$G(t)$	Control gain matrix
O	Compatible null matrix	$P(t)$	Riccati matrix
A	Structural matrix	A_c	Closed-loop plant/structural matrix
B	General Locator matrix	B_c	Closed-loop locator matrix
B_c	Control force locator matrix	K_p	Proportional gain
B_e	Earthquake excitation locator matrix	K_i	Integral gain
B_w	Wind excitation locator matrix	t_f	Control period
F	External and internal force vector	C_R	Reduced output/observation matrix
Y	Output vector	H_∞, H_2	Robust controllers
C	Output/observation matrix	F_{sk}	Skyhook force
D	Feedthrough matrix	C_{sk}	Damping coefficient of skyhook damper
$f(t)$	Arbitrary force input	\dot{v}_1	Velocity of suspended mass
$\delta(t)$	Dirac delta function	F_d	Damper force
$\hat{\lambda}$	Laplace transform	C_{sa}	Damping coefficient of semi-active device
\dot{X}_R	Reduced derivative of state vector	\dot{v}_r	Relative velocity of two masses
X_R	Reduced state vector	F_{sa}	Force of semi-active device
A_R	Reduced structural matrix	Y_R	Reduced output vector
B_R	Reduced locator matrix		

Chapter 1

Introduction

1.1 Background and Motivation

Substantial improvements in the field of structural engineering at the beginning of the 20th century, allowed engineers to design tall residential and office blocks based on the concept of “Unresponsiveness”. These high-rise “unresponsive” structures comprised super-rigid structural frames and stiff infills for their protection against lateral sway. Great examples of such structures are the Empire-State in New York and Sears Towers in Chicago. As opposed to these conventionally, strength-based designed structures, modern high-rise structures for the purposes of economy of space, material and foundation requirements, speed of erection and elegance as well as the associated desire for ever-improving sustainable and efficient structural designs, are designed with slender sections and lightweight materials. The increased flexibility and low damping associated with modern high-rise structures generally implies attendant problems such as excessive and long pertaining vibrations under dynamic loading which in turn negatively affect the structure’s serviceability in terms of structural integrity, material fatigue, and comfort of its operators and occupants (Irwin, 1978).

In order to fully satisfy both the additional serviceability and sustainability requirements, for more than half a century, alternative approaches are constantly being investigated. In this regard, many studies have been undertaken examining the possibility of incorporating passive, active and semi-active control devices in high-rise structures so as to alleviate their wind and seismic response. Passive control, which mobilises devices such as viscoelastic dampers, base isolation systems and tuned mass dampers (TMDs), is an adequately understood and widely accepted method for mitigating excessive vibrations in structures, with many on-site applications in Japan, USA and Europe. Their acceptability in the civil engineering field is primarily linked to their high reliability and ability to successfully mitigate excessive vibrations. Unfortunately, such purely passive systems because of

their fixed energy dissipation capacity lack adaptability to ever-changing loading conditions and parametric variation in the structural system.

The strategy developed to deal with the problem of adaptability is known as active control and acts by directly modifying the energy of the system through the application of control forces in a prescribed and controlled manner using actuators. The additional energy allows the structure to adjust its dynamic characteristics making it behave favourably under different environmental conditions. Although such systems are indubitably the most effective in terms of vibration attenuation performance, they suffer from high power demands, relevant implementation hurdles and potential unstable operation. Furthermore, from a cost perspective, when a new structural control system is designed, the designer needs to make appropriate choices so that the extra costs associated with the introduction of the control system will subsequently reduce costs of different nature or increase the global reliability of the system. For active control solutions, however, most of the codes state that the structural system upon failure of the active component must still be able to survive a foreseeable hazardous events (Casciati et al., 2012). Consequently, while the designer might accept the additional costs for promoting innovation, active control solutions might be outside strict market reasoning.

A combination of the advantages of both passive and active vibration control strategies gave birth to one of the most promising control techniques known as semi-active vibration control. Semi-active control achieves its objective through the use of a passive device working in conjunction with actively controlled elements. When this is the case, a large degree of adaptability can be achieved. Owing to the fact that a portion of the control objective is met by the passive device, the power demand is considerably lower and also the problem of reliability is addressed by the provision of a “fail-safe” mechanism. In other words, failure of the semi-active system will result in a purely passively controlled system, which for the case of civil engineering structures inherent stability is guaranteed (Casciati et al., 2006). For example a semi-active tuned mass damper (STMD) upon failure of its active elements (that being either variable stiffness or damping elements) will take the role of a purely passive tuned mass damper (TMD). On the contrary, a purely active system upon active component failure can either seize operation and remain unproductive

(i.e. the actuator driving the mass of an active mass damper (AMD) stops driving the mass) or work in an unexpected manner (i.e. the actuator puts the mass in-phase to the structural vibrations, resulting in larger response amplitudes and also carry the possibility of a global instability).

Due to the aforementioned reasons, semi-active control can be arguably considered the next step in improving the performance of civil engineering structural systems. However, as it is evident from recent constructions of super-tall and evidently technologically high-end structures, which among others include the famous Burj-Khalifa and Taipei 101, such structures are still constructed on the basis of strength/ductility and in some rare cases using passive control. As a matter of fact, according to a 2009 study, from the year 1990-2006 in Japan only 20 buildings have been constructed incorporating semi-active control devices (Ikeda, 2009). It would be therefore reasonable to conclude that the applicability of semi-active control in the construction and civil engineering fields is still at its infancy, suggesting the need for further work emphasising on the aspects that hinder the practical applicability of semi-active control technologies in structural systems.

From a practical applicability perspective, the major factors impeding the application of semi-active control in the civil engineering field are linked to the specific challenges that are not typically encountered in other areas of the control industry. For instance, when considering the processes involved in control system design as depicted in Figure 1, for the case of structural control of high-rise structures, disturbances are often unmeasurable particularly for the case of wind excitations, systems to be controlled are often unknown or contain a large degree of parametric uncertainty, sensors are often limited due to the large number of degree-of-freedom (DOF) and force delivering devices often cannot meet the large force and power demands.

To this end, and taking into account the obstacles impeding the application of semi-active and smart control, this study is interested in investigating methods for enhancing the selling strengths of semi-active control to the structural engineering community.

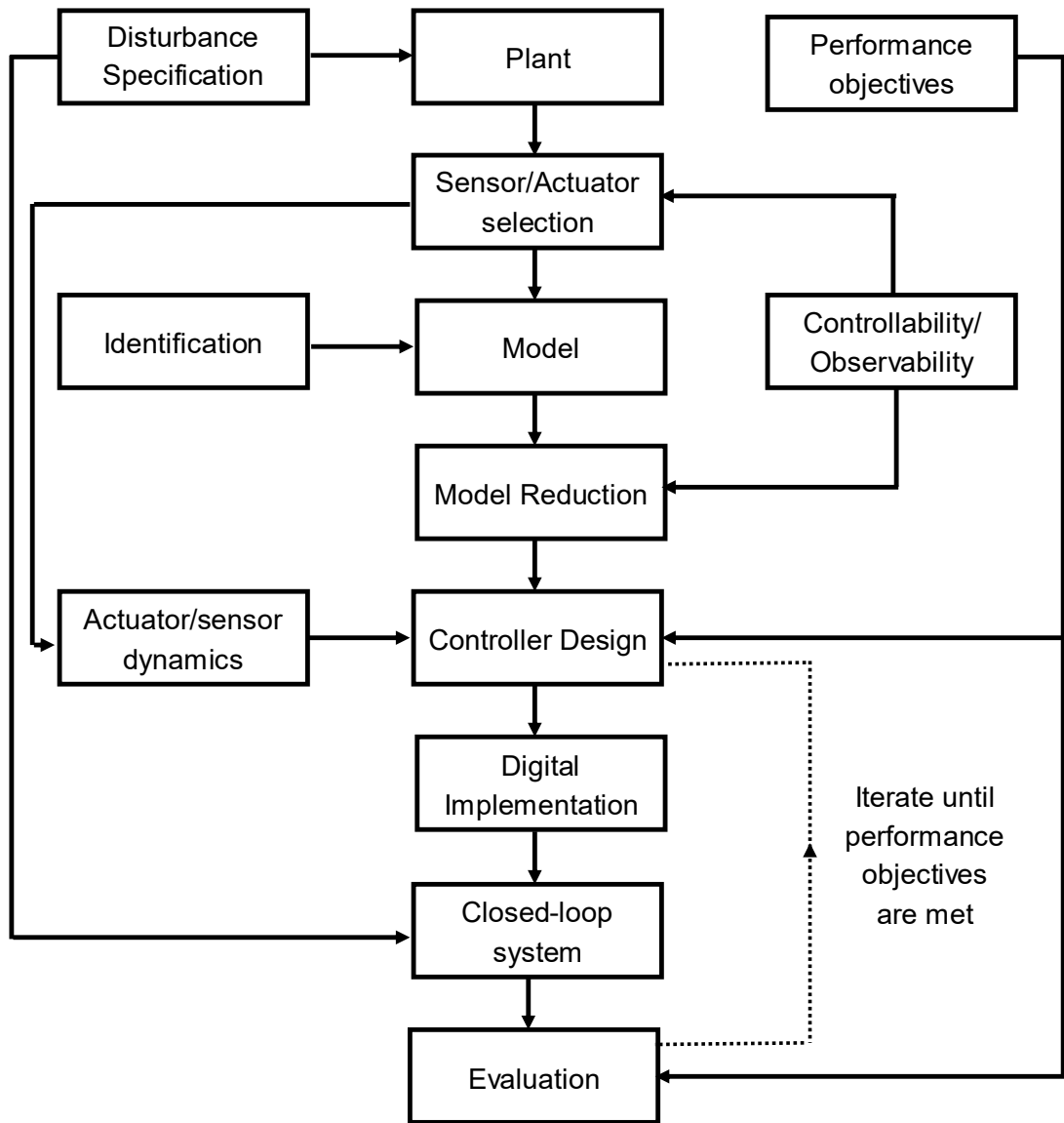


Figure 1. The various steps involved in control system design (Astrom and Hagglund, 1995)

1.2 Thesis Objectives

This research is undertaken with the aim of enabling the construction of slender and lightweight high-rise structures through the use of semi-active control technology and in particular semi-active (smart) tuned mass dampers (STMDs). En route to the attainment of this objective, an evaluation of the efficacy of this exact control strategy in high-rise structures is necessary. At an initial stage, this is achieved by the comparison of the relative performances of the traditional optimised tuned-mass damper in its passive and semi-active states under different loading conditions. Once the semi-

active control strategy is shown to be suitable for use in high-rise structures, the study is then focused on dealing with the complexity associated with practical control implementation, emphasising in the following three areas:

1. Algorithm selection and implementation:

In literature, a large volume of advanced control algorithms has been developed and reviewed for the case of semi-active control (Datta, 2003, Lienes, 2009). Most of these algorithms when compared with traditionally developed algorithms based on classical optimal and robust control theory have shown improved performance both in terms of disturbance rejection and robustness. While, it would be reasonably anticipated that the large number of newly developed and advanced algorithms would revolutionise the structural control field, the same time, classical conventional, robust and optimal controllers (LQR, H_2 , H_∞) remain the prevalent algorithms used in industrial applications. For this reason, categorising and comparing the control algorithms for both the control device and the problem specific (high-rise structures) case can be considered the next step in practical control system implementation. In this regard, questions such as: What is the effect of different algorithms in high-rise structures comprising STMDs? Is it worth using advanced and complex algorithms in STMD controlled systems or will conventional controllers perform satisfactory? Which algorithms can be applied to high-rise structure (at which limited state measurements are available)? need to be answered. By answering these questions, crisp information regarding the implementation of semi-active control algorithms in STMD controlled high-rise structures will be provided, thus the structural control engineering community both in research and practicing level will be facilitated in terms of selecting and implementing the most appropriate algorithm, focusing future efforts in the most promising directions.

2. Novel smart device configuration:

With the aim of promoting further the applicability of semi-active control, this study also aims to investigate the potential of reconfiguring the conventional design of the STMD to one that has the potential to achieve performance gains close to an active control system at considerably lower actuation and power demands while at the same time satisfying practical constraints and stringent

limitations governing the design of the structure and the control device, including but not limited to space availability, weight limitations and actuator strokes. Clearly, for such a novel configuration to be viable for use on civil engineering applications, the crucial provision of a fail-safe mechanism needs to be also satisfied.

3. Simple robust control option for smart damper configurations

Ensuring the robust stability of a smart tuned-mass damper configured system is a non-trivial procedure that typically causes unwanted delays in the design of such systems. In this study an effort will be made to develop a simple and robust control method for use in control system configurations encompassing such devices via the modification of one of the most widely used controllers, namely the proportional-integral-derivative (PID).

1.3 Readership and Organisation of the Thesis

In writing this thesis, the author had in mind that its potential end users will be civil engineers, consultants, and postgraduate students interested in the field of structural control and more specifically structural control of high-rise structures using smart tuned-mass dampers. It has been assumed that the reader is familiar with the concepts governing structural dynamics but only some basic knowledge on structural control and control theory concepts is acquired. For this reason, the thesis is set out in a way that it progressively covers most of the features of structural control design (Figure 1). When an in-depth knowledge is required to progress through the different design steps or whether the reader wants to enhance further their understanding, they can follow the references provided throughout the text.

With that in mind, this thesis is structured as follows: The current introductory chapter briefly laid down the motivation of the research along with the aims and objectives. The immediately following chapter presents a critical literature review on the aspects governing control system design, namely control strategy selection, control system formulation (modeling), etc. giving all the background information necessary for following the numerical work later presented. Chapter 3 introduces the different control algorithms along with the majority of mathematical models used throughout the thesis. The relative

performance of the control algorithms and in turn the investigation of the first objective is found in chapter 4. Chapter 5 introduces a novel configuration for STMD equipped structural systems. Chapter 6 presents a modified robust control method for use with conventional hybrid and novel semi-active hybrid configurations. The final chapter of the thesis summarises the findings of the research including recommendations for future work. A schematic representation of the thesis structure is shown in Figure 2.

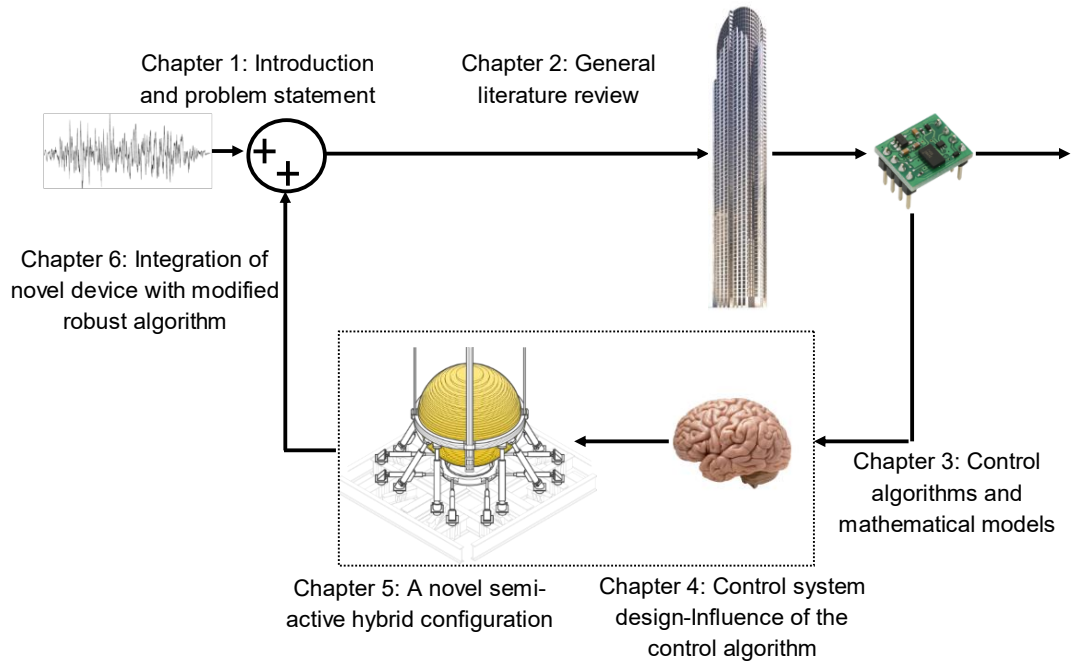


Figure 2. Organisation of thesis

Chapter 2

Literature Review

2.1 Problem Definition

It is justifiable to say that the construction of high-rise structures became a viable solution to the problems associated with urban society. However, the safety of such structures and their contents as well as the comfort of their occupants under external forces such as earthquakes and winds remains a significant engineering concern (Chai and Feng, 1997).

From a structural point of view, the increased height of structures is usually accompanied with low damping (Cheng et al., 2008, Kulkarni et al., 2012), which in turn reduces the ability of the structure to restrict lateral movements. As a result, flexible systems and particularly high-rise engineering structures, opposed to conventional low-rise rigid structures become more vulnerable under dynamic loading, increasing their failure possibilities and problems associated with their serviceability (Kulkarni et al., 2012).

Traditional design methods for mitigating the vulnerability of high-rise structures under dynamic loading, based on 'solidity' and 'massiveness' have often been equated to safety and reliability (Soong, 1990). However, this approach typically tends to overlook the serviceability of the structure and the comfort of its occupants (Kareem et al., 1999). Conventional low-rise structures designed to deal with the "physical design problem" by complying with code requirements, will typically satisfy with ease the serviceability criteria. As structures become taller, more flexible, complex and costly, serviceability criteria and performance requirements become increasingly stringent and more difficult to satisfy. These serviceability criteria are selected in a way that human comfort and structural safety is not compromised. More specifically, lateral deflections, accelerations and stresses must be kept low at all times in order to allow proper functioning of structural and non-structural components. Doing so, will help minimise the fatigue experienced by the structure, prevent excessive cracking, increase the structural lifespan and

preserve the comfort of the structure's occupants and operators (Islam et al., 2012).

2.2 The Civil Engineering Challenge

Protecting high-rise structures from serviceability or collapse failure, preserving human life as well as improving occupant's comfort, are all factors of paramount importance. Traditionally protecting structures from the dynamic effects of wind and earthquakes was achieved through structural stiffening of framing members and plastic deformation allowances (ductility). Designing for strength and ductility, however, does not necessarily ensure the serviceability of the structure and the comfort of its occupants (Housner et al., 1997, Kareem et al., 1999). The reason underlying the limited capacity of conventional 'rigid-unresponsive' structures in satisfying serviceability and collapse requirements is two-folded. Firstly, such structures rely solely on their inherently small material damping for energy dissipation. Secondly, they fail to adapt to ever-changing environmental excitations owing to their fixed capacity of load resistance and energy dissipation (Soong, 1990, Cheng et al., 2008).

In practice the limited capacity of conventionally designed structures was put in test during the late major earthquakes of Northridge in 1994 and Kobe in 1995, where the performance of the intended stiff and ductile structures was proved to be unsatisfactory and far below expectation, with extensive large-scale damages on many modern nominally earthquake-proof buildings (Housner, 1996). The limitations of the traditional design approach along with the urge to enhance structural safety and further resilience, led to the development of more reliable and effective techniques based on structural control concepts. The concept of structural control and its notion as an alternative approach for addressing the safety problem in structural engineering was first introduced by Yao (1972). Structural control aims to control the response of engineering structures through the modification of their rigidities, masses, damping or shape, or by modifying the energy in the system through the action of passive or active counter forces (Housner et al., 1997). Based on this concept, in the last decades considerable research has been undertaken for the development of passive, active, and semi-active control into workable technology, aiming to improve the dynamic performance of

structures (Housner et al., 1997, Spenser and Nagarajaiah, 2003, Cheng et al., 2008). The following subsections present a review of the range of techniques that can be used to mitigate wind and earthquake response in high-rise structures. In this context, the key topics of passive, active and semi-active control are discussed below followed by a brief discussion of the advantages and disadvantages of each technique. In order not to deviate from the initial scope of the study, in the following sections the effectiveness of different control methods is illustrated by focusing on examples and studies that examine the performance of tuned dynamic vibration absorbers (DVAs) in their passive, active and semi-active states.

2.2.1 Passive Control

Passive control is an adequately understood and widely accepted method for mitigating excessive vibrations in structures (Soong, 1990, Kwok and Samali, 1995, Cheng et al., 2008) with a large number of passive control devices being currently incorporated successfully in many high-rise structures for their protection against wind and earthquake excitation (Kulkarni et al., 2012). A passive system, consisting of one or more devices, is designed to alter the dynamic characteristics of the structure in a desirable manner without the requirement of an external power source or measurement of the structural response (Kulkarni et al., 2012). The fact that a passive control system does not require any external power implies that no energy can be added to the system, thus altering its mechanical properties for adaptability to ever-changing conditions is impossible (Hudson, 2013). While other control approaches make use of mechanical actuators for energy dissipation purposes, a passive control system uses the motion of the structure so as to produce relative motion within its damping devices that in turn dissipate energy. The basic configuration of a passive vibration control system is shown in Figure 3.

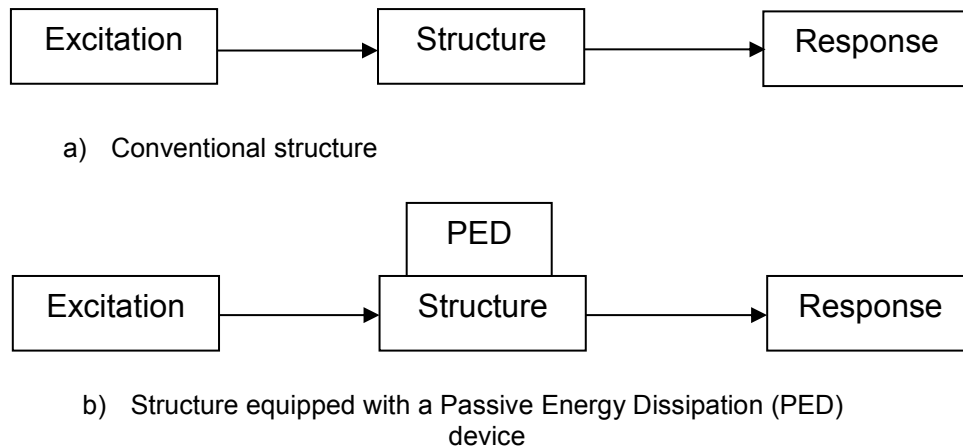


Figure 3. Passively controlled structure

Typical passive devices that can be attached on a structural system include mass and liquid dampers, viscous fluid and viscoelastic dampers, impact dampers and isolation systems. All of these auxiliary devices are characterised by their ability to dissipate energy either by conversion of kinetic energy to heat or by transferring energy among vibrating modes (Housner et al., 1997). Beyond the addition of damping to the system, passive devices can be also designed to alter the stiffness and strength of the structure, thus increase its energy storage capacity and/or avoid resonance through the application of forces generated in response to the movement of the structure (Soong and Spencer, 2002). Examples of such control schemes include base isolation systems that are designed to lengthen the fundamental period of a structure through modification of the structural stiffness at a particular location. Such systems, however, although being shown to be effective for low to medium rise structures and high frequency vibrations, the increased flexibility associated with slender high-rise, long period buildings would lead to large amplitude motions that would most likely be objectionable.

Due to the lack of effectiveness and practicality of passive structural control schemes based on the modification of mass and stiffness in high rise-structures, structural control schemes based on damping control are typically the preferred approach for structural response reduction (Cheng et al., 2008). For this reason, tuned mass dampers (TMDs) , tuned liquid dampers (TLDs) and other auxiliary damping devices of similar energy absorbing nature are considered more suitable for tall and super tall structures (Cheng et al., 2008).

Examples of famous buildings employing auxiliary damping devices include the Crystal Tower in Osaka, the John Hancock Tower in Boston, the CN tower in Toronto, the Citicorp Centre in New York City and the Sydney tower in Australia. The reader is referred to Kwok and Samali (1995) for explicit design details of the passive devices employed in these structures.

The effectiveness of the application of passive damping devices in high-rise structures and towers has been a subject of study by many researchers who suggest that passive vibration control is an effective method for reducing structural response under both wind and earthquake loading. A good example of such study is found in Xu et al. (1992). In this study the authors conducted parametric analyses on a 76-story, 306 m tall building and a 370m TV transmission tower equipped with TLDs and TMDs. The systems were modeled as lumped mass multi-degree-of-freedom (MDOF) systems representing the wind-sensitive slender structure. The authors showed that both devices when tuned to the fundamental frequency of the structure, managed to reduce base moments by 33%, top displacements by 20%, as well as top floor accelerations by 42%. On the other hand, through the frequency response functions of the structural system, they observed that neither of the damping devices had any beneficial effect on reducing the responses of higher modes. In a similar study, Kawaguchi et al. (1992) investigated the response of a 12-storey TMD equipped structure under wind excitation. While the authors observed a significant response reduction from the incorporation of a TMD in the structural system, ranging 45-60 % depending on the mass ratio chosen, they state that the TMD has virtually no effect on frequencies lower than the primary vibration frequency or on high-mode vibration of the building. Both studies suggest that care must be taken when dealing with high-rise slender structures since force and acceleration type responses of such structures may involve more vibration modes than the fundamental. Suggesting that taking into account only the first mode of vibration may lead to nonconservative errors.

In another study, Cao et al. (1997) studied the effect of the application of a TMD on a 340 m communication tower in Nanjing, China. The authors investigated the behaviour of the structure under both earthquake and wind excitation. Additionally, physical constraints and implementation issues such

as space availability, weight limitations, power-force relations and frictional effects were taken into account for obtaining accurate and realistic results. The study showed that the incorporation of a TMD in the structural system indeed reduced the structural response. However, they note that the target comfort limit of 15 mg acceleration was never achieved.

More recently, Liu et al. (2008) examined the effectiveness of a TMD at reducing structural vibrations of a 40-storey structure subjected to both along-wind and across-wind excitation. The authors investigated the sensitivity of the structure to different soil types by accounting for soil structure interaction. The presented results suggest that the TMD is successful at reducing the amplitude of oscillations of the high-rise structure. Furthermore, they observed that TMD suppress vibrations more effectively as the soil stiffness is increased.

In regards to controlling the vibratory motion of slender and low-damped structures, Casciati and Giuliano (2009) numerically investigated the dynamic response of a suspension bridge towers equipped with multiple TMDs. While, the authors observed that multiple TMDs are effective at attenuating wind vibration response, they also noted that such devices are intrinsically non robust owing to their sensitivity to mistuning. They also observed that supplementary provision of robustness by enlarging the operating frequency range results to a drop in the effectiveness of the control system.

Overall, reviewing literature suggests that passive control of high-rise structures and in particular TMD control of such structures is an effective method for alleviating structural response under generic dynamic loading. However, it is important to highlight some of the most important limitations of the use of this technique in high-rise structures. Firstly, TMDs being tuned to a single mode of the structure's vibration are limited to a narrow band of operating frequencies (Connor, 2003). Referring back to what has already been mentioned earlier, for high-rise structures excited in a mode other than the first this may lead to non-conservative errors. Secondly, at the presence of parametric variation in the structural system, a purely passive TMD unavoidably becomes de-tuned resulting in reduced vibration attenuation capacity and in some cases can even increase the levels of vibration in the

system (Sun et al., 1995, Nagarajaiah and Sonmez, 2007, Nagarajaiah, 2009).

2.2.2 Active Vibration Control

Active vibration control dates back in the 18th century. One of the early notions of active control is contained in Mallock (1905) who reported the application of active control on steam ships through synchronisation of the engines in opposite phase (Tokhi and Veres, 2002). Later, Hort (1934) reported the reduction of roll motion of ships by an actively driven Frahm tank where the water is pumped between tanks located on the two sides of the ship. In another study, Allan (1945) examined the roll stabilisation of ships by buoyancy control with activated fins. These gyroscopically controlled auxiliary rudders had the capacity to change their angle of attack to counteract roll caused by wind or waves acting on the ship.

Active control research in the field of civil engineering was not established until 1972 when Yao (1972) laid down a more rigorous control-theory based concept of structural control. In civil engineering structural systems, active vibration control technology makes use of sensors for measuring structural response or external excitations, real-time processing devices for calculation of control forces and mechanical actuators serving as force delivery devices. A schematic representation of an active control system is shown in Figure 4.

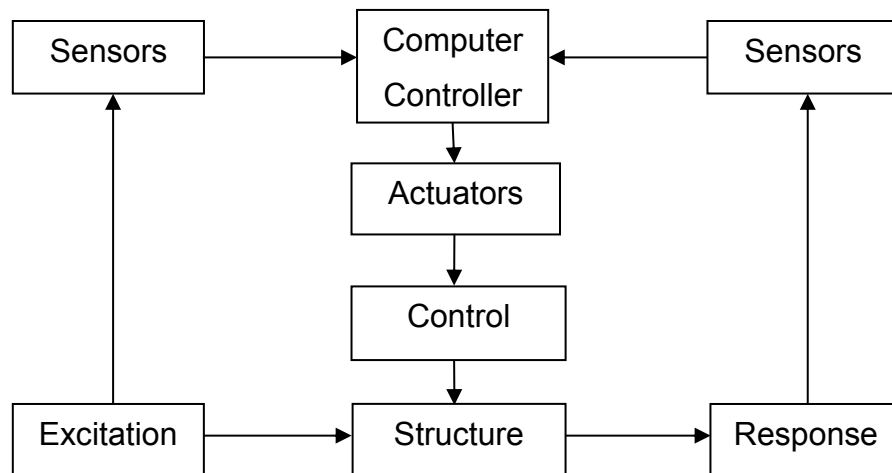


Figure 4. Schematic representation of active control, after Spencer and Soong (1999)

The main difference between an active system and its simpler yet more reliable passive predecessor is the reliance of the first on external energy sources for operation. The ability of a control system to add energy to the structural system implies time-varying energy dissipation capacity which in turn results into enhanced adaptability to ever-changing loading conditions. The adaptive nature of active vibration control systems also allows it to behave favourably under unpredictable dynamic situations and multiple loading conditions such as low frequency winds and high frequency earthquakes, a limitation often observed in purely passive systems which tend to be more effective when dealing with a particular frequency range of vibrations, depending strictly on the tuning of the device.

Active control systems often employ devices such as active mass drivers (AMDs), active tendons, active bracings or active isolators which are often driven by hydraulic, pneumatic, electromagnetic or motor-driven ball-screw actuation. While there are many studies examining the performance of such systems e.g. (Reinhorn et al., 1992, Preumont and Bossens, 2000, Spenser and Nagarajaiah, 2003), reviewing these devices is outside the scope of this thesis. For the purposes of this study, AMDs which represent the purely active version of the TMD will be considered. Such active devices consist of masses driven by mechanical actuators at the absence of which the masses will remain idle. A typical uniaxial AMD device is depicted in Figure 5a. In order to visualise the difference between a TMD and an AMD the mathematical model of an AMD controlled system is depicted in Figure 5b. It is worth noting that the values of K_d and C_d represent the inherent stiffness and damping of the 'purely' active device, which can be also ignored in the analysis due to their small influence when compared to the actuator force, F_a .

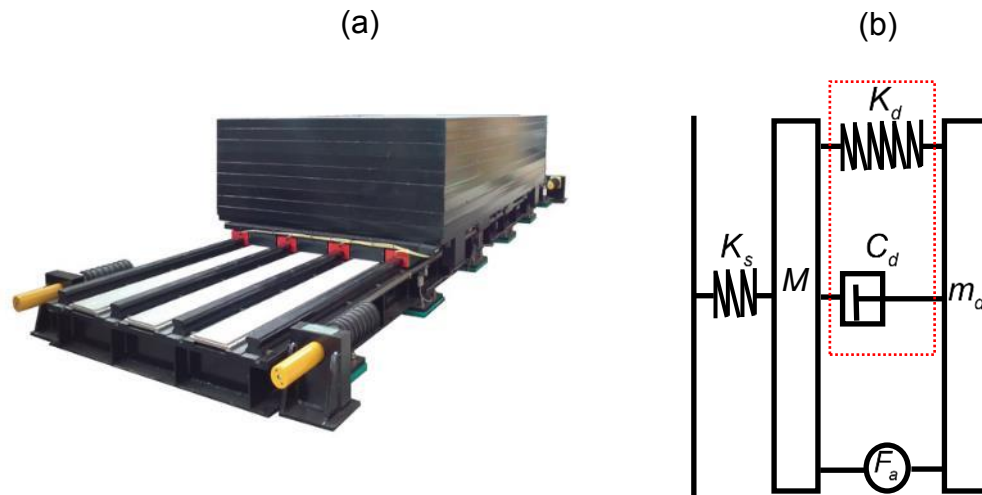


Figure 5 (a) Typical uniaxial AMD device (IHI Infrastructure Systems CO., 2013) (b) Model of SDOF structure equipped with AMD

The Kyobashi Seiwa building in Tokyo constructed in 1989 is believed to be the first building fitted with an AMD (Kwok and Samali, 1995, Spenser and Nagarajaiah, 2003) as well as the first ever practical application of active structural control in civil engineering (Ikeda et al., 2001). In this structural system, the two masses comprising the AMD device (one in each horizontal direction) are suspended by wire ropes and driven using servohydraulic actuators. This device, unlike a passive TMD is not tuned to a specific frequency of the structure. For this reason, a controller, in this particular case a linear quadratic regulator (LQR) was used to calculate corrective actions based on the relative velocity of the masses and the structure. According to Kwok and Samali (1995), the performance of the structure was put in practice under both earthquake and typhoon wind conditions. From the obtained measurements, it was shown that the incorporation of the AMD in the system helped reducing the system's acceleration response by approximately 50-60% compared to the uncontrolled structure (Koshika et al., 1992, Kwok and Samali, 1995).

In 2003, Ricciardelli et al. (2003) compared numerically the performance of SDOF and four-DOF structures equipped with a TMD and an AMD under white noise excitation. Interestingly enough the authors observed that although an AMD is effective at attenuating vibration response, its performance is constrained by large strokes, large control forces and power

requirements. Similar observations have been made by Boujari et al. (2012). In their study, the authors examined the response reduction of a PID-ATMD controlled three-DOF structural system under seismic excitation. It was observed that both acceleration and displacement responses were greatly reduced, however, the authors state that the values of active control force maybe so high that its realisation be non-economic.

In 2006, Al-Dawod et al. (2006) developed a five-storey experimental model equipped with an AMD and examined its behaviour under four earthquake excitation records. While, the fuzzy logic controlled device was shown to be effective at reducing the displacement responses of the structure under the four earthquakes, the authors reported that acceleration responses have been reduced for most loading cases but also increased for a few other cases. Additionally, the authors observed while the AMD device was able to reduce the responses of the fifth storey, lower floor responses were shown to be reduced by a different percentage or even larger for some cases. This suggests that attempting to control a certain mode of the overall system, spillover can occur increasing the amplitude of higher modes. To the author's understanding, due to the different frequency content of the four earthquake records the effectiveness of active control is reasonably not evident in every loading case.

Recently, Casciati and Chen (2012) investigated both numerically and experimentally the behaviour of a proportional-integral-derivative (PID) controlled AMD for suppressing the vibrations of a three-storey structure under sinusoidal movement of a shake table at a frequency of 1.25 Hz. The excitation frequency was selected such that it matches the fundamental frequency of the structure, thus at the absence of an AMD the frame would resonate until the amplitude of the top floor acceleration would reach a maximum steady state amplitude. In order to avoid destroying the frame, the shake table was stopped when the acceleration amplitude approached 0.5g. The authors observed that when the excitation stopped, the frame was damped in a very slow manner. On the contrary, for the AMD equipped structure, the acceleration amplitude was stabilised at approximately 0.2g and the structural system quickly damped its response when the excitation stopped. From these observations, the authors suggested that the PID

controlled AMD was successful at mitigating vibration responses.

The presented studies are a few amongst the many showing that incorporating active control (AMDs) in high-rise structures can be considered a promising method for alleviating dynamic vibration response. On the other hand, one needs to consider factors such as the apparent complexity of implementing active control in structural systems, reliability, cost, and safety. While the reliability, design and implementation complexity can be easily realised, a cost benefit analysis of such devices cannot be easily made. Additionally, due to code requirements and limitations, fully actively controlled systems have to be backed up by sufficient capacity in the uncontrolled system. Subsequently, the presence of the active device will have a performance enhancement role without allowing structural systems to be made with less material as suggested by the aforementioned researchers. Consequently, while in theory significant cost savings can result from the incorporation of active devices in the structural system, in practice, significant advances in technology need to be made so that codes accept that active component failure will not occur beyond any reasonable doubt.

2.2.3 Semi-Active Vibration Control

Semi-active control technology dates back in the 1920s when the first patents were issued for shock absorbers utilising power operated valves for directing flow (Symans and Constantinou, 1999). Semi-active control in structural engineering was not exploited until 1983 when Hrovat et al. (1983) suggested a semi-active tuned mass damper (STMD) for controlling structural vibrations. It is evident that his work was vastly influenced by work done in other engineering fields and particularly work undertaken in automotive vibration control. Since the introduction of this novel technology in the civil engineering community, a large amount of research has been undertaken establishing semi-active control as a viable alternative for mitigating structural vibrations. Semi-active vibration control systems are fundamentally controllable passive systems, which achieve their control objective through the indirect application of energy on the structure as shown schematically in Figure 6. In such systems, power is used to vary the mechanical properties of a passive device i.e. through varying the fluid discharge through an orifice, or by varying the

magnetic field around a ferrofluid piston (i.e. Magnetorheological (MR) damper). Depending on the varying parameter, semi-active devices are divided in two categories namely, variable stiffness and variable damping. Examples of such devices include electrorheological and magnetorheological dampers, viscous and tuned mass or liquid dampers. The reader is referred to Symans and Constantinou (1999) for a comprehensive state-of-the-art review on these devices.

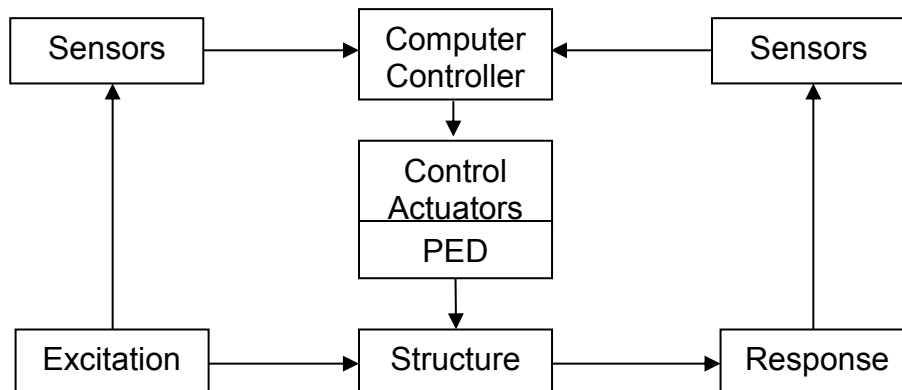


Figure 6. Schematic representation of a semi-active control scheme (Soong and Spencer, 2002)

Beyond the adaptability achieved in the system by the variation of the parameters of the semi-active device, a semi-actively controlled system is also benefitted by a considerably lower power demand compared to an active system (of the order of Watts as opposed to kWatt) owing to the ability of its devices to achieve a large portion of the control objective through their passive components, allowing such systems to be operated on small external power sources such as batteries (Nagarajaiah and Varadarajan, 2005). As a result, at the event of power failure e.g. during an earthquake, the reliability of the system will not be compromised. It is noteworthy that the reliability and low-energy consumption of these systems are amongst the primary factors that directed the attention from active systems to semi-actively controlled ones.

Referring back to the first application of semi-active control in civil engineering structures, Hrovat et al. (1983) demonstrated through numerical simulations that the use of variable-damping STMDs (VD-STMDs) controlled by an LQR algorithm is an effective method for controlling the wind induced motion of tall buildings. As a matter of fact, from the comparison of the VD-STMD with the

purely passive TMD and an active ATMD, the VD-STMD was shown to outperform the TMD exhibiting similar behaviour to the ATMD.

Validating the observations of Hrovat and his colleagues, Pinkaew and Fujino (2001) examined the behaviour of a VD-STMD attached to a SDOF structure subjected to free and harmonic excitation. The authors observed that the LQR controlled VD-STMD was able to substantially improve the steady-state response of the structure around the tuning frequency when compared to the TMD. It was also observed that the performance improvement is equivalent to an increase of the TMD's mass by about four times, suggesting that a VD-STMD configuration can be used to replace part of the TMD vibrating mass, achieving a lightweight vibration control solution or can be even used to improve the performance of the TMD given a certain mass.

Along the same lines, Setareh (2001) used an on-off control algorithm, where the damping of the mass damper was switched between maximum and minimum level depending solely on the direction of motion of the structure in regards to the direction of the damper's force. For example, if the structure and the damping force are in the same direction, the variable-damping component of the STMD is set to a high state, otherwise is set to a low state. The author observed that through this control method, the seismic response of a SDOF structure was successfully reduced, suggesting that there is still room for the improvement of the control effect on the VD-STMD structural system. A year later, Runlin et al. (2002) examined the behaviour of a five and a ten-storey structure equipped with a STMD. As opposed to the previous studies that used the LQR and on-off algorithms for the calculation of the corrective actions the authors used an off-towards-equilibrium (OTE) algorithm. Comparing the responses of the structures using both the on-off algorithm (used by Setareh (2001)) and the OTE algorithm the authors observed an additional (approximately 10%) response reduction using the latter algorithm.

Most recently, Demetriou et al. (2014) examined the behaviour of a benchmark three-DOF structure equipped with a VD-STMD under various earthquake excitation records. As opposed to the previous studies, the semi-active device was controlled using a PID controller. From the numerical

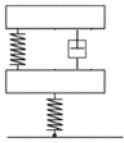
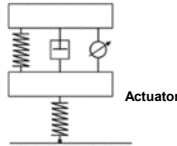
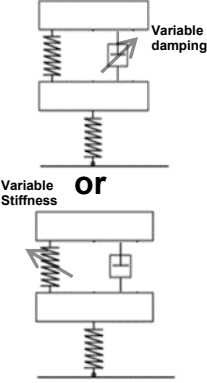
simulations, an increase of 5-10% in the system's vibration attenuation capacity was evident in terms of rms values when compared to the optimally designed TMD. The authors suggest that this increase in performance may not be enough to justify the use of sophisticated equipment; however, they note that with the development of cost effective control solutions this should be considered as part of the future civil engineering design agenda. Additionally, examining the long term performance of both the TMD and the VD-STMD by accounting for material degradation and damage in the system, it was observed that the latter devices are relatively insensitive to parametric variations in the structural system.

In terms of controlling structural systems with variable stiffness (VS)-STMD devices, Nagarajaiah and his colleagues launched a series of studies examining the performance of VS-STMD in structural systems. As opposed to damping variation in STMD controlled systems that exploit energy dissipation, VS-STMD controlled systems are associated with moving the system's natural frequency outside the resonance range and in a sense retune the STMD depending on the excitation frequency. A method for capturing the instantaneous localised timed-varying frequency content of any given signal is thus essential for the variable stiffness device to make appropriate adjustments. It will be therefore, reasonably anticipated that control algorithms which are applicable in VD-STMD will not be applicable to VS devices. As a matter of fact, most of the VD-STMD controlled systems use classical control methods for the derivation of the required actions, whereas VS-STMD systems use real time tuning algorithms based on Hilbert transform (HT) and short time Fourier transform (STFT). In this context, Nagarajaiah and Varadarajan (2005) examined the behaviour of a 76-Storey benchmark building using a VS-STMD demonstrating the robustness of the system to parametric uncertainty. The performance of the VS-STMD was shown to have similar performance to an ATMD but with an order of magnitude less power consumption. Along the same lines, Nagarajaiah and Sonmez (2007) proposed the application of single and multiple STMDs for response control of multi-storey structures (one and five-DOF) under harmonic, stationary and nonstationary excitation. It was observed that the VS-STMDs are superior to their passive counterparts at reducing structural responses under both force

and base excitations. Another remarkable observation was that at the presence of damage or deterioration, the TMD controlled system quickly became de-tuned losing significant vibration attenuation performance, whereas, the VS-STMD was shown to be insensitive to the parametric variation.

Summary: So far, each of the different control methods has been discussed. The effectiveness and the limitations of passive, semi-active and active control methods on mitigating the vibration response on high-rise structures were demonstrated through specific studies. A summary of the findings is presented in Table I.

Table I . Summary of the advantages and disadvantages of each control method

Control method	Advantages	Disadvantages
<p>Passive:</p> 	<ul style="list-style-type: none"> • Relatively inexpensive • No need for energy • Inherently stable • Effective in low-medium rise structures 	<ul style="list-style-type: none"> • Not adaptable to conditions • Relatively unsuitable for high-rise structures
<p>Active:</p> 	<ul style="list-style-type: none"> • Effective for all conditions and structural configurations • Less invasive than structural stiffening when retrofitting is required • Insensitive to parametric variation/ flexibility in tuning 	<ul style="list-style-type: none"> • May introduce instability • Spillover may occur on higher modes • Reliance on external power / Vulnerable to power failure • Its adaptability is limited by large stroke and control forces
<p>Semi-active:</p> 	<ul style="list-style-type: none"> • Significantly lower consumption than active methods • Ensured bounded input/output stability • More adaptable than passive methods/ closer performance to active methods • Less expensive than active control • Insensitive to parametric variation/ flexibility in tuning • Fail-Safe mechanism 	<ul style="list-style-type: none"> • Lower vibration attenuation performance than active control methods

2.3 Principles of Structural Control

The basic concept of response control of vibrating systems can be illustrated using a simple single-degree-of-freedom (SDOF) structural model and the equations governing its motion. The motion of a SDOF system subjected to earthquake excitation is governed by:

$$m\ddot{x}(t) + c\dot{x}(t) + kx(t) = -m\ddot{x}_g(t) \quad (2.1)$$

where m, c, k is the structural mass, damping coefficient and linear elastic stiffness respectively. $x(t), \dot{x}(t), \ddot{x}(t)$ are the response variables displacement, velocity and acceleration of the SDOF system when subjected to an external acceleration $\ddot{x}_g(t)$. Dividing all terms by m , substituting $\omega_n = \sqrt{k/m}$ and $\zeta = c/2m\omega_n$, Eq.(2.1) can be written as:

$$\ddot{x}(t) + 2\zeta\omega_n\dot{x}(t) + \omega_n^2x(t) = -\ddot{x}_g(t) \quad (2.2)$$

where, ζ is the damping ratio as defined earlier and ω_n is the undamped natural frequency. Using the theory of structural dynamics (Meirovich, 1990, Clough and Penzien, 1995) the response of the SDOF system subjected to ground acceleration $\ddot{x}_g(t)$ can be calculated by:

$$x(t) = e^{-\zeta\omega_n t} (C_1 \cos \omega_d t + C_2 \sin \omega_d t) - \frac{1}{\omega_d} \int_0^t \ddot{x}_g(\tau) e^{-\zeta\omega_n(t-\tau)} \sin \omega_d(t-\tau) d\tau \quad (2.3)$$

where, ω_d is the damped natural frequency, and C_1, C_2 are constants derived from initial conditions. The response of the same SDOF system under a single sinusoidal excitation $P \sin \theta t$ is:

$$x(t) = e^{-\zeta\omega_n t} (C_1 \cos \omega_d t + C_2 \sin \omega_d t) + \frac{P \sin(\theta t - \varphi)}{m\sqrt{(\omega_n^2 - \theta^2)^2 + 4\zeta^2 \omega_n^2 \theta^2}} \quad (2.4)$$

where,

$$\varphi = \tan^{-1} \left(\frac{2\zeta\omega_n}{\omega_n^2 - \theta^2} \right) \quad (2.5)$$

In which θ is the frequency of the excitation. Eq.(2.3) and Eq.(2.4) show that structural response can be altered either by reducing the magnitude, P , of the

external excitation, either by increasing the damping ratio ζ or by avoiding resonance through enlarging the difference of ω_n and θ (Cheng et al., 2008). This can be achieved through a variety of techniques such as modification of rigidities, masses, damping, or through the provision of passive or active counter forces (Housner et al., 1997).

Using Eq.(2.1) and the same SDOF system, Spencer and Soong (2002) demonstrated the effect of structural (passive and active) control on response reduction. Through the addition of active or passive elements (similar to the one depicted in Fig. 5) Eq.(2.1) becomes:

$$(m + \bar{m})\ddot{x}(t) + c\dot{x}(t) + kx(t) + \Gamma x(t) = -(m + \bar{m})\ddot{x}_g(t) \quad (2.6)$$

where; \bar{m} is the mass of the active or passive element, $\Gamma x(t)$ is the force corresponding to the device, and Γ represents an integrodifferential operator. The specific form of $\Gamma x(t)$ must be specified before analysing Eq.(2.6). A typical linear model of $\Gamma x(t)$ can be expressed as:

$$\Gamma x(t) = \bar{c}\dot{x}(t) + \bar{k}x(t) \quad (2.7)$$

where \bar{c} and \bar{k} are the damping coefficient and stiffness of the control device respectively. Eq.(2.6) becomes:

$$(m + \bar{m})\ddot{x}(t) + (c + \bar{c})\dot{x}(t) + (k + \bar{k})x(t) = -(m + \bar{m})\ddot{x}_g(t) \quad (2.8)$$

Eq.(2.8) shows that the application of a passive or active control force modifies the dynamic properties of the system in such a way so as to respond more favourably to the external excitation. For a purely active control system, the terms in Eq. (2.7) and Eq. (2.8) \bar{c} and \bar{k} characterise the control gains, which can be chosen in such a way that the structural response can be in principle eliminated (Datta, 2003). As it will be extensively discussed in the following chapters, the choice of gains depends on the control algorithm selected. Like any other engineering design process, the selection of control gains will be a compromise between different performance variables. In the case of structural control systems these performance variables are typically the robust stability and vibration attenuation capacity of the control system. It is also noteworthy that systems that are stable for some gain values become unstable after a

certain threshold. Identification of this threshold is thus of major importance.

Traditionally structural control of high-rise and large-scale structures is achieved through the addition of damping to the system as opposed to the alteration of the system's mass and stiffness (Cheng et al., 2008). This is primarily linked to performance and practical limitation associated with the latter two techniques. Mathematically, the impracticality of altering the stiffness and mass of high-rise structures through structural control is demonstrated using the same SDOF described previously. Using Eq. (2.4) the response amplitudes of the SDOF system to a resonant excitation $P \sin \omega_n t$ can be derived as:

$$x = \frac{P}{2\zeta m \omega_n^2}, \quad \dot{x} = \frac{P}{2\zeta m \omega_n}, \quad \ddot{x} = \frac{P}{2\zeta m} \quad (2.9)$$

From which the amplitudes of the restoring force, R , the damping force, D , and inertia force, I , are extracted as:

$$R = \frac{P}{2\zeta}, \quad D = P, \quad I = \frac{P}{2\zeta} \quad (2.10)$$

It can be seen that the magnitude of the restoring force R and the inertial force I (associated with the stiffness and the mass of the SDOF respectively) is substantially larger than the magnitude of the damping force (approximately 50 times for a lightly damped system with $\zeta \approx 1\%$). The same can be also observed by studying the root-mean-square (rms) response of the SDOF system under a white noise excitation (Cheng et al., 2008) validating the presented argument. The above observations suggest that controlling the magnitude of the inertia or restoring force would require numerous sizeable force-generating devices, which in turn implies a larger control effort and impracticality. Therefore, controlling the damping in the high-rise structural system would be typically the preferred approach. Damping, on the other hand, unlike mass and stiffness does not relate to a unique physical phenomenon, making it impossible to engineer without the addition of external damping devices (Kulkarni et al., 2012). What is more, inherent material damping cannot be estimated with accuracy; however, known levels of supplementary damping can be introduced using either passive or active devices (Housner et al., 1997).

The effect of the provision of additional damping on a SDOF structure can be also illustrated through the transmissibility of the system. Transmissibility is calculated as the ratio of the amplitude of vibration measured in the system to the amplitude of vibration entering the system and is a measure of how much vibration energy can be transmitted through the structure. By plotting the transmissibility of the SDOF system at different damping ratios, ζ , and frequency (of the excitation to the structural frequency ω / ω_n) ratios, β , as shown in Figure 7a, it can be seen that provision of additional damping will reduce the transmissibility around the system's natural frequency but will subsequently increase its response at higher frequencies relative to other control methods. This suggests that passively controlling the system through the provision of damping may have adverse effects on its performance, especially during transient response (Pinkaw and Fujino, 2001). By attaching an active or semi-active device on the purely passive system, the designer can make use of control algorithms in order to adjust its damping appropriately. In the example shown in Figure 7a, using a simple on-off control algorithm, the damping could be reduced to its minimum value at frequency ratios larger than $\sqrt{2}$. Figure 7b summarises the concept by illustrating the relative performance of a passive, active and semi-active control equipped system. The shaded area between the passive and active curves shows the possible operating range of a semi-actively controlled system, highlighting the potential of such configuration.

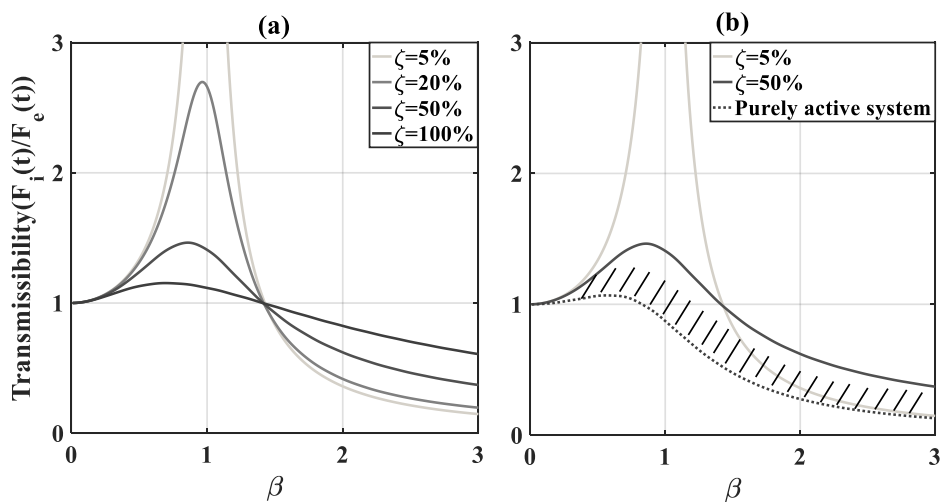


Figure 7. Transmissibility of a SDOF at (a) Different values of supplemental damping, (b) and the addition of a PID calculated active force

Summary points: In practice vibration control of structures is achieved in many different ways depending on the problem. Most common methods include stiffening, damping and isolation. Stiffening the structure allows shifting its resonance frequency beyond the frequency band of excitation, isolation prevents the propagation of disturbances to sensitive parts of the system and damping reduces the resonance peaks by dissipating energy (Preumont and Seto, 2008). Additionally, through investigation of Eq.(2.10) it is demonstrated that controlling the damping requires much less control effort than controlling stiffness particularly in high-rise low damped structures.

Structural vibration control in the form of stiffness, damping and isolation can be introduced in the system through structural modification, albeit considered the most structurally invasive and inefficient method, or through the provision of passive/active or semi-active forces as demonstrated in Eq.(2.8). In this regard semi-active and active control methods can be used to enhance the performance of passive control schemes through the modification of damping and/or stiffness when necessary. Furthermore, semi-actively controlled systems, when designed properly have the potential of achieving attenuation performance similar to active systems.

2.3.1 Structural control using semi-active and active dampers

A single mass damper's operational principle can be easily explained when considering a simple MDOF structure as the one shown in Figure 8. The dynamic behaviour of such a system when subjected to an arbitrary disturbance is fully captured by its matrix equation of motion:

$$M\ddot{x}(t) + C\dot{x}(t) + Kx(t) = Bu(t) + Dd(t) \quad (2.11)$$

where M, C and K are the $n \times n$ mass, damping, and stiffness matrices respectively; $x(t)$ and $d(t)$ are in order the displacement, and external force $n \times 1$ column vectors; $u(t)$ is the single scalar control force and B and D are the $n \times 1$ influence matrices assigning the control and external force contributions respectively to the individual DOFs. For each DOF in $x(t)$ being the displacement of the i^{th} ($i = 1 - n$) mass, M trivially becomes diagonal, while

for the pure viscous damping considered (and connections as in Figure 8) the damping matrix C attains a form identical to the symmetric stiffness matrix K . Without any loss of generality the mass damper device is attached to the $(n-1)^{th}$ DOF and its motion constitutes the n^{th} DOF.

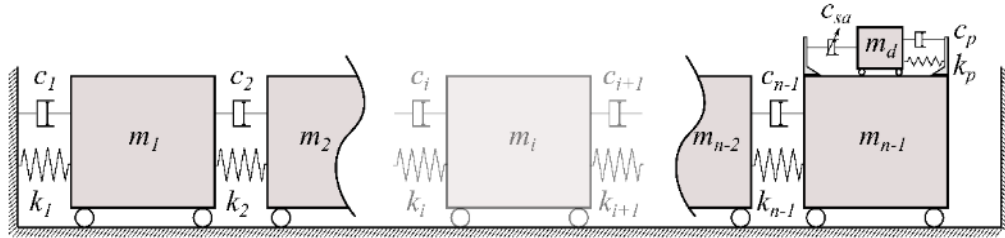


Figure 8. Idealised n-DOF structural system equipped with a dynamic vibration absorber (DVA)

The matrix Eq.(2.11) could describe a system equipped with any type of viscous dynamic absorbing device. The difference between passive, active and semi-active schemes would exclusively be captured by the nature of the control force $u(t)$. It would be probably more appropriately for this case to term $u(t)$ interaction force, yet for economy in presentation the term control is used throughout. To facilitate the derivation of a semi-active control force, it would be beneficial to first consider the case of a purely passive TMD. When the TMD is attached to the system of interest, the $u(t)$, takes the form of a purely passive action, $u_p(t)$, resulting solely from the motion of the absorber's mass. This passive force which couples the damper to the rest of the system can be mathematically expressed as:

$$u_p(t) = c_p \dot{x}_r(t) + k_p x_r(t) \quad (2.12)$$

In the equation above, c_p is the constant scalar damping coefficient and k_p is the constant scalar spring stiffness of the TMD, while $\dot{x}_r(t)$ and $x_r(t)$ are respectively the relative velocity and displacement between the n^{th} and $(n-1)^{th}$ DOFs (i.e. the structural and damper motion variables). It should be also noted that the n -element B becomes $[0 \dots 1 \ -1]^T$. Next step towards the derivation of the semi-active control force is to formulate an equivalent control force provided by a purely active-TMD (ATMD) (Pinkaw and Fujino, 2001). When an active control system is considered, the control force takes the form of a

desired action $u_a(t)$, determined by a control algorithm such as a Linear-Quadratic-Regulator (LQR), PID or similar. For an ATMD, the desired force is the summation of the passive forces generated by the mass damper's motion and an additional external force provided by means of mechanical actuation. Because the dynamic characteristics of the mass damper remain unaltered and the desired interaction force, $u_a(t)$, has been already calculated by the control algorithm, the required actuation force, $f_a(t)$, can be readily determined from:

$$u_a(t) = c_p \dot{x}_r(t) + k_p x_r(t) - f_a(t) \quad (2.13)$$

The final step of the derivation of the semi-active control force involves the calculation of a force that can be physically realised by the semi-active device. In this regards, because of the fact that no energy should be added directly to the system, the semi-active device will produce control forces only when required i.e. when the damper is to "consume" energy. Having already obtained an equivalent active force from Eq.(2.12), the final step is to apply semi-active force saturation limits such that the semi-active control force, $u_{sa}(t)$, is calculated by (Hrovat et al., 1983):

$$u_{sa}(t) = f_a(t) \left(\frac{1 - \text{sgn}[f_a(t)\dot{x}_r(t)]}{2} \right), \quad (2.14)$$

$$\text{sgn}(q_a) = \begin{cases} 1 & \text{for } q \geq 0 \\ -1 & \text{for } q \leq 0 \end{cases} \quad (2.15)$$

The product of $f_a(t)\dot{x}_r(t)$ is the power, q_a , of the whole active system device. Similarly, the power of just the semi-active component is defined as the product of the force that can be physically translated by the device, $u_{sa}(t)$, and its relative velocity, $\dot{x}_r(t)$:

$$q_{sa} = u_{sa}(t)\dot{x}_r(t) < 0 \quad (2.16)$$

A schematic representation of the power time histories of both an actively and a semi-actively controlled devices is shown in Figure 9. It can be observed that the active device has the advantage of both producing and consuming power while the semi-active device only consumes power. This verifies the fact that

an active control scheme can add energy to the system while a semi-active scheme can only dissipate energy.

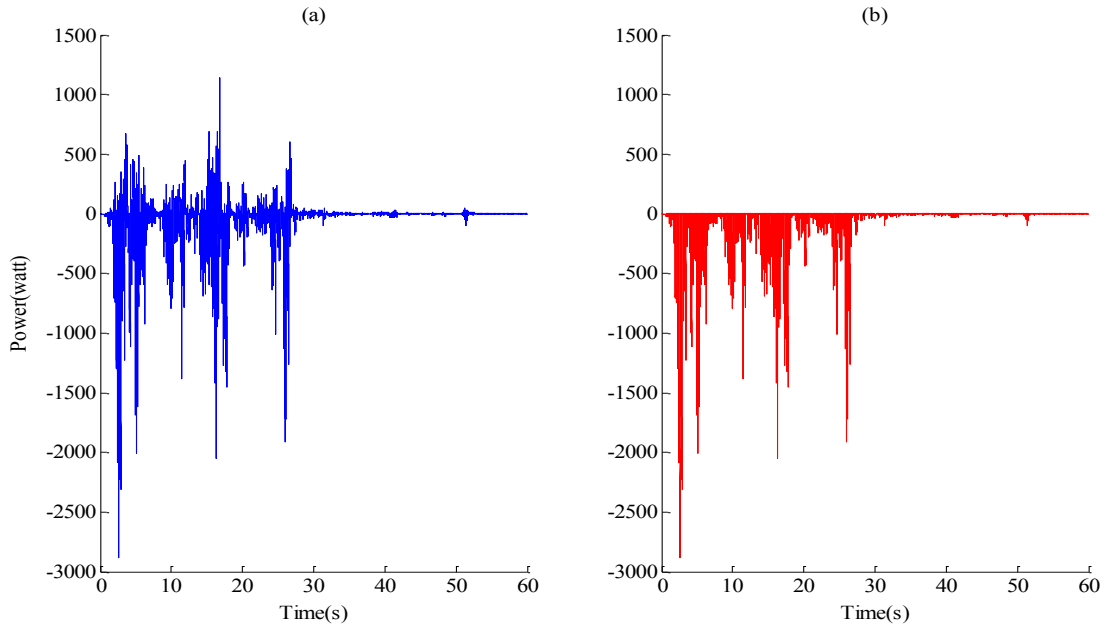


Figure 9 Indicative power demand of an (a) Active device and (b) Semi-active device

So far, the principle of obtaining a “desired” control force to be provided by a semi-active device has been discussed. When a VD-STMD is considered, the chosen way of achieving optimum performance, is by appropriately timely adjusting the damping coefficient of the device within bands, in order for the required control force to be reached. By referring back to the system presented in Figure 8, one can express the semi-active damping force contribution as $c_{sa}(t)\dot{x}_r(t)$. Inspection of Eq.(2.16) easily leads to $c_{sa}(t) < 0$. Updating Eq.(2.13), the resulting overall control force provided at each time instance by a VD-STMD can be expressed mathematically as:

$$u_a(t) = (|c_{sa}(t)| + c_p)\dot{x}_r(t) + k_p x_r(t) \quad (2.17)$$

In Eq.(2.17) the time varying semi-active damping coefficient, $c_{sa}(t)$, is the only unknown. Therefore, calculating the real-time variation of the damping coefficient is straight forward.

2.4 Control Strategies

Semi-active and active vibration control in engineering systems is divided primarily in two strategies, namely, feedback and feedforward. The classification of a control system in either of the two categories depends strictly on the type of information processed by the controller (data passed to the control algorithm). In structural engineering systems, feedback controllers measure structural response, whereas, feedforward controllers measure the external excitation for the calculation of control forces. It can be easily realised that vibration control of civil engineering structures is typically limited to feedback control strategies due to the apparent limitations of measuring the external excitation.

When referring to feedback control systems, the term closed-loop is commonly used. A system is considered a closed-loop system if its sub-systems are interconnected in a cycle. Figure 10a, demonstrates the idea of a closed-loop system characterised by two sub-systems and their transfer functions $H(s)$ and $G(s)$. It is worth noting that in a structural control system one might need to make use of a greater number of sub-systems to adequately capture the dynamic behaviour of sensors, actuators etc. In the closed-loop system of Figure 10a, the output signal $y(t)$ is compared to the reference (desired) signal, $r(t)$, for the calculation of an error $e(t)=r(t)-y(t)$. The error signal is then passed to $H(s)$ which is designed to minimise its magnitude through modifying the input signal $u(t)$ to the plant $G(s)$. The sub-system $H(s)$ which is known as the controller of the system, will simply generate a control command $u(t)$ aiming for an output $y(t)$ closer to the reference signal $r(t)$.

The aforementioned observations indicate that the dynamics of the sub-systems in a feedback control system are strongly coupled. Additionally, it can be also observed that even though a controller represents only a fraction of the overall system, it has a major influence on its overall performance. If the link between the output signal $y(t)$ and the reference signal, $r(t)$, is removed, the resulting system would be termed as an open-loop system as shown in Figure 10b. In the latter case, the output, $y(t)$, of system 2 will not have any influence on the input signal of system 1.

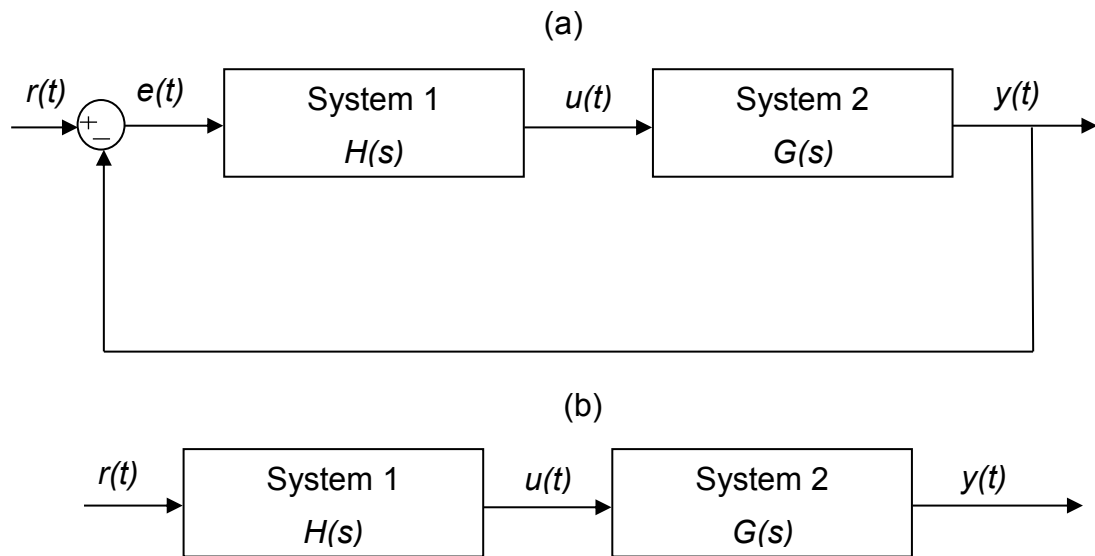


Figure 10. Control strategies (a) Closed-loop system and (b) Open-loop system (Astrom and Murray, 2012)

Beyond the apparent performance advantages of using a feedback control strategy, potential disadvantages may also arise. Feedback control systems are susceptible to dynamic instability which will be the result of oscillations with negative damping. Another drawback is that unwanted sensor noise can be introduced in the system, requiring careful filtering of the signals (Astrom and Murray, 2012). The engineering challenge is to find an appropriate controller-compensator ($H(s)$) for achieving a certain desired behaviour characterised in terms of both performance and reliability (stability and robustness) of the closed-loop system.

2.4.1 Evaluation of Control Strategy

The most obvious performance specification in a structural engineering control system is the rejection of external disturbances which will cause the system to deviate significantly from its equilibrium position, compromising the serviceability of the structure and the comfort of its occupants. Like all design problems, the controller synthesis problem involves trade-offs. The most obvious trade-off is that of performance and robust stability. In general, the more robust a system against variations or uncertainties in the system model, the less performance can be achieved (Dyke et al., 1996, Dietz, 2008). A successful controller would be the one that achieves the desired performance

level while at the same time being tolerant to variations in the system maintaining the system's stability at all times.

The evaluation of a controller and its effectiveness on the physical system can be performed with and without the use of mathematical models. Without the use of mathematical models, one would require to assess the controller effectiveness and ultimately the structural performance (both in terms of disturbance rejection and robustness) by repeated trials on the physical system (i.e. through trial and error tuning of the controllers) until an answer that satisfies intuitive reasoning is obtained (Housner et al., 1997). The impracticality of this method and its inability to capture the infinite number of feasible events and disturbances, acts as a major limitation prohibiting its use in practical applications. On the contrary, the use of mathematical models which are derived either from first principles or system identification techniques (i.e. input/output data, black box techniques) allows an approximation of the dynamics of the physical system. The resulting system model which includes the mathematical models of the actuators, the sensors, the compensator and the plant can be used to make analytical predictions which are not limited to individual events. For these reasons, in this thesis, the control objective is achieved using pure mathematical descriptions of the control systems.

2.5 Dynamics of High-Rise Structures

Modelling the structural system can be viewed as the first step involved in control system design. Flexible high-rise structures, due to their physical characteristics, can be often described as continuous or distributed parameter systems. Such systems have an infinite number of DOF and exact analytical solutions even for the case of the simple flexible beam are impossible to obtain (Cavallo et al., 2010, Rahimi and Nazemizadeh, 2014). Additionally, in terms of control implementation purposes, the infinite number of degrees of freedom can impose severe constraints on the design of controllers (Theodore and Ghosal, 1995). For these reasons, it is useful, advisable and sufficient (Preumont and Seto, 2008, Thorby, 2008, Cavallo et al., 2010) to replace the distributed parameter system by a discrete one.

In the literature three discretisation methods are presented for modelling flexible systems namely; the Lumped Parameter Method (LPM), the Finite Element Method (FEM) and the Assumed Modes Method (AMM). The simplest of the three, the LPM is an approach based on modelling the structural system as lumped masses at each floor location connected by spring and dampers, representing the column's behaviour under dynamic loading. Reviewing the literature shows that this method does not provide a powerful modelling tool when dealing with flexible structures due to its inability to handle the complexity and non-linearity associated with such structures (Rahimi and Nazemizadeh, 2014). The second discretisation method, AMM, makes use of the principle of virtual work or the Lagrange equations for obtaining the approximate solution. The suitability of the AMM for modelling flexible structures with complex cross sectional geometries, similarly to the LPM was deemed objectionable by various researchers (Theodore and Ghosal, 1995, Yousefi-Koma, 1997) and is recommended only for simple structures with uniform geometry. The universal application of the FEM which is based on a discrete approximation of the distributed parameter system by a finite dimensional system governed by a set of ordinary differential equations covers most of the practical tasks in structural dynamics (Thorby, 2008). Once the finite DOF system is constructed from a pure description of its geometric features and structural properties such as stiffness, damping and mass, the eigenproblem can be solved and the dynamic properties (natural frequencies, damping ratios and mode shapes) can be derived in great accuracy.

Whatever the discretisation technique adopted, the accuracy of the analysis can be improved by increasing the number of DOF. The constructed many-degree of freedom system is widely referred in literature as a full-order system (FOS). For control implementation purposes and computational considerations, however, the FOS needs to be further reduced to a smaller number of DOF. The reduced system is referred in literature as a reduced-order system (ROS). Whenever a ROS is used in control design, inevitable errors such as control and observation spillovers and possible instability may be introduced (Balas, 1978, Soong, 1990, Preumont and Seto, 2008). Dealing with spillover with ways such as locating sensors and actuators at the same location (collocated setup) will be examined in subsequent chapters.

An alternative to the three discretisation methods presented above is experimental modal analysis (EMA). Using this technique, the structure is excited with a known force and its response is measured using sensors at specified locations. The time-variant structural response (acceleration, displacement or velocity) and input force are used to construct graphical relationships in the time domain (i.e. acceleration vs. time etc.). These graphical relationships provide useful information to the control engineer, however, their representation in the frequency domain using techniques such as the fast Fourier transform (FFT) allows the computation of the system's frequency response functions (FRFs) which can be then used to determine the dynamic behaviour of the structure under excitations of various frequency components.

Summary points: Distributed parameter systems are not feasible to solve and their infinite number of DOF will impose severe constraints on the design of controllers. ROS are more appropriate but they might give rise to problems such as control and observation spillover and possible instability.

FEM has been shown to outperform AMM and LPM for the case of flexible and complex structural systems. However, attention should be paid when dealing with structures with a high number of DOF particularly when model reduction of the FOS is necessary for control implementation. EMA can be used as an alternative tool to verify experimentally the simulation results as well as a method used for model updating.

2.6 Control System Formulation

In engineering and applied sciences, the behaviour of dynamic systems is captured by sets of differential equations governing their motion. Each engineering discipline, however, formulates these differential equations in a way that facilitates manipulation, analysis and control implementation. Although the detailed analysis of the differential equations provides countless abilities to the control engineer to manipulate the system of interest in great accuracy, such methods become complex and impractical to use when dealing with high-order systems. To counteract the limitations of dealing with the second order differential equation of motion in a structural system, transfer

functions and state space representations are widely used in the control engineering community for system formulation and control implementation.

2.6.1 State Space Formulation

State space representations allow the structural dynamics system which is described by sets of second order differential equations to be decomposed to a set of first order differential equations. This set of first order differential equations will contain unknown variables which are necessary to describe the state of the system at any given time. For the case of a structural system, these states (variables) are typically the displacements and velocities of the system.

Decomposing the second order differential equation to a set of first order differential equations, one can take advantage of the algorithms developed for first order equation solution. For control implementation purposes the state space approach becomes even more important since it is central to the development of modern control theory (Soong, 1990). The adaptability of this approach to computer simulation and computation, its straightforward extension from single input single output (SISO) to multiple input-multiple output (MIMO) systems, from time-invariant to time variant, as well as from low-order to high-order systems are all factors that make this approach attractive to the structural control engineer.

The state space representation of any mechanical system can be derived by considering the second order differential equation governing the motion of any SDOF or MDOF system when it is subjected to a control force, $u(t)$, ground acceleration, $\ddot{x}_g(t)$, and wind excitation, $w(t)$, mathematically expressed as:

$$M\ddot{x}(t) + C\dot{x}(t) + Kx(t) = -Lu(t) - M\ddot{x}_g(t) - Dw(t) \quad (2.18)$$

where $x(t)$ is the $n \times 1$ displacement vector, M, C, K are the $n \times n$ mass, damping and stiffness matrices respectively, n is the number of DOFs, L is the $n \times \alpha$ actuator location matrix, α is the number of actuators, D is the $n \times n$ disturbance matrix. In order to present the dynamic system of Eq.(2.18) in state space, it is important to define the state variables: $X_1 = x$ and $X_2 = \dot{x}$. So that $\dot{X}_1 = \dot{x}$ and $\dot{X}_2 = \ddot{x}$. Therefore, $\dot{X}_1 = X_2 = \dot{x}$. Eq.(2.18) becomes: ((t)

omitted for simplicity)

$$M\dot{X}_2 + CX_2 + KX_1 = -Lu - M\ddot{x}_g - Dw \quad (2.19)$$

$$\dot{X}_1 = X_2 \quad (2.20)$$

Writing Eq.(2.19) and Eq.(2.20) in matrix form:

$$\begin{pmatrix} \dot{X}_1 \\ \dot{X}_2 \end{pmatrix} = \begin{bmatrix} 0 & I \\ -M^{-1}K & -M^{-1}C \end{bmatrix} \begin{pmatrix} X_1 \\ X_2 \end{pmatrix} + \begin{bmatrix} 0 \\ -M^{-1}L \end{bmatrix} (u) + \begin{bmatrix} 0 \\ -D \end{bmatrix} (\ddot{x}_g) + \begin{bmatrix} 0 \\ -M^{-1}D \end{bmatrix} (w) \quad (2.21)$$

where M^{-1} is the inverse mass matrix. Eq.(2.21) can be written in a generalised matrix notation form as:

$$\dot{X} = AX + B_c u + B_e \ddot{x}_g + B_w w \quad (2.22)$$

In which:

$$A = \begin{bmatrix} 0 & I \\ -M^{-1}K & -M^{-1}C \end{bmatrix}, \quad x = \begin{pmatrix} x \\ \dot{x} \end{pmatrix} = \begin{pmatrix} X_1 \\ X_2 \end{pmatrix}, \quad \dot{X} = \begin{pmatrix} \dot{X}_1 \\ \dot{X}_2 \end{pmatrix} \quad (2.23)$$

And,

$$B_c = \begin{bmatrix} 0 \\ -M^{-1}L \end{bmatrix}, \quad B_e = \begin{bmatrix} 0 \\ -D \end{bmatrix}, \quad B_w = \begin{bmatrix} 0 \\ -M^{-1}D \end{bmatrix} \quad (2.24)$$

where I is the $n \times n$ identity matrix and 0 is the compatible null matrix so that $A \in \mathbb{R}^{2n \times 2n}$, $B_c \in \mathbb{R}^{2n \times \alpha}$, $B_e \in \mathbb{R}^{2n \times 1}$, $B_w \in \mathbb{R}^{n \times 1}$. Eq.(2.22) can take the general form of:

$$\dot{X} = AX + BF \quad (2.25)$$

where vector \dot{X} represents the first order change of the state of the system, X contains the displacements and velocities, matrix A contains the system's parameters, B is referred as the locator matrix, indicating where the actuators are acting and vector F contains all internal and external excitations. It is worth noting that in Eq.(2.18) the vectors $\ddot{x}_g(t)$ and $w(t)$ are stochastic in nature, whereas the vector $u(t)$ is determined through optimisation and control. The form of Eq.(2.22) and its generalised form Eq.(2.25) are referred as state-space representation.

Once the nature of the input force and control gains have been established, the control engineer can obtain the information derived from the state space model through the use of the equation:

$$Y = CX + DF \quad (2.26)$$

where, Y is the output vector, C is the output matrix and D is the feedthrough (or feedforward matrix). In cases where the model does not have a direct feedthrough, D can be taken as a null matrix. Eq.(2.26) through manipulation of C and D matrices allows the engineer to observe the output of interest i.e. velocities and/or displacements.

2.6.2 Transfer Function Formulation

Transfer functions are a compact description of the input-output relation in a linear time invariant (LTI) system. They provide a complete representation of the LTI system in the frequency domain. In control design and implementation, transfer function formulations represent a powerful tool because of their ability to easily describe, manipulate and analyse linear feedback systems mathematically through algebraic manipulations of the differential equations governing the system or experimentally through system identification techniques. Decomposing the complex system into smaller and simpler pieces, one can use transfer functions to capture the dynamic behaviour of each component of the feedback loop and then combine them together using block diagrams so as to form the bigger and more complex system (Astrom and Murray, 2012).

Considering the simple case of the undamped oscillator subjected to an arbitrary input of $f(t)$, the equation of motion can be derived as:

$$m\ddot{x}(t) + kx(t) = f(t) \quad (2.27)$$

The impulse response of the system can be found by setting the input, $f(t) = \delta(t)$, where $\delta(t)$ is the Dirac delta function so that:

$$m\ddot{x}(t) + kx(t) = \delta(t) \quad (2.28)$$

The second order differential equation can be transferred in the Laplace domain through the generalised form of the Laplace transform:

$$L = \int_0^{\infty} f(t)e^{-st} dt \quad (2.29)$$

For the simple case of the undamped oscillator Laplace transform tables can be used:

Table 2. A simple Laplace transform table

$f(t)$	$F(s)$
$\delta(t)$	1
$x(t)$	$x(s)$
$\dot{x}(t)$	$sx(s) - x(0)$
$\ddot{x}(t)$	$s^2x(s) - sx(0) - \dot{x}(0)$

Assuming zero initial conditions ($x(0) = \dot{x}(0) = 0$), Eq.(2.28) becomes:

$$ms^2x(s) + kx(s) = 1 \quad (2.30)$$

Rearranging the above equation in terms of the output $x(s)$:

$$x(s) = \frac{1}{ms^2 + k} \quad (2.31)$$

The right hand term of Eq.(2.31) is known as the transfer function of the system (Note for the case of unit impulse input, the impulse response is the same with the transfer function of the system). Once the transfer function of the system is derived, the response of the system to arbitrary inputs can be obtained using simple multiplication of the transfer function and the Laplace transform of the input. For example: Assuming a ramp input of the form $f(t) = u(t) = t$, its Laplace transform can be derived from:

$$L = \int_0^{\infty} te^{-st} dt \quad (2.32)$$

Integrating by parts results:

$$L = \frac{1}{s^2} \quad (2.33)$$

Therefore the response function of the system to a ramp input can be given by a simple multiplication of the transfer function and the Laplace transform of

the input function:

$$x(s) = \left(\frac{1}{ms^2 + k} \right) \frac{1}{s^2} \quad (2.34)$$

The same procedure can be followed to obtain the response of the system to any type of loading condition. It is also noteworthy that transfer functions and Laplace transformations are a powerful tool for engineers, at the absence of which the procedure would be required to be carried out in the time domain. If that was the case, obtaining the response function of the system would involve the convolution integral which can be difficult and computationally inefficient to solve. Finally, it should be kept in mind that if the engineer decides to use state-space formulation for control implementation and then chooses to revert to transfer function formulation, they can easily do so by defining a transfer function $x(s)$ as a function of the state space matrices (Gu et al., 2005):

$$x(s) = C(sI - A)^{-1}B + D \quad (2.35)$$

2.7 Model Order Reduction

In a structural engineering system, it can be realised that the number of possible states grows exponentially with the system's size and the number of elements comprising it. Using state-of-the-art structural mechanics, sophisticated numerical models (such as FEM, which here are regarded as full order systems) can be constructed capturing the behaviour of the continuous system in great accuracy. The need to simplify the numerical simulation of such systems for the purposes of attaining a solution in the most time efficient manner as well as not exceeding the current capabilities of verification tools, requires the adoption of model reduction techniques. The underlying principle of these techniques is to project the original high-dimensional system by a smaller system having similar properties and thus not compromising the accuracy of the simulation.

In structural systems such as high-rise structures and long-span bridges, where there is one dominant dimension a preliminary form of model reduction can take the arrangement of masses concentrated at floor levels linked by

springs and dampers (Casciati and Faravelli, 2014). The system's partial differential equations describing the distributed system can be represented (as shown in earlier sections) using the state space formulation, such that:

$$\dot{X} = AX + BF \quad (2.36)$$

$$Y = CX \quad (2.37)$$

Using the state space representation, further model reduction can be achieved. Doing so the following relationships will be obtained:

$$\dot{X}_R = A_R X_R + B_R F_R \quad (2.38)$$

$$Y_R = C_R X_R \quad (2.39)$$

In which the subscript R accounts for the reduced matrices and vectors. For all model reduction techniques, there is a relationship between the primary degrees of freedom and the secondary (i.e. the one's to be deleted), which can be written in general terms as.

$$\{x_n\} = \begin{Bmatrix} x_b \\ x_a \end{Bmatrix} = [T] \{x_b\} \quad (2.40)$$

In which subscript n denotes all the dof of the system, b denotes the primary dof and a denotes the secondary or omitted dof. The nature of the transformation is defined by the adopted reduction technique. Using one of the most popular techniques, known as static condensation, the global stiffness matrix is partitioned and rearranged such that:

$$\begin{bmatrix} k_{aa} & k_{ab} \\ k_{ba} & k_{bb} \end{bmatrix} \begin{bmatrix} x_a \\ x_b \end{bmatrix} = \begin{bmatrix} F_a \\ F_b \end{bmatrix} \quad (2.41)$$

Multiplying the first matrix equation gives:

$$k_{aa} x_a + k_{ab} x_b = F_a \quad (2.42)$$

Solving for x_a :

$$x_a = k_{aa}^{-1} (F_a - k_{ab} x_b) \quad (2.43)$$

If no force is applied on the secondary dof, $F_a = 0$, Eq.(2.43) becomes:

$$x_a = k_{aa}^{-1} (-k_{ab} x_b) = -k_{aa}^{-1} k_{ab} x_b \quad (2.44)$$

Rewriting the displacement vector in terms of X_b only:

$$x = \begin{bmatrix} x_a \\ x_b \end{bmatrix} = \begin{bmatrix} -k_{aa}^{-1}k_{ab} \\ I \end{bmatrix} x_b = \begin{bmatrix} -k_{aa}^{-1}k_{ab}x_b \\ x_b \end{bmatrix} \quad (2.45)$$

Defining a transformation matrix for brevity:

$$x = \begin{bmatrix} x_a \\ x_b \end{bmatrix} = \begin{bmatrix} -k_{aa}^{-1}k_{ab} \\ I \end{bmatrix} x_b = \begin{bmatrix} T_a \\ x_b \end{bmatrix} x_b = Tx_b \quad (2.46)$$

where,

$$T_{ab} = -k_{aa}^{-1}k_{ab} \quad (2.47)$$

$$T = \begin{bmatrix} T_{ab} \\ I \end{bmatrix} \quad (2.48)$$

Substituting back into the original static equilibrium equation:

$$kx = k(Tx_b) = F \quad (2.49)$$

Multiplying both sides by T^T to reduce the number of dof from $(a+b)$ to b :

$$(T^T k T)x_b = T^T F \quad (2.50)$$

The reduced stiffness matrix can be obtained by expanding the parenthesis such that:

$$k_{bb}^* = T^T k T = \begin{bmatrix} T_{ab}^T & I \end{bmatrix} \begin{bmatrix} k_{aa} & k_{ab} \\ k_{ba} & k_{bb} \end{bmatrix} \begin{bmatrix} T_{ab} \\ I \end{bmatrix} = k_{bb} - k_{ba} k_{aa}^{-1} k_{ab} . \quad (2.51)$$

Summary: This chapter has presented a generalised literature review, progressively capturing the concepts and principles required for structural control implementation. The immediately following chapter presents the specific details of different control algorithm configurations along with the mathematical models to be used in the subsequent chapters of this thesis.

Chapter 3

Control Algorithms

3.1 Background

Even though the principle of control has been intuitively understood since antiquity, the development of controllers based on a well-established theory has more recent origins. The establishment of classical control theory as a result of extensive work carried out during and after the Second World War laid down a rigorous step-by-step approach for solving the control problem. In classical control schemes, the design involved by-and-large single-input single-output (SISO) systems that can be adequately captured by linear, single-variable, time-invariant and low order models. The simplicity and ease of physical implementation of classical control systems makes them the preferred choice in most industrial applications (Kappos, 2002). However, the limitations associated with classical controllers generate the need for development of more advanced ones able to deal with more sophisticated design problems. Such controllers are based on the newly developed modern control theory. In modern control theory, the subsystems comprising the main system can be multivariable, high-order, time-varying and poorly modelled (i.e. systems with large parametric uncertainty) allowing engineers to develop controllers with enhanced performance, stability and less control effort.

In structural vibration control literature both classical and modern feedback controllers are classified in two broad categories: (1) fixed parameter and (2) adaptive controllers. The former category of controllers, as their name suggests, have fixed parameters and control gains during the control stage, while the latter allows for some adaptation or training during control. Fixed parameter controllers are further divided in two subcategories namely: direct-output feedback (DOFB) and model based (MB) controllers. The main difference of the two subcategories of fixed parameter feedback controllers is that the latter one requires an accurate model of the system for determination of precise controller properties (Hudson, 2013). Adaptive controllers are also categorised as MB controllers. However, such MB controllers are modified in order to apply to systems with varying parameters, or systems that are initially

uncertain.

To avoid confusion and further enhance understanding, in this thesis the controllers are only divided in two main categories: fixed parameter and adaptive controllers. In the category of fixed parameter controllers, both DOFB and MB controllers exist, whereas in the category of adaptive controllers only the special case of MB controllers exists. A schematic diagram of control classification is presented in Figure 11.

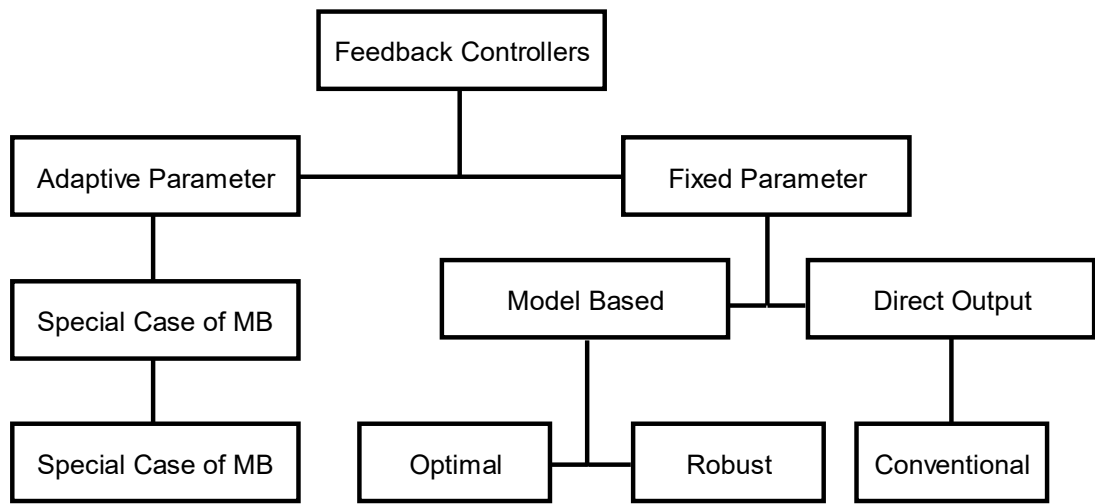


Figure 11. Classification of feedback controllers

3.2 Fixed parameter controllers

In classical single-input-single-output (SISO) systems, satisfactory performance both in terms of disturbance rejection and robust stability can be easily achieved through simply ensuring good gain and phase margins. Various frequency domain techniques for analysis and controller design (such as Bode plots, Root-locus, pole placement etc.) dominate SISO control system theory. Most industrial control systems, however, cannot be captured using the principles of SISO systems (Gu et al., 2005). The inevitable extension of SISO systems to multiple-input-multiple-output (MIMO) systems in the 1960s entailed the development of modern multivariable techniques. Such multivariable techniques are based on linear quadratic performance criteria and Gaussian disturbances. These methods, commonly referred as linear quadratic Gaussian (LQG) methods, which are bounded in the category

of optimal controllers, although being successfully implemented in aerospace applications, they exhibited poor robustness in industrial applications (Gu et al., 2005). In an effort to address the issue of robustness, substantial research has been undertaken for the development of robust controllers. The theory developed based on this concept is the well-known H_∞ optimal control theory. This section presents the most popular fixed parameter algorithms developed to date for the response reduction of structural systems incorporating active and semi-active control devices.

3.2.1 On-off Controllers

On-off controllers are amongst the simplest controllers found in classical control theory. When incorporated in semi-active control systems, such controllers are used to vary the parameters (stiffness or damping) of the auxiliary device between two states (maximum and minimum) so that the vibration response of the system is alleviated. Determination of whether a high state or a low state is required to be achieved by the device depends exclusively on the choice of control algorithm. Most common algorithms incorporated in semi-active control systems are based on skyhook, groundhook and bang-bang control.

3.2.1.1 Skyhook Control

Karnopp and Crosby (1974) in an attempt to reduce the response of vehicles using semi-active suspension systems developed the famous skyhook control scheme, the operational principle of which can be demonstrated through the SDOF semi-actively controlled system shown in Figure 12a. As a first step, the semi-actively controlled system is idealised by the hypothetical system shown in Figure 12b. In a skyhook control scheme, the system's mass is assumed to be "hooked" on a notional damper that is fixed on the "sky". The idea is that the semi-active damper shown in Figure 12a matches the ideal skyhook force of the hypothetical system shown in Figure 12b, however this is true only if both the skyhook and semi-active forces act in the same direction. If they do not act in the same direction, the damper force should be

unconditionally set to a minimum value. The force provided by the skyhook damper, F_{sk} is calculated by:

$$F_{sk} = C_{sk} \dot{V}_1 \quad (3.1)$$

where, C_{sk} is the damping coefficient of the skyhook damper, and \dot{V}_1 is the velocity of the suspended mass. The force that can be provided by the “real” damper is calculated by:

$$F_d = C_{sa} \dot{V}_r \quad (3.2)$$

where, C_{sa} is the damping coefficient of the semi-active damper, and \dot{V}_r is the relative velocity of the suspended mass and the base (i.e. $\dot{V}_1 - \dot{V}_2$). In order for the semi-active damper to emulate the ideal groundhook force, the skyhook force is set equal to the force provided by the semi-active damper, such that:

$$C_{sa} = C_{sk} \frac{\dot{V}_1}{\dot{V}_r} \quad (3.3)$$

By multiplying the damping coefficient, C_{sa} , of the semi-active device by the relative velocity of the masses, the semi-active force, F_{sa} , calculated with respect to the groundhook control law is obtained by:

$$F_{sa} = C_{sk} \frac{\dot{V}_1}{\dot{V}_r} \dot{V}_r = C_{sa} \dot{V}_1 \quad (3.4)$$

According to the system’s motion, the directionality condition of the forces needs to be examined in order to determine whether a high-state (i.e. $F_{sa} = C_{sa} \dot{V}_1$) or a low state (typically zero even though some damping is present in the system) is required. Depending on the motion of the mass and the base, four cases can be identified and damper forces can be calculated accordingly:

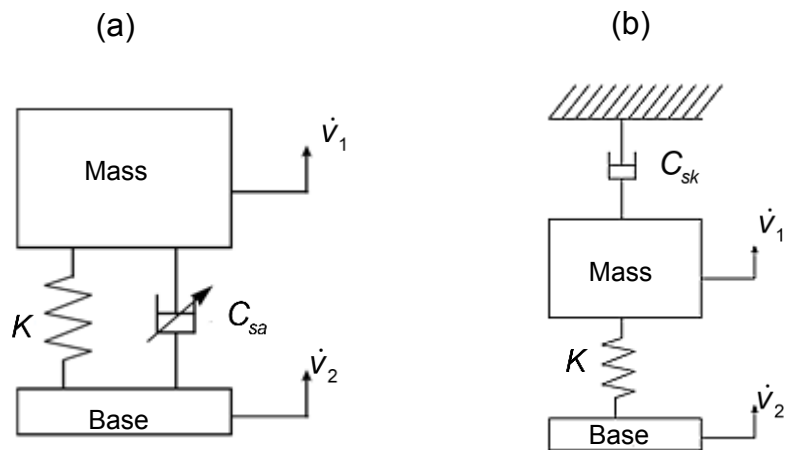


Figure 12. Skyhook control of a variable damping device (a) Semi-active variable damping control model (b) Ideal configurations

- 1) The mass moves away from the base (i.e. $\dot{v}_r > 0$) with a positive velocity (i.e. the mass moves upwards). As it can be observed, the mass moves away from the equilibrium. Since the notional skyhook damper is in compression, the force applied to the suspended mass is in the negative direction. Referring back to the “real” system of Figure 12a, when the system is subjected to the same motion, the non-notional semi-active damper will be put in tension, thus the force, F_d , acting on the suspended mass will still be in the negative direction, thus the force should take the maximum value.
- 2) The mass still moves away from the base (i.e. $\dot{v}_r > 0$) with negative velocity (i.e. the mass moves upwards). In this case, the skyhook force will be applied in the positive direction. On the other hand, the semi-active damper of the real system will remain in tension, thus the semi-active force will be in the negative direction. Since the skyhook and semi-active forces are in opposite directions, the best it can be achieved by the semi-active device is to minimise the damping force, thus a minimum state is required.
- 3) The mass and base are moving towards each other (i.e. $\dot{v}_r < 0$) and the suspended mass has a positive velocity. In this case, the skyhook damper is put in compression thus it subjects the mass to a negative force. On the contrary, the semi-active damper which is also in compression will exert a

positive force. Since the two forces are in opposite direction a minimum (damping) state is required.

4) The mass and base are moving towards each other (i.e. $\dot{v}_r < 0$) and the suspended mass has a negative velocity. In this case, the skyhook damper is put in tension thus it exerts a positive force on the mass and the semi-active damper is put in compression also subjecting the mass to a positive force. Therefore, a high state is required.

Summarising the four cases, the skyhook control algorithm can be directly derived by the product of the velocity of the suspended mass relative to the base, \dot{v}_r , and its velocity, \dot{v}_1 . This can be mathematically expressed as:

$$\dot{v}_1 \dot{v}_r \geq 0 \rightarrow F_{sa} = C_{sa} \dot{v}_1 \quad (3.5)$$

$$\dot{v}_1 \dot{v}_r < 0 \rightarrow F_{sa} = 0 \quad (3.6)$$

3.2.1.2 Groundhook Control

With reference to Figure 12, It can be realised that skyhook control in civil engineering applications could be potentially used to control semi-active damping or stiffness devices such as magnetorheological and electrorheological dampers placed between floors, but would not be of any particular use when a tuned vibration absorber such as a STMD is used for vibration mitigation in structural systems. This is due to the fact that the effort is placed on controlling the mass that the vibration absorber is mounted on (i.e. the base now represents the structural system and the sprung mass the vibration absorber). To overcome this limitation and extend the application of the control scheme to civil structures equipped with STMD devices, Koo et al. (2004) altered the original skyhook controller design. The resulting scheme is known as Groundhook control. This control scheme follows a similar operational principle to skyhook control, however, the latter controller primarily aims to control the sprung mass (i.e. the suspended mass shown in Figure 12a) as opposed to the unsprung mass (i.e. the base of the system shown in the same figure).

Figure 13, illustrates how the semi-active damper emulates the behaviour of an ideal passive damper “hooked” between the ground and the mass to be controlled. Using the same procedure followed for the determination of whether a high-state or a low-state of damping is required in the skyhook scheme, the same four cases depending on the motion of the masses need to be defined. To avoid repetition and enhance clarity, the four cases are summarised in Table 3.

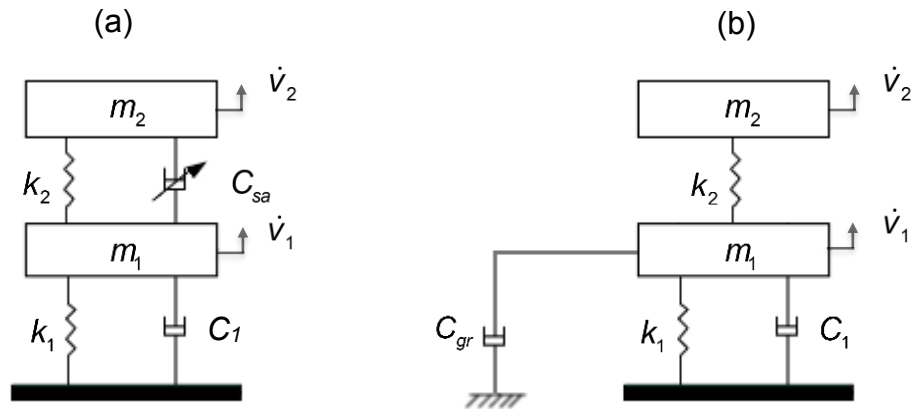


Figure 13. Groundhook control of a variable damping device (a) Semi-active variable damping control model (b) Ideal configuration

Table 3. Groundhook Control Logic

Sign Conventions	Damper Condition	Desired Damping State
$\dot{v}_1 > 0, \dot{v}_r < 0$	Extension	Off
$\dot{v}_1 > 0, \dot{v}_r > 0$	Compression	On
$\dot{v}_1 < 0, \dot{v}_r < 0$	Extension	On
$\dot{v}_1 < 0, \dot{v}_r > 0$	Compression	Off

Note* \dot{v}_r is defined similarly to the skyhook scheme as $\dot{v}_1 - \dot{v}_2$.

Groundhook control can be mathematically expressed by:

$$\dot{v}_1 \dot{v}_r \geq 0 \rightarrow F_{sa} = C_{sa}(t) \dot{v}_1 \quad \therefore C_{sa}(t) = c_{max} \quad (3.7)$$

$$\dot{v}_1 \dot{v}_r < 0 \rightarrow F_{sa} = C_{sa}(t) \dot{v}_1 \quad \therefore C_{sa}(t) = c_{min} \quad (3.8)$$

When the velocity of the unsprung mass, \dot{v}_1 is used for the calculation of the controlling actions (Eq.(3.7) and Eq.(3.8)), the resulting groundhook logic is termed velocity based groundhook (VBG). Alternatively, it is possible to replace the velocity of the unsprung mass by a primary system displacement term, resulting to a displacement based groundhook (DBG) control, mathematically expressed as follows:

$$v_1 \dot{v}_r \geq 0 \rightarrow F_{sa} = C_{sa}(t) \dot{v}_1 \quad \therefore C_{sa}(t) = c_{\max} \quad (3.9)$$

$$v_1 \dot{v}_r < 0 \rightarrow F_{sa} = C_{sa}(t) \dot{v}_1 \quad \therefore C_{sa}(t) = c_{\min} \quad (3.10)$$

Great examples of studies that highlight the performance advantage of both DBG and VBG algorithms over the optimal passive TMD can be found in (Koo et al., 2004, Liedes, 2009, Viet et al., 2014, Ji et al., 2005, Kang et al., 2011). A typical acceleration and displacement frequency response of an STMD controlled structure regulated by these two groundhook controllers is shown in Figure 14a and Figure 14b respectively.

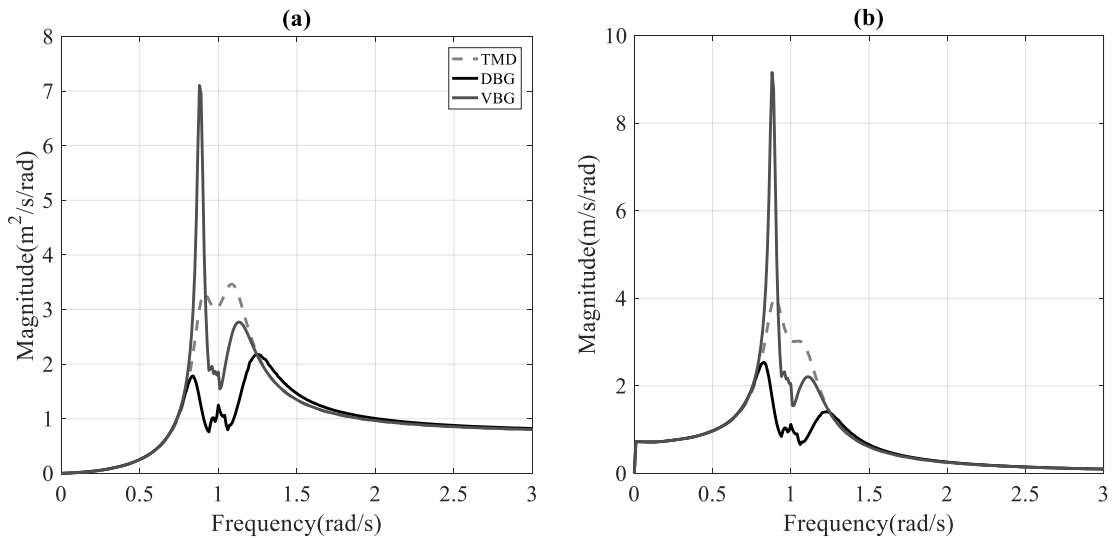


Figure 14. Typical (a) Acceleration response and (b) Displacement response of a groundhook controlled STMD equipped structure

Following the conclusions in the aforementioned studies, as well as the observations made by the author of this thesis (and the findings of Figure 14) it can be evidently said that the performance of the VBG groundhook algorithm is far inferior that its displacement based counterpart. Additionally, it can be observed that the VBG exhibits a poor performance in the low frequency part

(<1 rad/s) of the vibration response. To improve the performance of the arguably under-performing VBG algorithm, Liedes (2009) and Viet et al. (2014) examined the potential of combining the two algorithms to create an improved form of Groundhook control. In the first study, the authors made use of weighting coefficients so as to define how the displacement and velocity signals contribute to the combined signal. The resulting algorithm, termed displacement and velocity based groundhook (DaVBG), was shown to provide better performance and robustness against parameter variations in the system. In the second study, Viet et al. (2014) demonstrated analytically that if they combine three forms of groundhook control, including the DBG, VBG and the inverse of VBG termed IVBG (i.e. max force given when $\dot{v}_1 \dot{v}_r \leq 0$, effectively being a mirror image of the VBG response in the frequency domain), the effectiveness of each algorithm at different frequency ranges can be exploited and enhanced performance can be achieved.

3.2.2 PID controllers

The PID which stands for Proportional-Integral-Derivative controller is one of the most widely used control loop mechanisms in the industry because of its remarkable effectiveness and simplicity of implementation (Astrom & Hagglund 1995, Etedali et al. 2013). Like most classical controllers, the PID calculates the required corrective actions based on the feedback error $e(t) = r(t) - y(t)$. Once the feedback error is calculated, the controller attempts to minimise it (for the next iteration) by appropriately adjusting the inputs $u(t)$ to the plant at each time step in order to bring the output $y(t)$ as close to the reference signal $r(t)$. Using the “textbook” version of the PID controller, the inputs to the plant that minimise the feedback error are calculated by (Astrom and Hagglund, 1995):

$$u(t) = K_p \left(e(t) + \frac{1}{T_i} \int_0^t e(t) dt + T_d \frac{de(t)}{dt} \right) \quad (3.11)$$

where, K_p is the proportional gain, T_i is the integral time and T_d is the derivative time. Using simpler notation, the above equation can be written as:

$$u(t) = K_p e(t) + K_i \int_0^t e(t) dt + K_d \frac{de(t)}{dt} \quad (3.12)$$

In this equation, $K_i = K_p / T_i$ is the integral gain and $K_d = K_p \times T_d$ is the derivative gain. It can be observed from the above expressions that the (plant) input signal $u(t)$ is the summation of three terms: The proportional (P) term

$$K_p e(t) , \text{ the integral (I) term } K_i \int_0^t e(t) dt \text{ and the derivative (D) term } K_d \frac{de(t)}{dt}$$

. It can be also seen from the above relationships, that an accurate model of the plant is not necessary for control implementation in a PID control scheme. This is the main differentiation of conventional DOFB (PID) controllers to other MB controllers. The engineering challenge is to adjust “tune” the control gain K_p, K_i, K_d in such a way that given a feedback error $e(t)$ at any instance in time, the controller outputs will generate desirable plant inputs making it behave in accordance to predefined performance objectives such as rise time, overshoot ,settling time, steady state error etc. Using different tuning methods, the performance of the system in terms of the aforementioned objectives can be compared by subjecting the system to step inputs and examining its transient response as shown in Figure 15.

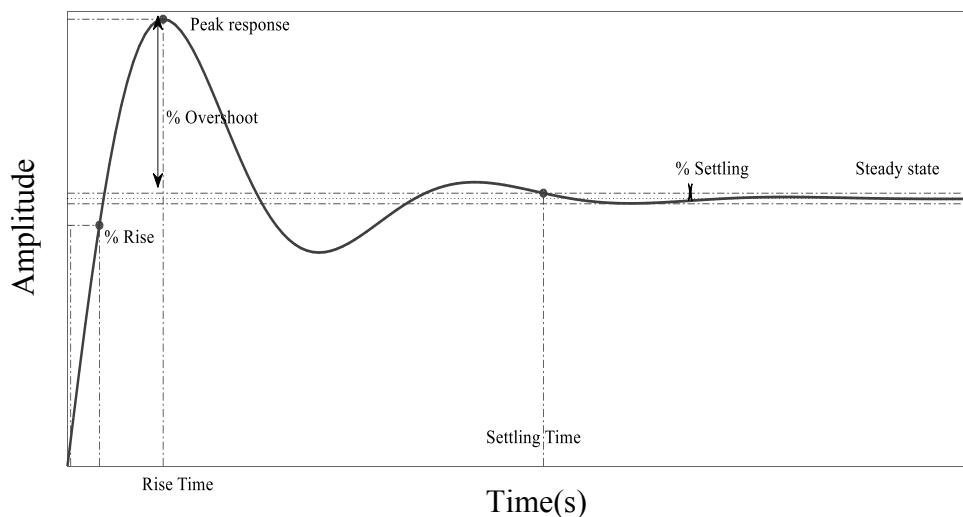


Figure 15. Second order system subjected to step input

Like any other design procedure, PID controller tuning involves trade-offs between performance and robust stability objectives. For example, reducing

the steady state response would require large proportional gains at which instability may be introduced. Therefore, tuning the controller to achieve the aforementioned time domain objectives, robust stability is not necessarily guaranteed. For this reason both time-domain performance and frequency domain robustness should be considered (Tan et al., 2006). The reader is referred to Tan et al. (2006) for a comprehensive comparison of different PID tuning strategies in terms of performance and robustness.

Although PID controllers occupy a big portion of industrial controllers, their use in structural control applications is scarce (Etedali et al., 2013). As a matter of fact, there are only a few studies regarding vibration control of structures using PID controllers, highlighting the fact that MB controllers are preferred in structural control applications (Korkmaz, 2011). This rejection of classical controllers might be primarily attributed to the fact that complex structural systems with uncertain and varying parameters subjected to unknown loading conditions cannot be captured through these schemes (Yang et al., 2006). For these reasons, a number of researchers suggest that robust control methods are offered for achieving the control objective.

Despite the drawbacks of conventional controllers, various studies have been undertaken examining their performance in structural engineering applications. Guclu and Sertbas (2005) examined the performance of a five-DOF structure incorporating ATMD subjected to earthquake excitation. The control actions were determined using a PID controller tuned using the Ziegler-Nichols method. They observed in their numerical analysis no valuable improvement in frequency response, suggesting that since structural systems have uncertainties and their parameters are subject to changes, robust controllers are preferable because of their robust character and applicability to nonlinear systems (Guclu and Sertbas, 2005). They validate their arguments in the same study by comparing the PID controller with a sliding mode controller (SMC) and demonstrated that the latter controller is much more effective.

Later, Guclu and Yazici (2007) examined the performance of a PID controller for vibration suppression of a fifteen-DOF structure using an active isolator. The results show an improved reduction in the displacement response but

only minimal effects on the acceleration responses of the top storey.

Casciati and Chen (2012) developed a PID controller for implementation in a three storey experimental structure incorporating an active mass damper (AMD). The experimental results clearly indicated reduction in top floor accelerations. In another similar study, Boujari et al. (2012) examined the performance of a three-storey structure subjected to four ground acceleration records. The structure was controlled by an ATMD and the control forces were calculated by a PID controller and its modified version – the 2DOF PID. In their numerical simulations, they observed a significant increase in performance both in terms of acceleration and displacement response of the actively controlled structure using both PID controllers. In this numerical study, however, the authors highlight the fact that the values of active control forces might be so high that the realisation of such a scheme might be non-economic. In other words, the machine saturation limits (i.e. the capacity of the hydraulic jack providing the required forces) have not been considered in the analysis. For this reason conclusions cannot be easily drawn in regards to the applicability of PID or 2DOF PID in such structural systems.

In another study, Chen et al. (2012) examined numerically and experimentally the reduction of floor vibrations using a prototype variable stiffness and damping ATMD controlled by a PID controller. The results obtained suggest a significant reduction in floor accelerations.

3.2.3 Riccati Optimal Controllers

The category of optimal controllers includes among others: the famous linear quadratic regulator (LQR) and linear Gaussian regulator (LGR). All these controllers work on the basis of minimising a quadratic performance index J through manipulation and optimisation of the control vector $u(t)$. The performance index J used in structural control applications when working with the state space formulation is defined as (Soong, 1990):

$$J = \int_0^{t_f} [x^T(t)Qx(t) + u^T(t)Ru(t)] dt \quad (3.13)$$

In the above equation, $Q \in \mathbb{R}^{2n \times 2n}$ and $R \in \mathbb{R}^{\alpha \times \alpha}$ are referred as the weighting

matrices relating to the trade-off between control effectiveness and control energy consumption respectively, t_f is the control period of consideration. Manipulating the magnitudes of Q and, R better disturbance rejection can be achieved at the expense of control effort and vice versa. For example, a better disturbance rejection and minimisation of the state error could be achieved by increasing the magnitude of the elements of the Q matrix relative to the R matrix. In contrast, increasing the magnitude of the R relative to the Q matrix would yield smaller control forces thus less control effort as well as reduced disturbance rejection. It is noteworthy that the values of elements of Q and R matrices are selected such as Q is a positive semi-definite matrix and R is a positive definite matrix. Doing so, it is ensured that Eq.(3.13) will never yield a negative result (Hudson, 2013).

As already mentioned, minimising the performance index J is achieved through manipulation and optimisation of the control vector $u(t)$. This control vector $u(t)$, for a closed-loop system comprising an optimal controller is described by:

$$u(t) = G(t)X(t) = -\frac{1}{2}R^{-1}B^T P(t)X(t) \quad (3.14)$$

where $G(t)$ is the control gain and $P(t)$ is the Riccati matrix defined as the matrix that satisfies the algebraic Riccati equation (ARE) which at the absence of an external excitation function is given by:

$$\dot{P}(t) + P(t)A - \frac{1}{2}P(t)BR^{-1}B^T P(t) + A^T P(t) + 2Q = 0 \quad (3.15)$$

Soong (1990) observed that in structural control applications in which the matrices Q and R are weighted arbitrarily, the Riccati matrix remains constant over the control interval, suggesting that $P(t)$ in most cases can be approximated by a constant matrix P without compromising the effectiveness of the control system (Yang et al., 1987, Soong, 1990, Cheng et al., 2008). As a result, Eq. (3.15) reduces to:

$$PA - \frac{1}{2}PBR^{-1}B^T P + A^T P + 2Q = 0 \quad (3.16)$$

The control gain $G(t)$ becomes also a constant matrix described by:

$$G = -\frac{1}{2}R^{-1}B^T P \quad (3.17)$$

Eq.(3.17) indicates that the constant gain G matrix can be precalculated for a structure with given parameters (i.e. A matrix known) and weighting matrices Q and R . It can be also observed that Eq.(3.13)-(3.17) are coupled and it can be realised that obtaining the optimal performance through the selection of appropriate control gains, can be achieved through iterations. Substituting Eq.(3.14) back in the state space formulation of the second order systems (Eq.(2.22)), the behaviour of the optimally controlled structure and the subsequent closed-loop system is described by:

$$\dot{X} = (A + B_c G)X + B_e \ddot{x}_g + B_w w \quad (3.18)$$

In this equation, the closed-loop plant matrix is defined as $A_c = A + B_c G$ and its eigenvalues define the closed-loop modal damping and natural frequencies. Throughout the years, the potential of optimal control has been explored by many researchers who through modifications of the basic algorithm aim to improve control performance by incorporating in the algorithm various factors such as non-linearity, external excitation, time delay etc. All of the developed algorithms, however, work on the same basic principle of optimal control.

3.2.3.1 Optimal and suboptimal Bang-Bang control

Similarly to optimal controllers, the objective of bang-bang control is to minimise a quadratic performance index of Eq.(3.13) (Wu and Soong, 1996). According to the Pontryagin Maximum Principle, the optimal control action is obtained by:

$$u(t) = -u_{\max} \operatorname{sgn}[B^T \lambda(t)] \quad (3.19)$$

where $\lambda(t)$ is the costate vector obtained by solving:

$$\dot{\lambda}(t) = -A^T \lambda(t) - Qx(t) \quad (3.20)$$

It is worth noting, that the optimal control action, is of bang-bang nature, i.e. it moves from a maximum to a minimum value when $B^T \lambda(t)$ changes sign. It is also easy to realise that obtaining the control actions, one needs to solve

online the differential equation ($\lambda(t)$) which will most likely increase the delays in the system and potentially degrade its performance. Alternatively, the control actions can be obtained by minimising the time derivative of a Lyapunov function of the system. Firstly a quadratic function of the state variable is defined as:

$$V(x) = x^T S x \quad (3.21)$$

where S is the solution of the Lyapunov matrix equation:

$$A^T S + S A = -Q \quad (3.22)$$

Once the solution to the Lyapunov matrix is found, the control actions can be then calculated from:

$$u(t) = -u_{\max} \text{sgn}[B^T S x(t)] \quad (3.23)$$

The law used in Eq.(3.23) for the calculation of the control action is called suboptimal bang-bang control. It is evident that using this approach no on-line evaluation of the differential Eq.(3.20) is required.

3.2.4 Pole Placement Algorithms

Pole placement algorithms also commonly referred to as pole assignment methods are amongst the most traditional algorithms found in modern control theory (Cheng et al., 2008) . Such algorithms perform on the simple basis of altering the eigenvalues of the system in such a way that either its damping capacity is increased or its frequencies move out of the resonant range.

As discussed in the previous sections, the plant matrix A captures the open-loop system dynamics. In the closed-loop system, however, the plant matrix A which initially contained all the modal characteristics of the structural system (i.e. damping ratios and frequencies) is now modified and takes the form of $A_c = A + B_c G$. The fact that the eigenvalues of A_c are different from those of A raises the question whether the selection of an appropriate feedback gain matrix G can give the closed-looped system matrix A_c prescribed eigenvalues (or poles as commonly referred in the control community) which will in turn yield desirable modal damping ratios and frequencies. The algorithms developed to achieve this objective are known as pole placement algorithms

and have been widely accepted and extensively used for many years in the mechanical and electrical engineering fields (Cheng et al., 2008).

In the structural engineering field, these algorithms can be very promising and convenient because of the fact that conventional engineering structures have only a few significant modes of vibration (Cheng et al., 2008). This suggests that the closed-loop eigenvalues can be easily selected for achieving the control objective. On the other hand, it is important to note that pole placement methods would not be acceptable in cases where high-order structural systems excited in more than the first few modes are considered (Soong, 1990, Datta, 2003). An additional important prerequisite of this technique is that the system is fully controllable (i.e. available force is sufficient to bring the system from any initial state to any desirable state). Lastly such controllers require trial and error for tuning while at the same time there is no measure of how close the performance is to optimal (Hudson, 2013) in which case optimal controllers might be the preferred option. For the aforementioned reasons, particular care should be taken when using the pole assignment method since it can be cumbersome for complex structures comprising many degrees-of-freedom (Yang et al., 1987).

Chang and Yu (1997) examined the performance of two structures, the first modelled as a SDOF subjected to a white noise ground excitation and the second one modelled as an eight-DOF structure subjected to the South-East component of the El-Centro earthquake of 1940. The selected control devices were an active mass driver and an active tendon system. The numerical simulations suggested that the pole placement technique can be successfully applied for mitigating the structural response due to earthquake excitation.

In another study, Pan et al. (2011) designed a universal pole placement controller for structures with known frequencies, damping ratios and mode shapes. The performance of the controller was evaluated by simulation using the dynamic model of a flat steel plate estimated from experimental data. Beyond the reduction in vibration, the authors also highlighted some issues/observations arising from the use of this technique:

1. An accurate model of the structure is required for the implementation of this method.

2. The selection of pole locations is a compromise between the speed of the response of the error vector and the sensitivity to disturbance and measurement noises.

3. A large control effort might be required in high-order problems. If the effort is too large, actuator saturation might occur which may lead to undesirable performance and even instability.

More recently, Rahman and Darus (2012) examined the response reduction of a flexible plate stabilised by a feedback controller using the pole placement method. They observed that pole placement algorithms have the ability of ensuring the stability of the system while at the same time alleviate its vibration response. Other studies including those of (Manning et al., 2000, Bu et al., 2003, Pan et al., 2011) successfully implemented pole placement control for controlling the first dominant modes of flexible beams.

3.2.5 Instantaneous optimal control:

From the above presented relationships it can be observed that the optimisation procedure performed for the derivation of appropriate control gain matrices does not take into account the external excitation component (see Eq.(3.15). It is therefore arguable that the control Riccati closed-loop algorithm (i.e. Procedure described in Eq.(3.16)-(3.17) is not truly optimal (Datta, 2003). As a matter of fact, most of the optimal control algorithms are not optimal in this sense since the external excitation is not known a priori. Yang et al. (1987) developed a “truly” optimal control algorithm named Instantaneous Optimal Control (IOC) which incorporates the earthquake excitation component as sensor acceleration measurements at any particular time interval. This algorithm, however, was demonstrated numerically (in the same study) and experimentally (Yang et al., 1987, Soong, 1988) to be only slightly more effective than the traditional Riccati closed-loop controller. On the other hand, the authors highlight the fact that unlike the Riccati control procedure, which requires a full structural parametric knowledge for the solution of the Riccati matrix, instantaneous control is independent of the uncertainty in structural identification.

3.2.6 Robust Controllers/ The H_2 and H_∞ compensator

As the name suggests, these control laws account for some degree of uncertainty in the plant and/or the external perturbation. Being able to deal with uncertainty, signifies the importance of such controllers in the civil engineering domain, in which both an accurate dynamic model of the plant is not always available, and also the external perturbation is stochastic in nature (Stavroulakis et al., 2006). In this field, the work of Zames (1981) entailed the development of two key controllers, namely, the H_2 and H_∞ which are predominantly based in the frequency domain (Gu et al., 2005). Such controllers aim to minimise the rms power of the error signal from a generalised plant as shown in Eq.(3.24) (Suhardjo et al., 1992) :

$$\|F_{wz}\|_2 \triangleq \left(\frac{1}{2\pi} \int_{-\infty}^{\infty} \text{trace} \left[F_{wz}(j\omega) F_{wz}(j\omega)^* \right] d\omega \right)^{1/2} \quad (3.24)$$

where F_{wz} is the transfer function between the exogenous signals, w , and the error signals, z . $(.)^*$ denotes the complex conjugate transpose of $(.)$. It is noteworthy, that it is possible to formulate a Riccati optimal controller from the generalised H_2 formulation by appropriately defining the error and the input signal (Skogestad and Postlethwaite, 2005, Montazeri et al., 2009).

3.3 Adaptive controllers

For the cases for which the uncertainty in the structural system and/or the external perturbation is so great that a fixed parameter controller cannot achieve the desired performance, an adaptive parameter controller might be more appropriate (Casciati et al., 2012). Adaptive controllers are often based on a fixed controller design in which a mechanism is added so as to evaluate and adjust controller parameters. The mechanism is thus designed to employ a real time evaluation of the controller's performance based on a predefined performance index and a mode through which the controller's parameters are adjusted (Housner et al., 1997). This adjustability mechanism, can either measure directly the error between the measured and desired outputs and update control parameters, or indirectly via updating the model of the uncertain structure and base the new controller parameters on this new model

(Housner et al., 1997). Regardless the approach, the control objective is to find a control force that satisfies:

$$\lim_{t \rightarrow \infty} [x(t) - x_m(t)] = \lim_{t \rightarrow \infty} [e(t)] = 0 \quad (3.25)$$

In which, $x(t)$ and $x_m(t)$ are the measured and desired (model) outputs respectively. Two of the most widely, used methods of adaptive control that can use both direct and indirect approaches are model-reference adaptive (MRAC) and self-tuning controllers (STC). In the latter category of adaptive controllers, an on-line plant parameter estimator is added in the control loop for simultaneous parameter identification. The controller parameters are then computed from the estimates of the plant parameters as if they were the true ones. In the former category, MRAC control synthesis entails the choice of adaptive laws (on-line parameter updates) such that the time-derivative of the Lyapunov function decreases along the error dynamics trajectories.

Another category of adaptive controllers identifies the frequency bands for which different control algorithms (or tuning of a particular algorithm) work better than an alternative one. Using short-time Fourier transformations the operating frequency can be thus obtained in real time, and an appropriate predesigned algorithm can be selected. A great example of an adaptive controller based on a series of fixed semi-active control laws is found in the study of Viet et al. (2014). In this study, the authors examined the potential of combining three versions of the groundhook controller (DBG, VBG and inverse VBG (IVBG) in a single mixed-groundhook control. This adaptive controller, exploits the effectiveness of each individual controller at different frequency response ranges.

Summary: Having presented, the principles of structural active and semi-active control and the mathematical models associated with different control algorithm configurations, the next chapter focuses on the first objective of the thesis.

Chapter 4

Control System Design-Influence of the control algorithm

This chapter introduces a novel and more ‘transparent’ approach for the selection and use of control algorithms that significantly influence the performance of systems equipped with STMD devices of variable damping. To this end, both a SDOF system excited using mono-harmonic loading and a benchmark high-rise structure subjected to wind excitation are used in the investigation. It has been demonstrated that when realistic constraints are taken into account the algorithms that increase significantly the performance of the controlled structure do so at the expense of damper strokes. When the maximum damper strokes are capped to progressively lower limits, the efficacy of different algorithms, measured through a number of performance objectives, drastically alters, totally changing the performance ranking of them and pointing out the need for an extensive study of the interplay between loading, control algorithm and allowable stroke within the design of semi-active tuned mass dampers devices. The contents of this chapter are an adapted form of the conference papers presented in the 6th International Conference of Structural Control and the 8th International Conference on the Behaviour of Steel Structures, and finally a journal paper published in the Journal of The structural Design of Tall and Special Buildings. Details of these papers are as follows:

Demetriou, D. et al. 2014. Performance of Proportional-Integral-Derivative Controlled Variable Damping Tuned Mass Dampers. In: *6th International Conference of Structural Control, 15-17 July, Barcelona, Spain*.

Demetriou, D. et al. 2015. Performance of Fixed-Parameter Control Algorithms on High-Rise Structures Equipped With Semi-Active Tuned Mass Dampers. In: *8th International Conference on the Behavior of Steel Structures in Seismic Areas, July 1-3, Shanghai, China*.

Demetriou, D. et al. 2016. Performance of fixed-parameter control algorithms on high-rise structures equipped with semi-active tuned mass dampers. *The Structural Design of Tall and Special Buildings*. **25**(7), pp.340-354.

4.1 Introduction

Since the introduction of the dynamic vibration absorber (DVA) to the engineering community by Frahm in 1911 (Frahm, 1911), a large number of studies have been published validating the applicability and effectiveness of passive TMDs on high-rise and slender structures (Kawaguchi et al., 1992, Xu et al., 1992, Cao et al., 1997, Liu et al., 2008, Casciati and Giuliano, 2009, Sadek and Mohraz, 1998). In an attempt to improve further the effectiveness and flexibility of the device, researchers across the world have successfully altered the original design by incorporating sophisticated passive, semi-active and active elements. While the approach of upgrading the performance of the TMD using enhanced and innovative passive elements is reasonable from a technological, practical and economical perspective (Pinkaew and Fujino, 2001, Marian and Giaralis, 2014), this might not be always the case for semi-active and active control of structures because of the costs associated with the requirement of expensive actuators and specialised control components (such as electrorheological and magnetorheological dampers), which can be considered prohibitive for use on structural applications (Casciati et al., 2012). Due to such limitations, over the years an attempt has been made to improve the performance of actively and semi-actively controlled systems via the relatively easier design and selection of appropriate control algorithms, suitable for implementation in full-scale civil structures.

In literature, most of the algorithms adopted for use on STMD equipped structures are based on finding optimal control forces through the minimisation of some cost function or performance index such as in the case of the linear quadratic regulator (LQR) and linear quadratic Gaussian (H_2 /LQG) control. Hrovat et al. (1983), were the first to suggest the use of variable damping dynamic absorbers on civil structures. They proposed an optimal control method for reducing the wind induced vibration of a model two degree of freedom structure, demonstrating the superiority of the proposed system over a relevant traditional passive. Later, on a similar study Pinkaew and Fujino (2001) demonstrated the gains of the LQR controlled STMD variable damping device on reducing the response of structures under harmonic excitations. They reported substantial improvements on the steady-state response of the

structure around the tuning frequency but only minor gains for the transient component of the vibration. Over the same years, another class of optimal control laws, the so-called “bang-bang” control method has been investigated. Wu and Soong (1996), and Jansen and Dyke (2000) investigated the performance of optimal and suboptimal bang-bang controllers on semi-actively controlled structures comparing their effectiveness against other algorithms on the benchmark of earthquake excited structures. Later, Koo et al. (2004) developed a semi-active control algorithm, termed “groundhook control” for use on STMD variable damping devices. This algorithm was developed as an extension to the “skyhook control” algorithm proposed by Karnopp and Crosby (1974) for use on vehicle suspension systems. The flexibility of the former lies on its simplicity of implementation, its computational efficacy and its demand for only two sensors in order to achieve the calculation of control actions. Validating the effectiveness of the groundhook control scheme, Kang et al. (2011) examined the performance of different semi-active device configurations on wind excited tall structures, demonstrating that (displacement based) groundhook controlled STMD devices can substantially reduce the response of the structure when compared to passive TMD solutions. These authors also observed that using an optimally tuned displacement based groundhook (DBG) controller, the predefined stroke limitations could not be satisfied, thus an additional passive damper was required for satisfying the stroke limitations. Most recently, Demetriou et al. (2014) demonstrated that PID controllers can also be tailored for use on VD-STMD equipped structures subjected to earthquake excitations and outlined the benefits from the use of such a control strategy.

Even though all the quoted studies inarguably drew conclusions on the enhanced performance of the STMD equipped system over its conventional passive analogue, it is evident that the once small and meaningless damper strokes (i.e. not being translated to practical applicable values) arising either due to the nature of the external perturbations (harmonic, white noise or short earthquake) and the system’s geometric and dynamic properties (low-rise and high-frequency structures) cannot be overlooked when it comes to high-rise structures subjected to long term wind actions. For these reasons, no truly conclusive argument can be made regarding the relative performance of 1)

STMD over TMD equipped structures and 2) the gains arising from different algorithms on high-rise structures equipped with STMD variable damping devices; particularly when the main performance limiting factor is the stroke of the damper this evidently needs to be taken into account for reaching any performance verdict.

Adding to the aforementioned arguments, in the studies referenced above, the design of the control system (i.e. both the control algorithms and control device/actuator) is based on the assumption that all the components behave linearly. However, for real structures equipped with dynamic vibration absorbers (DVAs) this is not always the case. Even though the structure to be controlled is assumed to be linear, in other words its mechanical characteristics remain unaltered in time, the control device will inflict non-linearity as a result of the device's force and stroke saturation limits (Rohlfing et al., 2011b). In this regard, force saturation occurs when the current in the coil exceeds the allowable limits, whilst stroke saturation occurs when the movement of the DVA's mass exceeds the allowable displacement, which in practice will cause the device to hit the stops on either side of the static component of the actuator, which in turn can impart destabilising impulses into the structure and even permanently damage the actuator (Rohlfing et al., 2011a). It is noteworthy, that stroke saturation is generally only a problem at low frequencies because of the large displacements required in order to generate forces at these frequencies (Hudson, 2013). Consequently, for the case of low frequency high-rise structures for which the DVA is an attractive control option, stroke saturation needs to be taken to account in every step of the control design process.

Typical measures taken to avoid saturation and its non-linear adverse effects on the performance of control systems, involve the use of command limiters and high pass filters (Hudson, 2013). Using a command limiter, the maximum force that can be generated by the actuator(s) is limited by capping the voltage to the device, whereas the high pass filter is used to remove the low frequency components from the command signal (i.e. the signal used as the controller input). Obviously, removing the low frequency components of the command signal reduces the controllers ability to affect the first (lower) modes of vibrations (which arguably are the most important to control for the case of

high-rise structures). For these reasons, this thesis negates the use of high pass filters and additional passive damping that degrade performance and add to the life-time cost of the control system, through a novel approach for limiting actuators strokes based on the selection of appropriate algorithms.

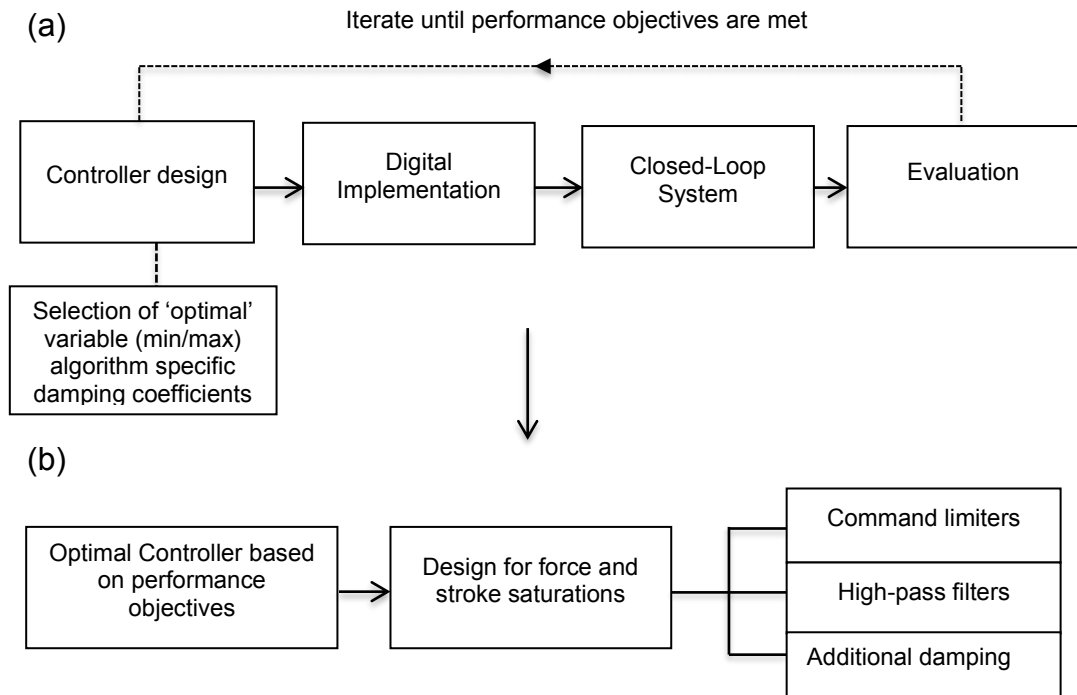


Figure 16. Conventional 2-step control design approach for a) Selecting appropriate control algorithm and (b) accounting for force and stroke saturation

With reference to Figure 16, the control design procedure requires the selection of (any) active/semi-active control algorithm, followed by iterative analyses that would aid the selection of damping (min/max) coefficients, based solely on the predetermined performance objectives, that typically involve (as in the case of the aforementioned studies) minimisation of the structural response quantities (acceleration and/or displacement). If no stroke saturations are taken into account, a comparison of different control algorithms based exclusively on the structural response quantities can be considered fair. Still, for the case of low frequency, high-rise structures equipped with DVAs stroke saturations cannot be overlooked. For this reason, in the second step of the control design procedure (Figure 16b), the designer takes into account stroke saturation limits based on one of the two performance degrading methods described earlier (additional damping and

high pass filtering). For example, the iterative process of Figure 16a, suggested that the best algorithm for a particular structural system is the DBG with variable max-min damping coefficients 30 Ns/m and 1Ns/m respectively. At this configuration the resulting damper stroke at a particular excitation time history exceeds the assumed allowable limit of 80cm. Therefore, the designer caps the stroke by either increasing the max and/or min damping coefficients until the stroke of the damper satisfies the limit. Generally speaking, the more the deviation of the max/min damping coefficients from the optimal damping coefficients (30Ns/m and 1Ns/m for this example) the more the performance degrades. Alternatively, a high pass filter could be employed, rendering the control system 'unresponsive' to the low frequency components of the vibration, defeating the purpose of using a DVA as a control device.

This thesis exploits the potential of making stroke limits an integral part of the performance objectives, through which the selection of variable damping coefficients at different stroke saturation limits is achieved. In other words, each given control algorithm is optimised (damping coefficient wise) at different stroke saturation limits. Therefore, depending on the stroke saturation required, the control algorithm of choice will always have optimal max/min damping coefficients. Consequently, there might be a case that what was traditionally considered to be the most 'effective' control algorithm for controlling the response of STMD equipped structures under wind vibration, underperform at lower stroke saturation limits.

Naturally in this study, the effectiveness of a variable damping STMD device on alleviating dynamic response of both a simplified SDOF system and a benchmark high-rise structure is investigated and the relative performance of five of the most popular fixed parameter feedback algorithms, namely the groundhook (DBG and VBG), clipped optimal, bang-bang (BANG), and PID controls, is reassessed. The dynamic input takes the form of a wind buffeting type load, always of interest to high-rise buildings. Discussions on both quantitative and qualitative gains arising from the use of each control algorithm are sought, while at the same time the fairness of all comparisons is explicitly preserved. As a novel feature, the possibility of switching to an appropriate algorithm for improving performance at the expense of low damper strokes is exploited in an attempt to avoid performance deterioration,

and cost due to the addition of an auxiliary damper when limited strokes are imposed.

4.2 Numerical investigation

The steps followed in the construction of the numerical simulation model and its evaluation at different algorithm and control devices configurations are presented. For clarity, each of the steps involved in the design procedure is described in the following subsection as illustrated in the flow chart of Figure 17. Clearly, for the case of passive control, there is no need for sensors and computer controllers, therefore the design procedure is limited to the bottom half of the diagram (below red dotted line). Whereas, for the case of semi-active control, the arrangement of sensors and the choice of appropriate control algorithms is an integral part of the design process.

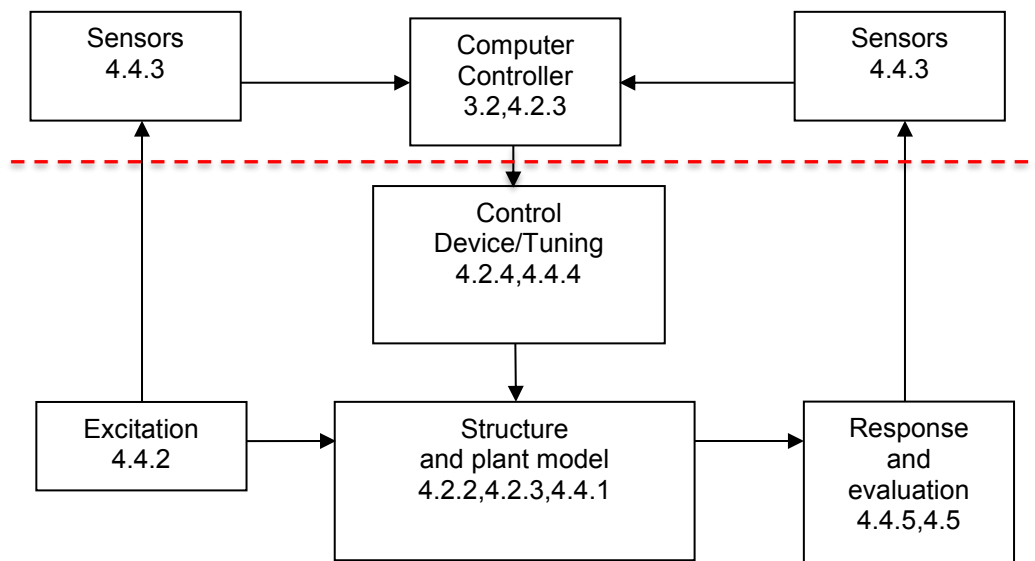


Figure 17. Control system design procedure

As a first step, the investigation initiates with the analysis of a SDOF system coupled with an optimally designed passive (TMD) and semi-active (STMD) dynamic vibration absorber. From this, the frequency response functions of the resulting systems are examined at different mass and stiffness uncertainty ratios. Following this, the analysis extends to a 76-storey high-rise structure on which practical constraints such force, stroke as well as DVA mass constraints been taken to account.

4.2.1 Frequency domain analysis of simplified SDOF system

In order to enhance the understanding on the design and optimisation of different algorithms, as well as aiding the establishment of fair criteria for the comparison of the different control algorithm configurations, this section of the thesis initiates with the investigation of the response of an equivalent SDOF system in the frequency domain. In this regard, a series of sinusoidal waves have been used as external input until the system reached steady state response. Arguably for non-linear systems the response magnification factor may depend on the type and magnitude of the excitation and the resulting structural response might be of random non-periodic nature. Yet, following the proof of Hac and Youn (Hac and Youn, 1992, Pinkaew and Fujino, 2001), the response of piecewise linear second order systems (such as the ones presented herein) to periodic excitation, is also periodic and the amplitude ratio is independent of the excitation amplitude. In other words, exciting the structure using a periodic wave of notional amplitude allows for meaningful performance information in the frequency domain for such piecewise linear systems.

4.2.2 Description of the SDOF and 2DOF (DVA equipped) system

The SDOF system has a mass of 1000 Kg and stiffness of 1000 N/m. When coupled with a DVA designed using Den Hartog's equations (Eq.(4.1)) (Hartog, 1956) for optimal TMD design, the resulting system attains an additional DOF (2DOF system) and is described by the matrices shown in Eq.(4.2).

$$a_p = \frac{1}{1 + \mu}, \quad \zeta_{opt} = \sqrt{(3\mu/8)/(1 + \mu)} \quad (4.1)$$

In which a_p and ζ_{opt} is the optimal stiffness tuning and damping ratio for mass ratio $\mu = m_d / m$ respectively.

$$M = \begin{bmatrix} m & 0 \\ 0 & m_d \end{bmatrix}, \quad K = \begin{bmatrix} k_s + k_d & -k_d \\ -k_d & k_d \end{bmatrix}, \quad C = \begin{bmatrix} c_s + c_d & -c_d \\ -c_d & c_d \end{bmatrix} \quad (4.2)$$

In Eq.(4.2), k_s and C_s is the spring stiffness and damping coefficient of the SDOF respectively. The optimum values of damper stiffness k_d and damping coefficient C_d of the auxiliary damper are calculated by:

$$k_d = a_p \omega_n^2 m \quad (4.3)$$

$$C_d = 2\zeta_{opt} m \omega_n \quad (4.4)$$

4.2.3 Development of models/ state space representation

Having already obtained the mechanical properties (M , C , K) of the system, the next step is to incorporate (mathematically) a semi-active DVA. In order to do so, consider the dynamic behaviour of a generic, linear, controlled building structure modelled as a sway n -degree-of-freedom lumped mass system when subjected to an arbitrary disturbance through its matrix equation of motion:

$$M\ddot{x}(t) + C\dot{x}(t) + Kx(t) = Bu(t) + Dd(t) \quad (4.5)$$

where $x(t)$ and $d(t)$ are in order the displacement, and external force n -element vectors; $u(t)$ is a single scalar control force (for the case of a single DVA) calculated using an appropriate control algorithm, and B and D are the $n \times 1$ influence matrices assigning the control and external force contributions respectively to the individual DOFs. For each DOF in $x(t)$ being the displacement of the i^{th} ($i = 1, \dots, n$) mass, M trivially becomes diagonal, while for the specific viscous damping considered the damping matrix C is assumed to have a form identical to the symmetric stiffness matrix K (i.e. classical damping approach). Without loss of generality, the system considered is equipped with a mass damper system attached to its $(n-1)^{th}$ DOF, with the devices motion variable constituting the n^{th} DOF. Adopting a state-space formulation, Eq.(4.5) becomes:

$$\dot{z}(t) = Az(t) + Fu(t) + Ed(t) \quad (4.6)$$

where, $\dot{z}(t)$ represents the first order time-change of the states $z(t) (= [x(t) \ \dot{x}(t)]^T)$ of the system, A is the system block matrix containing

the system's mass, damping, stiffness properties, F is the control force locator block matrix, and E is the external perturbation locator block matrix, such that

$$A = \begin{bmatrix} 0 & I \\ -M^{-1}K & -M^{-1}C \end{bmatrix}, \quad F = \begin{bmatrix} 0 \\ M^{-1}B \end{bmatrix}, \quad E = \begin{bmatrix} 0 \\ M^{-1}D \end{bmatrix} \quad (4.7)$$

with I being the identity matrix of appropriate dimensions (i.e. $n \times n$). Unlike a conventional passive TMD equipped system that produces an unregulated control force as a result of the relative motion ($\dot{x}_r(t)$, $x_r(t)$) of its mass against its supports (i.e. between the n^{th} and $(n-1)^{\text{th}}$ DOFs) such that,

$$u(t) = k_p x_r(t) + c_p \dot{x}_r(t) \quad (4.8)$$

where, c_p and k_p is the passive damping and stiffness coefficients of the TMD; a VD-STMD can be modulated damping-wise between two values, referred to as passive maximum (c_{max}) and passive minimum (c_{min}) as depicted in Figure 18. By employing a chosen control algorithm, the calculation of the appropriate maximum and minimum damping coefficients either directly or through the calculation of a desired active force $u_a(t)$, one allows for enhanced overall energy dissipation capacity for the damper and improved performance of the vibration control system.

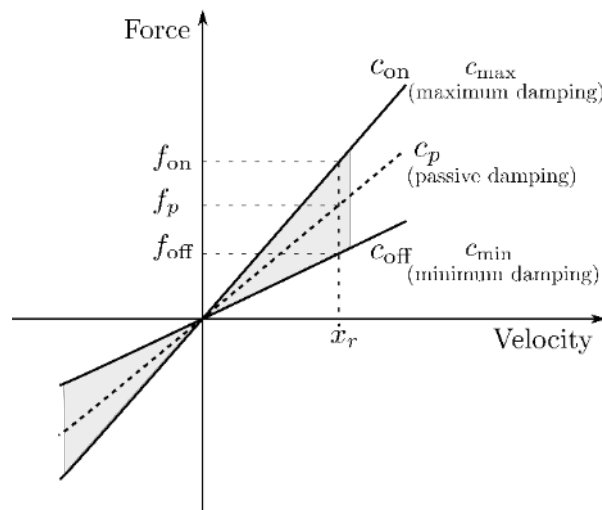


Figure 18. Force-velocity relationship for the performance bands of a variable damping device

For the cases where a purely active algorithm such as the LQR or the PID is used for the calculation of c_{\max} and c_{\min} , the desired active force $u_a(t)$ needs to be calculated and tailored to an equivalent semi-active force which can be physically realisable by the device. To this respect, because a semi-active device can, by definition, only consume energy, functioning criteria need to be applied on the active control force. Namely the semi-active force $u_{sa}(t)$ is calculated by:

$$u_{sa}(t) = u_a(t) \left(\frac{1 - \text{sgn}[u_a(t)\dot{x}_r(t)]}{2} \right) \quad (4.9)$$

$$\text{sgn}[u_a(t)\dot{x}_r(t)] = \text{sgn}(q_a) = \begin{cases} 1 & \text{for } q_a \leq 0 \\ -1 & \text{for } q_a > 0 \end{cases} \quad (4.10)$$

From this, the relevant power “dissipation” of the semi-active device q_{sa} can be calculated by:

$$q_{sa} = u_{sa}(t)\dot{x}_r(t) < 0 \quad (4.11)$$

where, the negative sign is only indicating the flow of energy from the structure to the semi-active control device. Having obtained the physically attainable semi-active force, the time-varying semi-active damping coefficient $c_{sa}(t)$ can be directly calculated as:

$$c_{sa}(t) = \left| \frac{u_{sa}(t)}{\dot{x}_r(t)} \right|, \text{ where } c_{\min} \leq c_{sa}(t) \leq c_{\max} \quad (4.12)$$

4.2.4 Optimisation of algorithms/PID Gains and LQR control effort

A numerical response optimisation procedure based on Nelder-Mead simplex search algorithm (Nelder and Mead, 1965) is followed for deriving the controller parameters (such as gains and control effort matrices r for the cases of PID and full state feedback LQR control respectively). Similarly to Den Hartog’s optimisation approach for the passive DVA design, in this thesis, the optimisation is based on reducing the rms acceleration response of the structure in the frequency band of interest. To this end, the less the area under

the acceleration response curve, the lower the rms acceleration over the frequency band of interest.

4.2.4.1 Full state feedback controllers, LQR.

With reference to Figure 19, It is evident, that decreasing the magnitude of the scalar quantity r (weighting variable of the controller effort) and hence increasing the controller effort, the performance of the LQR controlled semi-active system drastically improves. This is illustrated by the reduced magnitude of both the displacement and acceleration response quantities. It is also noteworthy that with increased effort, the relative phase of the two masses approaches the optimal 90 degree phase difference. In order to maintain the fairness of the comparison between the different control algorithm configured semi-active systems, the controller parameters that achieve lower response at the frequency range of interest are selected.

As already mentioned, lower response over the wider range of frequencies is indicated by the area under the response curves. In this regard, Figure 19e and Figure 20e demonstrate how the area under the acceleration response curve is progressively reduced with increased controller effort, to a point that no more response can be alleviated. Therefore, with reference to Figure 20e the optimum performance (always with respect to rms acceleration response) is achieved when the control effort quantity r attains a value between 0.0025-0.006.

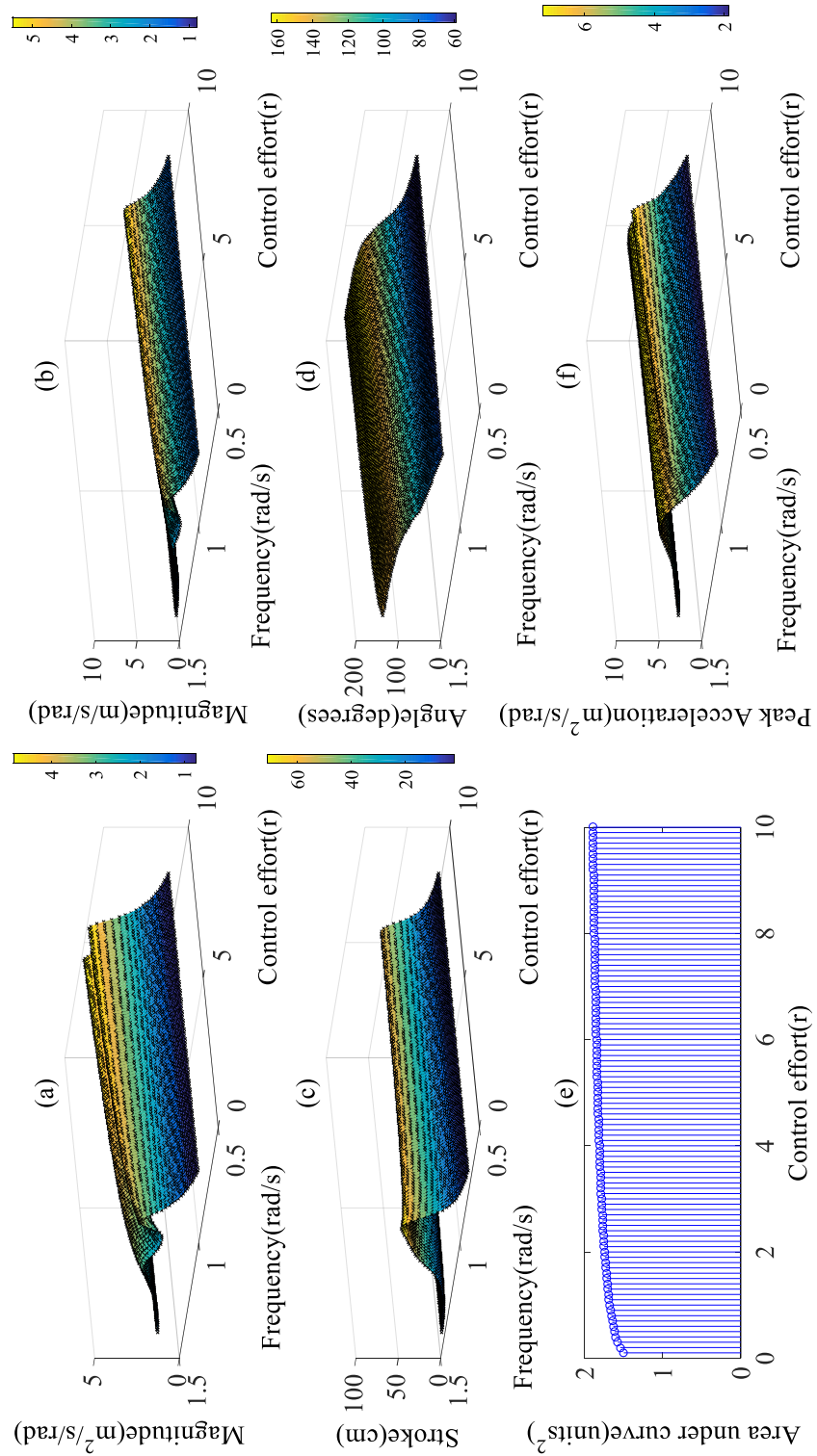


Figure 19. (a) Acceleration response, (b) Displacement response, (c) Damper stroke, (d) Relative phase, (e) Area under acceleration response curve (f) Peak acceleration response with varying controller effort r ranging from 0.1-10.

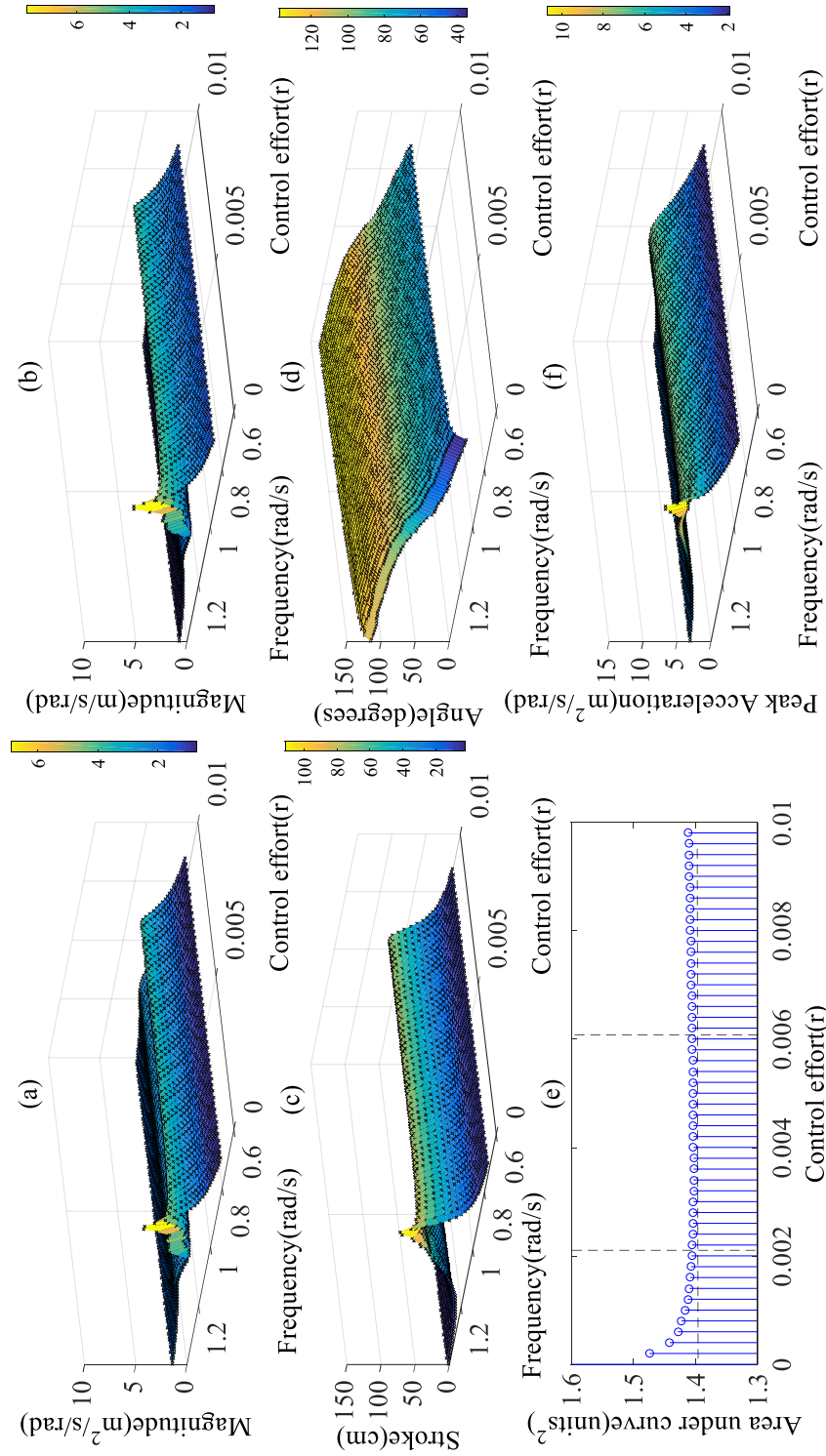


Figure 20. (a) Acceleration response, (b) Displacement response, (c) Damper stroke, (d) Relative phase, (e) Area under acceleration response curve (f) Peak acceleration response with refined controller effort r ranging from $5e^{-5}$ – 0.01 .

4.2.4.2 PID optimisation

Owing to the absence of a rigorous approach for the optimisation of semi-active PID controlled structures, in this section of the study, eleven trial PID and PD controllers have been investigated. The control gains of the different trial controllers have been selected such that the controller response time is progressively reduced (the exact value of the controller gains can be seen in the appendix). Following that, an optimal PID controller was derived through numerical optimisation which requires the gains to achieve maximum rms acceleration reduction over the whole frequency band of interest. The resulting performance of the optimised, PID_{opt} , controller compared with the remaining ten trial controllers and the DBG baseline controller is illustrated in Figure 21.

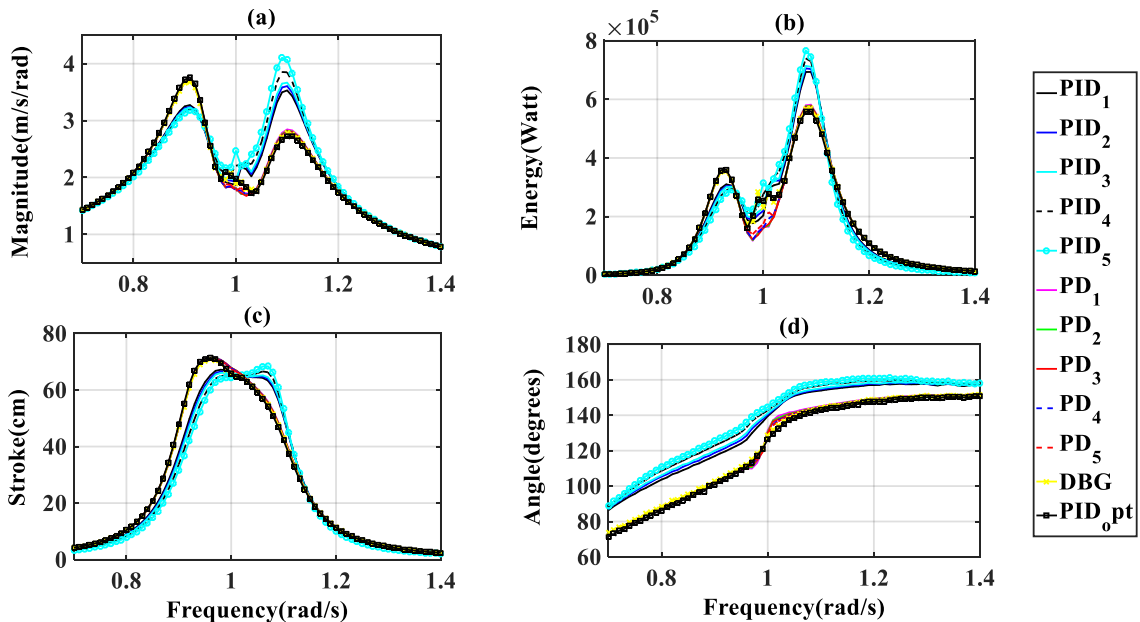


Figure 21. (a) Displacement response, (b) Extracted energy, (c) Maximum stroke, (d) Relative phase of the eleven trial PID and PD controllers and their comparison with the baseline DBG controller

Figure 21, shows that PID and PD control of STMD devices allows for some flexibility when it comes to PID gain tuning. In this respect, it is observed that it is possible to select appropriate gains such that desired performance is achieved in the frequency band of interest (either in the low frequency region <1 Hz, or the higher frequency region >1Hz). Theoretically, the existence of a rigorous approach for the design of linear controllers for non-linear systems

such as the one presented herein, would allow for controllers to be designed with performance variations between the limits of the least aggressive PID controller, termed PID_5 and the most aggressive PD controller, termed PD_1 . Nevertheless, as the tuning becomes more aggressive (and the integral component of the PID controller is eventually dropped, resulting to an ultra-aggressive PD controller), it is observed that performance gains similar to that of a baseline DBG controller are achieved. Because of this, from an active/adaptive control perspective, the tuning flexibility of the PID controller over the baseline DBG controller could signify tremendous performance gains particularly when gain scheduling is performed (i.e. selection of controller gains depending on the operating frequency).

4.2.5 Semi-active maximum damping optimisation

Having optimised the algorithms, the next step in the semi-active controller design procedure is the selection of maximum damping coefficients. To this end, the acceleration response of each control configuration was examined at damping ratios (ζ) ranging from 1%-100% of the critical damping. From this the maximum damping coefficient c_{\max} can be readily calculated using:

$$c_{\max} = 2m_d \omega_n \zeta \quad (4.13)$$

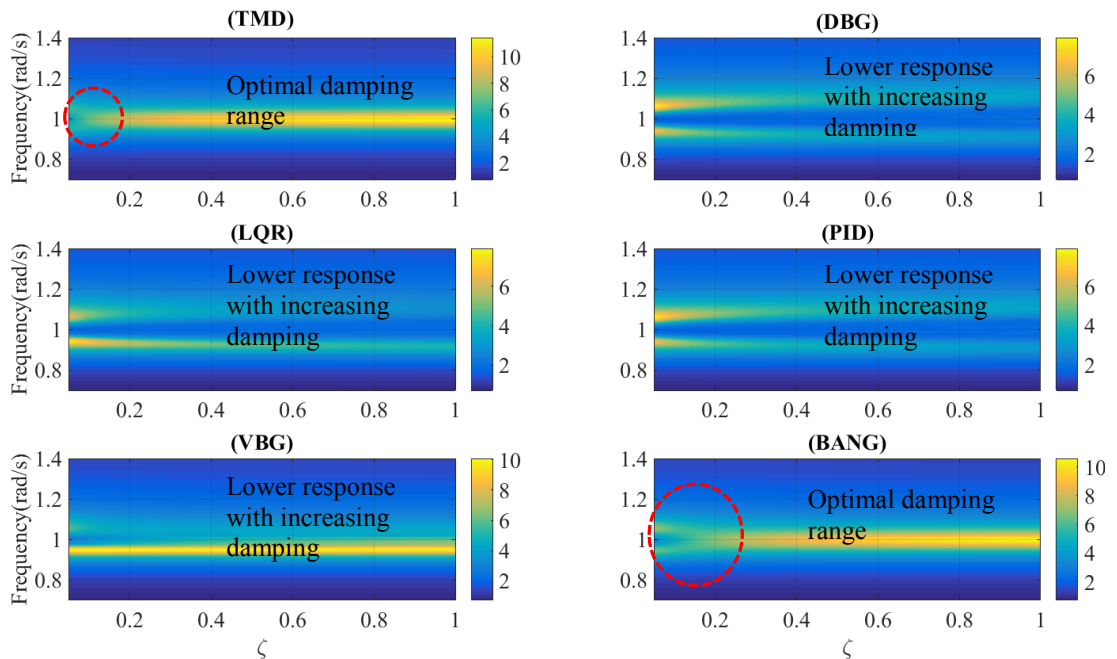


Figure 22. Acceleration response of the different control configurations as a function of the damping ratio (ζ)

Figure 22 shows that for the passive TMD case with $\mu = 1\%$, the optimal damping values range between 5%-10% (6.1% using Den Hartog's equations for optimal design with mass ratio of 1%). At higher damping ratios, it is observed that the TMD does not create the desirable side-lobes that split the response around the tuning frequency, but act as an additional (unresponsive) mass, moving in-phase with the structural system. Similar to the passive TMD case, the semi-active BANG configuration requires low damping ratios (approximately 5%-15%) for optimal behaviour. On the contrary the remaining semi-active control configuration algorithms improve system performance with increasing damping ratio.

4.3 Effect of mass ratio and stiffness uncertainty

In this section of the thesis, the effect of mass ratio ($\mu = m_d / m$) and stiffness uncertainty ($k_s \times \% \text{ uncertainty}$) on the frequency response functions of the system is investigated. For the purposes of realism and clarity of the results, the selected mass ratios ranged between 1%-10%, while the stiffness uncertainty ratio was varied between 80% and 120% (indicating reduction and increase in stiffness respectively). Figure 23 shows that as the mass of the TMD increases, so does the reduction in response at the frequency that the TMD is tuned to. Additionally, as the mass ratio increases the distance between the side-lobe peaks also increases. In regards to the stroke of the auxiliary mass, it is shown that damper strokes reduce with increased mass. With respect to the uncertainty in stiffness and Figure 24, as expected optimum performance is achieved when no parametric uncertainty is found in the system ($k_s \times \% \text{ uncertainty} = 1$), thus the auxiliary device remains in-tune to the structural system. For the cases that the structural stiffness is over-predicted ($k_s \times \% \text{ uncertainty} < 1$), the response of the system in the lower frequency range (<1Hz) amplifies. Similarly, when the stiffness of the system is under-predicted ($k_s \times \% \text{ uncertainty} > 1$) the response of the system in the higher frequency range (>1Hz) amplifies. These observations, are a clear illustration of the sensitivity of the TMD device to tuning.

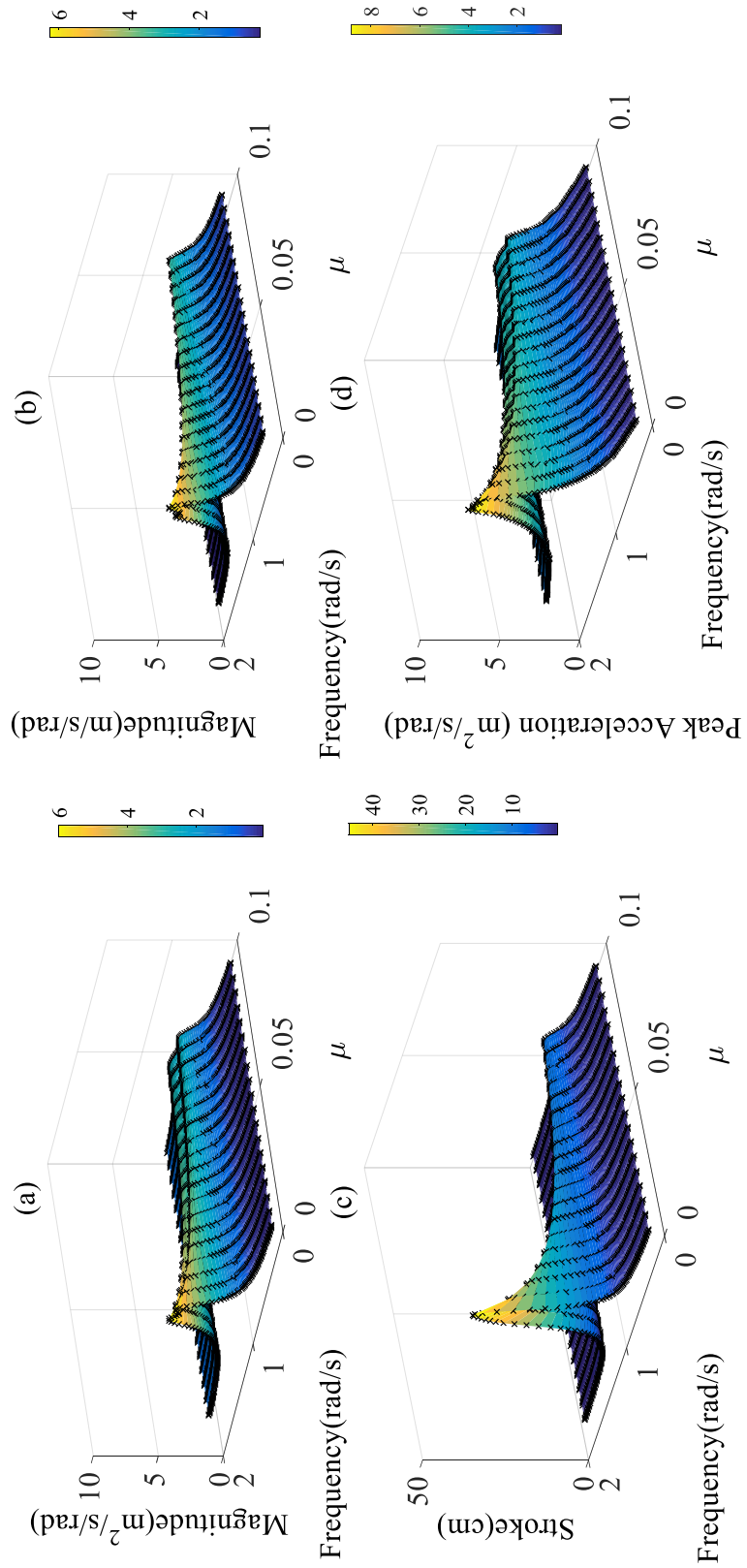


Figure 23. (a) Acceleration response, (b) Displacement response, (c) Maximum stroke, (d) Peak acceleration as a function of the mass ratio for the TMD case

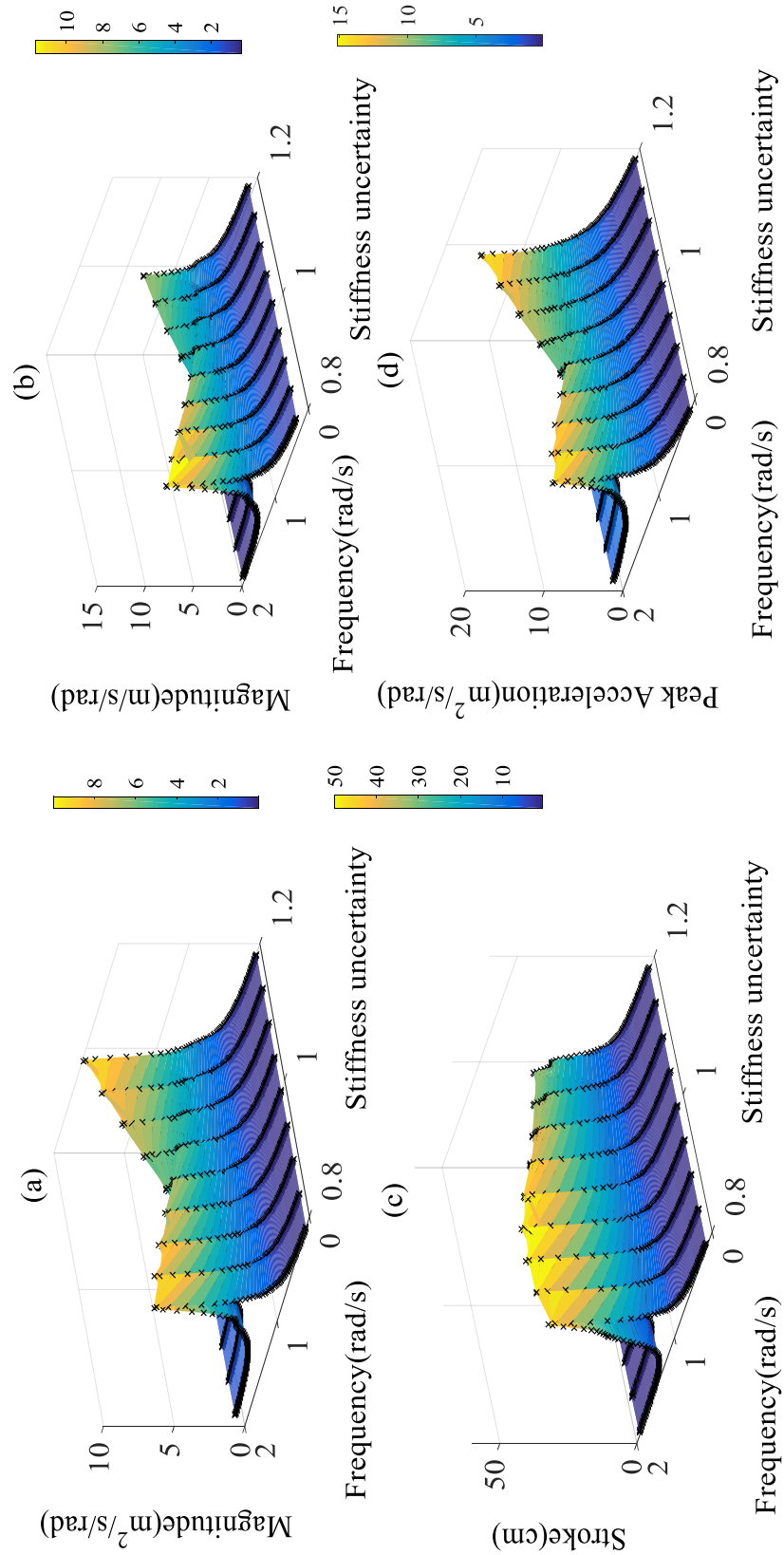


Figure 24. (a) Acceleration response, (b) Displacement response, (c) Maximum stroke, (d) Peak acceleration as a function of the stiffness uncertainty for the TMD case

4.3.1 Frequency response comparison

Similar procedure to the one presented in the former section has been followed for the comparison of the different semi-active control algorithms. The results (and three-dimensional plots) of the analysis can be found in Appendix A. For clarity and ease of comparison, this section presents the two-dimensional contour plots of the different control and algorithm configurations. Similarly to the passive TMD case, the acceleration response (being the tuning/optimisation parameter) of the semi-active controlled systems reduces with increasing mass ratio. Although the distance between the peaks of the side-lobes increases with increasing mass ratio for both the passive and semi-active configurations, it is clear that semi-active configurations push the side-lobe peaks further apart from the tuning frequency. In the same figure, it is observed that the semi-active configuration implemented with a BANG control becomes effective at higher mass ratios (>5-6%). For a mass ratio of 5%, the comparison of the algorithms in terms of acceleration, displacement, peak stroke and peak acceleration as a function of frequency is shown in Figure 26. Arguably, from the five semi-active control algorithm configurations the BANG control and VBG are shown to be the least promising, while the DBG, LQR and PID show significant response reduction.

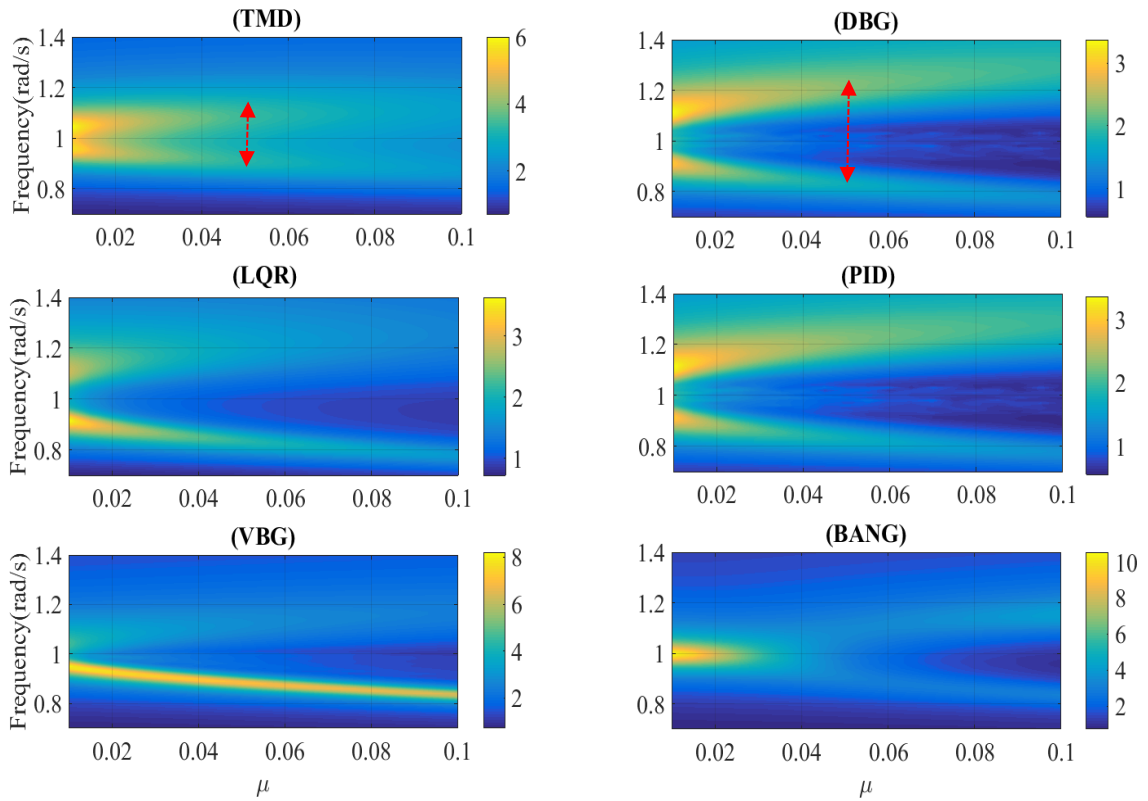


Figure 25. Acceleration response as a function of the mass ratio for the different control and algorithm configurations

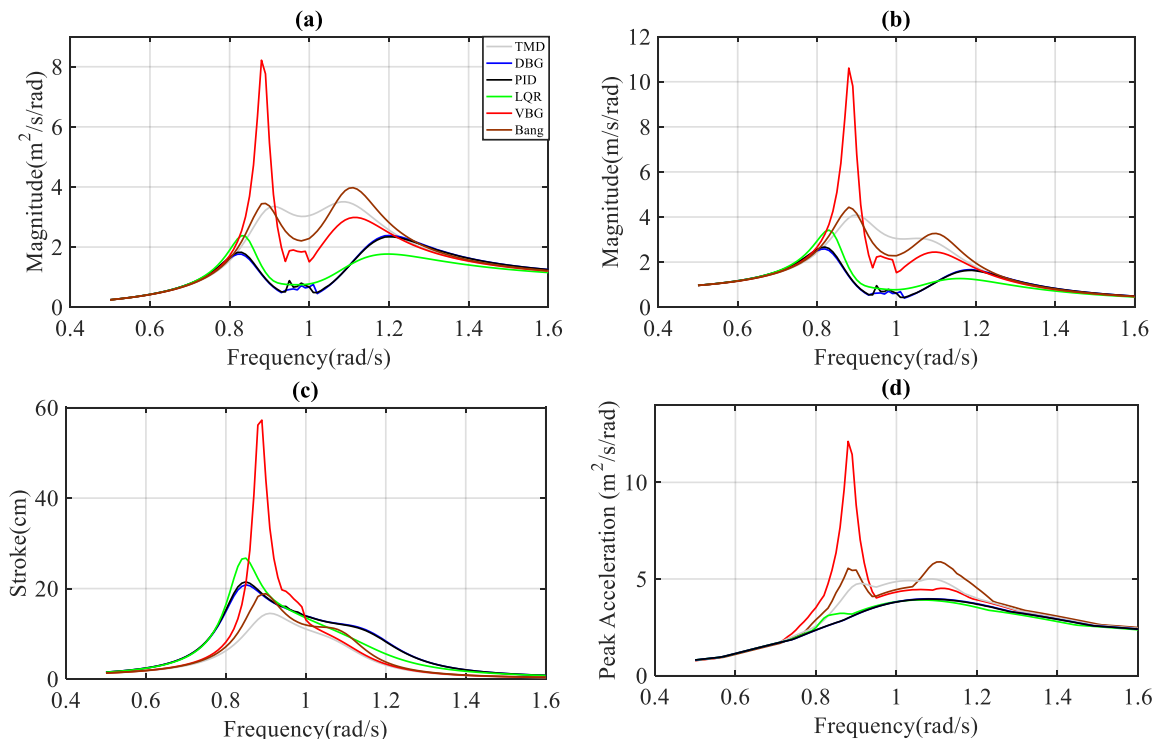


Figure 26. (a) Acceleration response, (b) Displacement response, (c) Maximum stroke, (d) Peak acceleration of different algorithms for 5% mass ratio and 1/1 stiffness uncertainty ratio.

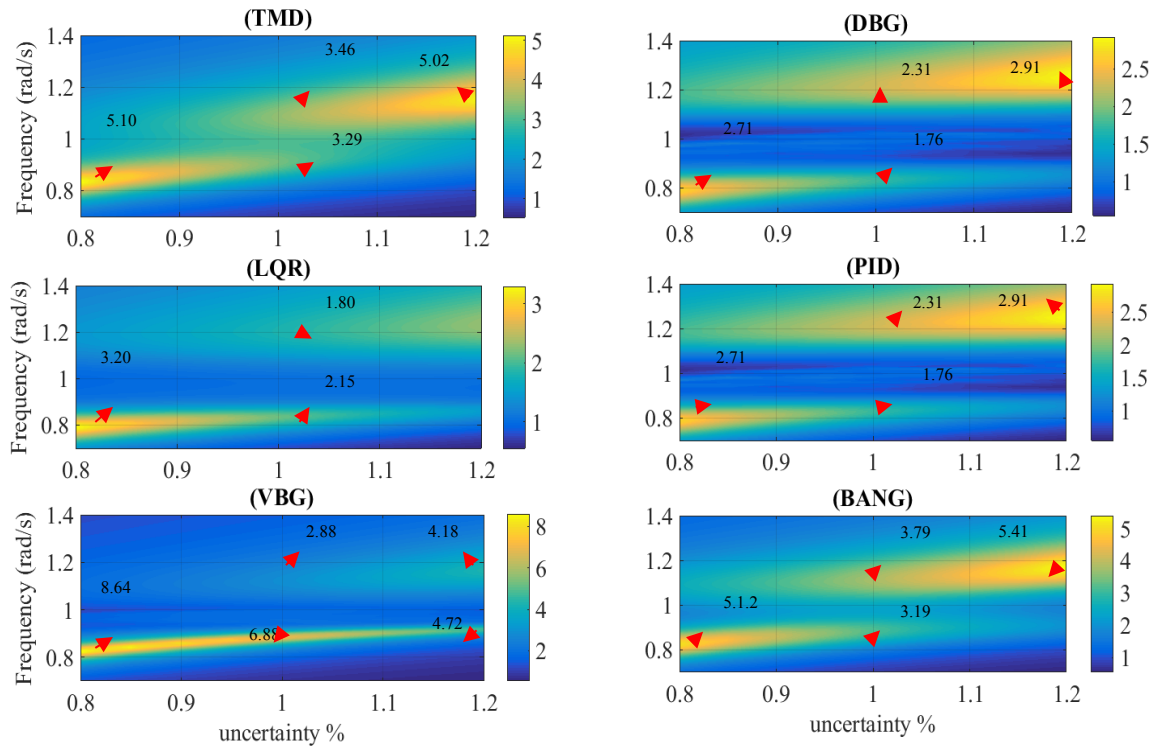


Figure 27. Acceleration response as a function of stiffness uncertainty for the different control and algorithm configurations for 5% mass ratio

By observing the effectiveness of the different control configurations at varying stiffness uncertainty, it is illustrated in Figure 27 that the LQR is the configuration that is better at dealing with parametric uncertainty, particularly when the structural stiffness is underestimated ($ks \times \% \text{uncertainty} > 1$). Additionally, it can be observed that for the case of the passive TMD, an increase of acceleration by 45% for the extreme case of 20% under-prediction in stiffness ($ks \times \% \text{uncertainty} = 1.2$) occurs, while for the DBG and PID counterpart only 26% increase occurs.

4.4.1 Description of the benchmark structural system

To illustrate the effectiveness of different algorithms at alleviating structural response based on the new suggested procedure that accounts for damper stroke saturation, the 76-storey and 306m tall benchmark wind-sensitive structure proposed by Yang et al. (2004) is considered. This office tower building proposed for construction in the city of Melbourne, Australia, has a square 42m x 42m cross-section, with a height to width aspect ratio of 7.3 and

a low natural frequency that lends it the wind sensitivity attribute. The structural system is comprised by a concrete core located in the centre and a concrete frame located at the perimeter of the structure. For such structural designs, the stiff core acts as the main mode of resisting the lateral loads, whereas the concrete frame is primarily designed to carry the gravitational loads and only part of the lateral loads. The structural configuration can be seen in Figure 28. The total mass and volume of the building is 153,000 metric tons and $510,000 \text{ m}^3$ respectively, resulting in a mass density of 300 kg/m^3 , typical for concrete structures.

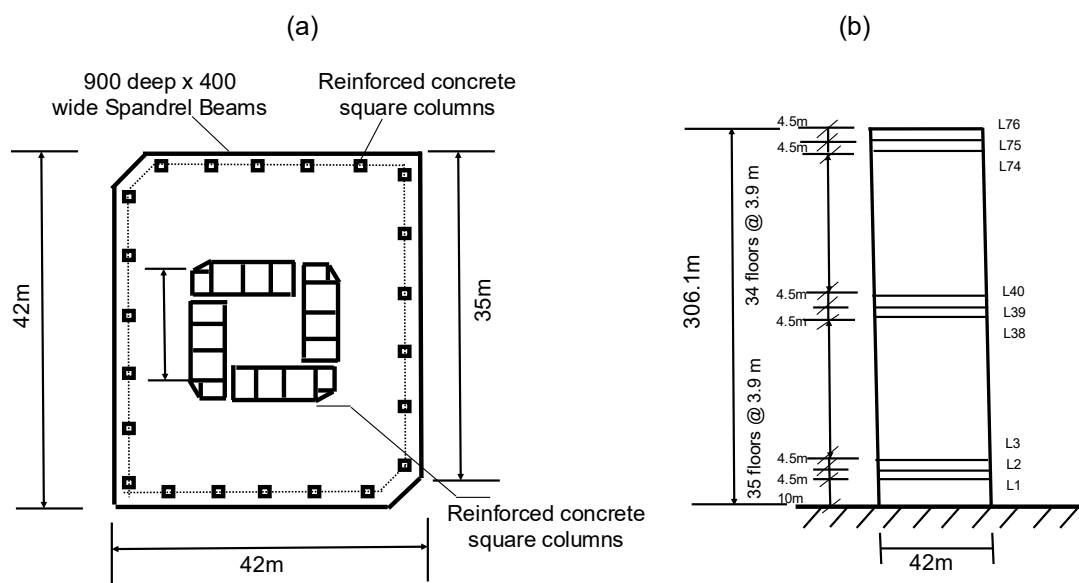


Figure 28. (a) Plan view and (b) elevation view of the 76-story benchmark structure (Yang et al., 2004)

A simplified planar finite element model of the structure is constructed by considering the portion of the building between two adjacent rigid floors as a classical beam element of uniform thickness, leading to 76 rotational and 76 translational degrees of freedom. From these, all the rotational degrees of freedom have been removed using static condensation, leading to a lumped mass sway model with 76 degrees of freedom, representing the displacement of each floor in the lateral direction. The resulting simulated structure has a total mass of 153,000tons, with the first six frequencies at 0.16, 0.765, 1.992, 3.790, 6.395 and 9.45 Hz, and corresponding modal structural damping ratios of 1% calculated using Rayleigh's approach. The mode shapes corresponding to the six first frequencies of the building are shown in Figure 29.

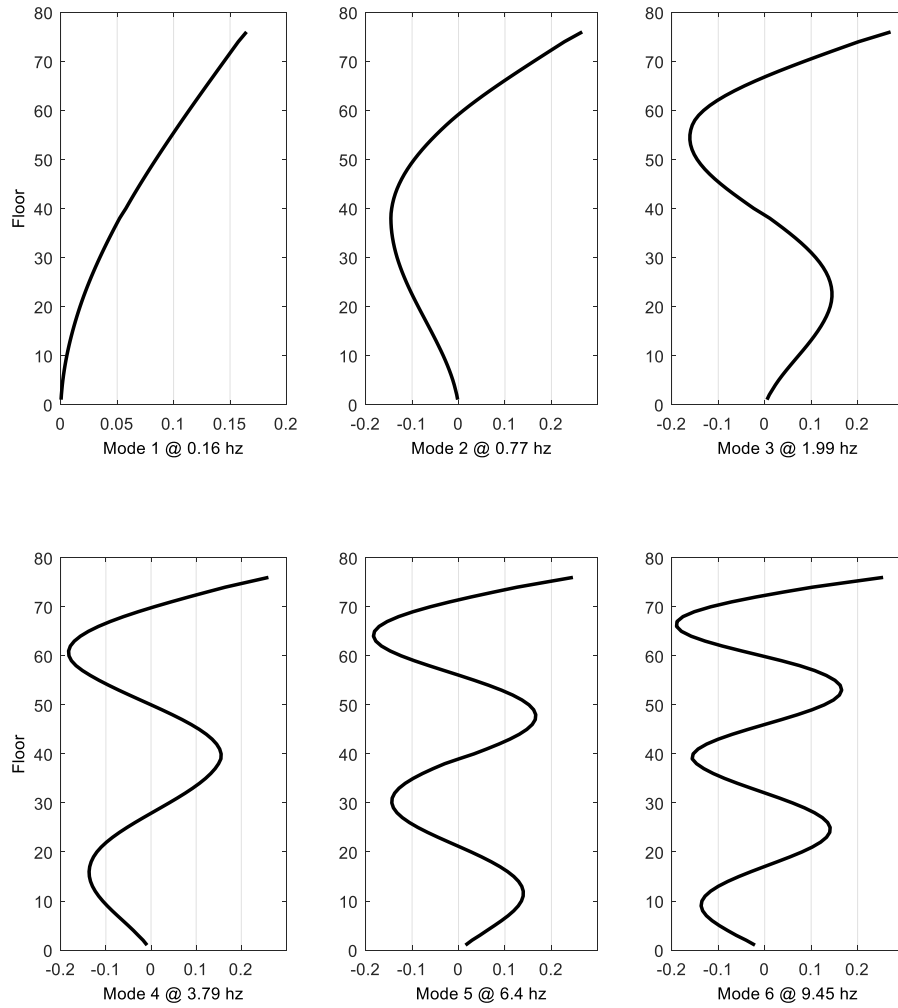


Figure 29. Mode shapes of the first six modes of the building

4.4.2 The excitation

The wind excitation input is derived from wind tunnel tests performed on a rigid model of the 76-storey benchmark structure constructed and tested in the Department of Civil Engineering, at the University of Sydney, Australia. The wind velocities used in the tests were derived from ASS1170.2-1989 (Australian Wind Code (Australian, 1989)) for winds with return period of 10 years. 32 pressure panels (16 panels on either side of the test structure) were combined to give a single pressure coefficient at the centre of each panel. The combined pressure coefficients are converted into across wind forces using:

$$F(t) = 0.5\rho U^2 C_{Pr}(t) A_{pan} \quad (4.14)$$

where ρ is the density of air (kg/m^3), U is the mean wind speed at the top of the building (m/s), A_{pan} is the corresponding single panel area (m^2) and $C_{Pr}(t)$ is the dimensionless instantaneous combined pressure coefficient. For more information on the exact details used for the derivation of the wind forces, the reader is referred to Samali et al. (2004). Indicatively, Figure 30a) and Figure 30b) illustrate the resulting dynamic part of the wind force for the first and last occupied floors along with the frequency content of each loading case. Evidently any motion correlated component is excluded from this wind force description (i.e. no interaction of the motion with the wind force is enabled).

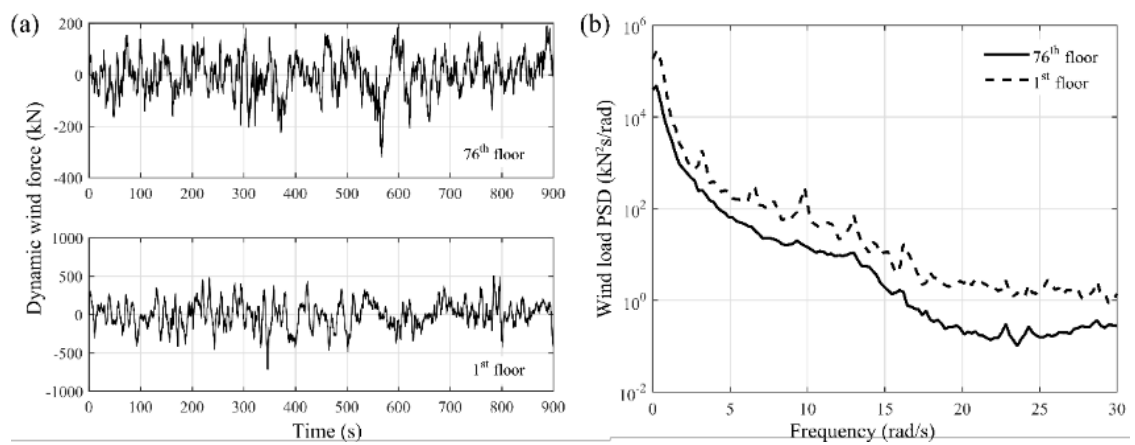


Figure 30. (a) Dynamic wind force time histories of last and first occupied floor, (b) frequency content of the wind excitation fluctuation

4.4.3 Sensor arrangement

In order to enforce practical and realistic constraints on the numerical model, a maximum limit of six sensors is imposed. In other words, at most six output variables can be used for feedback. For the cases where full state feedback is required (such in the case of LQR control), Kalman filtering is applied in accordance to (Kalman, 1960). For the assumed acceleration sensors used in this numerical model, the measurement noises are modelled as Gaussian rectangular pulses with pulse width of 0.001s and two sided spectral density of $10^{-9} m^2/s^4/Hz$. This corresponds to a diagonal covariance matrix in which each diagonal element is $10^{-9} \delta(\tau) m^2/s^3$, where τ is the time interval between two time instants considered. The resulting noise corresponds to approximately 1-5% of the uncontrolled acceleration response of the building.

4.4.4 Tuning and optimising the passive and semi-active devices

In the analysis, two structural configurations are considered: 1) Structural model with an optimally designed TMD, and 2) with a STMD at different control algorithm configurations. A schematic representation of the two different structural configurations is found in Figure 31. Both the TMD and VD-STMD devices comprise an inertial mass of 500tons that corresponds to 0.356% of the total structural mass. Because of the long period of the structural system and the associated motion generally governed by the first modal response, it was deemed appropriate to tune both the devices on the fundamental frequency of the structure (i.e. $\approx 1\text{rad/s} \approx 0.16\text{ Hz}$).

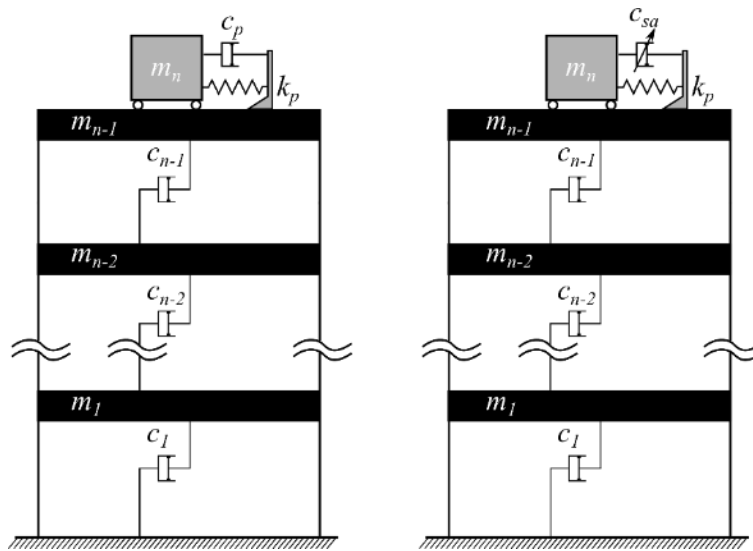


Figure 31. Ensemble of the structural configurations; left TMD equipped structure and right VD-STMD equipped structure

Obviously, optimising the min/max damping coefficients for the case of semi-active control as well as the passive damping coefficient for the case of passive control, will have substantial effects on the performance of the control system. To this date, most of the tuning of the mechanical parameters of a TMD device is achieved via closed-form expressions derived from the minimisation of the rms acceleration response of a SDOF subjected to white noise or harmonic excitation (see section 4.2.2). While this approach is broadly accepted, representing civil engineering structures with an equivalent SDOF system can lead to significant errors in the estimation of their dynamic response. The problem amplifies when one considers the probabilistic nature

of the knowledge of the system's properties and the fact that the estimated properties can vary with time (e.g. amplitude dependence, fluid-structure interaction etc.). Moreover, obtaining TMD mechanical parameters through the use of harmonic or flat spectrum inputs may not always yield optimum values (Ricciardelli et al., 2000). For these reasons, in this thesis and due to the fact that the motion of long period structures is generally governed by the first modal response, both the TMD and STMD are tuned to the fundamental frequency of the structure. On the other hand, tentative damping values are given to the damping devices based on existing formulas found in literature (Hartog, 1956, Ghosh and Basu, 2007) validated and adjusted when necessary through numerical/response optimisation on the MDOF system. Following this principle, and maintaining consistency between the comparisons, the numerical optimisation procedure is based on minimising the rms structural acceleration response. Figure 32a shows the frequency response of the TMD equipped structure under mono-harmonic excitation around the tuning frequency of 1rad/s for different damping ratios of the device, while Figure 32b shows the rms acceleration response of the structure at different floors, under wind excitation at the range of different damping ratios considered within Figure 32a.

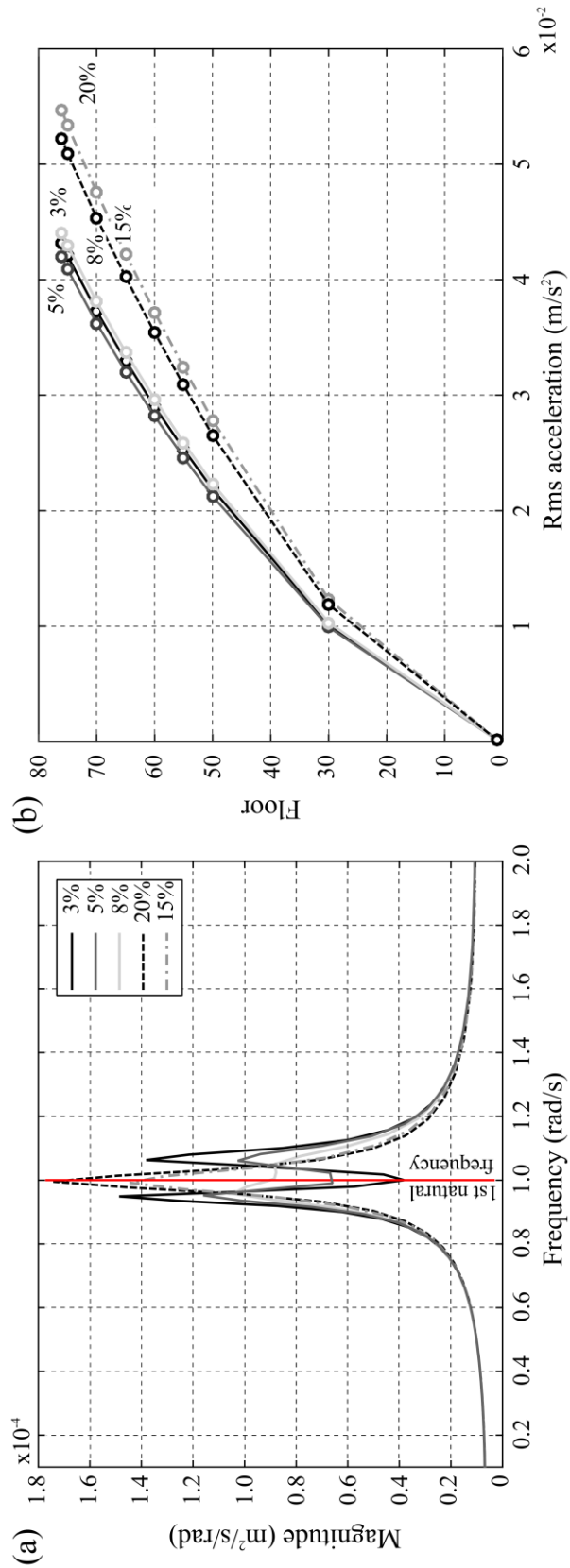


Figure 32. (a) Power spectral density of the acceleration of the 7th floor under harmonic loading and (b) rms acceleration response of different floors under the across wind loading derived from the static wind-tunnel tests

From these two figures, it is evident that under both harmonic and wind excitation, the TMD equipped structure has a better performance when the damping ratio is between 3-5%. By employing a simplex search algorithm for iterative/numerical response optimisation of the rms acceleration response of the wind excited 76-storey structure, a damping ratio of 4.7% was selected for the later analysis. Similar to obtaining the appropriate fixed damping ratio for the TMD device, numerical optimisation using the Nelder-Mead simplex search algorithm (Nelder and Mead, 1965) was employed for deriving the maximum and minimum damping ratios for the STMD device. The implementation of the simplex algorithm was performed using MATLAB response optimisation toolbox. It is worth noting that similarly to the optimisation of the TMD the optimisation of the STMD device is carried out solely on the basis of reducing the rms structural acceleration response of the last occupied floor (75th). Figure 33a and Figure 33b, demonstrate how the algorithm alters non-uniformly the c_{max} and c_{min} values at each of its iterations in an attempt to minimise the rms acceleration metric.

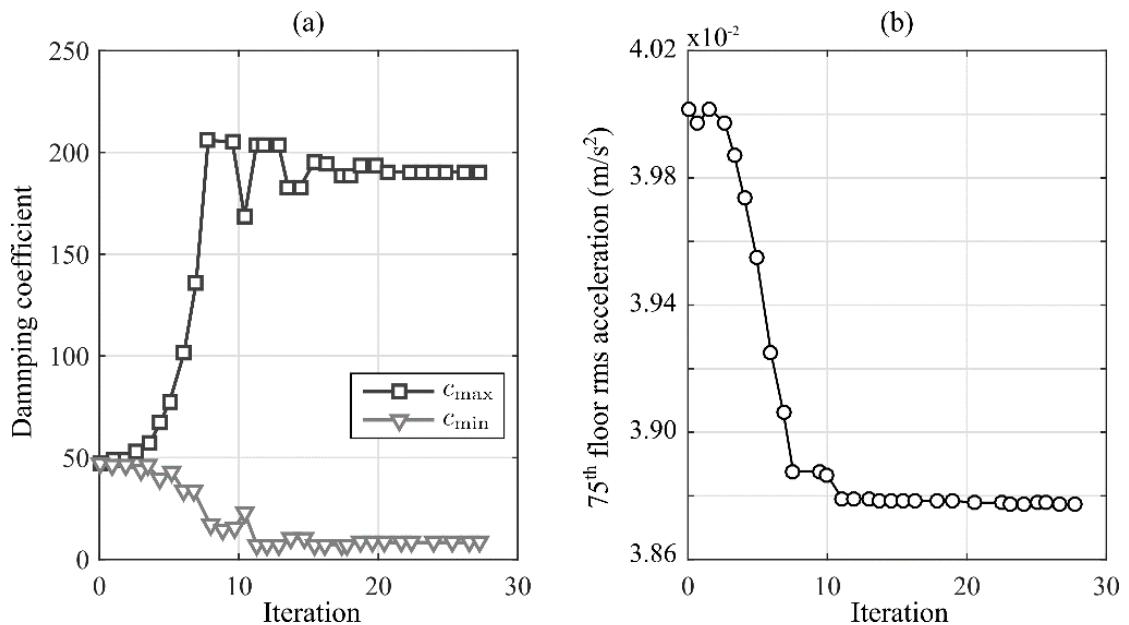


Figure 33. Numerical response optimisation using the Nelder-Mead simplex method; (a) damping band convergence and (b) rms response convergence

Figure 34, shows the resulting damping ratios for each algorithm configuration on the VD-STMD equipped system, along with the damper strokes obtained

from the response optimisation procedure. It is important to notice that the device stroke was implemented as an additional variable to the problem in order to study the stroke limitations and interactions with the overall vibration mitigation performance it enables. The same scale was used throughout for comparative assessments.

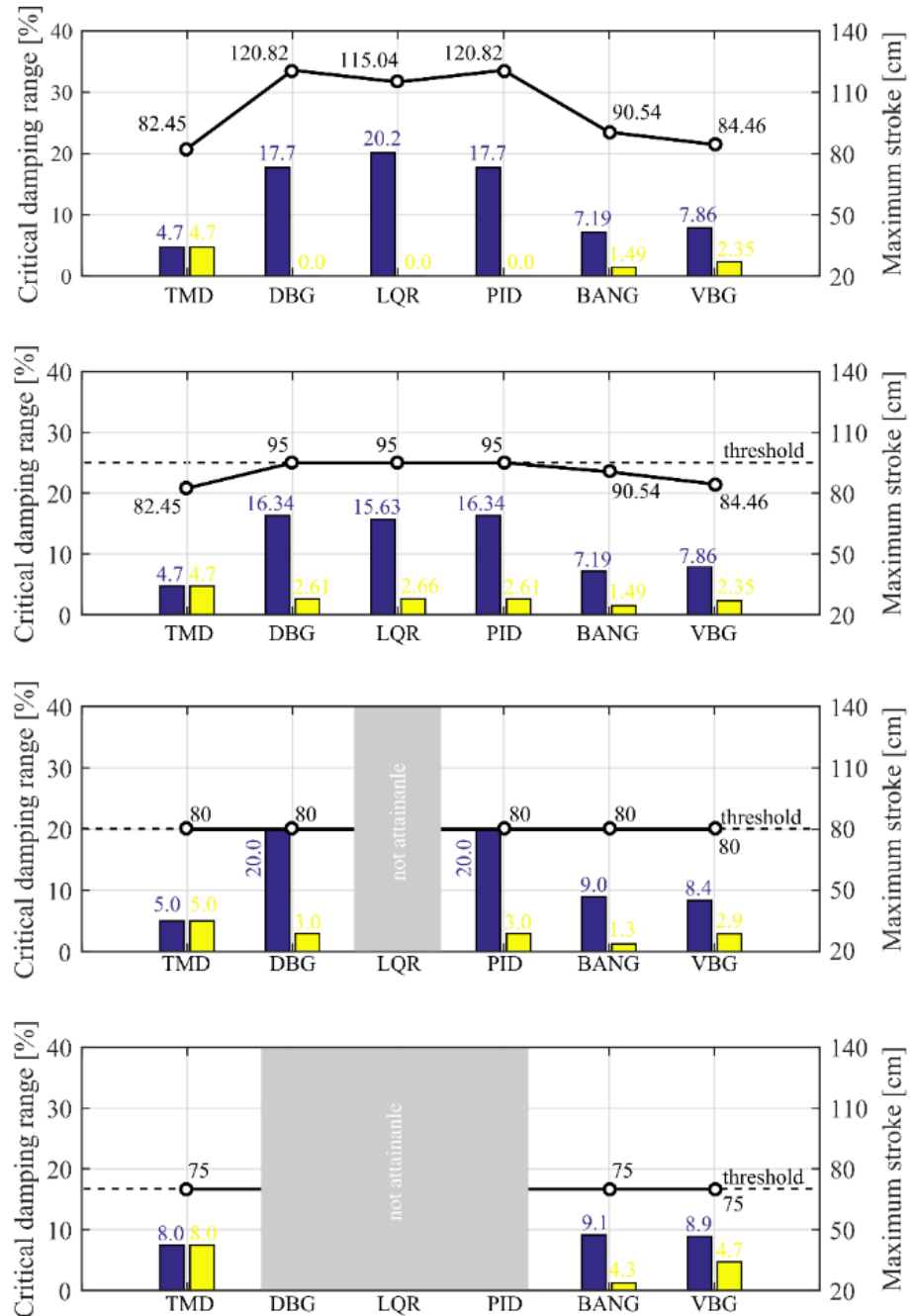


Figure 34. Optimal damping max-min ranges and damper strokes for the different VD-STMD control scenarios for the cases (top to bottom) of uncapped damper strokes, strokes capped at 95cm, 80cm and 75cm

It can be observed that as the stroke of the damper is progressively reduced, some of the algorithms could not achieve enhanced performance compared to the TMD equipped system in respect to the optimisation variable (rms acceleration). The phrase “not-attainable” in Figure 34 is used to graphically illustrate the aforementioned argument. In this respect “not-attainable”, demonstrates that the optimisation of the LQR-STMD ensemble for strokes $\leq 80\text{cm}$, both minimum and maximum damping ratios converge to that of the TMD. Similarly, the DBG, LQR and PID control STMD ensembles for damper strokes $\leq 75\text{ cm}$ converge to the same minimum and maximum damping ratios of the passive TMD. In addition to the aforementioned observations, the results of the optimisation suggest that two categories of algorithms can be distinguished. In this respect, a category of algorithms requiring a large high/low damping ratio (i.e. c_{\max} / c_{\min}) with a high c_{\max} coefficient, and a category of algorithms that requires a small high/low damping ratio with relatively low c_{\max} coefficient. In the former category, the DBG, PID and LQR algorithms are found, while the latter category contains the remaining two algorithms, the VBG and BANG.

4.4.5 Evaluation criteria

The comparison of the different control algorithms is based on the stationary response properties of the different controlled structures. In order to capture the participation of different modes to the structural response, the rms and peak accelerations and displacements at different storeys are extracted from the associated time-histories. From the obtained values, twelve performance criteria were identified and described for the benchmark wind-sensitive sway structure proposed by Yang et al. (Yang et al., 2004). The first criterion, J_1 , appraises the ability of the control strategy to reduce rms accelerations at different building heights:

$$J_1 = \max(\sigma_{\ddot{x}_1}, \sigma_{\ddot{x}_{30}}, \sigma_{\ddot{x}_{50}}, \sigma_{\ddot{x}_{55}}, \sigma_{\ddot{x}_{60}}, \sigma_{\ddot{x}_{65}}, \sigma_{\ddot{x}_{70}}, \sigma_{\ddot{x}_{75}}) / \sigma_{\ddot{x}_{75o}} \quad (4.15)$$

where, $\sigma_{\ddot{x}_i}$ is the rms acceleration of the i^{th} storey and $\sigma_{\ddot{x}_{75o}}$ is the rms acceleration of the 75th floor (last occupied floor) without any control action.

The second performance criterion evaluates the average performance of six floors above the 49th floor:

$$J_2 = \frac{1}{6} \sum_i (\sigma_{\ddot{x}_i} / \sigma_{\ddot{x}_{i0}}) \text{ for } i = 50, 55, 60, 65, 70, 75 \quad (4.16)$$

where, $\sigma_{\ddot{x}_{i0}}$ is the rms of the i^{th} floor without control. The third and fourth performance indices assess the ability of the control system to reduce top floor displacements:

$$J_3 = \sigma_{x_{76}} / \sigma_{x_{76o}} \quad (4.17)$$

$$J_4 = \frac{1}{7} \sum_i (\sigma_{x_i} / \sigma_{x_{i0}}), \text{ for } i = 50, 55, 60, 65, 70, 75 \quad (4.18)$$

where, σ_{x_i} is the rms displacement of the i^{th} floor, $\sigma_{x_{i0}}$ is the rms displacement of the i^{th} storey without control and $\sigma_{x_{76o}}$ is the rms displacement of the 76th floor without control. The fifth and sixth indices take into account the rms stroke of the damper and the average power respectively:

$$J_5 = \sigma_{x_m} / \sigma_{x_{76o}} \quad (4.19)$$

$$J_6 = \left\{ \frac{1}{t_f} \int_0^{t_f} [\dot{x}_m(t)u(t)]^2 dt \right\}^{1/2} \quad (4.20)$$

In which, σ_{x_m} is the rms stroke of the damper, $\dot{x}_m(t)$ is the damper velocity and t_f is the total time of integration. Similarly to the first performance indices, the next four criteria (i.e. J_7 to J_{10}) evaluate the performance in terms of peak response quantities:

$$J_7 = \max(\ddot{x}_{p1}, \ddot{x}_{p30}, \ddot{x}_{p50}, \ddot{x}_{p55}, \ddot{x}_{p60}, \ddot{x}_{p65}, \ddot{x}_{p70}, \ddot{x}_{p75}) / \ddot{x}_{p75o} \quad (4.21)$$

$$J_8 = \frac{1}{6} \sum_i (\ddot{x}_{pi} / \ddot{x}_{pio}), \text{ for } i = 50, 55, 60, 65, 70, 75 \quad (4.22)$$

$$J_9 = x_{p76} / x_{p76o} \quad (4.23)$$

$$J_{10} = \frac{1}{7} \sum_i (x_{pi} / x_{pio}), \text{ for } i = 50, 55, 60, 65, 70, 75, 76 \quad (4.24)$$

where, \ddot{x}_{pi} is the peak absolute acceleration of the i^{th} floor with control and \ddot{x}_{pio} is the peak acceleration of the i^{th} floor without control. Similarly, x_{pi} is the peak displacement of the i^{th} floor and x_{pio} is the peak displacement of the i^{th} floor without control. The 11th criterion assesses the ability of the control strategy to minimise the stroke of the damper:

$$J_{11} = x_{pm} / x_{p76o} \quad (4.25)$$

in which, x_{pm} is the peak stroke of the actuator. The last criterion examines the control effort by calculating the maximum required power by:

$$J_{12} = \max |\dot{x}_m(t)u(t)| \quad (4.26)$$

From the above defined criteria, it can be observed that the better the performance, the smaller the performance indices J_1, J_2, \dots, J_{12} (Yang et al., 2004). Table 4, summarises the 12 performance criteria introduced by the creators of the published benchmark case in hand (see ref. Yang et al., 2004).

Table 4. Summary of performance criteria

Index	Description
J_1	Maximum floor rms acceleration (among a floor selection)
J_2	Average rms acceleration for selected floors
J_3	Maximum rms displacement of top floor
J_4	Average rms displacement for selected floors
J_5	Rms actuator stroke
J_6	Rms control power
J_7	Maximum floor peak acceleration (among a floor selection)
J_8	Average peak acceleration for selected floors
J_9	Maximum peak displacement of top floor
J_{10}	Average peak displacement for selected floors
J_{11}	Peak actuator stroke
J_{12}	Peak control power

4.5 Simulation results

Two structural configurations consisting of passive and semi-active control devices are used for investigating the performance of five different control algorithms on semi-actively controlled high-rise structures. Numerical

optimisation of the damping ratios for the TMD and STMD is carried out at different damper stroke states. The optimised devices are incorporated to the benchmark problem for numerical simulation. From this, the obtained structural response properties are used to calculate the 12 predefined performance indices for four different damper stroke cases. Figure 35–Figure 38 present the results of the comparison. In these figures, the performance indices J_1 to J_4 and J_7 to J_{10} are associated with rms and peak response properties, respectively, while the remaining four performance indices J_5 , J_6 , J_{11} and J_{12} are associated with the stroke and the power consumed by the device.

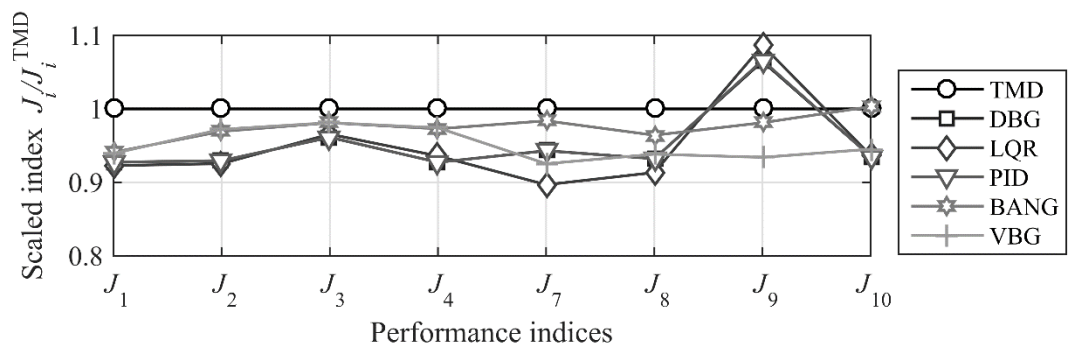


Figure 35. Scaled (over the TMD performance) performance indices for uncapped damper strokes

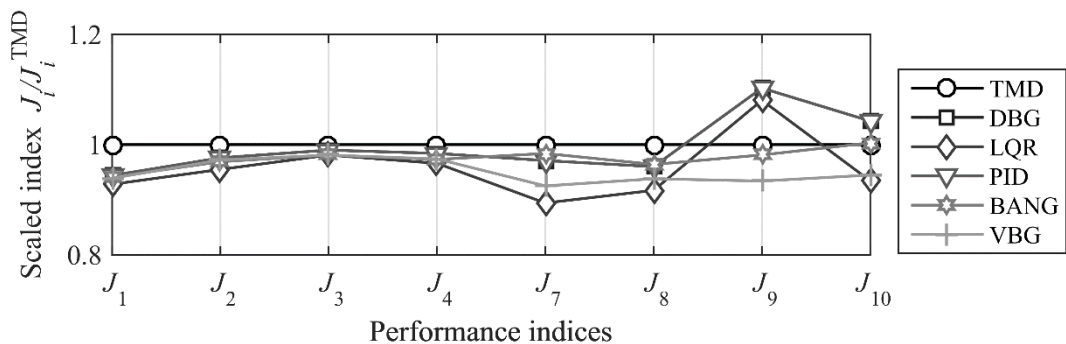


Figure 36. Scaled (over the TMD performance) performance indices J_1, \dots, J_4 , J_7, \dots, J_{10} for damper strokes ≤ 95 cm.

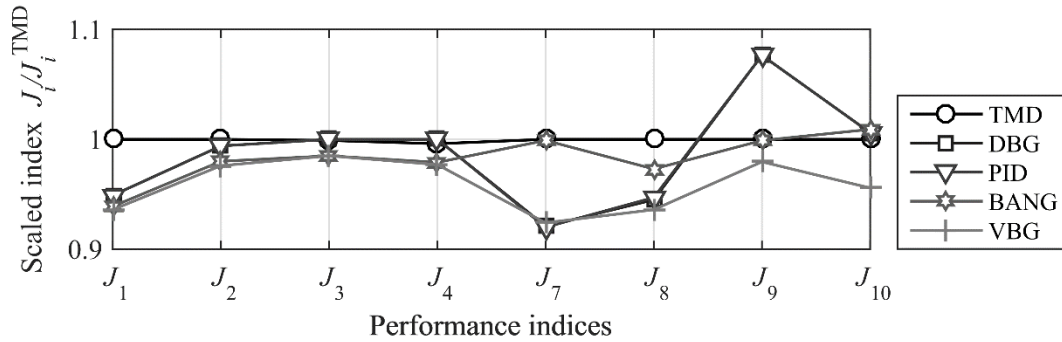


Figure 37. Scaled (over the TMD performance) performance indices J_1, \dots, J_4 , J_7, \dots, J_{10} for damper strokes ≤ 80 cm.

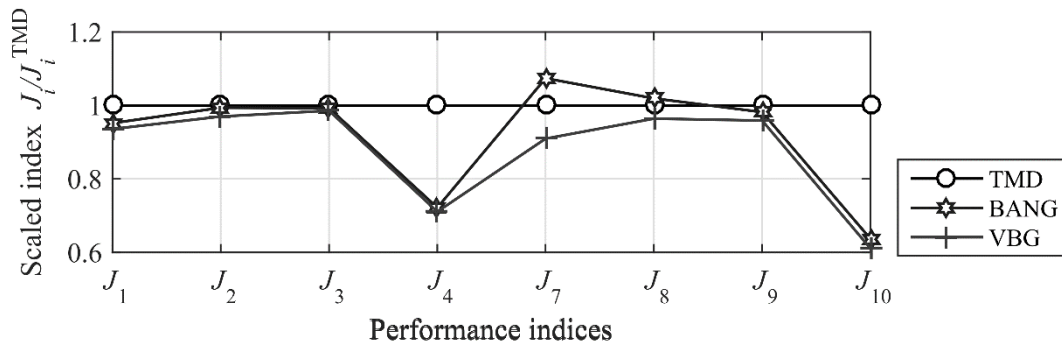


Figure 38. Scaled (over the TMD performance) performance indices $J_1, \dots, J_4, J_7, \dots, J_{10}$ for damper strokes ≤ 70 cm.

As probably expected, when the stroke of the damper is unrestrained the performance of the STMD equipped structure at any control algorithm, configuration is superior on the majority of the performance objectives to that of the TMD-equipped one. This is illustrated through the lower values attained by performance indices J_1 to J_4 and J_7 to J_{10} excluding J_9 . Note that for illustrative purposes, a scaled form was opted for all later graphs whereby the performance is scaled over the TMD performance.

For the comparison between the different semi-active control configurations, the results from the uncapped damper stroke case indicate that it would be appropriate to divide the control algorithms into two categories. The first category contains the more ‘aggressive’ algorithms, indicated by a higher

performance index J_{11} , and the second category of less 'aggressive' or more conservative algorithms that achieve performance gains at the expense of lower damper strokes (see also Figure 34 in its uncapped variant). In this regard, the DBG, LQR and PID controllers are termed 'least-conservative', while the BANG and VBG controllers are termed 'conservative'. Subsequently, when considering rms response properties (indicated by J_1 to J_4), there is a noticeable difference between conservative and least conservative algorithms. As a matter of fact, the latter category of algorithms achieves rms response reduction ranging from 6% to 8% when compared with the TMD-equipped structure and from 3% to 5% when compared with the STMD-equipped structure coupled with conservative algorithms. On the other hand, when peak response properties are considered (indicated by J_7 to J_{10}), conservative algorithms better match the performance of least conservative ones and even show superior performance when peak top floor displacements are considered (indicated by J_9). It can be also observed that 'aggressive' tuning of the PID controller, makes the system behave identically to the system ensemble with a DBG controller. Nevertheless, different PID tuning methods for optimal behaviour are not exploited in this chapter; thus, conclusions on the similarity of PID to other control algorithms cannot be definitive. By restraining the damper stroke to a maximum allowable value of 95 cm as suggested by Yang et al. (2004), with reference to

Figure 36, it can be observed that conservative algorithms succeed in reaching the performance of least conservative algorithms and even noticeably surpassing it in the case of peak response values, with the only exception of the LQR that appears to be more robust to the drop of damper strokes, maintaining better rms and peak response performance than every other algorithm. By further reducing the stroke to ≤ 80 cm (Figure 37), similar observations can be made. However, the LQR that initially showed to be robust to the reduction of damper strokes failed to produce control actions that reduce the rms response of the structure without exceeding the stroke limit. This is evident from the fact that during the optimisation, both damping coefficients c_{\max} and c_{\min} of the STMD device converged to a value of 4.7%, which is the optimum damping coefficient for the TMD device. In other words,

at these (low) damper strokes, the LQR ensemble STMD cannot exceed the performance of a passive TMD with respect to the tuning property (rms acceleration). From the two conservative algorithms, the VBG shows better performance when compared with BANG both in terms of rms and peak responses. For damper strokes ≤ 70 cm, none of the least conservative algorithms is able to produce control actions that will reduce the performance objective. From the two remaining conservative algorithms, VBG remains preeminent, while the BANG-STMD ensemble demonstrated inferior performance compared with the TMD system with respect to peak acceleration response properties indicated by performance index J_7 and J_8 . From the above findings and with reference back to Figure 34, it is evident that regardless of the damper stroke, all three of the least conservative algorithms require high c_{\max} damping ratios for achieving optimum performance, while their c_{\min} coefficient is set to a relatively low value. This observation suggests that least conservative algorithms make better use of the minimum damping ratio for increasing stroke (and thus optimally increase the velocity of the damper so that the damping force is also increased), and thoroughly use their high damping only when necessary. This is similar to reducing the damping ratio of the passive device (thus increasing the stroke) up to a point where no more performance can be gained. Supporting this observation, the results obtained from the optimisation of minimum and maximum damping ratios for the cases of damper strokes ≤ 95 cm, least conservative algorithms restrain the stroke by increasing the c_{\min} coefficient while at the same time attempt to maintain the c_{\max} coefficient close to the optimal. Undoubtedly, in order to maintain the performance of least conservative algorithms close to the optimal, the resulting large c_{\max} dictates the requirement of large forces (and in turn control power indicated by performance index J_6 and J_{12}), which in turn influence the size and number of devices required for control.

4.5.1 Remarks

A variety of fixed parameter control algorithms proposed for semi-actively controlled structural systems have been evaluated for use on high-rise

structures incorporating STMD devices, through numerical simulations on a simplified SDOF system and a wind-excited 76-storey benchmark structure. The implementation of each algorithm was conducted based on available measurements of the structural system including absolute accelerations, displacements and velocities. The STMD-equipped structure at each of the algorithm configurations resulted in an improved performance when compared with the best passive case, with only exception the case of peak displacements in which the passive system was superior to the semi-active one. Still, for the semi-active case, the response of the structure varied significantly, depending on the choice of algorithm. In this regard, it is found that when no consideration is given on the damper strokes, three of these algorithms are found to be most suited for use with STMD on wind-excited structures. The LQR, the DBG and the PID that maximise damper strokes, thus termed 'least-conservative', achieved significant response reductions. On the other hand, it has been demonstrated that by progressively reducing the damper strokes, the remaining two algorithms, the VBG and BANG, the algorithms that significantly restrain the damper strokes and thus termed 'conservative' managed to reach and even surpass in some cases the performance of previously 'best' algorithms. From the category of least conservative algorithms, the LQR was shown to be more effective for use on the structure of interest, yet the requirement for full state feedback that translates to additional state measurements and computational burdens suggests that DBG and PID might be practically superior. From the category of conservative algorithms, the VBG is shown to be unconditionally superior to the BANG. From this, it has been demonstrated that appropriate selection of a control algorithm can be considered as an alternative method of limiting damper strokes while maintaining expedient performance without the requirement of an external auxiliary damping device or high pass filtering for limiting the damper's stroke. Finally, by investigating the tuning of the damping ratios for the different configurations, it is found that the main difference of the two categories of control algorithms is the requirement of the least conservative algorithms for high damping ratios for achieving optimal behaviour, whereas conservative algorithms require significantly lower values. As a matter of fact, for relatively similar performance gains, a DBG would

require a maximum damping ratio of 16% as opposed to 8% required by a VBG. This suggests that the choice of an algorithm from the latter category would translate to a reduced size/number of auxiliary devices used, control forces and power, which in turn relate back to the practical applicability and cost of the STMD device on high-rise structures.

Chapter 5

A Novel Semi-active Hybrid Configuration

In this chapter of the thesis, a novel, energy and cost efficient ‘smart’ hybrid semi-active mass damper configuration for use on structural applications has been developed. For this task, an arrangement of both active and semi-active control components coupled with appropriate control algorithms are constructed and their performance is evaluated on both single and multi-degree of freedom structures for which practical constraints such as stroke and force saturation limits are taken into account. It is shown that under both free and forced vibrations, the novel device configuration outperforms its more conventional passive and semi-active counterparts, while at the same time achieving performance gains similar to the active configuration at considerably less energy and actuation demands, satisfying both strict serviceability and sustainability requirements often found to govern most modern structural applications. The contents of this chapter are an adapted form of the conference paper presented in the proceedings of the IJSSD symposium on progress in structural stability and dynamics, and a journal paper published in the Journal of Applied Sciences. Details of these papers are as follows:

Demetriou, D.; Nikitas, N.; Tsavdaridis, K.D. A Novel Hybrid Semi-active Tuned Mass Damper for Lightweight Steel Structural Applications. In Proceedings of the IJSSD Symposium on Progress in Structural Stability and Dynamics, Lisbon, Portugal, 21–24 July 2015.

Demetriou, D.; Nikitas, N. A Novel Hybrid Semi-Active Mass Damper Configuration for Structural Applications. *Appl. Sci.* **2016**, *6*, 397.

5.1 Introduction

Alleviating the vibration response of tall and slender structures under wind action becomes an increasingly challenging task. Generally speaking, the response of such structures subjected to wind excitation can be thought of as the summation of three components, namely static, background aerodynamic, and resonant dynamic, in the relevant modes of vibration. Mitigating the static and background aerodynamic response can be achieved through supplemental structural stiffness and/or reduction of the mean excitation forces through manipulation of the structural aerodynamics (shape). Still, as structures become taller and more slender, resonant contributions become more and more significant and eventually dominate (Holmes, 2007).

One method of successfully and conveniently mitigating the resonant response of structures is by modifying their dynamic properties (frequencies and damping). Amongst the most popular devices used for resonant response reduction are the dynamic vibration absorbers (DVAs), which can be found in passive, active, hybrid and semi-active forms. The passive form of the DVA, the tuned mass damper (TMD), has been studied for more than a century and is shown to be effective and reliable at alleviating structural response under generic dynamic loading; however, this device being tuned to a single vibration mode of the structure thus has performance limited to a narrow band of operating frequencies that in turn compromise the system's attenuation capacity when excited beyond the targeted mode. Overcoming the limitations of the passive TMD, the active version of the DVA, the active mass damper (AMD), achieves resonant response reduction by generating control forces via acceleration and deceleration of auxiliary masses using actuators in a way that at any given time and independent of the excitation and system's characteristics, maximum energy is absorbed. Clearly, while the flexibility and adaptability of active devices allows for better vibration response reduction, this performance enhancement is achieved at the expense of considerable power-force demands and reliability. Adding to the limitations of the purely active AMD configuration, the performance of such devices on high-rise structures is typically limited by the capacity of the installed actuator and the auxiliary mass strokes (Ricciardelli et al., 2003, Yang et al., 2004, Zhang and Ou, 2015). Despite the attempts made to overcome these limitations, either

by using different, more efficient and novel-at-the-time AMD configurations such as the swing-style AMD presented in (Haertling, 1994), or the electromagnetic device with semi-active control properties presented in (Scruggs and Iwan, 2003), amongst many other configurations (Zhang and Ou, 2015, Zhang et al., 2016), the crucial absence of a fail-safe mechanism limits the options to structural engineers to an approach that is based on the hybridisation of the AMD device with a component able to prevent instability upon active component failure. To this extent, most practical structural control configurations comprising a form of active DVA are found in an active-passive hybrid state (Ikeda, 2009), with an inspiring recent application on the 101-storey Shanghai World Financial Centre, highlighting the prospects of hybrid control.

The conventional hybrid configuration of a DVA, entitled as active-tuned mass damper (ATMD), is one that requires a passive TMD device to work in conjunction with active control elements such as hydraulic, motor, ball-screw actuators, etc. Such devices are shown to achieve a compromise between performance and reliability at the expense of lower strokes and actuator demands. Studies such as those found in (Fujinami et al., 2001, Nakamura et al., 2001, Watakabe et al., 2001, Mitchel et al., 2012) are a few amongst the many illustrating the performance gains arising from the use of ATMDs on structural systems under both earthquake and wind excitations. Pushing the boundaries of hybrid control and innovation, Tan et al. (2012) proposed a hybrid mass damper configuration for Canton Tower in Guangzhou China. This configuration requires an AMD to work in parallel with a two-stage TMD, demonstrating significant vibration attenuation under strong wind and earthquake excitations. Following the same path, Li and Cao (2015) later proposed a hybrid configuration that uses two interconnected ATMDs for the supply of the control action. More recently, Tso et al. (2016) proposed an alternative approach to the design of the hybrid vibration absorber that incorporates detached passive and active parts, resulting in a non-colocated setup that was shown to achieve better performance than the traditionally bundled ATMD. In the field of mechanical engineering and away from DVA applications, but following the same logic, Khan et al. (2016) proposed a hybrid configuration that requires a magnetorheological semi-active damper to work

in conjunction with an active actuator placed at the base of the structural system, claiming the first-ever hybrid semi-active/active configuration. The aim of the study was to show how an active actuator can assist the semi-active device in a non-colocated configuration, in an attempt to achieve performance as close to that of a fully active system as possible. Prior to the publication of Khan et al. (2016), a different configuration that still makes use of semi-active and active elements has been proposed by the authors of this chapter in (Demetriou et al., 2015a). The fundamental novelty of the configuration and the main difference to any prior hybrid configuration is the use of colocated semi-active and active elements for the supply of control power directly to the DVA that in turn controls the structural system. In this chapter, boundaries of innovation and the limitations of the TMD, AMD and ATMD are surpassed and the idea proposed by Demetriou and Nikitas (Demetriou et al., 2015a) is extended through the use of a novel semi-active hybrid mass damper (SHMD) configuration proposed in this chapter. This device extends the conventional ATMD logic, by employing semi-active dampers working in conjunction with actively controlled elements in a way that, by combining the two components using appropriately designed control algorithms, the potential of timed maximum energy extraction is exploited. To this end, the operating principle of the novel SHMD configuration requires the semi-active elements to be designed such that maximum kinetic energy is extracted from the system at the expense of low energy demands required to control: power operated valves, the fluid discharge through orifices, the magnetic field around a ferrous fluid piston, etc., and then allowing for energy addition to the system using active (hydraulic) actuators, that in turn enhance the system's adaptability to ever-changing loading conditions. In other words, the active control components of the hybrid device are restricted to add energy while the semi-active components perform as usual by extracting energy. Critically, the control algorithm needs to be designed such that when energy is added to the system (and DVA's mass is accelerated), the semi-active component drops to its minimum value such that it does not counteract the action of the active component.

In order to demonstrate the performance gains from the use of this novel SHMD device, comparative studies on a low frequency single-degree-of-

freedom (SDOF) system subjected to free and forced vibrations are carried out. The selection of the input conditions was performed in an attempt to quantify the performance gains of the novel configuration over a wider band of operating conditions, through capturing a broader band of excitation frequencies. The study naturally extends the application of the novel configuration on a more realistic 76-storey benchmark structure on which realistic wind loading, actuation and damper stroke limits are applied.

5.2 Modeling Principles

5.2.1 General Dynamic Vibration Absorbers Modeling Approach

Modeling the novel SHMD device requires a thorough understanding of the modeling principles and procedures followed in the design of passive, active and semi-active systems. In order to do so, the dynamic behaviour of an n -DOF system coupled with a DVA (as depicted in Figure 39) under a random dynamic loading needs to be considered through its equation of motion:

$$M\ddot{x}(t) + C\dot{x}(t) + Kx(t) = Bu(t) + Dd(t) \quad (5.1)$$

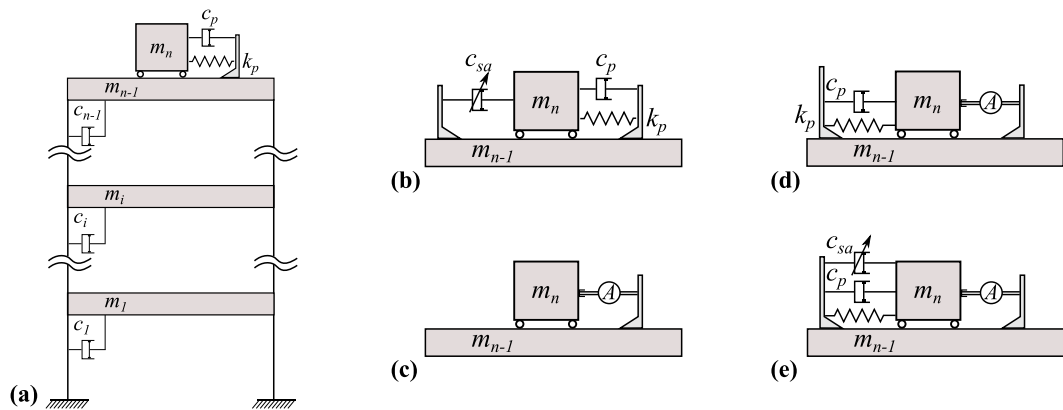


Figure 39. Structural configuration and mathematical models for (a) tuned mass damper (TMD); (b) semi-active tuned mass damper (STMD); (c) active mass damper (AMD); (d) active-tuned mass damper (ATMD); and (e) semi-active hybrid mass damper (SHMD) systems.

In Eq.(5.1), each overdot declares single differentiation with respect to time, M , C and K are the $n \times n$ mass, damping, and stiffness matrices, respectively; $x(t)$ and $d(t)$ are in order of the displacement, and external force $n \times 1$ column vectors; $u(t)$ is the single scalar control force and $B(n \times 1)$ and

$D(n \times n)$ are the influence matrices assigning the control and external force contributions, respectively, to the individual degree of freedoms (DOFs). For each DOF in $x(t)$ being the lateral displacement of the i th ($i = 1, \dots, n$) mass, M becomes diagonal, while for the classical viscous damping considered the damping matrix C attains a form identical to the symmetric stiffness matrix K . Without any loss of generality, the DVA is attached to the $(n - 1)$ th DOF and its motion constitutes the n th DOF. For control implementation purposes, Eq.(5.1) can be represented in the state space domain using a first order differential equation, such that:

$$\dot{z}(t) = Az(t) + Fu(t) + Ed(t) \quad (5.2)$$

where, $\dot{z}(t)$ represents the first order time-change of the states $z(t) = [x(t) \quad \dot{x}(t)]^T$ of the system, A is the system block matrix containing the system's mass, damping, stiffness properties, F is the control force locator block matrix, and E is the external perturbation locator block matrix, such that:

$$A = \begin{bmatrix} 0 & I \\ -M^{-1}K & -M^{-1}C \end{bmatrix}, \quad F = \begin{bmatrix} 0 \\ M^{-1}B \end{bmatrix}, \quad E = \begin{bmatrix} 0 \\ M^{-1}D \end{bmatrix} \quad (5.3)$$

5.2.1.1 Passive Tuned Mass Damper (TMD) Control

A TMD device produces control actions as a result of the relative motion of its mass against the structural mass such that the control force term, $u(t)$ in Eq.(5.2) is calculated at each time step by:

$$u(t) = k_p x_r(t) + c_p \dot{x}_r(t) \quad (5.4)$$

In this equation, $\dot{x}_r(t)$ and $x_r(t)$ are respectively the relative velocity and displacement between the n th and $(n - 1)$ th DOFs and c_p and k_p , are the passive damping and stiffness coefficients respectively. To this date, most of the tuning of the mechanical parameters c_p and k_p of a TMD device is achieved via closed-form expressions derived from the minimisation of the rms acceleration response of a single degree of freedom (SDOF) subjected to white noise or harmonic excitation. While this approach is broadly accepted, representing civil engineering structures with an equivalent SDOF system can

lead to significant errors in the estimation of their dynamic response. The problem amplifies when one considers the probabilistic nature of the knowledge of the system's properties and the fact that the estimated properties can vary with time (e.g., amplitude dependence, fluid–structure interaction, etc.). Moreover, obtaining TMD mechanical parameters through the use of harmonic or flat spectrum inputs may not always yield optimum values (Ricciardelli et al., 2000). In this chapter, because the motion of long period structures is generally governed by the first modal response, the stiffness coefficient of the auxiliary device is selected just as the mass damper is tuned to the fundamental frequency of the structure, whereas the damping coefficient is obtained using the expressions found in (Hartog, 1956, Ghosh and Basu, 2007), and validated and adjusted when necessary through numerical optimisation based on (Nelder and Mead, 1965, Demetriou et al., 2015b) for the case of the more complex, wind-excited multi-degree of freedom (MDOF) structural system.

5.2.1.2 Active Mass Damper (AMD) Control and Hybrid Active-Tuned Mass Damper (ATMD) Control

For a purely active system, the passive control force takes the form of a desired action, $u_a(t)$ determined via a control algorithm such as the Linear-Quadratic-Regulator (LQR), proportional-integral-derivative (PID) controller or similar. With reference to Figure 39c, for the case of AMD control, the force is delivered solely by means of mechanical actuation; thus the actuation force $f_a(t)$ is equal and opposite to the calculated desired action:

$$u_a(t) = -f_a(t) \quad (5.5)$$

Obviously, for the purpose of limiting the stroke and the requirement of a fail-safe mechanism, an ATMD is found in most practical applications (Yang et al., 2004, Ikeda, 2009). To this end, and with reference to Figure 39d, for an ATMD, the desired force is mathematically expressed as the summation of the passive forces generated by the motion of the mass damper and an additional external force provided by means of mechanical actuation. Because the dynamic characteristics of the mass damper remain unaltered and the

desired interaction force has been already calculated by the control algorithm, the required conventional hybrid actuation, $f_{a_atmd}(t)$ is determined from:

$$u_a(t) = c_p \dot{x}_r(t) + k_p x_r(t) - f_{a_atmd}(t) \quad (5.6)$$

In Eq.(5.6), the mechanical properties c_p , k_p of the device can be selected similarly to a purely passive device. Still, typically a higher damping coefficient c_p is used along with the ATMD device for stroke-restraining purposes (Yang et al., 2004, Demetriou et al., 2015b).

5.2.1.3 Semi-Active Tuned Mass Damper (STMD) Control

Similar to an active system, the semi-active counterpart makes use of control algorithms for the selection of appropriate control actions. The first step in the calculation of the semi-active control forces is the calculation of an equivalent active force using active algorithms and Eq.(5.5). Next, the active force is tailored so that it can be physically realised by the semi-active device. In this regard, because of the fact that no energy can be added directly to the system, the semi-active device will produce control forces only when required, i.e., when the damper is requested to “consume” energy. This is achieved by applying semi-active force saturation limits such that the semi-active control force, $u_{sa}(t)$ is calculated by (Hrovat et al., 1983):

$$u_{sa}(t) = f_a(t) \left(\frac{1 - \text{sgn}[f_a(t)\dot{x}_r(t)]}{2} \right) \quad (5.7)$$

$$\text{sgn}[f_a(t)\dot{x}_r(t)] = \text{sgn}(q_a(t)) \triangleq \begin{cases} 1 & \text{for } q_a \geq 0 \\ -1 & \text{for } q_a < 0 \end{cases} \quad (5.8)$$

The product of $f_a(t)\dot{x}_r(t)$ is the power, $q_a(t)$, of the whole active system device. Similarly, the power of just the semi-active component, $q_{sa}(t)$, is defined as the product of the force that can be physically translated by the device, $u_{sa}(t)$, and its relative velocity, $\dot{x}_r(t)$:

$$q_{sa}(t) = u_{sa}(t)\dot{x}_r(t) < 0 \quad (5.9)$$

A schematic representation of the power time histories of both an actively and a semi-actively controlled device is shown in Figure 40. It can be observed

that the active device has the advantage of both adding and dissipating energy, as indicated by positive and negative powers, while the semi-active device only consumes power (indicated by only negative power—and its integral energy is also negative).

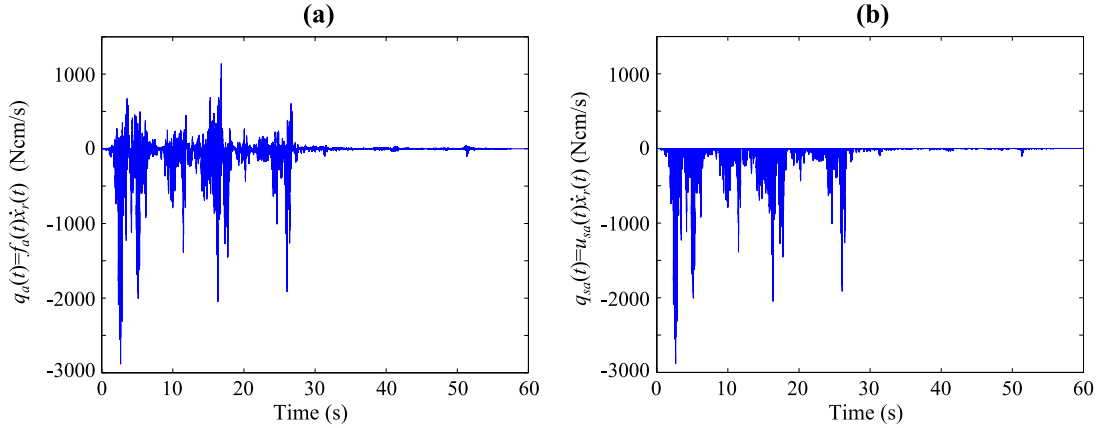


Figure 40. Indicative example of the “power” scheme/demand practised in (a) Active; and (b) Semi-active control.

When a variable damping (VD) STMD is considered, the method of achieving enhanced performance is by appropriately and in a timely fashion adjusting the damping coefficient of the device within bands, in order for the required control force to be reached. By referring back to the system presented in Figure 39, the semi-active damping force contribution can be expressed as $c_{sa}(t)\dot{x}_r(t)$. Inspection of Eq.(5.9) easily leads to $c_{sa}(t) < 0$. Updating Eq.(5.6), the resulting overall control force provided at each time instant by a VD-STMD can be expressed mathematically as:

$$u_{sa}(t) = (|c_{sa}(t)| + c_n)\dot{x}_r(t) + k_p x_r(t) \quad (5.10)$$

In Eq.(5.10), c_n is a small damping coefficient representing the inherent damping of the connection of a semi-active device and the structural system. In this equation, the time-varying semi-active damping coefficient, $c_{sa}(t)$, is the only unknown, making the calculation of the real-time variation of the damping coefficient straightforward.

5.2.2 Modeling the Semi-Active Hybrid Mass Damper

Through the use of an SHMD, the energy-dissipation capacity of a semi-active device is exploited and energy is added only when required through force

actuators. The main difference between an ATMD and the novel SHMD configuration lies in the fact that the actuators of the ATMD both add and dissipate energy, whereas the forcing provision of the SHMD can only add energy. To this end, it can be realised that when the actuators of the ATMD are required to add energy to the system, sufficient power should be provided so that the “braking” force acting on the DVA’s mass by the passive damping elements of the ATMD is surpassed for the mass to be accelerated, and sufficient control force can then be applied to the system. On the contrary, the novel SHMD configuration lowers the active actuation demands by lowering the semi-active damping component to its minimum value throughout the period of active actuation. The steps required for the implementation of this configuration and the calculation of the envisaged control action, $u_{shmd}(t)$, are explicitly introduced below and summarised in Figure 41:

- (1) Design of a semi-active controller based either on an active controller that is clipped using Eq.(5.7) for semi-active control purposes or using direct output feedback control algorithms such as the ones found in the groundhook control scheme for alleviation of the online computational burden of Eq.(5.7) and Eq.(5.8).
- (2) Design an active controller using active control algorithms such as LQR, PID or similar designed to satisfy performance and robustness specifications of the non-linear system (i.e., system including the semi-active controller).

- (3) Limit the capacity of the active actuator to only add power to the system:

$$q_a(t) = f_a(t)\dot{x}_r(t) > 0 \quad (5.11)$$

- (4) Incorporation of both active and semi-active forces to the system using:

$$u_{shmd}(t) = u_{sa}(t) + f_a(t) \quad (5.12)$$

- (5) Optimisation of maximum and minimum damping ratios of the semi-active control device for the case of on-off control.

Using the steps described, the resulting control signals relative to the active control counterpart should attain the form shown in Figure 42(b),(c). Evidently, the active control component of the novel device configuration (Figure 42(c)) can only supply force in the $q_a \geq 0$ regions, whereas the semi-active control component is able to only supply force in the $q_a \leq 0$ regions. With reference to Figure 42(b), the fifth and final step of the SHMD design procedure, the optimisation of the maximum and minimum damping coefficients of the semi-active component determines the slope and the magnitude of the control signal which in turn severely influence the performance of the hybrid system.

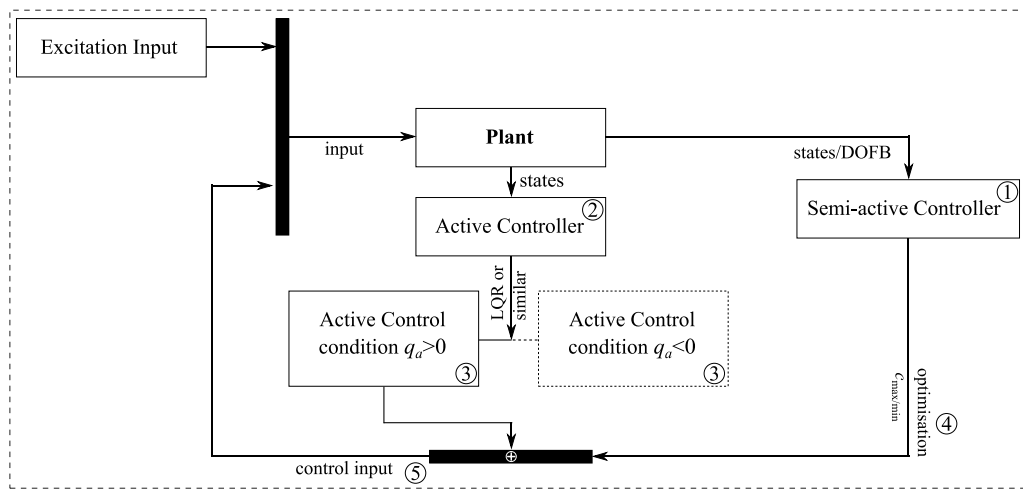


Figure 41. A schematic representation of the procedure followed for modeling the semi-active hybrid mass damper.

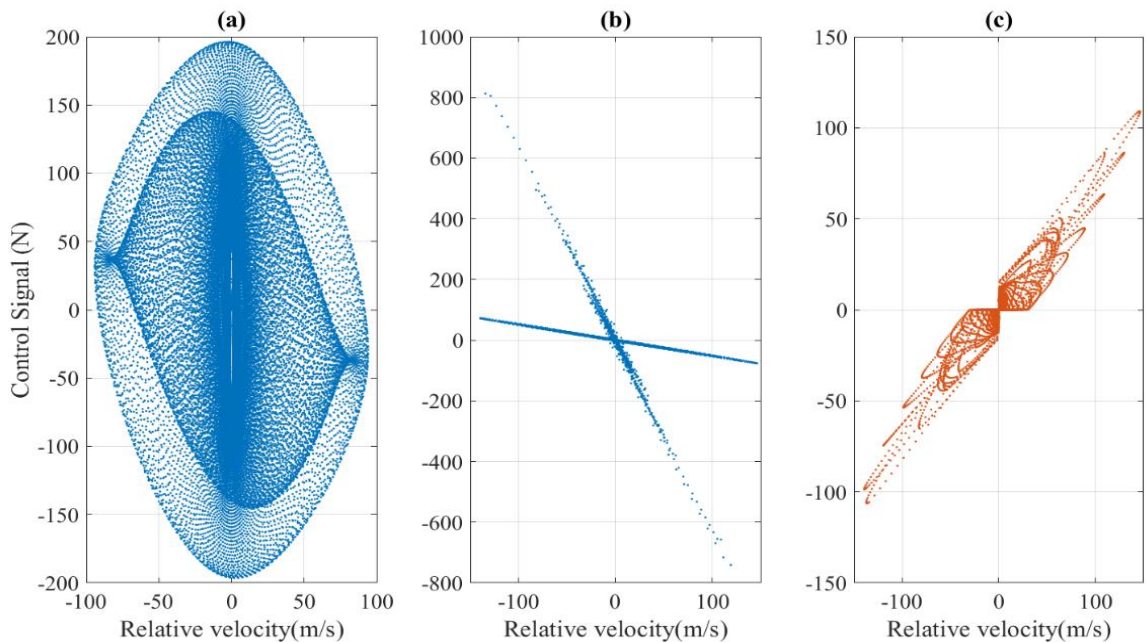


Figure 42. Control signals as a function of relative velocity for the (a) Purely active system; (b) Semi-active component; and (c) Active component of the hybrid configuration subjected to a white noise excitation.

5.3 Control Methods

Obtaining the semi-active and active forcing components is achieved via the use of control algorithms. In this study, for the purely active control case, the algorithm of choice is the optimal LQR that was proven suitable in a series of studies (Yang et al., 1987, Soong, 1990, Yang et al., 2004, Cheng et al., 2008) for use on flexible structural applications. The design of the controller (i.e., the determination of the weighting matrices which are required in the determination of the control gains) is based on the performance index defined in (Soong, 1990). For the case of semi-active control, the displacement based groundhook algorithm that belongs to the category of direct output feedback controllers (i.e., the control actions are calculated based on a limited number of measurements) is selected. The choice of this direct output feedback controller for the case of semi-active control is based on the reduction of the computational effort required for the online calculation of Eq.(5.7) and Eq.(5.8), requirement of minimum state measurements as well as its enhanced performance over other conventional direct output feedback controllers as shown in the studies of (Viet et al., 2014, Demetriou et al., 2015b). The mathematical expressions describing the control algorithm used in the derivation of the control actions are found in (Koo, 2003, Koo et al., 2004).

With reference to Section 2.2, and because of the fact that semi-active control precedes the design of the active controller, the incorporation of semi-active control to the system results in a configuration that is no longer linear but piecewise linear, generating the need for linearisation before a purely active controller is designed. In this study, the linearisation of the piecewise linear system is performed via input/output subspace SSARX identification using MATLAB's (MATLAB2016a, The MathWorks Inc., Natick, MA, USA, 2016) system identification toolbox. To this end, a purely harmonic signal with known frequency and amplitude is used as the external input to the system. The displacement of the structural mass was used as the output. From this, a four-state equivalent linear system is constructed and the state matrices are extracted for use in the active controller design procedure.

5.4 Numerical Investigation

5.4.1 Single Degree of Freedom (SDOF) Structural Configuration

In order to quantitatively capture the performance gains of the proposed system on both the transient and steady-state components of the vibration response, four alternatives, namely passive (TMD), semi-active (STMD), active (ATMD) and semi-active hybrid (SHMD)-equipped (low-damped) SDOF structures, are investigated. For the simulations, the mass and stiffness of the SDOF structure is selected such that the resulting mass ratio of the structural mass to the mass of the damper is 1% and the frequency of the system is approximately 1 rad/s, typical for high-rise structural applications. The resulting mass, stiffness and damping matrices used in the simulations are:

$$M = \begin{pmatrix} 1000 & 0 \\ 0 & 10 \end{pmatrix} \text{Kg} \quad K = \begin{pmatrix} 1009.9 & -9.9 \\ -9.9 & 9.9 \end{pmatrix} \text{Ns/m} \quad (5.13)$$

$$C = \begin{pmatrix} 51.22 & -1.22 \\ -1.22 & 1.22 \end{pmatrix} \text{Ns/m} \quad C_w = \begin{pmatrix} 50.04 & -0.04 \\ -0.04 & 0.04 \end{pmatrix} \text{Ns/m}$$

In Eq.(5.13), C is the damping matrix used for the case of TMD control, and C_w is the damping matrix used for the case of STMD, ATMD and SHMD control. It is evident that for the case of passive control, a damping ratio of 6.1% and stiffness tuning ratio of 0.9 derived using Den Hartog's expressions found in (Hartog, 1956) are used for optimal passive behaviour and maximum rms reduction at steady state. For the remaining three control cases, a minimal damping ratio of 0.2% is used in order to capture the inherent damping of the connection of the damper and the structural mass.

5.4.1.1 Variable Damping Coefficient Configuration

For the fairness of the comparison and consistency with the optimisation procedure followed for the case of passive TMD control, the selection of the variable damping coefficients for the case of the semi-active and hybrid controlled SDOF systems is performed via examination of the rms acceleration response of the system at steady state. To this end, an investigation of the acceleration response for maximum damping ratios (

$\zeta_{\max} = c_{\max} / 2m_d\omega_n$) ranging from 1% to 100% of the critical damping is carried out, the results of which are presented in Figure 43 and Figure 44. With reference to Figure 43a, for the STMD-equipped system, at higher damping ratios, the acceleration response of the structural mass reduces and the distance between the side lobes increases. On the contrary, for the SHMD-equipped system (Figure 43b), it can be observed that at low damping ratios, it has a performance inferior to its STMD-equipped counterpart. Nevertheless, as the damping ratios increase beyond the value of 0.3, the performance of the SHMD-equipped system drastically improves, reducing the acceleration response while at the same time pushing the side-lobes of the response further apart. The comparison of the two systems as a function of the damping ratio is shown in Figure 43c which presents the difference of the acceleration responses of the two systems (i.e., $\ddot{x}_{shmd}(\omega) - \ddot{x}_{stmd}(\omega)$). Owing to the selected sign convention, negative values in Figure 43c indicate performance gains of the SHMD over the STMD system, while positive values indicate performance loss. For clarity, the two-dimensional acceleration response of the STMD and SHMD controlled systems for maximum damping ratios of 0.3, 0.5, 0.75 and 1 is presented in Figure 44. The average response of the systems over the wider range of frequencies is captured by the area under the response curves as illustrated in the same figure.

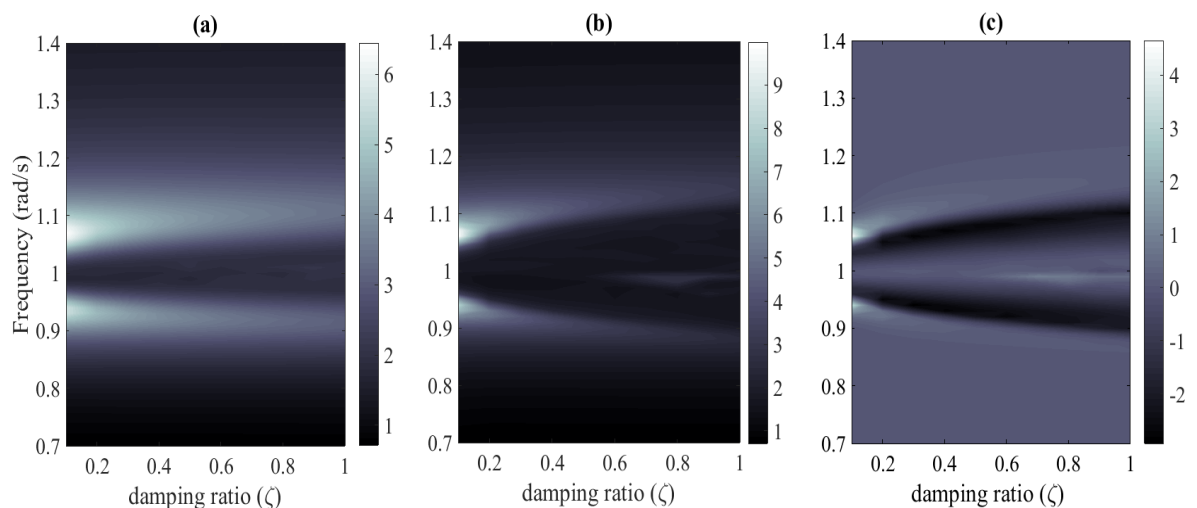


Figure 43. Acceleration response of (a) STMD; and (b) SHMD; and their (c) Difference at different damping ratios. (Units of acceleration response in $m^2 / s^3 / rad$).

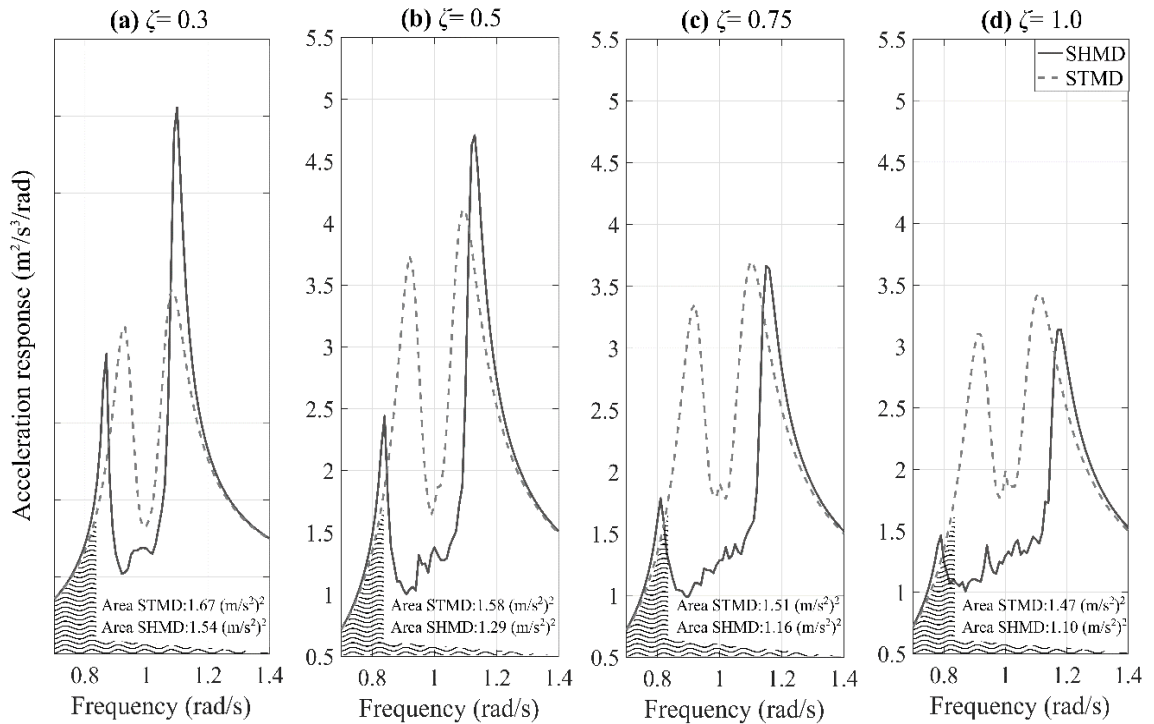


Figure 44. Acceleration response at steady state for damping ratios of (a) 0.3; (b) 0.5; (c) 0.75; and (d) 1. Shaded area illustrates average system response.

For the case of the SDOF, the performance of the novel hybrid configuration is investigated at the average maximum damping ratio of 0.5. Similar to the passive (TMD) optimisation procedure, when practical constraints are applied such as force and stroke saturation limits (for the case of the MDOF system), further numerical optimisation is carried out and appropriate values of maximum damping coefficients are selected. For the fairness of the comparison, the SDOF the STMD configuration is also designed with a maximum damping ratio of 0.5.

5.4.1.2 Free vibration analysis

For the first set of simulations, the SDOF is given an arbitrary initial displacement of 10 cm and is allowed to vibrate freely. Figure 45(a),(b) illustrate the system's displacement along with the active and semi-active forces required by the SHMD system.

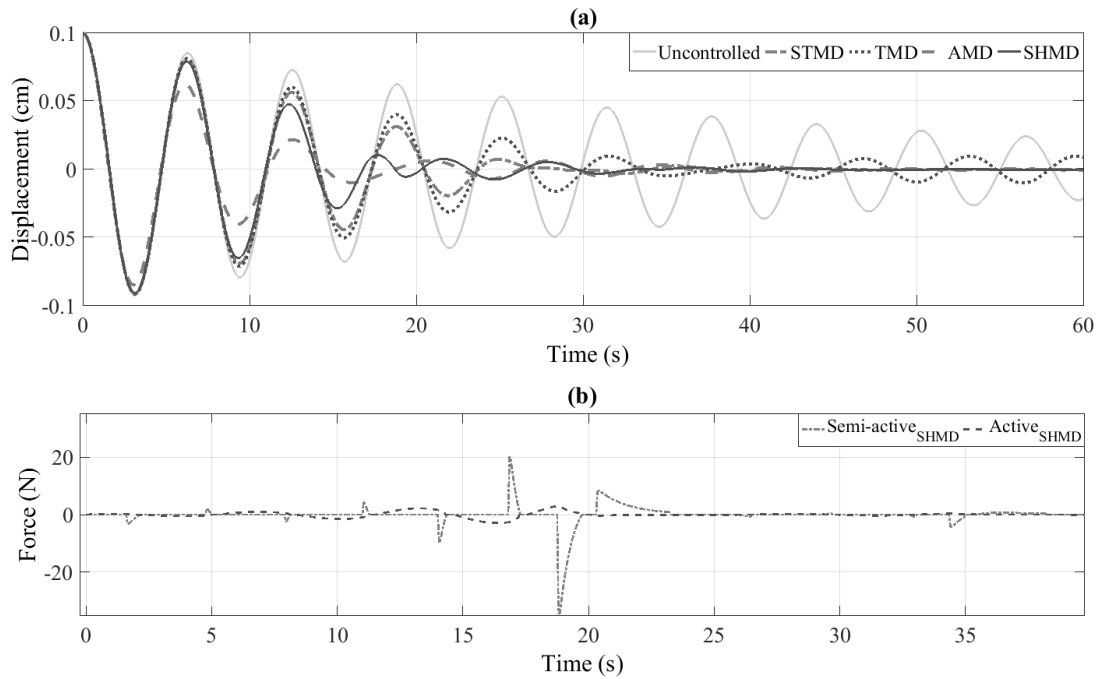


Figure 45. (a) Displacement response time history of different control configurations; (b) Control signal of active component and semi-active component of the hybrid configuration.

Clearly, the rate of decay of the system's response is a good primary indication of its effective damping. In this regard, it is shown that at the absence of a DVA, the low damped structure requires a much longer settling time. On the other hand, once a DVA is employed in the form of TMD, STMD, ATMD and SHMD the settling times drastically decrease, thereby demonstrating the effective damping of each of the five structural configurations. More specifically, out of the four DVA configurations, the SHMD and ATMD seem to be superior to their purely passive and semi-active counterparts. As a matter of fact, it is evident that the system coupled with an SHMD device follows closely the trajectory of the AMD-equipped, one particularly at the late part of the vibration response.

5.4.1.3 Forced vibration

Systems equipped with devices such as STMD (and also SHMD) are no longer linear but piecewise linear. For many non-linear systems, the response magnification factor may depend on the type and magnitude of the excitation and the resulting structural response might be of random non-periodic nature. Yet, following the proof of Hac and Youn (Hac and Youn, 1992, Pinkaew and

Fujino, 2001), the response of piecewise linear second-order systems to periodic excitation is also periodic, and the amplitude ratio is independent of the excitation amplitude. In other words, exciting the structure using a periodic wave of notional amplitude allows for meaningful performance information in the frequency domain. Figure 46 exhibits the time history response of the structural configurations under harmonic excitation with frequency equal to the structural frequency. For clarity, only the response time histories for the cases of STMD, ATMD and SHMD and TMD are presented. Complementing these results, Figure 47 illustrates the continuous (running) displacement rms for each of the different structural configurations.

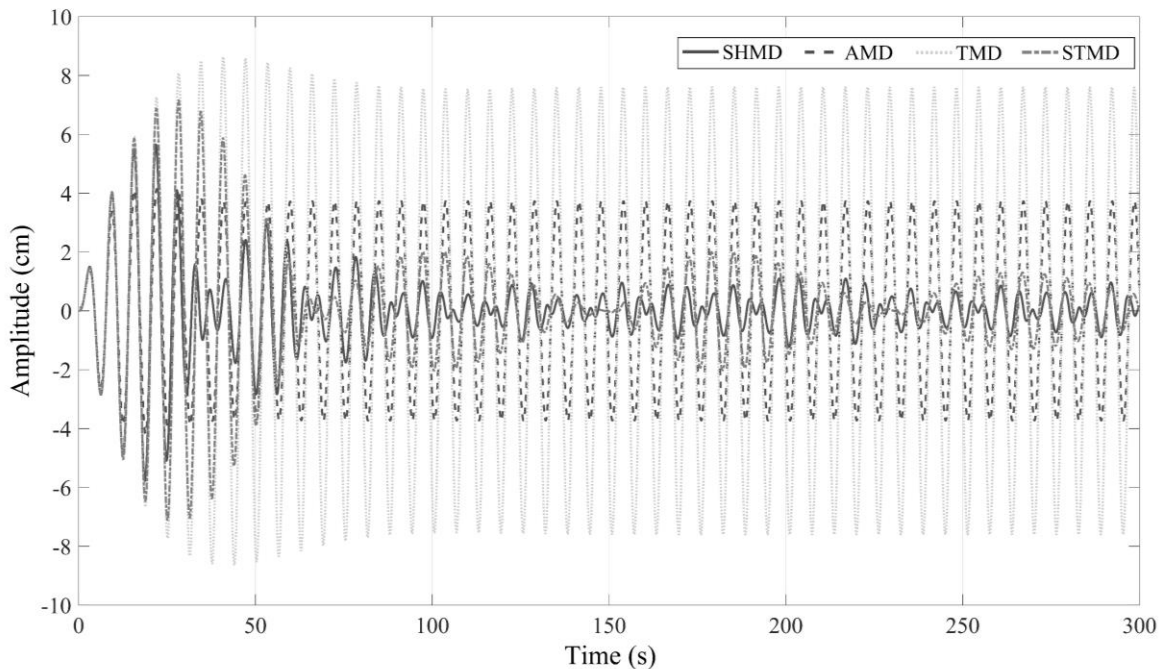


Figure 46. Transient and steady-state response of the different control device configuration under harmonic loading at tuning frequency (excitation frequency 1 rad/s).

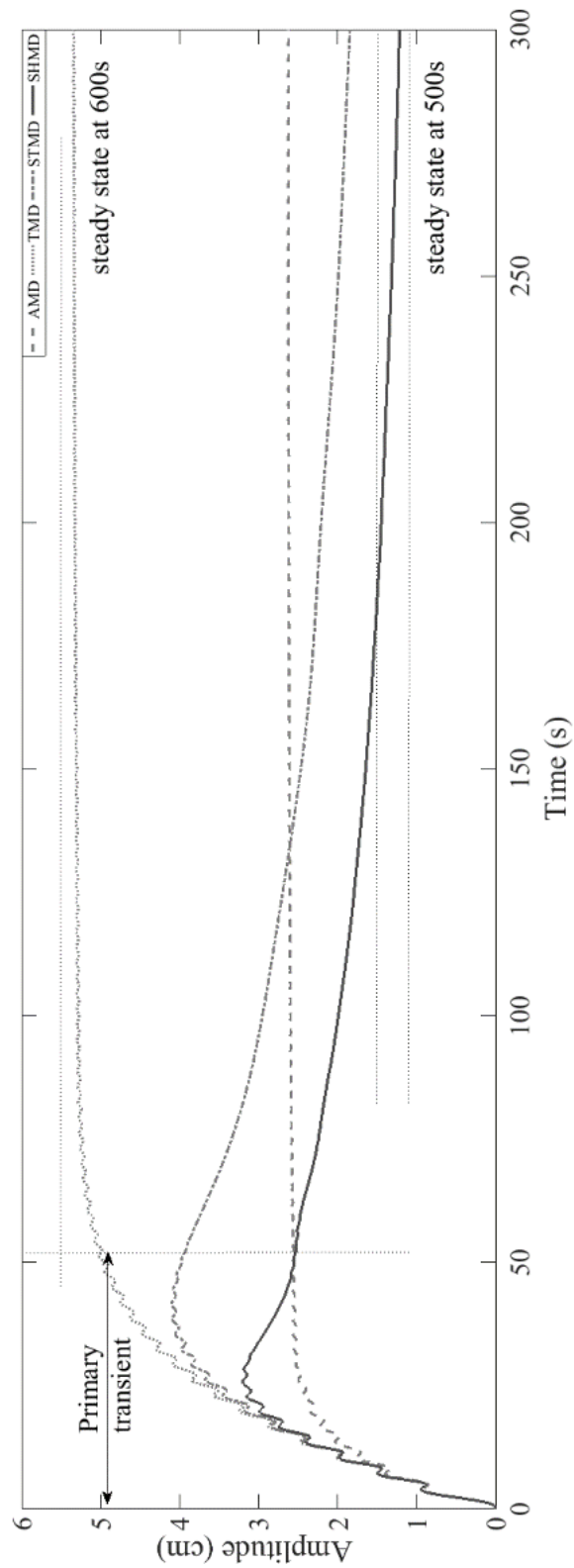


Figure 47. Transient and steady-state Crms response of the different control device configuration under harmonic loading at tuning frequency (excitation frequency 1 rad/s).

It is evident that under resonant forced vibration, the ATMD, STMD and SHMD clearly outperform the more conventional passive TMD under both the transient and steady-state parts of the vibration. Additionally, under the transient component of the vibration, the ATMD and SHMD devices are superior to the STMD. On the other hand, under steady state, the STMD is shown to be significantly better than the ATMD configuration, achieving steady-state response closer to the system equipped with the novel SHMD configuration. Similar remarks can be made after investigating the steady-state and peak frequency response functions (the response of the system at different frequencies, shown here as the ratio of the frequency of the external perturbation, F_e and the natural frequency, F_n of the structure) of the systems. Figure 48a,b illustrate that the novel device configuration achieves the best compromise between steady-state and transient performance.

5.4.2 Effect of mass and stiffness variation

In this section of the thesis, the effect of mass ratio ($\mu = m_d / m$) and stiffness uncertainty ($k_s \times \% \text{ uncertainty}$) on the frequency response functions of the novel structural configuration is investigated. For the purposes of realism and clarity of the results, the selected mass ratios ranged between 1%-10%, while the stiffness uncertainty ratio was varied between 80% and 120% (indicating reduction and increase in stiffness respectively). In contrast to the parametric analysis run in section 4.3, the purpose of this parametric study is to illustrate the performance of the control system for the case where a baseline optimal controller is applied. Clearly, if optimal performance is desired, system identification based on the procedures described in section 5.3 and optimal control design at each mass ratio should be carried out. It is reasonable however that such parametric analyses are important in showing the trends of the novel configuration at different mass ratios and stiffness uncertainty. Additionally, it is believed that such parametric analyses serve as a good first indication on the robust stability of the novel configuration.

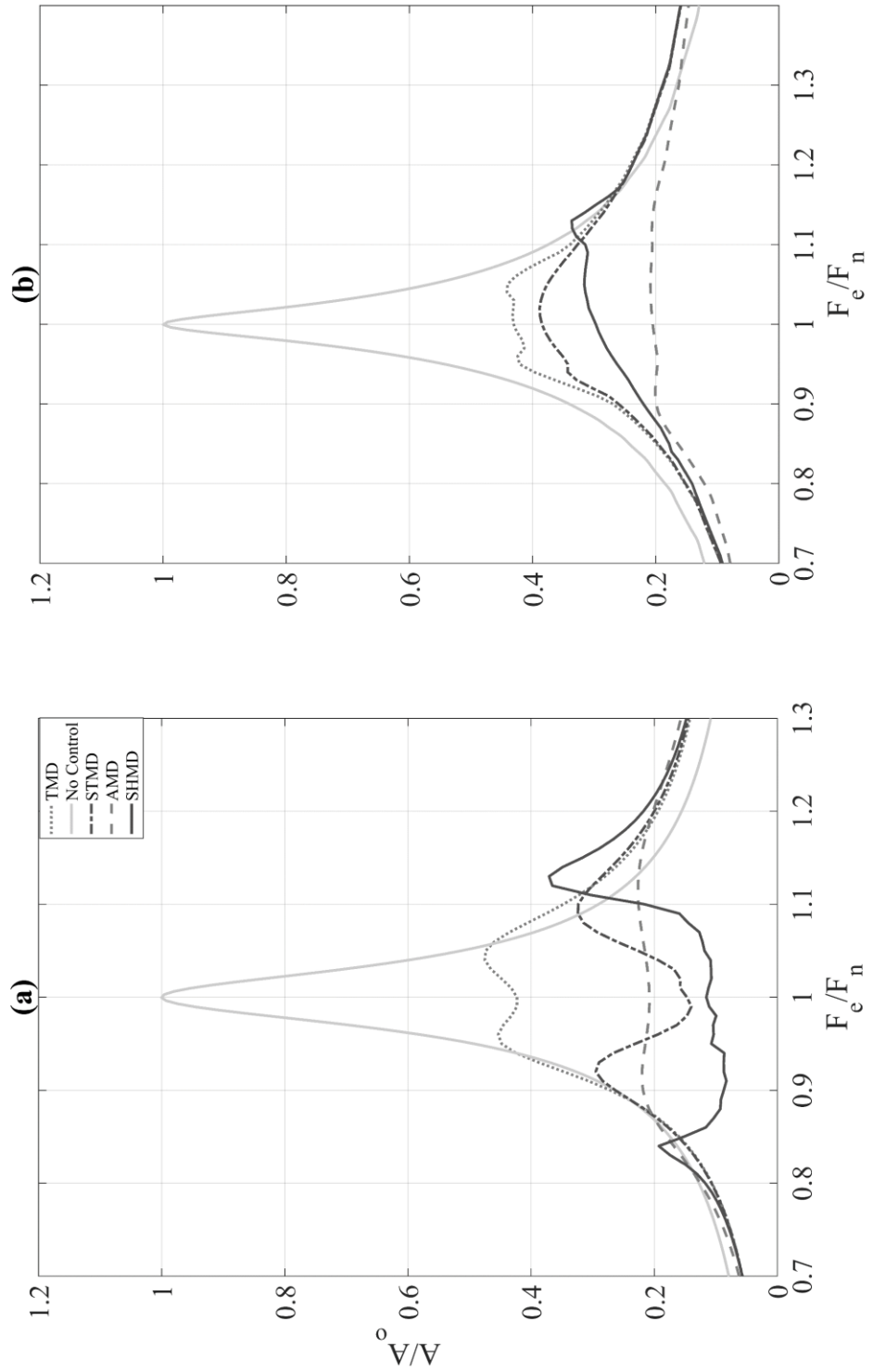


Figure 48. (a) Steady-state; and (b) Peak frequency acceleration response of the different structural configurations.

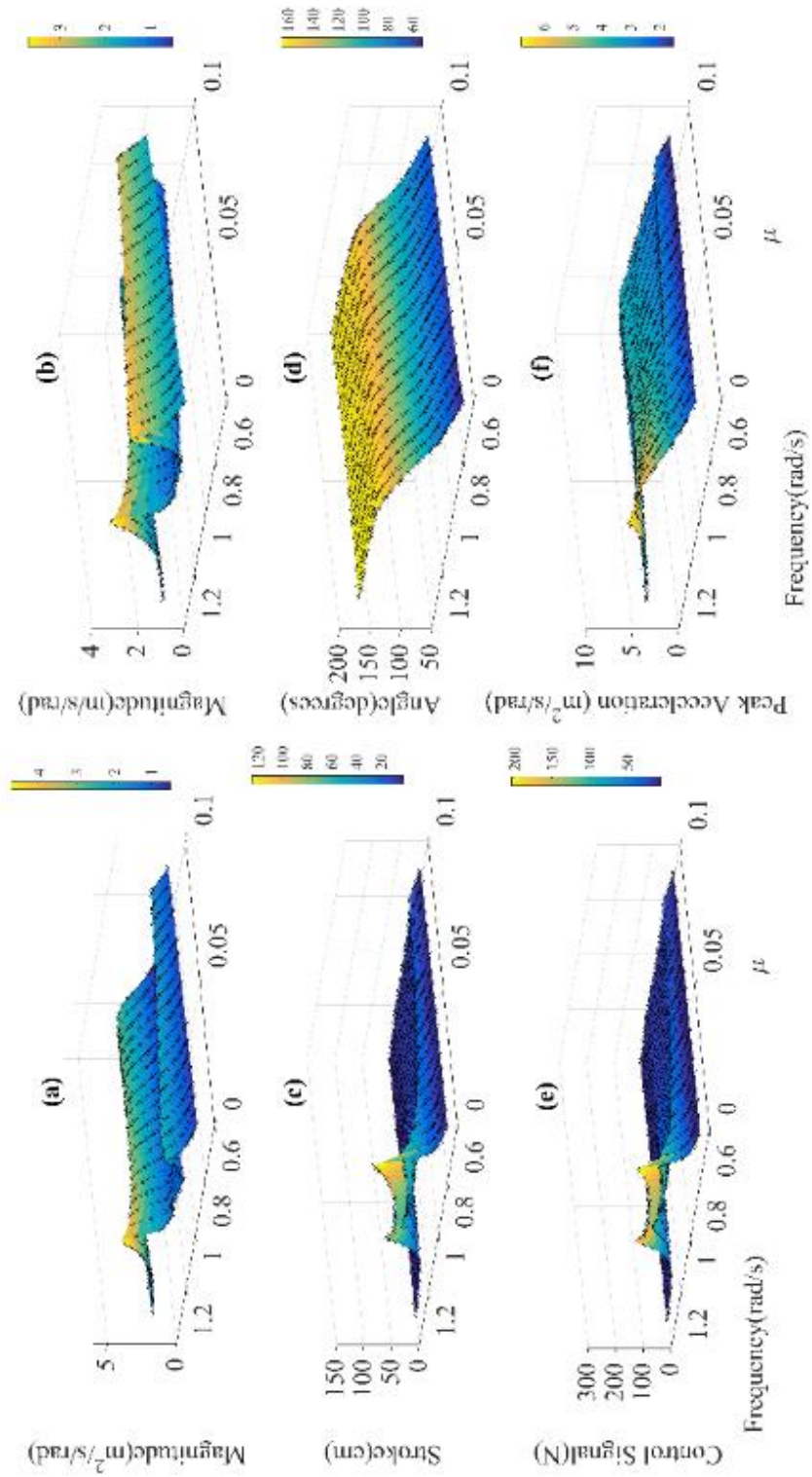


Figure 49. (a) Acceleration response, (b) Displacement response, (c) Maximum stroke, (d) Angular phase, (e) Control signal, and (f) Peak acceleration as a function of the mass ratio (μ) and frequency.

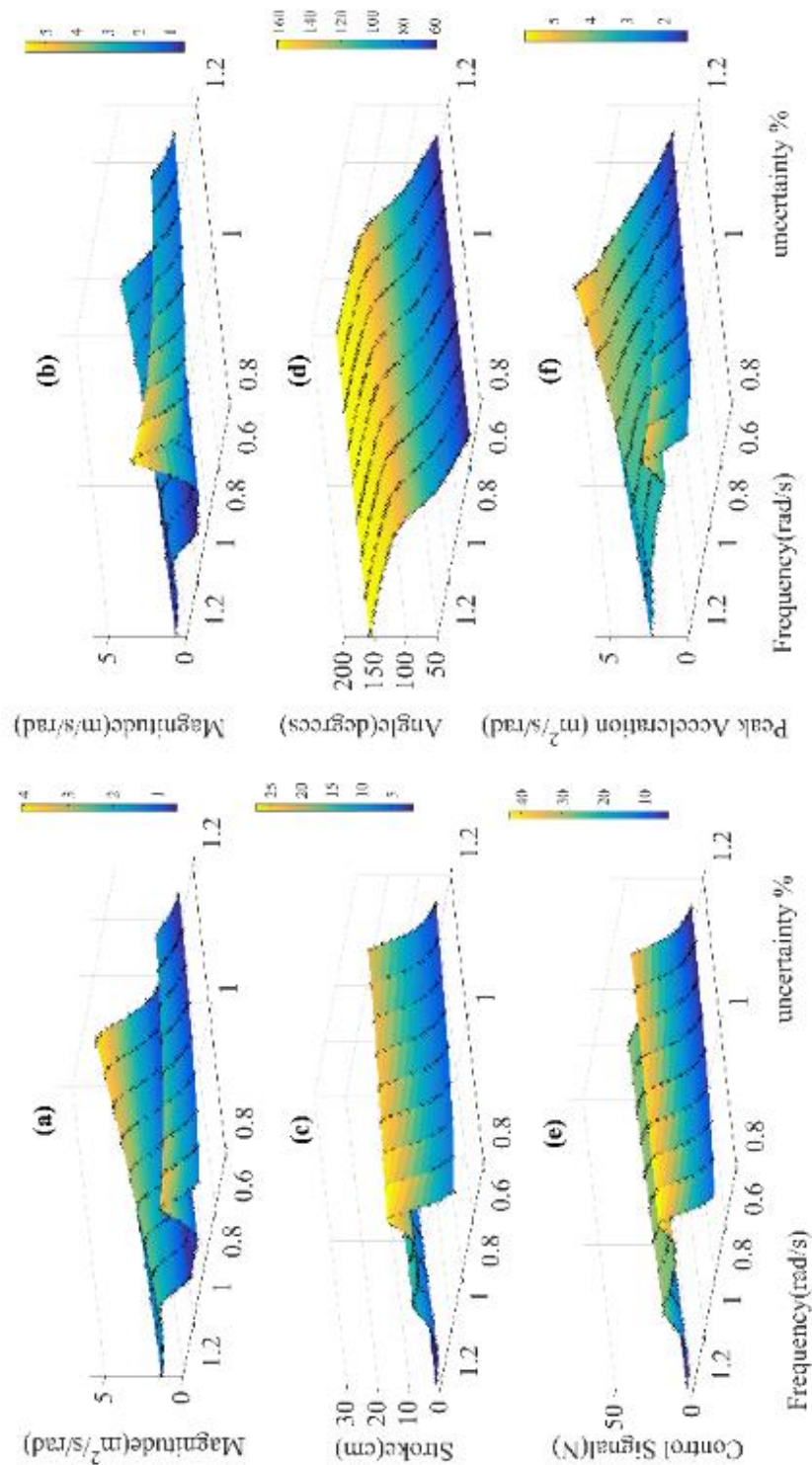


Figure 50. (a) Acceleration response, (b) Displacement response, (c) Maximum stroke, (d) Angular phase, (e) Control signal, and (f) Peak acceleration as a function of stiffness uncertainty percentage and frequency ($\mu = 0.05$).

With respect to Figure 49 and Figure 50 some remarks can be made. Firstly, for given control gains, at increasing mass ratios an improvement in performance is observed, while the stability of the system is maintained (indicated by the angular phase of the system (Figure 49d). In addition to this, as the mass ratio is increased, the active control system attains less and less importance as indicated by the reduction in the control force (Figure 49). This is to compliment the arguments made earlier, suggesting the need for system identification. The reduced contribution of the active control force to the response of the system is also shown in Figure 51b. In this figure, at increasing mass ratios, the energy consumed by the novel configuration converges to the energy consumed by the conventional STMD device. With regards to parametric stiffness uncertainty and for given mass ratios (5%), the device maintains stability (Figure 51a) while also maintaining expedient performance over the STMD and TMD devices.

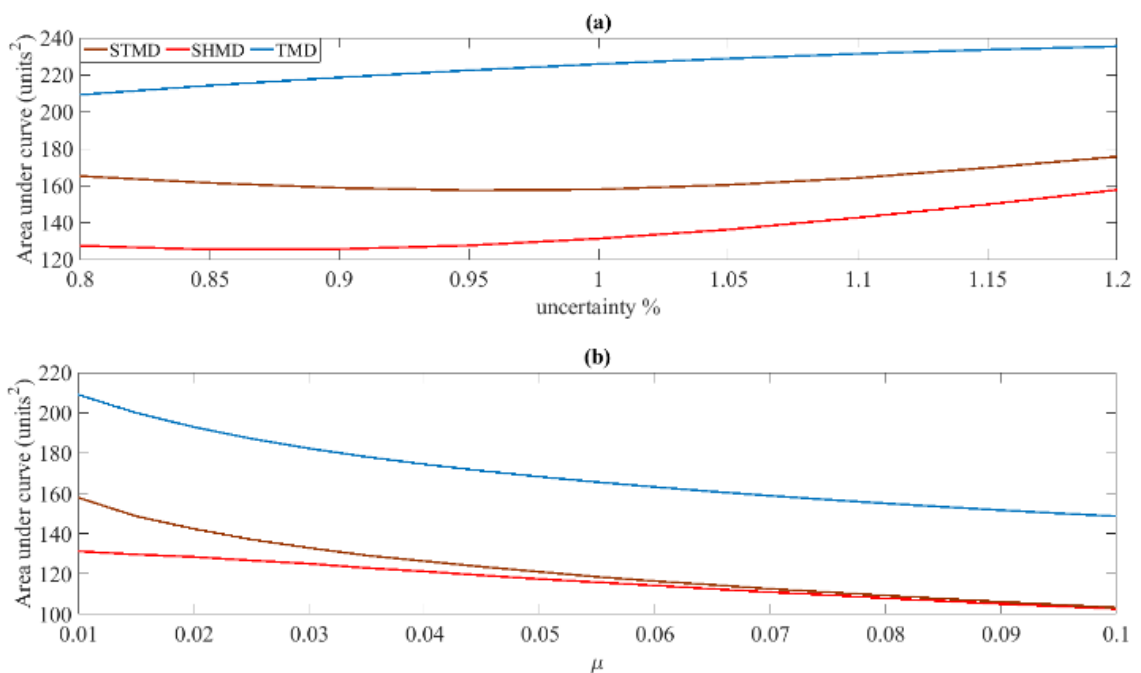


Figure 51. Energy dissipation as a function of (a) Stiffness uncertainty and (b) Mass ratio for the different structural configurations

5.4.2 High-Rise Structural Configuration

In order to establish the robustness of the novel device and its ability to reduce wind vibration response, it is important to evaluate its performance on realistic

high-order systems for which constraints such as actuator force-power demands and damper strokes can be taken into account. To achieve this, the 76-storey benchmark wind-sensitive sway structure proposed by Yang et al. (Yang et al., 2004) is used in this study. The building has a square $42\text{ m} \times 42\text{ m}$ cross-section, with a height to width aspect ratio of 7.3 and a low natural frequency that lends it the wind sensitivity attribute. A simplified planar finite element model of the structure is constructed by considering the portion of the building between two adjacent rigid floors as a classical beam element of uniform thickness, leading to 76 rotational and 76 translational degrees of freedom. From these, all the rotational degrees of freedom have been removed using static condensation, leading to a lumped mass sway model with degrees of freedom, representing the displacement of each floor in the lateral direction. The resulting simulated structure has a total mass of 153,000 tons, with the first five frequencies at 0.16, 0.765, 1.992, 3.790 and 6.395 Hz, and corresponding modal structural damping ratios of 1% calculated using Rayleigh's approach. In this study, four alternatives, namely: passive (TMD), semi-active (STMD), active (ATMD) and semi-active hybrid (SHMD) controlled structures are used for the establishment of the comparison metrics. The assemblage of the different control configurations is depicted in Figure 52.

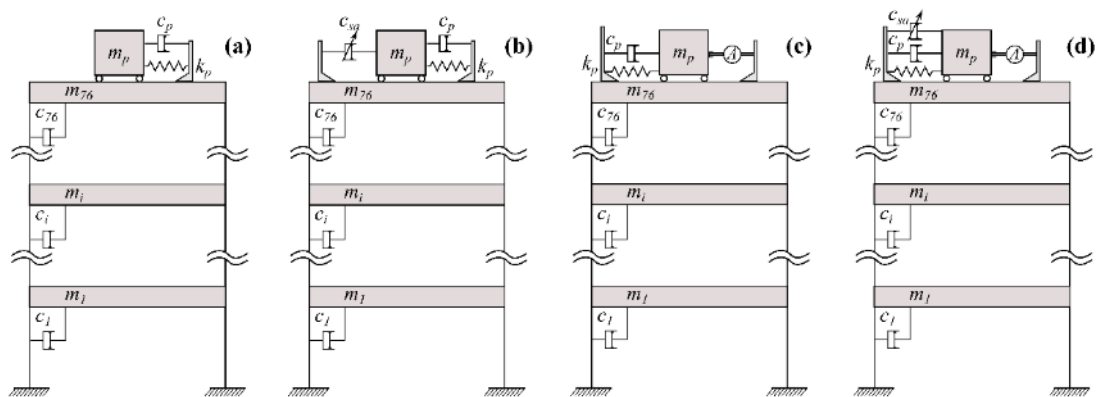


Figure 52. Ensemble of all the different control options (a) TMD; (b) STMD; (c) ATMD; (d) SHMD studied herein for the model 76-storey structure of Yang et al. (Yang et al., 2004).

In every control configuration, the dynamic absorber comprises an inertial mass of 500 tons that corresponds to 0.356% of the total structural mass, limited by realistic structural design constraints. For DVA configurations that require tuning of the device (i.e., TMD, SHMD and STMD), appropriate spring

stiffness, k_p , is chosen such that the device is tuned to the fundamental frequency of the structure (i.e., ≈ 0.16 Hz). In order to ensure the fairness of the comparison, it was deemed necessary to restrain the maximum damper stroke of each of the alternatives by increasing the damping coefficient of the device appropriately so as to limit strokes to a maximum of 95 cm. Because control configurations that damper strokes are not a cause of concern, such as the case of the TMD, the damping ratio is numerically optimised (and kept low, approximately to the value calculated using Den Hartog's equations (Hartog, 1956)) for maximum rms acceleration response reduction. The resulting damping coefficients that equalise the maximum strokes at maximum rms acceleration response reduction are outlined in Table 5 below:

Table 5. Damping coefficients.

Control Strategy	Max Damping Coefficient (kNs/m)	Min Damping Coefficient (kNs/m)	Equivalent Damping Ratio
TMD	47	47	4.7%
STMD	163.4	2.61	16%–2.6%
ATMD	100	100	10%
SHMD	168	39	16.8%–4%

5.4.3 Evaluation Criteria

For the evaluation of the relative performance of the different structural control configurations the same 12 evaluation criteria defined earlier in section 4.4.5 and summarised below in Table 6 are used.

Table 6. Summary of evaluation criteria

Index	Description
J_1	Maximum floor rms acceleration (among a floor selection)
J_2	Average rms acceleration for selected floors
J_3	Maximum rms displacement of top floor
J_4	Average rms displacement for selected floors
J_5	Rms actuator stroke
J_6	Rms control power
J_7	Maximum floor peak acceleration (among a floor selection)
J_8	Average peak acceleration for selected floors
J_9	Maximum peak displacement of top floor
J_{10}	Average peak displacement for selected floors
J_{11}	Peak actuator stroke
J_{12}	Peak control power

5.4.4 Simulation Results and Discussion

Four structural configurations consisting of passive, semi-active, hybrid active and semi-active hybrid control devices were considered for investigating the efficacy of the SHMD device for the vibration control of high-rise structures. Figure 53 summarises the peak and rms (displacement and acceleration) responses at every floor. The results of the evaluation for the different performance criteria J_1, J_2, \dots, J_{12} are presented in Figure 54.

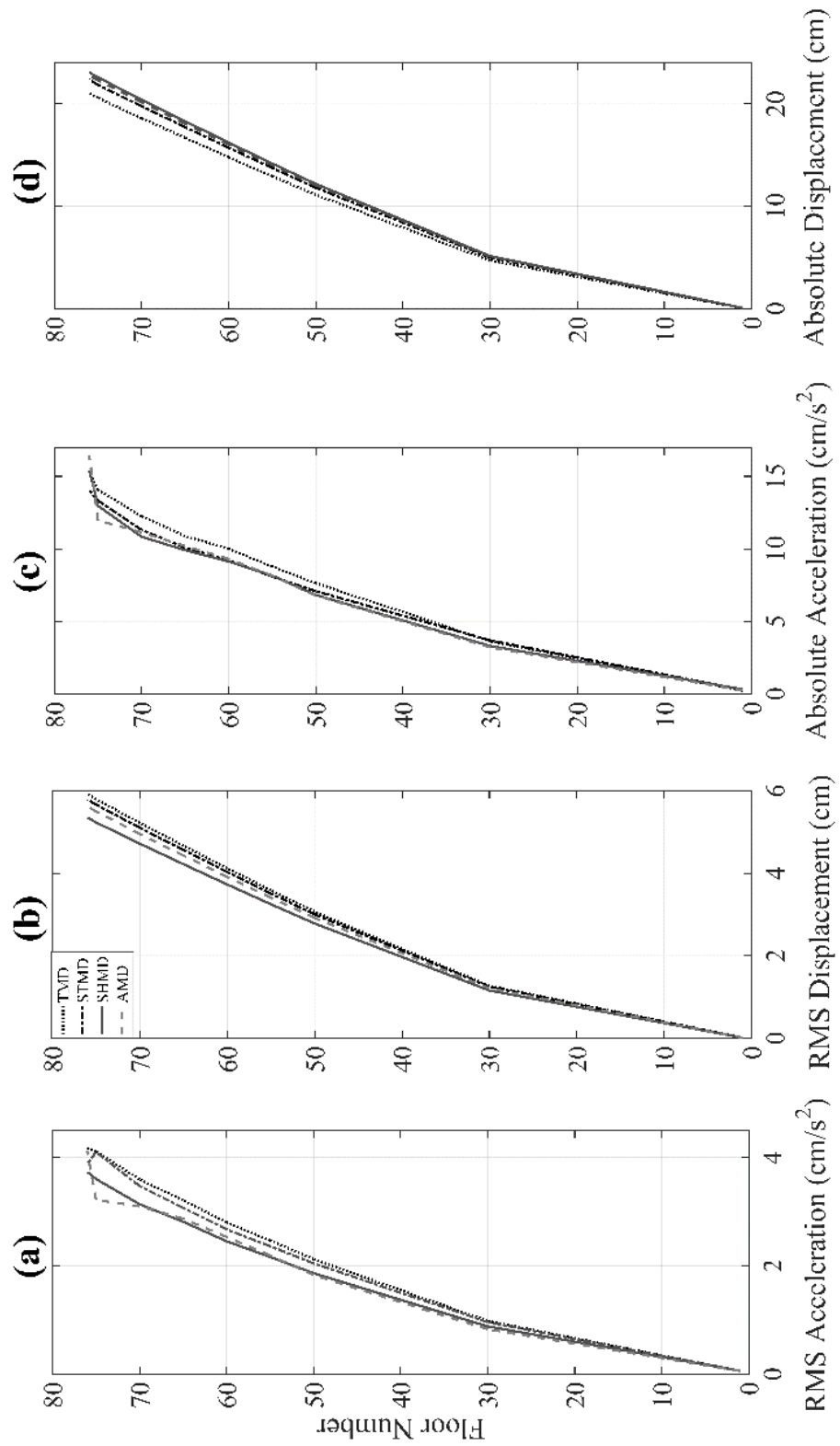


Figure 53. Illustration of the performance of different control measures in terms of (a) rms acceleration; (b) rms displacement; (c) Absolute acceleration; and (d) Absolute displacement at different floor levels.

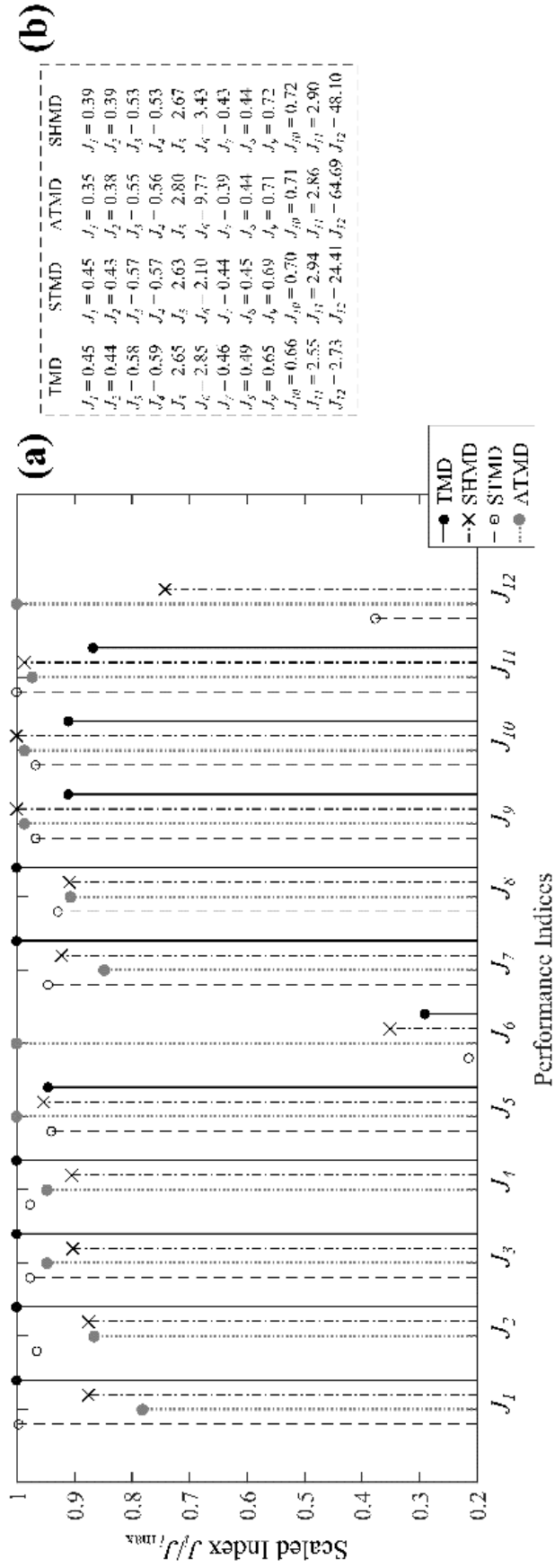


Figure 54. (a) Normalised; and (b) Non-normalised performance indices (lower index indicates better performance).

The results indicate that, for approximately the same damper strokes ($J_{1,1}$), the SHMD-equipped structure is able to achieve similar performance as the ATMD-equipped one, while clearly outperforming the passive and semi-actively controlled alternative.

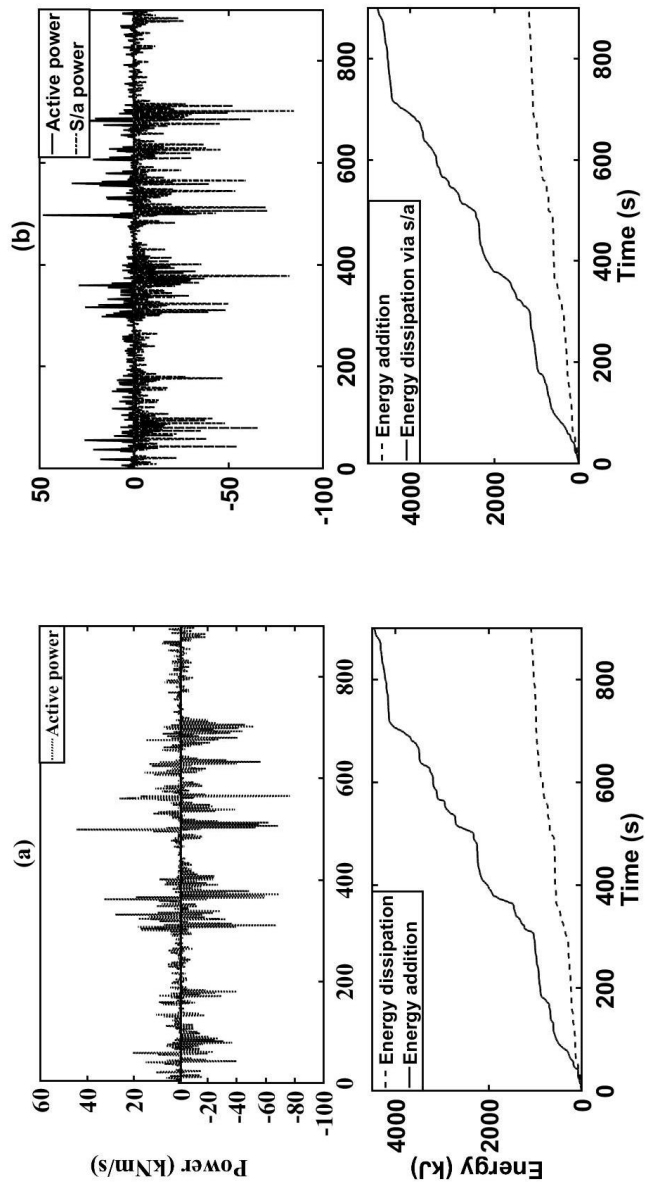


Figure 55. Power and its time integral energy for (a) ATMD; and (b) SHMD configuration. Positive stands for energy addition and negative for energy dissipation.

With reference to Figure 54 and Figure 55, it is evident that the SHMD device requires much less energy and actuation demands for achieving the aforementioned performance increase. As a matter of fact, the SHMD device requires approximately 26% of the total energy required by the ATMD device (1245 kJ compared to 4863 kJ). This is due to the large control effort and consequently the large amount of energy required to be added by the active actuators (approximately 4125 kJ or 82% of the total required active energy) in order to effectively accelerate the mass so that sufficient control force is provided in order to overcome the “braking” force acted by the passive component of the ATMD. Conversely, in the SHMD configuration, while the actuators are accelerating the mass, the semi-active damping component attains its minimum value, minimising the “braking” force needed to be counteracted by the actuators, thus requiring a lower control power (Figure 55b top). The energy required to be added in the SHMD configured structure is only 1245 kJ compared to 4125 kJ (which accounts for the 82% of the total energy required) (Figure 55). On the other hand, for energy dissipation purposes (Figure 55a,b bottom), the ATMD configuration is required to supply only a fraction (737 kJ and the remaining 18% of the total energy) of energy, while the SHMD-equipped structure requires consumption of a staggering 4600 kJ. However, since energy dissipation in the SHMD configuration occurs exclusively in the semi-active elements, the required energy depends solely on the selected semi-active device. Still, regardless of the device, the energy required for semi-active control is not expected to exceed the order of a few watts (Nagarajaiah and Varadarajan, 2005).

For more tolerant damper stroke limits, a lower passive damping ratio can be chosen for the ATMD which will reasonably lower the actuation demands for energy addition. On the contrary, lower damping ratios of the damping device will require the actuators to work harder in dissipating energy by decelerating the mass (and essentially work as an energy-expensive passive damper). The aforementioned arguments are illustrated in Figure 56, in which the power required by a purely active AMD device (i.e., absence of passive damping component) is investigated. As can be observed, the AMD is required to expend most of its energy for dissipation (4500 kJ as opposed to the 720 kJ required by the ATMD counterpart), while only a small fraction of that energy

is required for energy addition (approximately 1100 kJ). It should be clarified that no further comparisons can be made with the purely active AMD system, as its performance is theoretically uncapped (the larger the control effort, the lower the response).

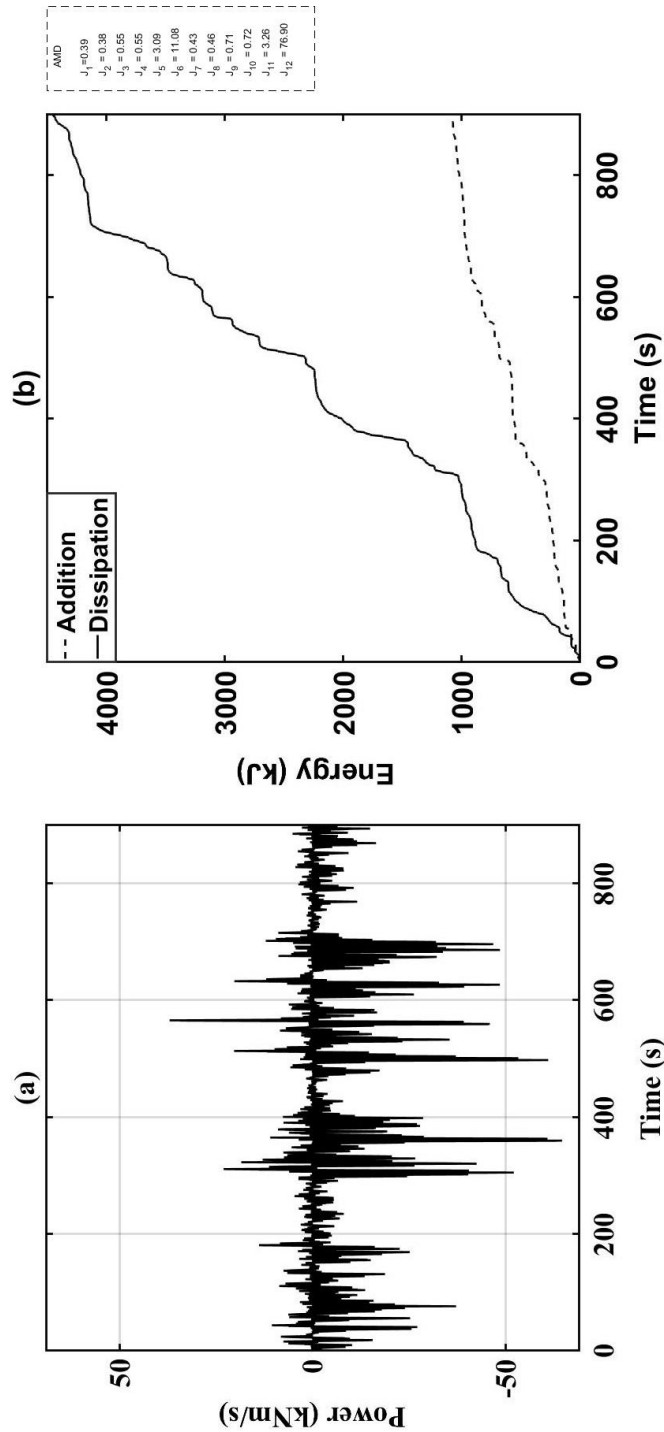


Figure 56. Power and its time integral (dotted line) energy of a purely active mass damper (AMD) system (no passive damping component) along with the corresponding performance indices. Positive stands for energy addition and negative for energy dissipation.

5.5 Conclusions

In this chapter of the study, a novel hybrid control device configuration termed semi-hybrid mass damper (SHMD) has been proposed as an alternative design to the traditional hybrid active-tuned mass damper (ATMD) for vibration suppression of dynamic structural systems. The fundamental novelty of this configuration is that it enables modulation of the instantaneous effective system damping via the successive and appropriate action of active and semi-active elements. For this case, the active components of the SHMD device are regulated by an optimal Linear-Quadratic-Regulator (LQR) controller, while the semi-active components are controlled via a direct output feedback displacement based groundhook (DBG) controller. A numerical step-by-step procedure for the calculation of the control actions and the coupling of the devices has been proposed in this chapter. Under vibration analyses run on both single degree of freedom (SDOF) and multi-degree of freedom (MDOF) SHMD configured structures, it is shown that the device is effective in reducing both the steady-state, as well as the peak frequency responses of the structural system, achieving similar performance gains to that of an ATMD-equipped structure. However, its achievement is not only the use of this novel hybrid mass damper configuration as a vehicle for enhancing vibration attenuation performance or providing a fail-safe mechanism, it is also shown that the successive action of active and semi-active elements allows an improvement in efficiency both in terms of power and actuation demands. By providing a feasible, reliable, effective and efficient alternative structural control approach, this novel hybrid configuration allows the concept of active control of structures to be extended to one of “active” structures for which both active and semi-active components are integrated and simultaneously optimised to produce a new breed of slenderer, longer and taller structures and structural forms.

Chapter 6

In Search of a Suitable Method for SHMD Control

In this chapter of the thesis, an assessment of the correlations between performance and control algorithm selection is performed seeking to optimise the “software” part of the novel SHMD control solution, paying particular attention on the stability of the control system which has not been discussed to this date. In this context, a recently proposed robust control algorithm for implementation with hybrid mass dampers has been tailored for the control of the novel SHMD configuration. The conditions for which this robust controller is applicable in the case of SHMD control have been identified and explicitly stated in this section of the thesis. As an additional step, a modification of the conventional PID controller and robust tuning of its parameters has been proposed in order to provide a more rigorous procedure for the design of active and hybrid (semi-active) control systems using simple and widely used control system architectures. The contents of this chapter are an adapted form of the paper submitted to be included in the Proceedings of Eurodyn 2017 Conference (abstract accepted).

Demetriou, D.; Nikitas, N. Hybrid Semi-Active Mass Dampers in Structures; Assessing and Optimising Their Damping Capacity. X International Conference on Structural Dynamics, EURO DYN 2017, Rome, September 2017. (Submitted)

6.1 Introduction

One of the main limitations of active control is the inability of the system to ensure safe operation upon active component failure. In a more generalised context, active component failure is described by the failure of active elements to provide feedback forces to the structure, rendering the control system unable to guarantee neither performance nor stability. To overcome this limitation and as a minimum stability warrantee, the provision of a fail-safe mechanism via the addition of auxiliary passive devices, as in the case of hybrid (ATMD) mass dampers is considered necessary and appears to govern most practical applications (Ikeda, 2009, Fisco and Adeli, 2011, Hiramoto and Grigoriadis, 2014). Despite ATMDs sharing the property of being fail-safe, they do not always satisfy another aspect of active control design, that is the stability of the system at varying gains, arising either from system parameter variation (due to deterioration of the system, uncertainty in the model etc.) or controller gains.

The traditional approach of examining robust stability of single-input-single-output systems (SISO) using root-locus diagrams is a good indication of the system's ability to maintain stability at varying gains. With reference to Figure 57 which presents a conventionally controlled direct velocity feedback (DVF) ATMD system subjected to a random input, it is observed that as the control gains increase, the low-frequency poles of the mass damper which follow closely the trajectories of the loci (the coloured lines in the root-locus diagram) tend to rapidly destabilise (move in the right-hand plane of the pole-zero map, attaining negative damping values, even at low gains. As a consequence, lowering the feedback gains of the controller to ensure stability will result in a reduction of the effective damping in the actuator, suggesting that the force output (stroke of the mass damper) will be increased.

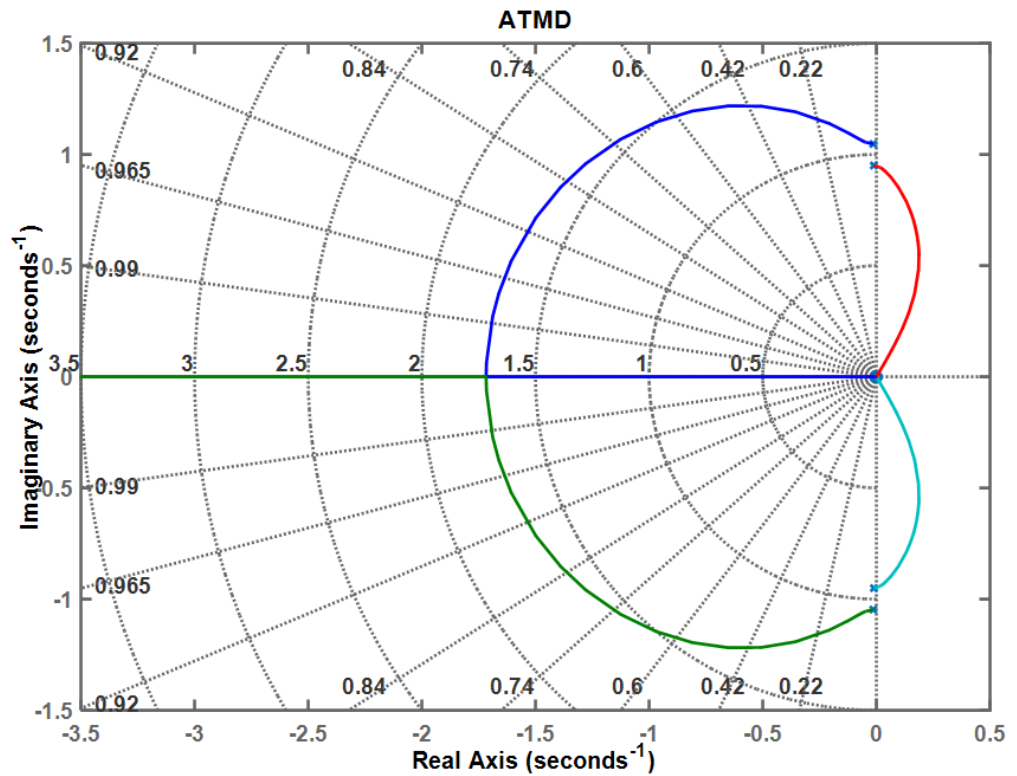


Figure 57. Root locus diagram of the ATMD-SDOF configuration described in Chapter 5

It is understood that the absence of a zero between the pole of the damper (low-frequency pole) and the first pole of the structure is the reason why the loci of the system move rapidly in the right-hand plane. This limitation of rapidly destabilising poles at increasing gains, as well as the associate increase in damper strokes at low gains is believed to be the primary reason why many elaborated control strategies have been introduced for the case of ATMD control. To this end, over the years classical (Burgos et al., 2004), fuzzy (Battaini et al., 1997, Movassaghi, 2012, Zhijun et al., 2014), pole placement (Chang and Yu, 1997, Pan et al., 2011, Rahman and Darus, 2012), Lyapunov (Kim et al., 2004), optimal (Amini et al., 2013), H-infinity (Baoya and Chunxiang, 2012), slide mode (Guclu and Sertbas, 2005) controllers have been presented in literature. Still, none of the aforementioned control strategies is able to guarantee the robust stability of the system at all gains. To overcome this limitation, most recently Collette and Chesné (2016) proposed a robust direct velocity feedback controller based on the principle of

hyperstability for the control of hybrid tuned-mass dampers. To this end, the authors of this publication identify hyperstability as the ability of the system to attain stable poles irrespective to the feedback gain provided. In order to achieve this, they address the root cause of the problem via the placement of a pair of zeros at the right locations of the pole/zero map assuring the closed-loop stability of the system.

In this chapter of the thesis, the control solution proposed by (Collette and Chesné, 2016) is tailored for application with the novel SHMD configuration, discussing whether such control approach and under which conditions can be useful. Following this, the concept of hyperstability is extended in the modification of the conventional PID controller in an attempt to provide a simple and robust (at all control gains) method for the control of both ATMD and SHMD systems. As a comparison metric, the robust stability of the resulting systems and their performance relative to the LQR-SHMD configuration presented in Chapter 5 is investigated.

6.2 Robust ATMD control design (a-ATMD)

The proposed robust controller is designed as the assemblage of two filters in the 's' domain. The first filter is responsible for the placement of zeros in the appropriate locations, whereas the second filter is a high-pass filter that prevents a constant component in the feedback loop. The resulting control action $U(s)$ is calculated by:

$$U(s) = G_c(s)G_{Hp}(s)\dot{x}(s) \quad (6.1)$$

In which, $G_c(s)$, $G_{Hp}(s)$ is the controller and high pass filter respectively and $\dot{x}(s)$ is the velocity of the unsprung mass (structural mass). Since the velocity of the structural mass is used as the control variable, the resulting scheme is a modified version of the simplest form of active control, termed direct velocity feedback. To this end, the controller and high-pass filter are defined as:

$$G_c(s) = \frac{g(s+a)^2}{s^2}, \quad G_{Hp}(s) = \frac{s}{s + \omega_c}, \quad \omega_c = f(a) \quad (6.2)$$

In which a is the tuneable parameter that makes the controller hyperstable (i.e. the poles of the system attain positive damping values irrespective to the

gain), g is the controller gain, the tuning of which depends on the objectives of the controller, and ω_c is the cut-off frequency of the high-pass filter. For the tuning of the a parameter, the frequency of the poles of the system post-application of the TMD must be determined. In this regard, the low frequency pole of the system has a frequency ω_a and a structural frequency ω_b . The robust controller entails that as long $a \in [\omega_a; \omega_b]$ the branches of the root locus go immediately in the left hand-plane satisfying the Routh- Hurwitz criterion (Collette and Chesné, 2016). Figure 58 illustrates how the application of the two filters on the SDOF system(2-DOF post-ATMD application) described in chapter 5 alters the root-locus diagram, moving the loci in the left-hand plane.

6.3 Application of robust control to SHMD device (a-SHMD)

By definition a transfer function is a representation in terms of spatial or temporal frequency, of the relation between the input and output of a linear time-invariant system. Therefore, constructing the transfer functions of the semi-active (STMD) system for application of the robust controller filters and performing stability analyses on the resulting a-SHMD system, necessitates the linearisation of the non-linear STMD system. To this end, and as a first step, system identification is required for the attainment of the linearised state matrices. Following the same procedure described for the tuning of the LQR controller in section 5.3, input/output subspace SSARX identification using MATLAB's (MATLAB2016a, The MathWorks Inc., Natick, MA, USA, 2016) system identification toolbox has been performed. In this case and for consistency with literature, the velocity of the structural mass is used as the output variable (direct feedback output control). The resulting input/output transfer function of the linearised plant is given by:

$$G_p(s) = \frac{0.001s^3 - 1.32e^{-11}s^2 + 3e^{-12}s - 1.32e^{-11}}{s^4 + 0.05s^3 + 2s^2 + 0.0495s + 0.99} \quad (6.3)$$

Solving for the roots of the denominator, the poles of the open loop system are obtained as:

$$\begin{aligned}
 P_1 &= -0.0138 + 1.0471i \\
 P_2 &= -0.0138 - 1.0471i \\
 P_3 &= -0.0112 + 0.9501i \\
 P_4 &= -0.0112 - 0.9501i
 \end{aligned}$$

(6.4)

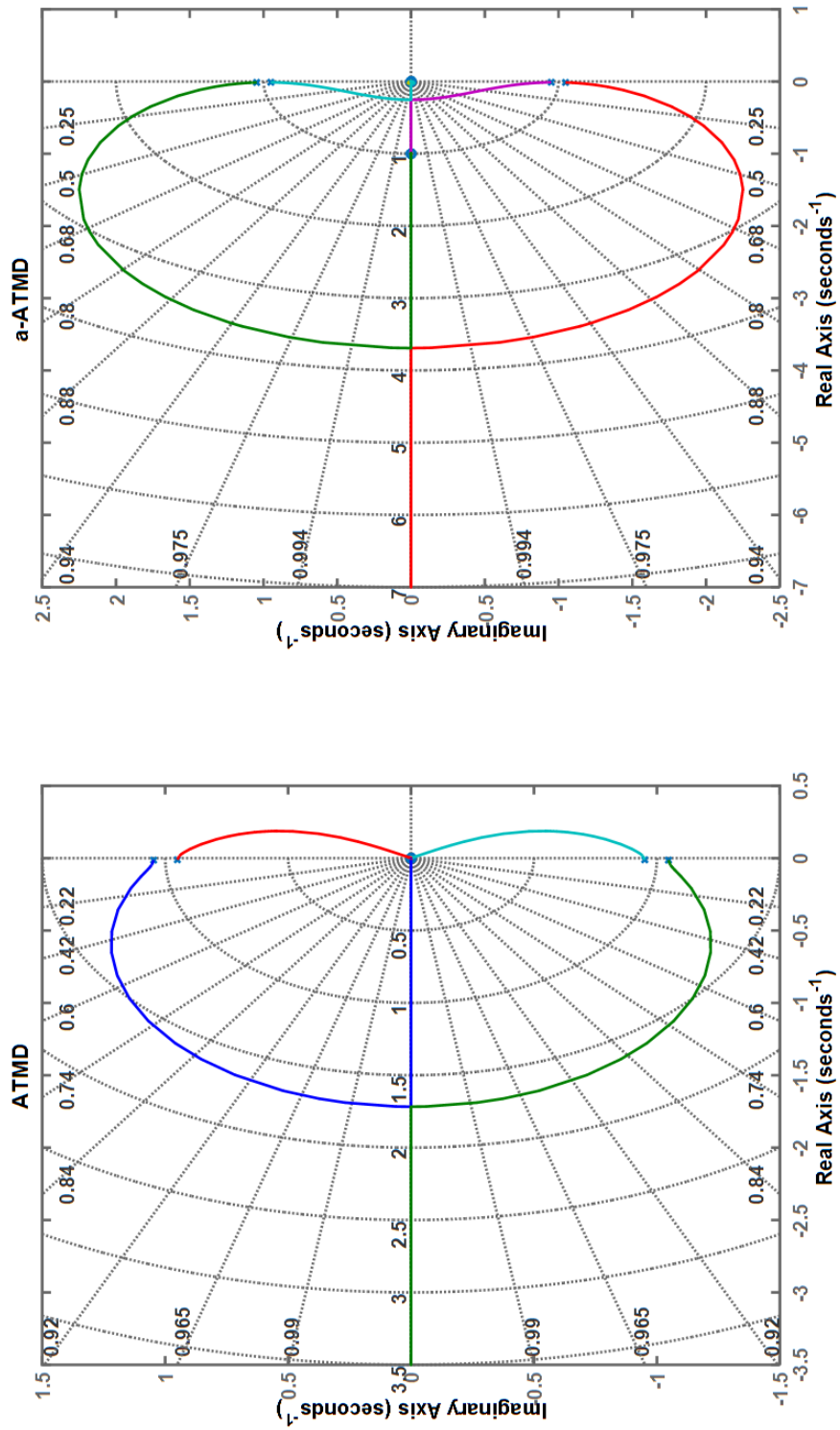


Figure 58. Root-locus diagram of the hybrid ATMD (left) and robust hybrid a-ATMD(right) configurations

From this, $\omega_a = 0.95$ rad/s and $\omega_b = 1.047$ rad/s. Since parameter a has to satisfy $a \in [\omega_a; \omega_b]$ in order to ensure stability, a value of $a = 1$ is selected. Obviously, for cases such as the SHMD, the designer might elect to use some form of online system identification (similar to the methods used by of self-tuning adaptive controllers) in order to ensure that the side lobes ω_a, ω_b of the system are correctly identified throughout the life-span of the system. From this, the transfer function of the closed loop system is constructed by:

$$G_{cl}(s) = \frac{G_c(s)G_p(s)}{1 + G_c(s)G_{Hp}(s)G_p(s)} \quad (6.5)$$

With reference to Figure 59, for the robust a-SHMD controller similarly to the a-ATMD case the loci stay in the left hand plane (for any given value of $g \in [0; \infty]$). It is worth noting however, that this condition is satisfied only for the case where active forces can both add and dissipate energy from the system. Still, revisiting the definition of the SHMD device, the application of active forces are capped to only add energy to the system with no ability to extract energy, rendering the system non-linear. For this reason, multiplication of the equivalent linear plant transfer function with the transfer functions of the filter and the robust controller is not possible. It is therefore fair to say that the designer has to select between a system that guarantees either robust stability independent to the gain variation by retaining the output of the linear controller (i.e. the uncapped case), or a system that minimises energy consumption via capping the actuation capacity to only add energy to the system (i.e. capped case).

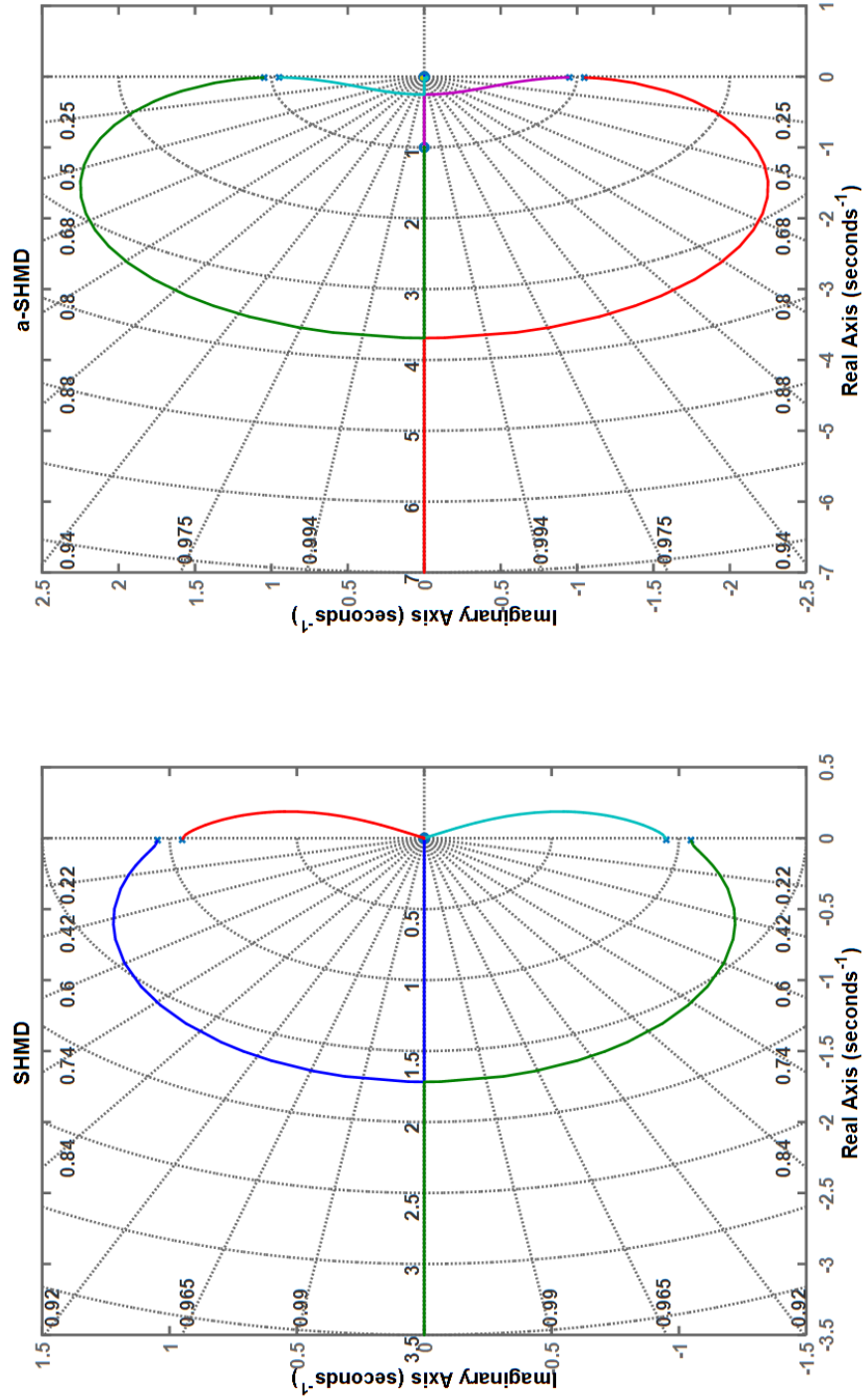


Figure 59. Root-locus diagram of the SHMD (left) and a-SHMD (right) system

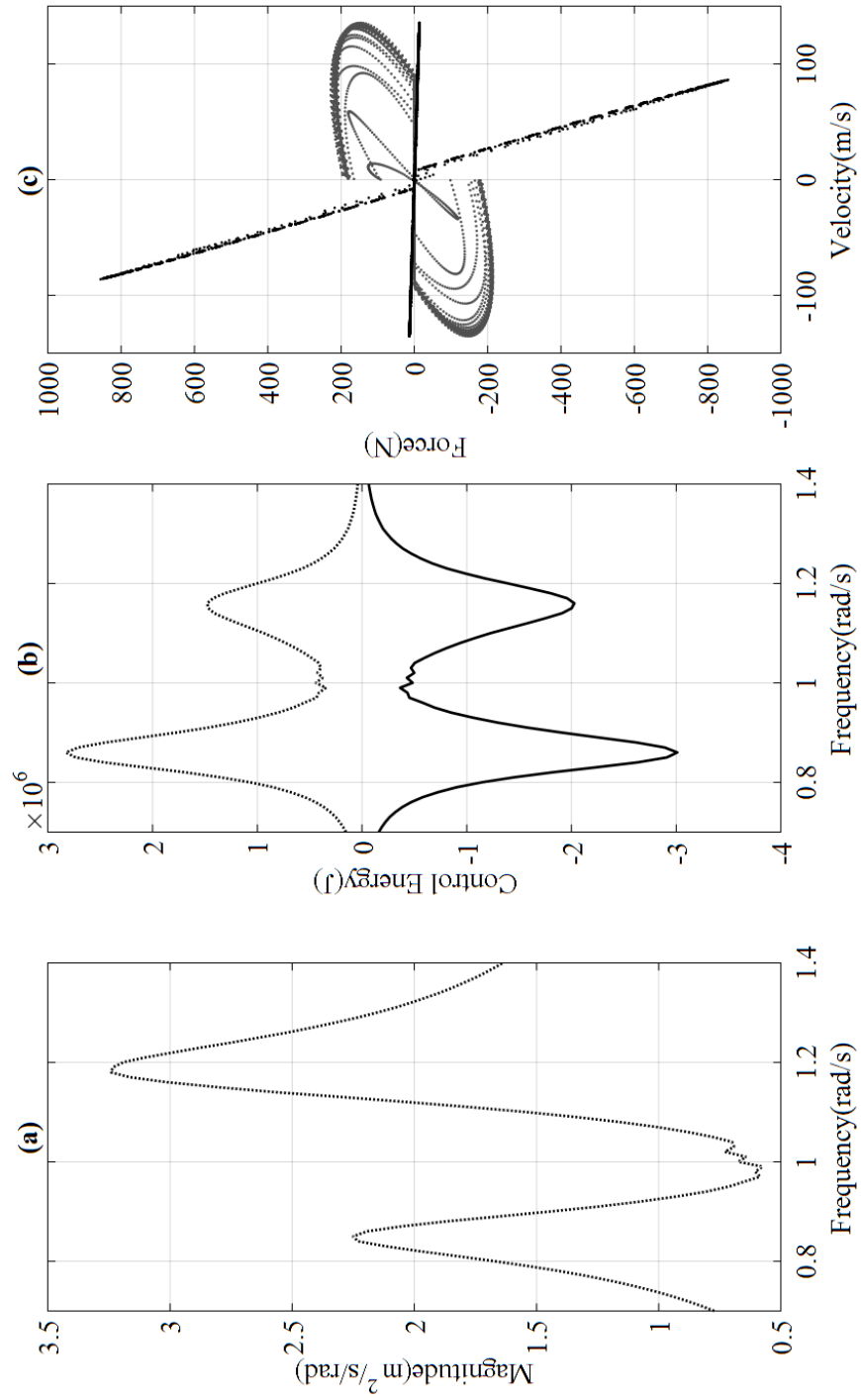


Figure 60. (a) Acceleration response (b) Control energy and (c) Force/velocity relationship for the case of the capped a-SHMD configuration

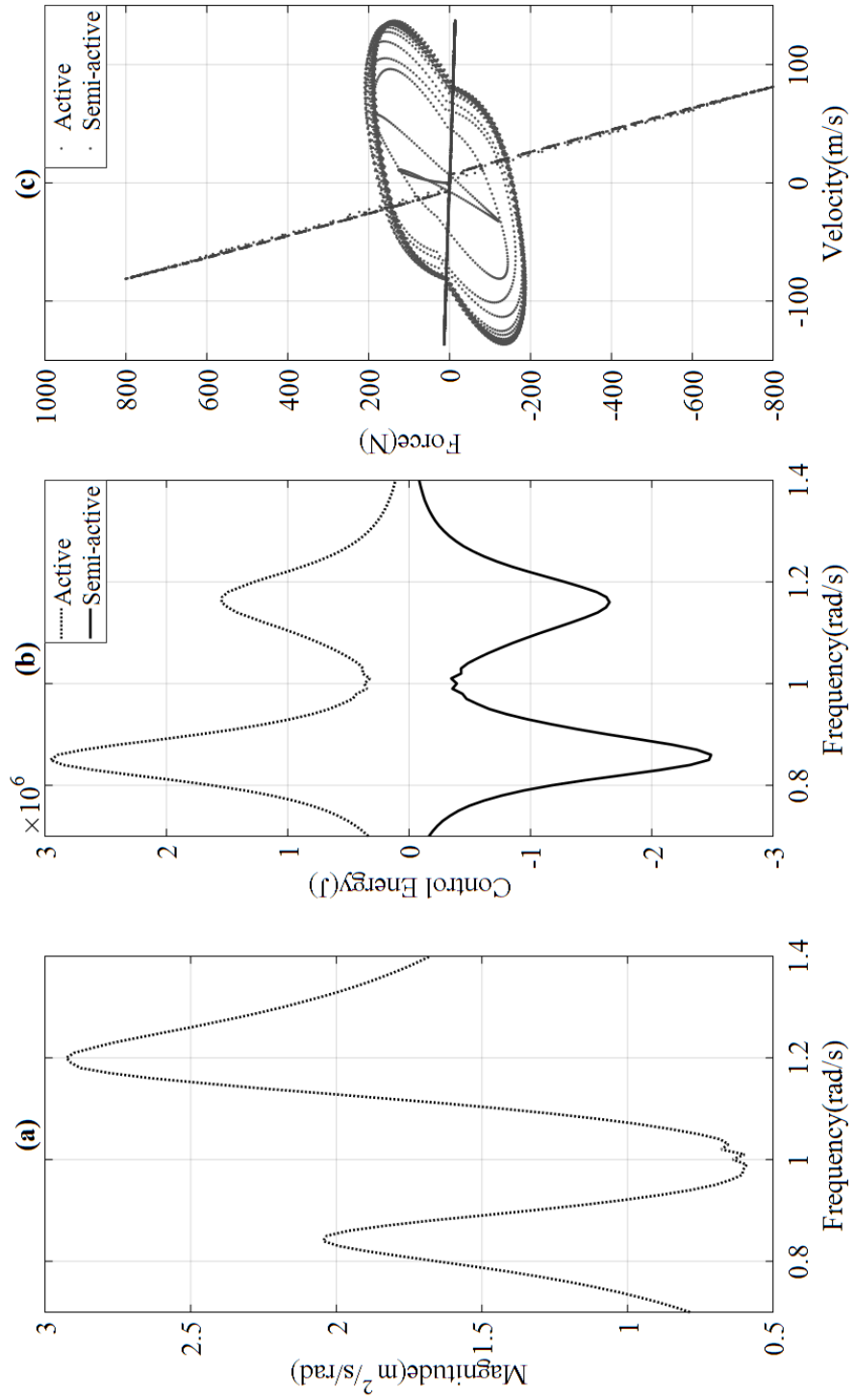


Figure 61. (a) Acceleration response (b) Control energy and (c) Force/velocity relationship for the case of the uncapped a-SHMD configuration

With reference to Figure 60 and Figure 61 a few observations can be made. Firstly, and as expected the ability of the uncapped SHMD configuration to also extract energy through its active components, further enhances the performance of the control system. This is indicated by reduction in acceleration response (Figure 60a-Figure 61a) across the frequency band of interest. Secondly, validating the initial hypothesis of lower energy consumption owing to the capping of the actuation capacity, the uncapped system is shown to require a fraction more energy for active control (Figure 60b-Figure 61b). At the same time the dissipation of energy through the active elements, alleviates some of the semi-active control burden. This is illustrated by the lower maximum semi-active force required by the uncapped system (Figure 60c-Figure 61c)

6.4 Modification of PID to aPID

Based on the same concept, a modification of the conventional PID controller via the addition of a first order filter (integrator) and appropriate tuning of the controller's gains has been proposed. This modification, ensures that the resulting closed-loop poles always remain in the left-hand plane of the pole/zero map, satisfying the Routh-Hurwitz criterion for $g \in [0; \infty] \leftrightarrow a \in [\omega_a; \omega_b]$. The control architecture considered is shown in Figure 62 (the corresponding Simulink block diagrams are shown in Figures A11 and A12 in the appendix):

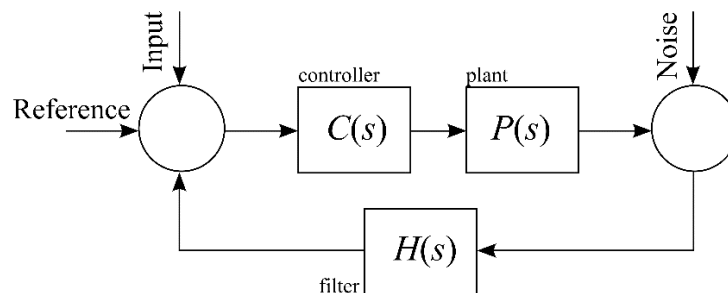


Figure 62. aPID control system architecture

For the particular control system architecture, $H(s)$ is defined as a second order filter described by the transfer function:

$$H(s) = \frac{s}{as(s + \omega_c)/2} = \frac{s}{s + \omega_c} \times \frac{1}{as/2} = G_{hp}(s)H_{int}(s) \quad (6.6)$$

The second order filter is designed such that the high-pass filter of Eq.(6.2) is connected in series with an integrator of the form:

$$H_{int}(s) = \frac{1}{as/2} \quad (6.7)$$

The PID controller's transfer function is defined by:

$$C(s) = K_p + \frac{K_i}{s} + K_d s = K_p \left(1 + \frac{1}{T_i s} + T_d s \right) = K_p \frac{T_i T_d s^2 + T_i s + 1}{T_i s} \quad (6.8)$$

In which, K_p , K_i and K_d are respectively the proportional, integral and derivative gains of the PID controller, and $T_i = K_p / K_i$ and $T_d = K_d / K_p$ are the integral and derivative time constants respectively. In order to achieve hyperstability (via the placement of the zeros between the poles of the structural system and the absorber), the following parameter tuning is proposed.

$$K_p = a^2 g, \quad K_i = \frac{a^3 g}{2}, \quad K_d = \frac{ag}{2} \quad (6.9)$$

where, $g \in [0; \infty]$ is the constant gain of the controller and the hyperstability parameter $a \in [\omega_a; \omega_b]$.

6.4.1 Proof of stability at varying a and g parameters

Due to the fact that the resulting closed-loop system is of high-order, it is impractical to determine stability from the solution of the characteristic polynomial at different values of a and g . For this reason, the Routh-Hurwitz stability test can be used to determine whether the roots of the characteristic polynomial have negative real parts. In this method, tables are constructed from the coefficients of the characteristic polynomial. The number of sign changes in the first column of each table indicates the number of non-negative poles. To this end, the characteristic polynomial of the PID controlled ATMD system (aPID-ATMD) must be first extracted from the closed loop transfer function of the control system architecture depicted in Figure 62.

$$G_{cl}(s) = \frac{C(s)P(s)}{1 + C(s)P(s)H(s)} \quad (6.10)$$

In Eq.(6.10) the only unknown is the transfer function $P(s)$ of the plant. To obtain $P(s)$, first Consider the 2-dof lumped parameter ATMD controlled system of Figure 63:

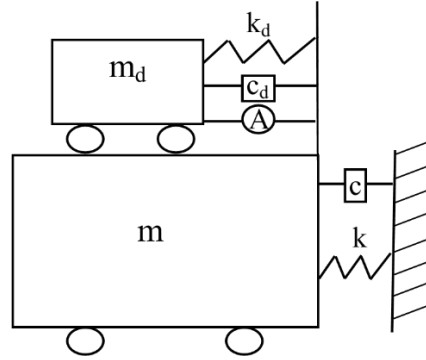


Figure 63. ATMD configuration

And its state space representation:

$$\begin{aligned} \dot{x}(t) &= Ax(t) + Bu(t) \\ y(t) &= Cx(t) \end{aligned} \quad (6.11)$$

In which:

$$A = \begin{bmatrix} 0 & 0 & 1 & 0 \\ 0 & 0 & 0 & 1 \\ -\frac{k+k_d}{m} & \frac{k_d}{m} & -\frac{c+c_d}{m} & \frac{c_d}{m} \\ \frac{k_d}{m_d} & -\frac{k_d}{m_d} & \frac{c_d}{m_d} & -\frac{c_d}{m_d} \end{bmatrix}, \quad B_c = \begin{bmatrix} 0 \\ 0 \\ \frac{1}{m} \\ -\frac{1}{m_d} \end{bmatrix}, \quad C = [0 \ 0 \ 1 \ 0] \quad (6.12)$$

From which the transfer function $P(s)$ is obtained by:

$$P(s) = C(sI - A)^{-1}B + D \quad (6.13)$$

Substituting Eq.(6.6) and Eq.(6.13) in Eq.(6.10) the 7th order characteristic polynomial of the closed loop transfer function is derived as:

$$\begin{aligned}
 f(m, m_d, k, k_d, c, c_d, a, g, \omega_c) = & \\
 m m_d s^7 + (c m_d + c_d m + c_d m_d + g m_d + m m_d \omega_c) s^6 + & \\
 [c c_d + k m_d + k_d m + k_d m_d + \omega_c (c m_d + c_d m + c_d m_d) + 2 a g m_d] s^5 + & \quad (6.14) \\
 (g m_d a^2 + \omega_c (c c_d + k m_d + k_d m + k_d m_d) + c k_d + c_d k) s^4 + & \\
 [k k_d + \omega_c (c k_d + c_d k)] s^3 + k k_d \omega_c s^2 &
 \end{aligned}$$

Clearly, for the case of SHMD control, the equivalent linear transfer function of the system must be obtained using identification techniques similar to the ones described earlier. In this regard, substituting Eq.(6.3), Eq.(6.8) and Eq.(6.6) in Eq.(6.10) the characteristic polynomial of the closed loop transfer function is obtained by:

$$c_7 s^7 + c_6 s^6 + c_5 s^5 + c_4 s^4 + c_3 s^3 + c_2 s^2 + c_1 s \quad (6.15)$$

In which:

$$c_1 = 1.32e^{-11} a^2 g, \quad c_2 = 3.02e^{-12} g a^2 - 2.65e^{-11} g a + 0.99 \omega_c \quad (6.16)$$

$$c_3 = -1.3e^{-11} g a^2 - 6.30e^{-12} g a - 1.32e^{-11} g + 0.05 \omega_c + 0.99 \quad (6.17)$$

$$c_4 = 3.02e^{-12} g - 2.65e^{-11} a g + 1e^{-3} a^2 g + 2 \omega_c + 0.05 \quad (6.18)$$

$$c_5 = 2e^{-3} a g - 1.33e^{-11} g + 0.05 \omega_c + 2, \quad c_6 = 1e^{-3} g + \omega_c + 0.05 \quad (6.19)$$

$$c_7 = 0 \quad (6.20)$$

Example: Solving Routh matrix for $a = g = 1$ and $\omega_c = a / 50$:

As a first step, the first two rows of the Routh matrix need to be filled with the coefficients of the characteristic polynomial. The next entry, is determined from the pattern shown in the matrix of Eq.(6.21)

$$R_m = \begin{array}{c} \begin{array}{cccc} c_7 & c_5 & c_3 & c_1 \\ c_6 & c_4 & c_2 & 0 \\ x = \frac{c_6 c_5 - c_7 c_4}{c_6} & y = \frac{c_6 c_3 - c_7 c_2}{c_6} & z = \frac{c_6 c_1 - c_7 0}{c_6} & 0 \\ \omega = \frac{x c_4 - c_6 y}{x} & \phi = \frac{x c_2 - c_6 z}{x} & 0 & 0 \\ \eta = \frac{\omega y - x \phi}{\omega} & \theta = \frac{\omega z - x 0}{\omega} & 0 & 0 \\ \psi = \frac{\eta \phi - \omega \theta}{\eta} & 0 & 0 & 0 \\ \zeta = \frac{\psi \theta - \eta 0}{\psi} & 0 & 0 & 0 \\ 0 & 0 & 0 & 0 \end{array} \end{array} \quad (6.21)$$

Substituting for $a = g = 1$ and $\omega_c = a / 50$:

$$R_m = \begin{array}{c} \begin{array}{cccc} 0 & 2.00 & 0.99 & 1.32e-11 \\ 0.07 & 0.09 & 0.02 & 0 \\ 2.00 & 0.99 & 1.32e-11 & 0 \\ 0.06 & 0.02 & 0 & 0 \\ 0.27 & 1.32e-11 & 0 & 0 \\ 0.02 & 0 & 0 & 0 \\ 1.32e-11 & 0 & 0 & 0 \\ 0 & 0 & 0 & 0 \end{array} \end{array} \quad (6.22)$$

It is shown that the sign of all numbers in the first column of the matrix does not change, suggesting no unstable poles. The same procedure is followed for all the values of $g \in [0; \infty] \leftrightarrow a \in [\omega_a; \omega_b]$. For convenience and clarity, the values of the first column of the Routh matrix are plotted in Figure 64.

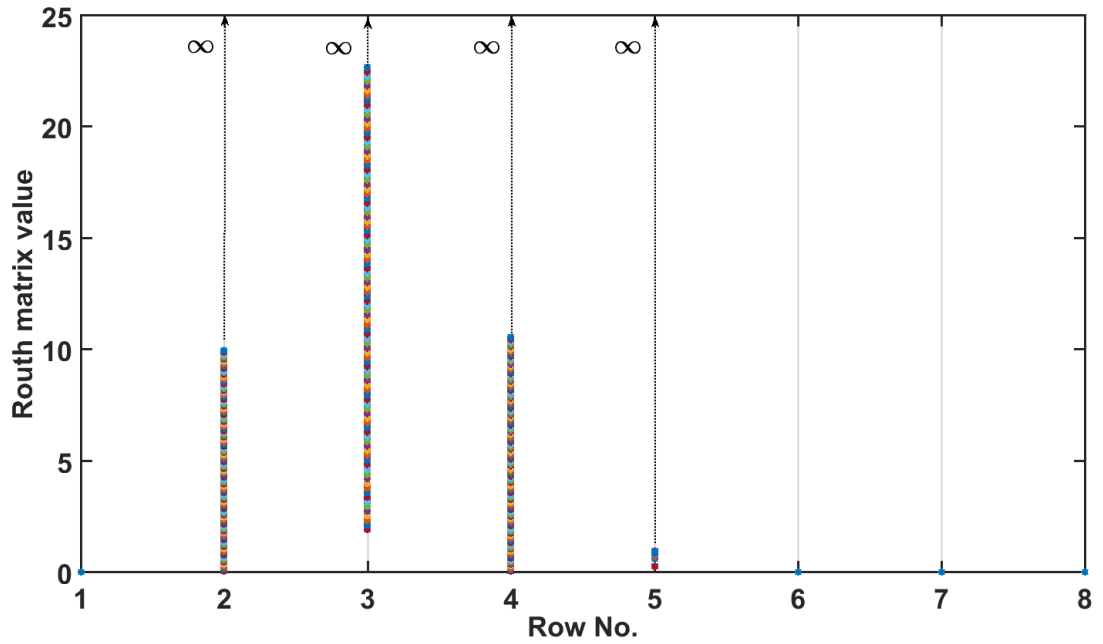


Figure 64. Values in the first column of the Routh matrix for $g \in [0; \infty] \leftrightarrow a \in [\omega_a; \omega_b]$

With reference to Figure 64, it is evident that for $g \in [0; \infty] \leftrightarrow a \in [\omega_a; \omega_b]$, all the values in the first column of the Routh matrix attain positive values (i.e. no sign change) which suggests no unstable poles, validating the robust stability of the system irrespective to the control gains.

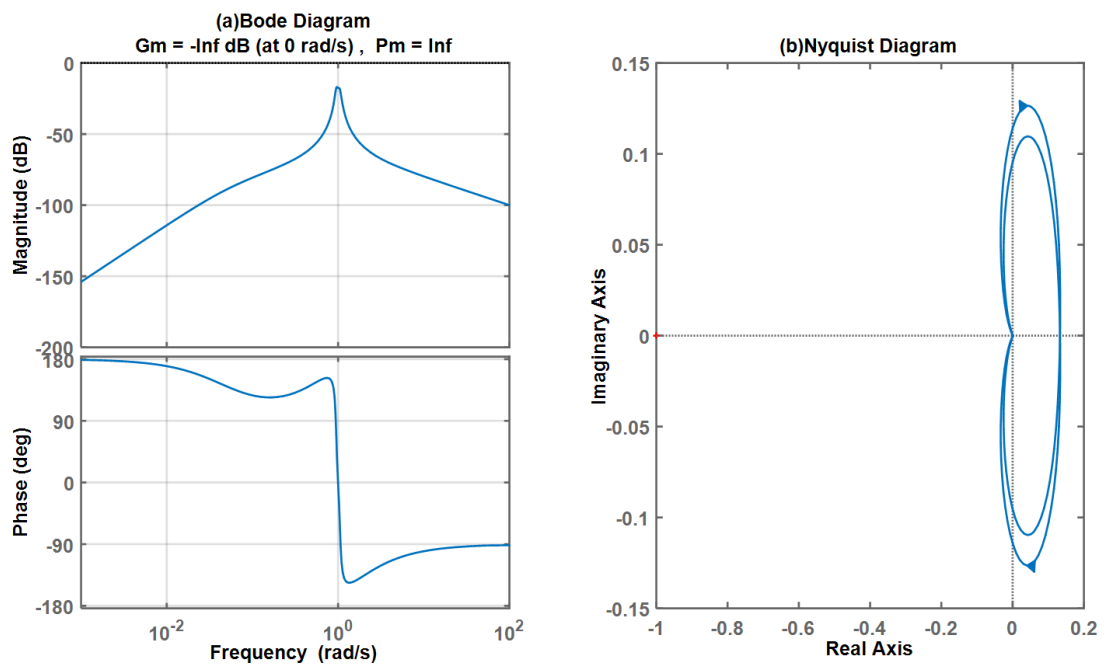


Figure 65. (a) Bode plot and (b) Nyquist plot for the aPID-SHMD system

Similar observations can be made from observation of the Bode-plot and Nyquist diagrams of Figure 65. It is evident that the system, post-application of the robust controller, has infinite gain and phase margins.

6.4.2 Trial aPID controllers

In this section of the study, the performance of the aPID equipped SHMD system (aPID-SHMD) is examined at increasing values of constant gain, g , for which $g \in [0; \infty] \leftrightarrow a \in [\omega_a; \omega_b]$. At each gain interval, the PID robust control gains are calculated using Eq.(6.9). A second order filter with cut-off frequency $\omega_c = a / 50$, is then applied in accordance to Eq.(6.6) and the robust controller parameter, a , is selected as unity ($a \in [\omega_a; \omega_b]$). It is noteworthy that for a robust controller parameter $a = 1$ the proportional gain of the PID attain the value of the constant gain g , while the integral and derivative gains of the PID are equal (Eq.(6.9)). As an additional demonstration of robust stability, the constant gain parameter varied from low to extremely large values. The results of the analysis are presented in Figure 66.

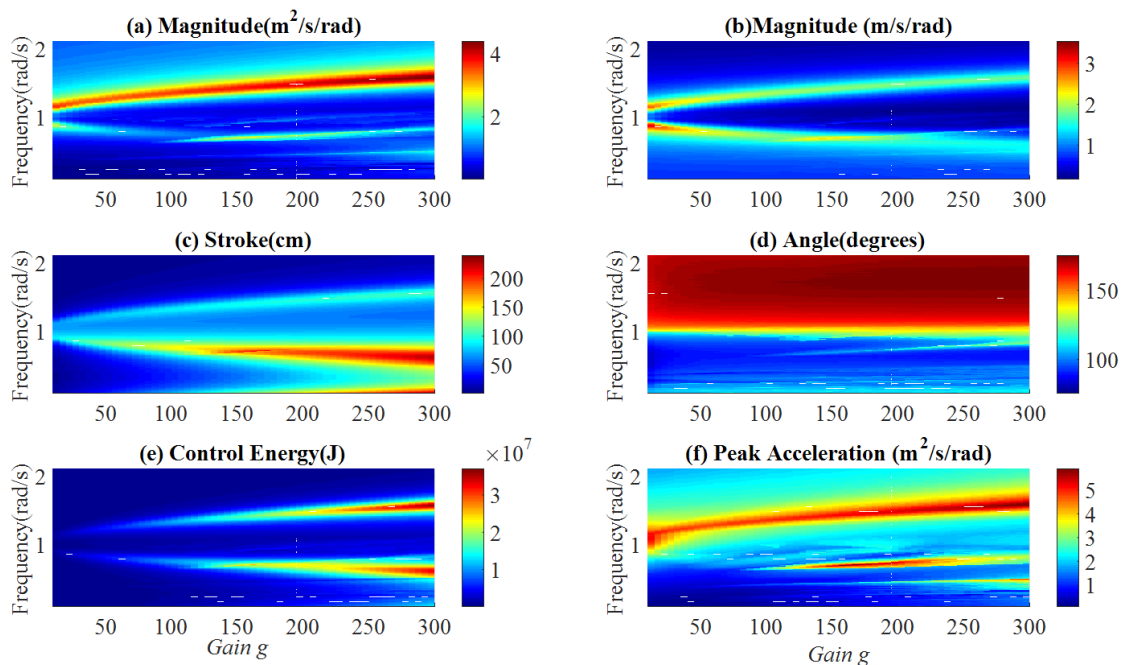


Figure 66. aPID-SHMD configured system response as a function of gain

With reference to Figure 66, the first observation to be made is the location of the peaks in the frequency response diagrams (Figure 66a-b). The location of

each peak indicates the location of the system poles in the pole/zero map. As anticipated from the design, and the corresponding root locus diagrams (Figure 59), at increasing gains the poles of the system move away from each other going left (into the negative values) and away of the imaginary axis. Moving away from the imaginary axis suggest increasing damping ratio in the system. The increased damping ratio of each pole is indicated by the spread of the peaks in the response diagrams of figure(Figure 66a-b)(for clarity refer to the 2-D version in Figure 68). With respect to Figure 66c-d, it is observed that as a consequence of the increasing gain, the stroke of the actuator also increases. Still, as the stroke increases the relative phase of the mass-damper and the structure remains unaltered, signifying the robustness of the system.

To complement the results of Figure 66, Figure 67b presents the total percentage response reduction (area under the curve) as a function of the gain. It is observed that the response reduction trend follows a curvilinear trajectory, suggesting that the rate at which the overall performance improves reduces at larger gains. Similarly, the rms force (Figure 67a) follows a similar curvilinear trajectory. It can be observed, that beyond a value of $g \approx 120 - 150$, the rms force values hit a plateau, while the maximum force keeps increasing. This suggests isolated spikes occurring in the actuation. Regarding the control energy supplied in the system, Figure 67c illustrates that total supplied energy follows a bilinear trend. A correlation between the point of which the rms force and the total energy hit the plateau is also observed($g \approx 120 - 150$).

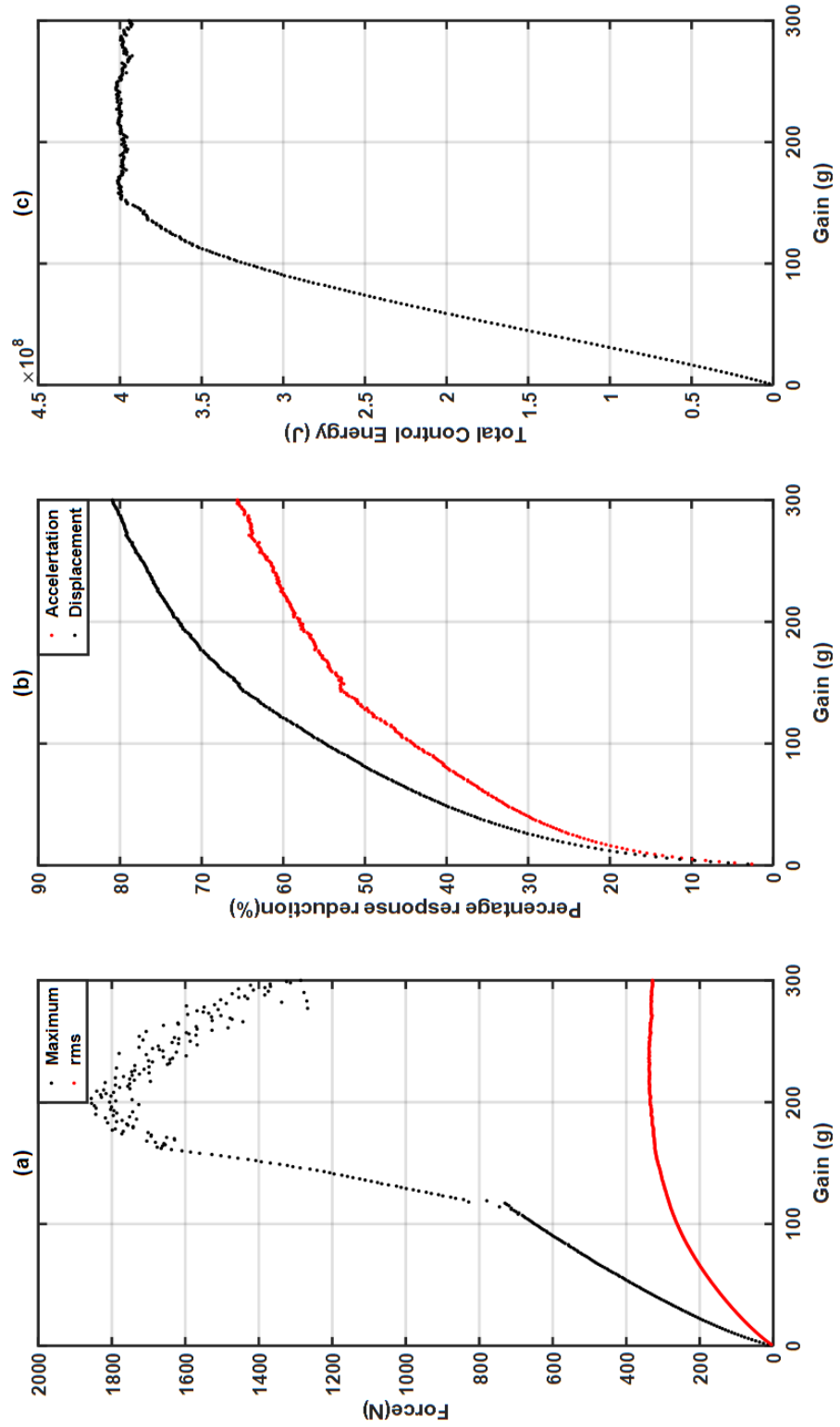


Figure 67. (a) Supplied maximum and rms force, (b) Total acceleration and displacement response reduction, and (c) Total control energy supplied by the aPID-SHMD system

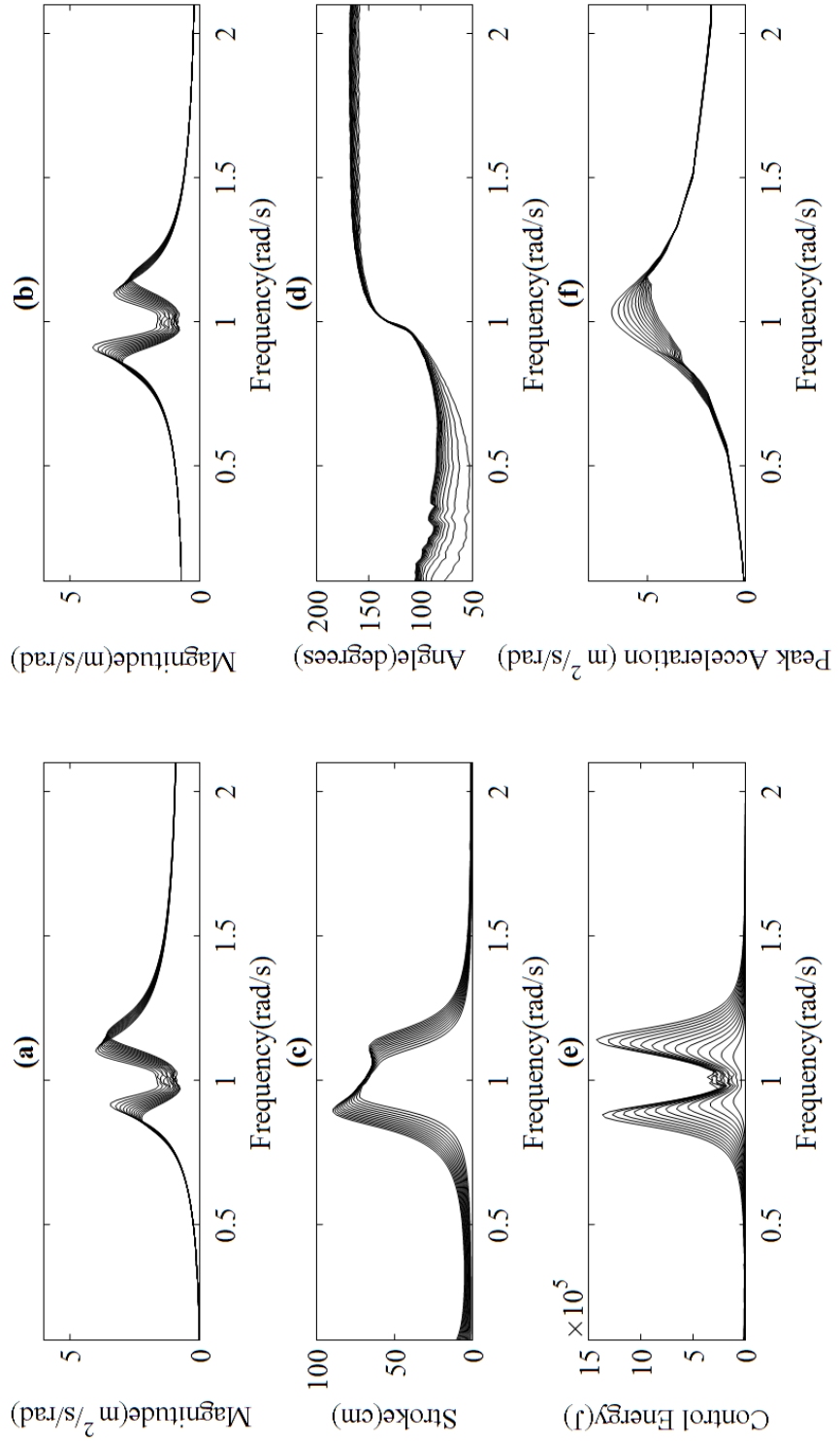


Figure 68. (a) Acceleration response, (b) Displacement response, (c) Damper stroke, (d) Relative phase, (e) Control energy and (f) Peak acceleration response for the aPID-SHMD at low control gains

6.5 Comparison with optimal LQR controllers

In this section, a LQR controller has been designed for comparison with the proposed robust controller. The design of the LQR is based on the linearised semi-active system following the description found in (Demetriou and Nikitas, 2016). In this approach, the Q and R weighting quantities have been iteratively selected such that maximum performance (i.e. vibration attenuation) has been extracted from the system with no regards to the control effort. This performance-wise optimised LQR allowed the establishment of a performance based comparison reference with the a-SHMD counterpart. The response of the LQR system in terms of acceleration, control energy and force demands is shown in Figure 69.

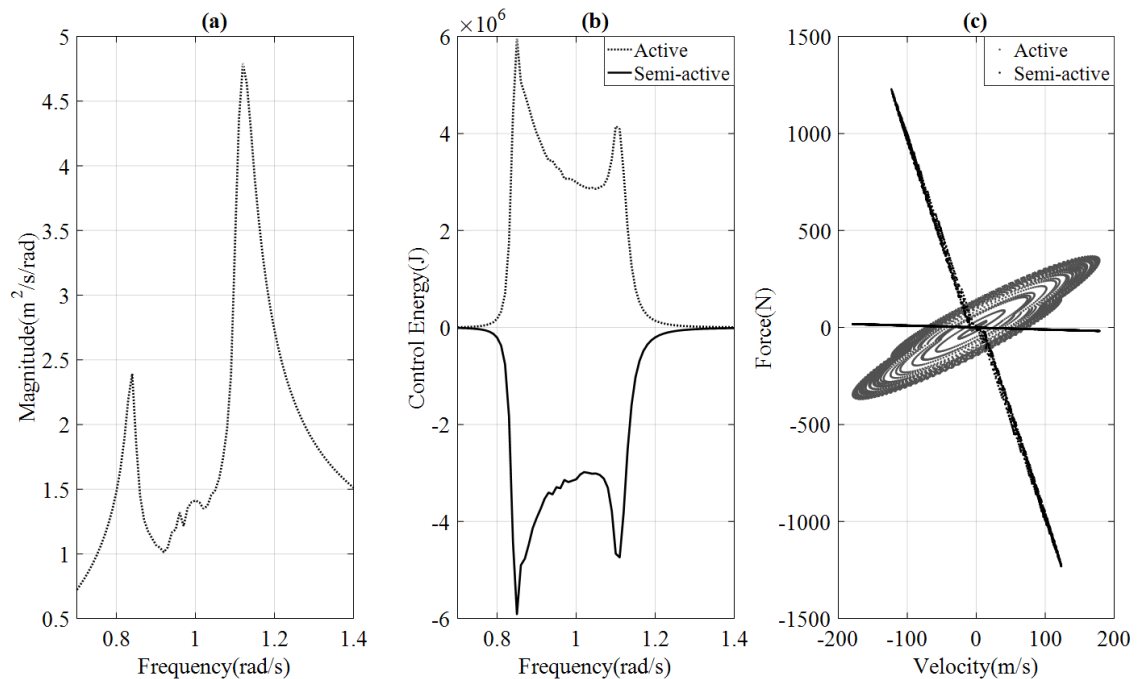


Figure 69. (a) Acceleration response (b) Control energy and (c) Force/velocity relationship for the case of the performance optimised LQR-SHMD system

For the fairness of the comparison, an aPID robust controller has been designed with gains selected such that similar actuation and control energy demands to that of the LQR-SHMD are achieved. To this end, the resulting aPID-SHMD system's response in terms of acceleration, control energy and force is shown in Figure 70.

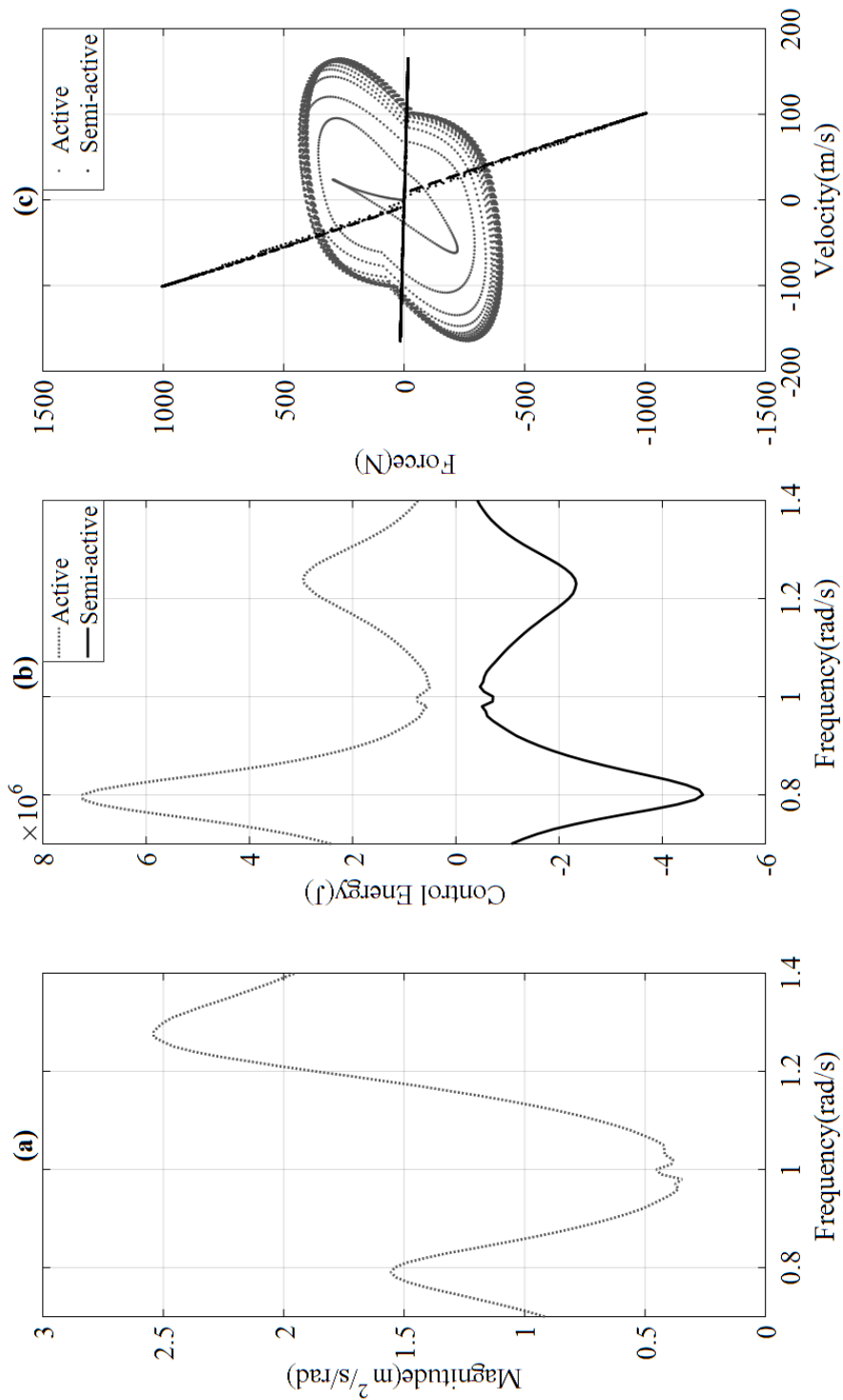


Figure 70. (a) Acceleration response (b) Control energy and (c) Force/velocity relationship for the case of the a-SHMD system gains matching control effort of LQR-SHMD

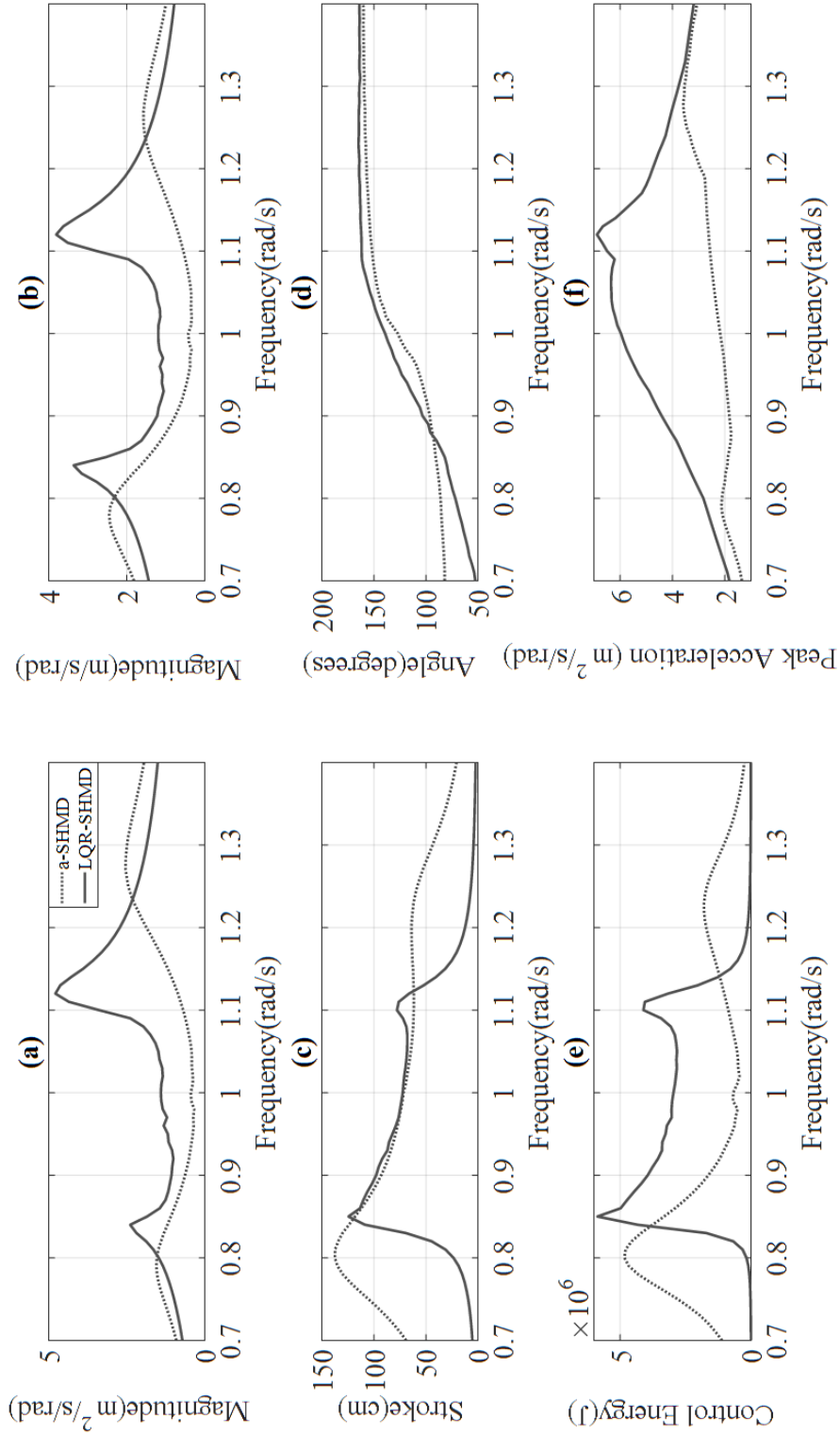


Figure 71. (a) Acceleration response, (b) displacement response, (c) damper stroke, (d) relative phase, (e) Control energy and (f) peak acceleration response for the aPID-SHMD and LQR-SHMD systems

Direct comparison of the two algorithms (Figure 71)) based on similar actuation and control energy demands, demonstrates a clear superiority of the a-SHMD over the LQR-SHMD configuration in almost every control design aspect, with only exception the higher strokes required by the aPID-SHMD. But it is not only the enhanced performance of the aPID-SHMD in terms of vibration response reduction that make it superior to the LQR-SHMD. The requirement of the latter configuration for system identification for deriving the state matrices to be used in the solution of the Riccati matrix, make it a complex and non-trivial task. Additionally, using a LQR, full state feedback is required either from direct measurement of all the states (one sensor at each DOF) or using state observers (Kalman filters etc.) further increasing the complexity and practicality. On the other hand, an aPID is based on simple direct velocity feedback control principles, capable of providing control actions using the measurement of only one state.

6.6 Conclusions

In this chapter of the thesis, a new robust algorithm proposed for the control of hybrid vibration absorbers has been applied to the novel SHMD configuration. This robust control law which belongs to the class of hyperstable controllers is shown to be suitable for use in conjunction with SHMD devices. Importantly, it has been shown that modification of the SHMD device to allow for energy dissipation using active actuation is essential in order for the robust controller to be hyperstable. The steps required for the design of the controller have been presented and guidelines on how to choose the tuning parameters of the controller have been proposed.

Additionally, one of the most widely used controllers in the control industry, the PID, has been modified based on the principle of hyperstability in an attempt to provide a simple and effective solution for the control of hybrid ATMD and SHMD devices. To this end, hyperstability conditions have been identified and tuning of the resulting robust aPID controller has been proposed. Proof of stability of the resulting aPID-SHMD system has been demonstrated using Routh-Hurwitz tests, bode plots, Root-locus and Nyquist diagrams. Finally, a comparison with the performance-wise optimised LQR-

SHMD system presented in Chapter 5, showed that beyond the simplicity in design and need for a single state measurement of the aPID-SHMD system, the latter system is shown to be superior to the LQR-SHMD configuration in almost every control design aspect, with only exception the higher strokes required by the aPID-SHMD.

Chapter 7

Conclusions and Future Work Recommendations

The primary goal of this thesis was to deal with some of the most important obstacles impeding the application of semi-active and smart control in the structural field with particular emphasis on high-rise structural applications using mass dampers. To this end, a number of key research aims were provided in Chapter 1. The research detailed in this thesis has worked towards meeting these aims, and as such a number of conclusions can be drawn. This chapter draws concluding remarks based on the previously described work, and provides recommendations for where future work could be focused.

7.1 Summary of contributions and impact

A comparison of different control algorithms on semi-actively controlled structural systems for which practical constraints such as stroke and force saturations can significantly affect their performance has been carried out. For consistency with literature and as an initial step, the performance of the different algorithms has been investigated on a SDOF harmonically excited system at the absence of practical constraints. Control system performance in terms of disturbance rejection and robustness to parametric uncertainty has been evaluated and a primary ranking/rating of the algorithms has been established. In this regard, the LQR and DBG algorithms which have been consistently shown in literature to outperform algorithms such as the VBG and BANG are also shown in the first part of this study to be the 'best' algorithms. However, when the study progressed to the investigation of a wind excited high-rise structure on which practical constraints have been applied, it has been shown that different control algorithms have different stroke operating ranges, signifying the importance and interplay between performance and damper strokes. To this end, it has been found that when no consideration is given to damper strokes, some of the investigated algorithms are found to be more suitable for use with STMD devices. The LQR, the DBG and the PID algorithms that maximise damper strokes, thus termed 'least-conservative',

achieve significant response reductions. On the other hand, it has been demonstrated that the remaining of the investigated algorithms, the VBG and the BANG, the algorithms that significantly restrain the damper strokes, thus termed 'conservative', can reach and even surpass in some damper stroke restrained scenarios the performance of the previously thought 'best' algorithms. As a result, it can be realised that making the damper strokes an integral part of the performance objectives, appropriate control algorithm selection can be performed as an alternative method of limiting damper strokes while maintaining expedient performance without the requirement of external auxiliary damping devices, command limiters or high-pass filters.

In addition to this, through investigation of the tuning of the damping ratios for different configurations, it is found that the main difference of the two categories of control algorithms is the requirement of the least conservative algorithms for high damping ratios for achieving optimal behaviour, whereas conservative algorithms require significantly lower values. As a matter of fact, for relatively similar performance benefits, a DBG would require a maximum damping ratio of 16% as opposed to 8% required by a VBG. This suggests that the choice of an algorithm from the latter category would translate to a reduced size/number of auxiliary devices used, control forces and power, which in turn relate back to the practical applicability and cost of the STMD device on high-rise structures.

In the second part of the study, the research was focused on dealing with the limitations of existing smart damper devices in terms of power and force actuation demands. In this regard, a novel semi-active hybrid mass damper (SHMD) configuration has been proposed. The novel configuration makes use of active and semi-active components coupled with appropriate control algorithms for achieving the desired control objective. In the proposed configuration, the active elements of the damper are designed to only add energy to the system, whereas the semi-active components are responsible for energy dissipation. This sequential action of the semi-active and active components ensures that energy dissipation occurs at considerably lower energy demands, while the energy addition whenever necessary is not hindered by forces acting in the opposite direction by the passive elements. Based on these concepts, it is shown that for approximately the same damper

strokes, the SHMD configuration is able to achieve similar performance to the conventional ATMD counterpart, while clearly outperforming the passive and semi-actively controlled alternative. Most importantly, it has been shown that the novel device configuration requires much less energy and actuation demands for achieving the aforementioned performance increase. As a matter of fact, the SHMD device requires only 26% of the total energy required by the ATMD device. This is due to the large control effort and consequently the large amount of energy required to be added by the active actuators (approximately 82% of the total required energy), necessary for overcoming the “braking” force acted by the passive components of the ATMD. Apart from the aforementioned benefits arising from the use of such low energy demand configurations, the SHMD device could potentially make novel energy regenerative force actuation technologies viable in the structural engineering field.

Even though the gains from appropriate configuration selection are evident, a successful control system does not rely exclusively on the individual performance of the hardware, but it is the combined action of both hardware and software that make a control system superior to another. For this reason, the final part of the thesis attempted to integrate software and hardware performance via the suitable selection of a control algorithm for SHMD devices. To this end, a recently proposed robust controller has been tailored for application to the novel configuration, showing great potential both in terms of vibration attenuation and stability. Based on the concept of hyperstability, a modification of the conventional PID controller and robust tuning of its parameters has been proposed in search of a more rigorous procedure for the design of hybrid control systems using simple and widely used control system architectures. The resulting robust aPID control algorithm is shown to satisfy all stability requirements regardless the control gain, as long as the robustness parameter is selected appropriately.

7.2 Future work recommendations

An interesting observation from the simulations performed in chapter 4, is that aggressive tuning of the PID controller, results in a control system similar to the one equipped with the baseline direct output feedback DBG algorithm.

Investigating how mathematically different algorithms produce exactly the same results is intriguing for future work. With reference to the same chapter, the potential of creating an adaptive control scheme by switching to an appropriate algorithm so that performance is improved at the expense of low damper strokes should be also investigated. To achieve this, the proposed adaptive control scheme could potentially use 'conservative' algorithms when stroke limitation is required and 'least conservative' algorithms for maximising the performance gain. The challenge is to identify the conditions for which switching of algorithm occurs.

Secondly, it is understood that the work in this thesis is based exclusively on simulations and it is important to verify the conclusions of this work through experimentation. To the author's opinion the key experiment to be conducted is implementing the SHMD configuration on a scaled model and subjecting it to various types of excitations. Additionally, different algorithms (including the modified aPID) should be implemented on the scaled structure so that the conclusions drawn in this thesis are experimentally verified. Although it is understood that there are practical limitations to this, i.e. the availability of suitable structures, availability of shaking table equipment, expense of setting monitoring systems etc. the potential benefit that could be derived through this work is significant. To complement this, a life-cycle analysis of the SHMD configured system should be performed.

References

- AL-DAWOD, M., SAMALI, B. & LI, J. 2006. Experimental verification of an active mass driver system on a five-storey model using a fuzzy controller. *Structural Control and Health Monitoring*, 13, 917-943.
- ALLAN, J. F. 1945. The stabilization of ships by activated fins. *Transactions of the Royal Institute of Naval Architects*, 87, 123-159.
- AMINI, F., HAZAVEH, N. K. & RAD, A. A. 2013. Wavelet PSO-Based LQR Algorithm for Optimal Structural Control Using Active Tuned Mass Dampers. *Computer-Aided Civil and Infrastructure Engineering*, 28, 542-557.
- ASTROM, K. J. & HAGGLUND, T. 1995. *PID Controllers: Theory, Design and Tuning.*, NC, ISA and Research Triangle.
- ASTROM, K. J. & MURRAY, R. M. 2012. *Feedback Systems-An introduction for scientists and Engineers*, New Jersey 08540, Princeton University Press.
- AUSTRALIAN, S. 1989. Minimum design loads on structures. II: Wind loads. *AS1170.2-1989*.
- BALAS, M. J. 1978. Active Control of Flexible Systems. *Journal of Optimization Theory and Applications*, 25, 415-436.
- BAOYA, C. & CHUNXIANG, L. Design of active tuned mass damper based on robust control. 2012 IEEE International Conference on Computer Science and Automation Engineering (CSAE), 2012. 760-764.
- BATTAINI, M., CASCIATI, F. & FARAVELLI, L. Implementing a fuzzy controller into an active mass damper device. American control conference, 1997. 888-892.
- BOUJARI, M., GHORBANI-TANHA, A. K., RAHIMIAN, M. & RAHAMI, H. 2012. Two Degrees of Freedom PID Control for Active Vibration Control of Structures. *15 int. WCEE*. Lisbon.
- BU, X., YE, L. & WANG, C. 2003. Active control of a flexible beam using a system identification technique based on ARMAX. *Smart Materials and Structures*, 12, 845-850.
- BURGOS, O., HIZON, J. & SISON, L. Comparison of classical and fuzzy control in active mass damping of flexible structure using acceleration feedback. IEEE Region 10 Conference, 2004 TENCON.
- CAO, H., REINHORN, A. M. & SOONG, T. T. 1997. Design of an active mass damper for a tall tv tower in Nanjing China. *Engineering Structures*, 20, 134-143.
- CASCIATI, F. & FARAVELLI, L. Structural control design on reduced order models. Sixth World Conference on Structural Control and Monitoring, 15-17 July 2014 Barcelona, Spain. International Center for Numerical Methods in Engineering, 713-719.
- CASCIATI, F. & GIULIANO, F. 2009. Performance of multi-TMD in the towers of suspension bridges. *Journal of Vibration and Control*, 15, 821-847.

- CASCIATI, F., MAGONETTE, M. & MARAZZI, F. 2006. *Technology of Semiactive Devices and Applications in Vibration Mitigation*, West Sussex PO19 8SQ, England, John Wiley & Sons Ltd.
- CASCIATI, F., RODELLAR, J. & YILDIRIM, U. 2012. Active and semi-active control of structures - theory and applications: A review of recent advances. *Journal of Intelligent Material Systems and Structures*, 23, 1181-1195.
- CASCIATI, S. & CHEN, Z. 2012. An active mass damper system for structural control using real-time wireless sensors. *Structural Control and Health Monitoring*, 19, 758-767.
- CAVALLO, A., MARIA, G., NATALE, C. & PIROZZI, S. 2010. *Active control of flexible structures from modeling to implementation*, Springer.
- CHAI, W. & FENG, M. Q. 1997. Vibration control of super tall buildings subjected to wind loads. *Journal of Non-linear Mechanics*, 32, 657-668.
- CHANG, C. C. & YU, L. O. 1997. A simple optimal pole location technique for structural control. *Engineering Structures*, 20, 792-804.
- CHEN, S. M., HUNG, C. F., CHANG, L. M., CHANG, S. H., ZENG, J. H. & LU, T. R. 2012. Semi-Active Tuned Mass Damper for Vibration Control in High-Tech Fab. *Second International Conference on Mechanical, Production and Automobile Engineering(ICMPAE'2012)*. Singapore.
- CHENG, F. Y., JIANG, H. & LOU, K. 2008. *Smart structures: Innovative systems for seismic response control*, New York, Taylor & Francis Group.
- CLOUGH, R. W. & PENZIEN, J. 1995. *Dynamics of Structures*, Berkley, CA 94704, Library of Congress Cataloging-in-Publication Data.
- COLLETTE, C. & CHESNÉ, S. 2016. Robust hybrid mass damper. *Journal of Sound and Vibration*, 375, 19-27.
- CONNOR, J. J. 2003. *Introduction to Structural Motion Control*, Upper Saddle River, New Jersey 07458, Prentice Hall.
- DATTA, T. K. 2003. A state-of-the-art review on active control of structures. *ISET Journal of Earthquake Technology* 40, 1-17.
- DEMETRIOU, D. & NIKITAS, N. 2016. A Novel Hybrid Semi-Active Mass Damper Configuration for Structural Applications. *Applied Sciences*, 6, 397.
- DEMETRIOU, D., NIKITAS, N. & TSAVDARIDIS, K. D. Performance of Proportional-Integral-Derivative Controlled Variable Damping Tuned Mass Dampers. 6th International Conference of Structural Control, 15-17 July 2014 Barcelona, Spain.
- DEMETRIOU, D., NIKITAS, N. & TSAVDARIDIS, K. D. 2015a. A Novel Hybrid Semi-active Tuned Mass Damper for Lightweight Steel Structural Applications. *IJSSD Symposium on Progress in Structural Stability and Dynamics*. Lisbon, Portugal.
- DEMETRIOU, D., NIKITAS, N. & TSAVDARIDIS, K. D. 2015b. Performance of Fixed-Parameter Control Algorithms on High-Rise Structures Equipped With Semi-Active Tuned Mass Dampers. *8th International Conference on the Behavior of Steel Structures in Seismic Areas*. Shanghai, China.

- DIETZ, S. G. 2008. *Analysis and Control of Uncertain Systems by Using Robust Semi-Definite Programming*.
- DYKE, S. J., SPENSER, B. F., QUAST, P., KASPARI, D. C. & SAIN, M. K. 1996. Implementation of an AMD Using Acceleration Feedback Control. *Microcomputers in Civil Engineering*.
- ETEDALI, S., SOHRABI, M. R. & TAVAKOLI, S. 2013. An Independent Robust Modal PID Control Approach for Seismic Control of Buildings. *Journal of Civil Engineering and Urbanism*, 3, 279-291.
- FISCO, N. R. & ADELI, H. 2011. Smart structures: Part II — Hybrid control systems and control strategies. *Scientia Iranica*, 18, 285-295.
- FRAHM, H. 1911. *Device for damping vibration of bodies*. United States patent application.
- FUJINAMI, T., SAITO, Y., MASAYUKI, M., KOIKE, Y. & TANIDA, K. 2001. A hybrid mass damper system controlled by Hinfity control theory for reducing bending-torsion vibration of an actual building. *Earthquake Engineering & Structural Dynamics*, 30, 1639-1643.
- GHOSH, A. & BASU, B. 2007. A closed-form optimal tuning criterion for TMD in damped structures. *Structural Control and Health Monitoring*, 14, 681-692.
- GU, D. W., PETKOV, P. H. & KONSTANTINOV, M. M. 2005. *Robust Control Design with Matlab*, Springer.
- GUCLU, R. & SERTBAS, A. 2005. Evaluation of Sliding Mode and Proportional-Integral-Derivative Controlled Structures with an Active Mass Damper. *Journal of Vibration and Control*, 11, 397-406.
- GUCLU, R. & YAZICI, H. 2007. Fuzzy Logic Control of a Non-linear Structural System against Earthquake Induced Vibration. *Journal of Vibration and Control*, 13, 1535-1551.
- HAC, A. & YOUN, I. 1992. Optimal semi-active suspension with preview based on a quarter car model. *ASME Journal of Acoustic Vibration*, 84-92.
- HAERTLING, G. 1994. Rainbow ceramics: A new type of ultra-high displacement actuator. *Am Ceram Soc Bull*, 93-96.
- HARTOG, D. 1956. *Mechanical Vibrations*, New York, McGraw-Hill Book Company.
- HIRAMOTO, K. & GRIGORIADIS, K. M. 2014. Active/semi-active hybrid control for motion and vibration control of mechanical and structural systems. *Journal of Vibration and Control*, 22, 2704-2718.
- HOLMES, D. J. 2007. *Wind Loading of Structures*, CRC Press
- HORT, H. 1934. Beschreibung und versuchsergebnisse ausgeführter schiffstabilisierungsanlagen. *Jahrbuch der Schiffbautechnischen Gesellschaft*, 35, 292-312.
- HOUSNER, G. W. 1996. Book review/Proceedings of the first world conference on structural control. *Soil Dynamics an Earthquake Engineering*, 15, 147-149.
- HOUSNER, G. W., BERGMAN, L. A., CAUGHEY, T. K., CHASSIAKOS, A. G., CLAUS, R. O., MASRI, S. F., SKELTON, R. E., SOONG, T. T., SPENSER,

- B. F. & YAO, J. T. P. 1997. Structural control: Past, present, and future. *Journal of Engineering Mechanics*, 123, 897-971.
- HROVAT, D., BARAK, P. & RABINS, M. 1983. Semi-Active Versus Passive or Active Tuned Mass Dampers For Structural Control. *Journal of Engineering Mechanics*, 109, 691-705.
- HUDSON, E. J. 2013. *Incorporating Active Control of Human-Induced Vibrations in Floors into Buildings*. University of Sheffield.
- IHI INFRASTRUCTURE SYSTEMS CO., L. 2013. *Linear Motor Active Mass Damper* [Online]. Available: https://www.ihico.jp/iis/english/products/damper_mass.html [Accessed 20th July 2016].
- IKEDA, Y. 2009. Active and semi-active vibration control of buildings in Japan – Practical applications and verification. *Structural Control and Health Monitoring*, 16, 703-723.
- IKEDA, Y., SASAKI, K., SAKAMOTO, M. & KOBORI, T. 2001. Active mass driver system as the first application of active structural control. *Earthquake Engineering & Structural Dynamics*, 30, 1575-1595.
- IRWIN, A. W. 1978. Human response to dynamic motion of structures. *The structural Engineer*, 56A, 237-244.
- ISLAM, M. M., SIDDIQUE, A. & MURSHED, A. 2012. Sustainable Development in Drift Control of Tall Buildings Due to Wind Load: Critical Analyses of The Structural Systems. *International Conference on Civil Engineering for Sustainable Development*. Bangladesh.
- JANSEN, L. M. & DYKE, S. J. 2000. Semi-Active Control Strategies for MR Dampers: A Comparative Study. *Engineering Mechanics*, 126, 795-803.
- JI, H. R., MOON, Y., KI, C. & LEE, I. 2005. Structural vibration control using semiactive tuned mass damper. *The Eighteenth KKCNN Symposium on Civil Engineering-KAIST6*. Taiwan.
- KALMAN, R. E. 1960. A New Approach to Linear Filtering and Prediction Problems. *Journal of Basic Engineering*, 82.
- KANG, J., KIM, H.-S. & LEE, D.-G. 2011. Mitigation of wind response of a tall building using semi-active tuned mass dampers. *The Structural Design of Tall and Special Buildings*, 20, 552-565.
- KAPPOS, E. 2002. *Classical Control Theory: A Course in the Linear Mathematics of Systems and Control*, University of Sheffield.
- KAREEM, A., KIJEWski, T. & TAMURA, Y. 1999. Mitigation of motions of tall buildings with specific examples of recent applications. *Wind Struct.*, 2, 201-251.
- KARNOPP, D. C. & CROSBY, M. J. 1974. Vibration control using semi-active force generators. *Journal of engineering for Industry*, 5, 619-626.
- KAWAGUCHI, A., TERAMURA, A. & OMOTE, Y. 1992. Time history response of a tall building with a tuned mass damper under wind force. *Journal of Wind Engineering and Industrial Aerodynamics*, 41-44, 1949-1960.

- KHAN, I. U., WAGG, D. & SIMS, N. D. 2016. Improving the vibration suppression capabilities of a magneto-rheological damper using hybrid active and semi-active control. *Smart Materials and Structures*, 25, 085045.
- KIM, C., HONG, K. & LODEWIJKS, G. Anti-sway control of container cranes: an active mass-damper approach. SICE 2004 Annual Conference, 2004. 939-944.
- KOO, J. H. 2003. *Using Magneto-Rheological Dampers in Semiactive Tuned Vibration Absorbers to Control Structural Vibrations*. Virginia Polytechnic Institute and State University.
- KOO, J. H., MURRAY, T. M. & SETAREH, M. 2004. In search of suitable control methods for semi-active tuned vibration absorbers. *Journal of Vibration and Control*, 10, 163-174.
- KORKMAZ, S. 2011. A review of active structural control: challenges for engineering informatics. *Computers & Structures*, 89, 2113-2132.
- KOSHIKA, N., SAKAMOTO, M., SASAKIM, K., IKEDA, Y. & KOBORI, T. Control effect of active mass driver system during earthquakes and wind. 1st International Conference on Motion and Vibration Control, 1992 Yokohama, Japan. 261-266.
- KULKARNI, S., JADHAV, D. & KHADKE, P. 2012. Passive control systems for tall structures. *International Journal on Theoretical and Applied Research in Mechanical Engineering(IJTARME)*, 1, 87-91.
- KWOK, K. C. & SAMALI, B. 1995. Performance of tuned mass dampers under wind loads. *Engineering Structures*, 17, 655-667.
- LI, C. & CAO, B. 2015. Hybrid active tuned mass dampers for structures under the ground acceleration. *Structural Control and Health Monitoring*, 22, 757-773.
- LIEDES, T. 2009. *Improving the Performance of the Semi-Active Tuned Mass Damper*. University of Oulu.
- LIU, M.-Y., CHIANG, W.-L., HWANG, J.-H. & CHU, C.-R. 2008. Wind-induced vibration of high-rise building with tuned mass damper including soil-structure interaction. *Journal of Wind Engineering and Industrial Aerodynamics*, 96, 1092-1102.
- MALLOCK, A. 1905. A method of preventing vibration in certain classes of steamships. *Transactions of the Royal Institute of Naval Architects*, 47.
- MANNING, W. J., PLUMMER, A. R. & LEVESLEY, M. C. 2000. Vibration Control of a Flexible Beam with Integrated Actuators and Sensors. *Smart Materials and Structures*, 9, 932-939.
- MARIAN, L. & GIARALIS, A. 2014. Optimal design of a novel tuned mass-damper-inerter (TMDI) passive vibration control configuration for stochastically support-excited structural systems. *Probabilistic Engineering Mechanics*.
- MEIROVICH, L. 1990. *Dynamics and Control of Structures*, Canada, John Wiley & Sons.

- MITCHEL, R., KIM, Y. & EL-KHORCHI, T. 2012. Wavelet neuro-fuzzy control of hybrid building-active tuned mass damper system under seismic excitations. *Journal of Vibration and Control*, 1881-1894.
- MONTAZERI, A., POSHTAN, J. & CHOBDAR, A. 2009. Performance and robust stability trade-off in minimax LQG control of vibrations in flexible structures. *Engineering Structures*, 31, 2407-2413.
- MOVASSAGHI, Z. Considering active tuned mass dampers in a five storey structure. Control Conference (AUCC), 2012 2nd Australian, 2012. 320-323.
- NAGARAJAIAH, S. 2009. Adaptive passive, semiactive, smart tuned mass dampers: identification and control using empirical mode decomposition, hilbert transform, and short-term fourier transform. *Structural Control and Health Monitoring*, 16, 800-841.
- NAGARAJAIAH, S. & SONMEZ, S. 2007. Structures with Semiactive Variable Stiffness Single/Multiple Tuned Mass Dampers. *Journal of Structural Engineering* 133.
- NAGARAJAIAH, S. & VARADARAJAN, N. 2005. Short time Fourier transform algorithm for wind response control of buildings with variable stiffness TMD. *Engineering Structures*, 27, 431-441.
- NAKAMURA, Y., TANAKA, K., NAKAYAMA, M. & FUJITA, T. 2001. Hybrid mass dampers using two types of electric servomotors: AC servomotors and linear-induction servomotors. *Earthquake Engineering & Structural Dynamics*, 30, 1719-1743.
- NELDER, J. & MEAD, R. 1965. A simplex method for function minimization. *Computer Journal*, 7, 308-313.
- PAN, X., MOORE, S. & FORREST, J. A. Design and Evaluation of a Pole Placement Controller for Controlling Vibration of Structures. Proceedings of Acoustics, 2011 Gold Coast, Australia.
- PINKAEW, T. & FUJINO, Y. 2001. Effectiveness of semi-active tuned mass dampers under harmonic excitation. *Engineering Structures*, 23, 850-856.
- PREUMONT, A. & BOSSENS, F. 2000. Active Tendon Control of Vibration of Truss Structures: Theory and Experiments. *Journal of Intelligent Material Systems and Structures*, 11, 91-99.
- PREUMONT, A. & SETO, K. 2008. *Active control of structures*, John Wiley & Sons, LTD, Publication.
- RAHIMI, H. N. & NAZEMIZADEH, M. 2014. Dynamic analysis and intelligent control techniques for flexible manipulators: a review. *Advanced Robotics*, 28, 63-76.
- RAHMAN, T. A. & DARUS, Z. M. Active Vibration Control using Pole Placement Method of a Flexible Plate Structure Optimise by Genetic Algorithm. IEEE Conference on Control, Systems and Industrial Informatics (ICCSII), 2012 Bandung, Indonesia.
- REINHORN, A. M., SOONG, T. T., LIN, R. C., RILEY, M. A., WANG, Y. P., AIZAWA, S. & HIGASHINO, M. 1992. Active Bracing System: A Full Scale Implementation of Active Control. University of New York at Buffalo, Chung-Hwa Polytechnic Institute, and Takenaka Corporation.

- RICCIARDELLI, F., OCCHIUZZI, A. & CLEMENTE, P. 2000. Semi-active tuned mass damper control strategy for wind-excited structures. *Journal of Wind Engineering and Industrial Aerodynamics*, 88, 57-74.
- RICCIARDELLI, F., PIZZIMENTI, A. D. & MATTEI, M. 2003. Passive and active mass damper control of the response of tall buildings to wind gustiness. *Engineering Structures*, 25, 1199-1209.
- ROHLFING, J., ELLIOTT, S. J. & GARDONIO, P. 2011a. Compensation filter for feedback control units with proof-mass electrodynamic actuators, simulations and experimental studies. *University of Southampton, Institute of Sound and Vibration Research (ISVR Technical Memorandum No. 991)*.
- ROHLFING, J., GARDONIO, P. & ELLIOTT, S. J. 2011b. Base impedance of velocity feedback control units with proof-mass electrodynamic actuators. *Journal of Sound and Vibration*, 330, 4661-4675.
- RUNLIN, Y., XIYUAN, Z. & XIHUI, L. 2002. Seismic structural control using semi-active tuned mass dampers. *Earthquake Engineering and Engineering Vibration*, 1, 111-118.
- SADEK, F. & MOHRAZ, B. 1998. Semiactive control algorithms for structures with variable dampers. *Journal of Engineering Mechanics*, 981-990.
- SAMALI, B., KWOK, K., WOOD, G. & YANG, J. 2004. Wind tunnel tests for wind-excited benchmark building. *Journal of Engineering Mechanics, ASCE*, 130, 447-450.
- SCRUGGS, J. & IWAN, W. 2003. Control of a civil structure using an electric machine with semiactive capability. *Journal of Structural Engineering:ASCE*, 129, 951-959.
- SETAREH, M. 2001. Application of semi-active tuned mass dampers to base-excited systems. *Earthquake Engineering & Structural Dynamics*, 30, 449-462.
- SKOGESTAD, S. & POSTLETHWAITE, I. 2005. Multivariable Feedback Control. *John Wiley & Sons Ltd, Sussex, 2nd edition*.
- SOONG, T. T. 1988. Active Structural Control in Civil Engineering. *Engineering Structures*, 10, 74-84.
- SOONG, T. T. 1990. *Active structural control: Theory and practice*, New York, John Wiley & Sons, Inc.
- SOONG, T. T. & SPENCER, B. F. 2002. Supplemental energy dissipation: state-of-the art and state-of-the practice. *Engineering Structures*, 24, 243-259.
- SPENCER, B. F. & NAGARAJAIAH, S. 2003. State of the art of structural control. *Journal of Structural Engineering*, 845-856.
- STAVROULAKIS, G. E., MARINOVA, D. G., HADJIGEORGIOU, E., FOUTSITZI, G. & BANIOPOULOS, C. C. 2006. Robust active control against wind-induced structural vibrations. *Journal of Wind Engineering and Industrial Aerodynamics*, 94, 895-907.
- SUHARDJO, J., SPENCER, B. F. & KAREEM, A. 1992. Active control of wind excited buildings: A frequency domain based design approach. *Journal of Wind Engineering and Industrial Aerodynamics*, 41-44, 1985-1996.

- SUN, J. Q., JOLLY, M. R. & NORRIS, M. A. 1995. Passive, Adaptive and Active Tuned Vibration Absorbers-A Survey. *Journal of Mechanical Design* 117, 234-242.
- SYMANS, M. D. & CONSTANTINOU, M. C. 1999. Semi-active control systems for seismic protection of structures: a state-of-the-art review. *Engineering Structures*, 21, 469-487.
- TAN, P., LIU, Y., ZHOU, F. & TENG, J. 2012. Hybrid Mass Dampers for Canton Tower. *CTBUH Journal*, 24-29.
- TAN, W., LIU, J., CHEN, T. & MARQUEZ, H. J. 2006. Comparison of some well-known PID tuning formulas. *Computers & Chemical Engineering*, 30, 1416-1423.
- THEODORE, R. J. & GHOSAL, A. 1995. Comparison of the assumed modes and finite element models for flexible multi-link manipulators. *The International Journal of Robotics Research*, 14, 91-111.
- THORBY, D. 2008. *Structural Dynamics and Vibration in Practice*, Hungary, Elsevier.
- TOKHI, O. & VERES, S. 2002. *Active and sound vibration control*, London, UK.
- TSO, M. H., YUAN, J. & WONG, W. O. 2016. Hybrid vibration absorber with detached design for global vibration control. *Journal of Vibration and Control*.
- VIET, L. D., NGHI, N. B., HIEU, N. N., HUNG, D. T., LINH, N. N. & HUNG, L. X. 2014. On a combination of ground-hook controllers for semi-active tuned mass dampers. *Journal of Mechanical Science and Technology*, 28, 2059-2064.
- WATAKABE, M., TOHDP, M., CHIBA, O., IZUMI, N., EBISAWA, H. & FUJITA, T. 2001. Response control performance of a hybrid mass damper applied to a tall building. *Earthquake Engineering & Structural Dynamics*, 30, 1655-1676.
- WU, Z. & SOONG, T. T. 1996. Modified Bang-Bang Control Law For Structural Control Implementation. *Journal of Engineering Mechanics*, 122, 771-777.
- XU, Y. L., SAMALI, B. & KWOK, K. C. 1992. Control of along-wind response of structures by mass and liquid dampers. *Journal of Engineering Mechanics*, 118, 20-39.
- YANG, N. J., AKBARPOUR, A. & GHAEMMAGHAMI, P. 1987. New Optimal Control Algorithms for Structural Control. *Journal of Engineering Mechanics*, 113, 1369-1386.
- YANG, N. Y., AGRAWAL, A. K., SAMALI, B. & WU, J. C. 2004. Benchmark Problem for Response Control of Wind-Excited Tall Buildings. *Journal of Engineering Mechanics*, 130, 437-446.
- YANG, S. M., CHEN, C. J. & HUANG, L. 2006. Structural Vibration Suppression by a Neural-Network Controller with a Mass-Damper Actuator. *Journal of Vibration and Control*, 12, 495-508.
- YAO, J. T. P. 1972. Concept of Structural Control. *Journal of Structural Division*, 1567-1574.

YOUSEFI-KOMA, A. 1997. Active vibration control of smart structures using piezoelements. Carleton University.

ZAMES, G. 1981. Feedback and optimal sensitivity: Model reference transformations, multiplicative seminorms, and approximate inverses. IEEE Transactions on automatic control, 26, 301-320.

ZHANG , C. & OU, J. 2015. Modeling and dynamical performance of the electromagnetic mass driver system for structural vibration. Engineering Structures, 93-103.

ZHANG, Y., LI, L., CHENG, B. & ZHANG, X. 2016. An active mass damper using rotating actuator for structural vibration control. Advances in Mechanical Engineering, 8.

ZHIJUN, L., SHUANGYANG, J. & YUANYUAN, L. Fuzzy sliding mode control for smart structure with atmd. Control Conference (CCC) 2014 33rd Chinese, 2014.

Appendix A

Appendix A presents the performance of the different control algorithms as a function of the selected mass ratio and stiffness uncertainty. The figures presented herein are used to complement the statements made in chapter 4.

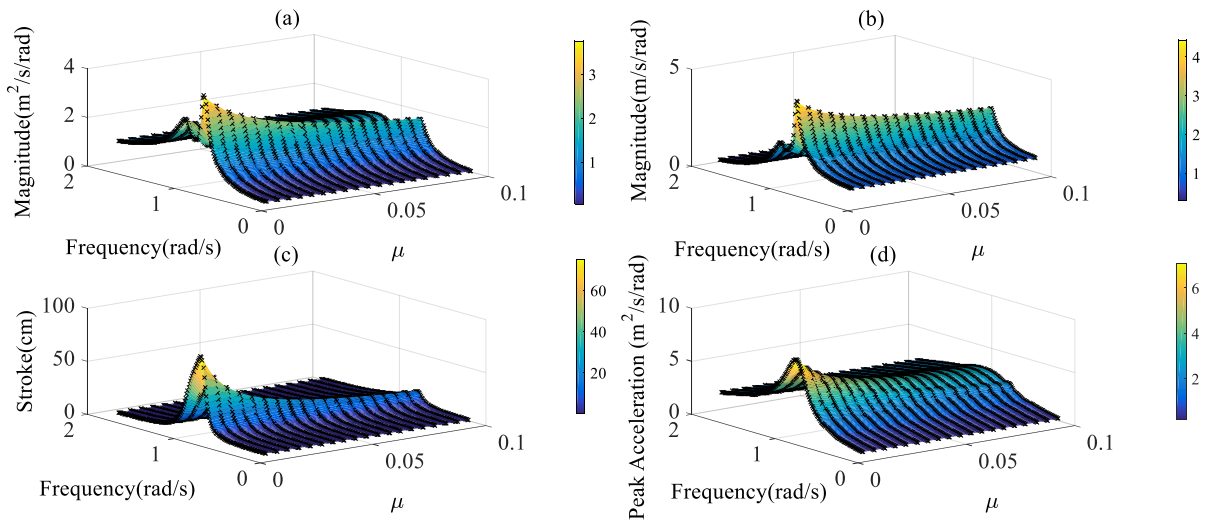


Figure A1.(a) Acceleration response, (b) Displacement response, (c) Maximum stroke, (d) Peak acceleration as a function of the mass ratio for the LQR case

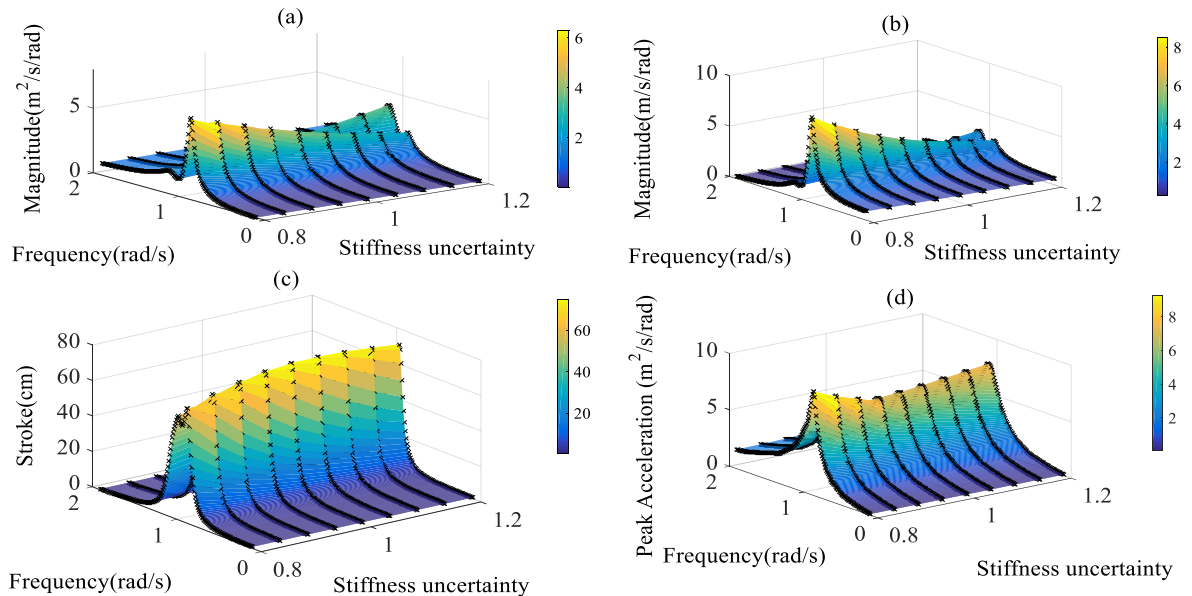


Figure A2.(a) Acceleration response, (b) Displacement response, (c) Maximum stroke, (d) Peak acceleration as a function of the stiffness uncertainty for the LQR case

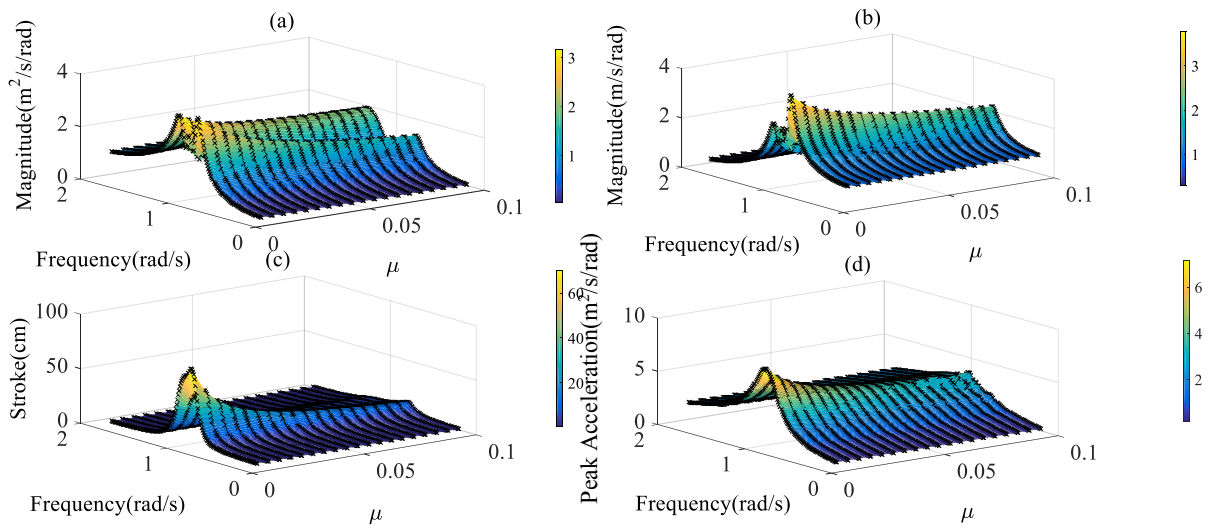


Figure A3.(a) Acceleration response, (b) Displacement response, (c) Maximum stroke, (d) Peak acceleration as a function of the mass ratio for the DBG case

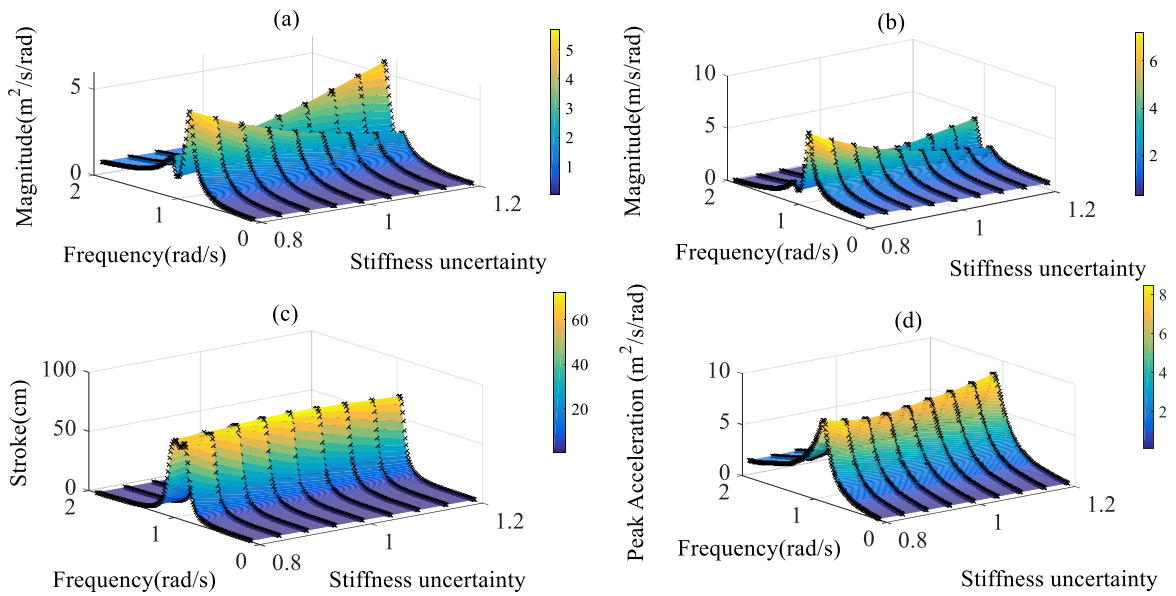


Figure A4.(a) Acceleration response, (b) Displacement response, (c) Maximum stroke, (d) Peak acceleration as a function of the stiffness uncertainty for the DBG case

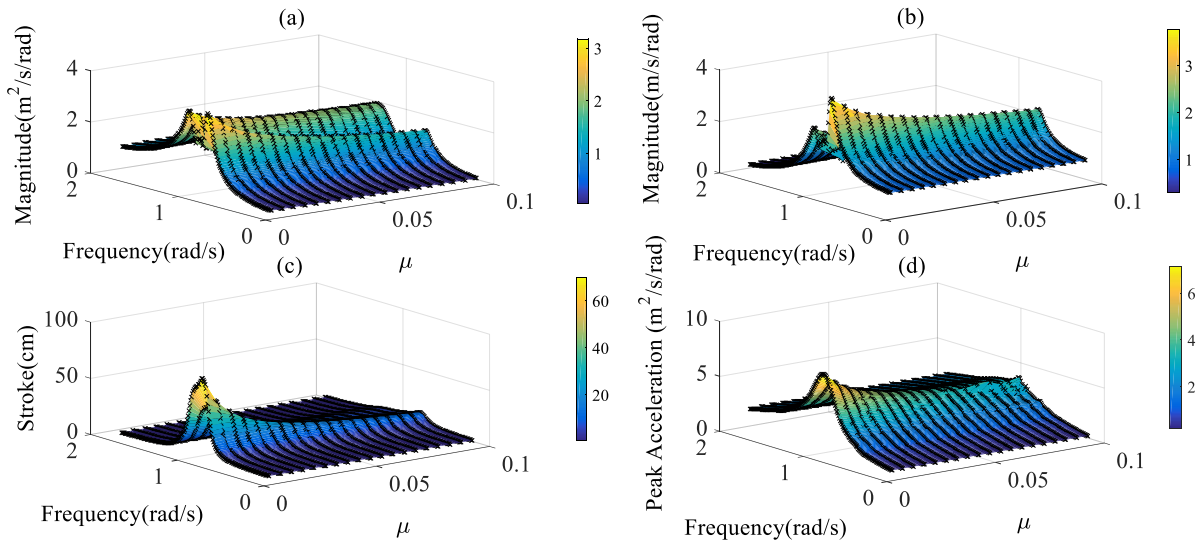


Figure A5.(a) Acceleration response, (b) Displacement response, (c) Maximum stroke, (d) Peak acceleration as a function of the mass ratio for the PID case

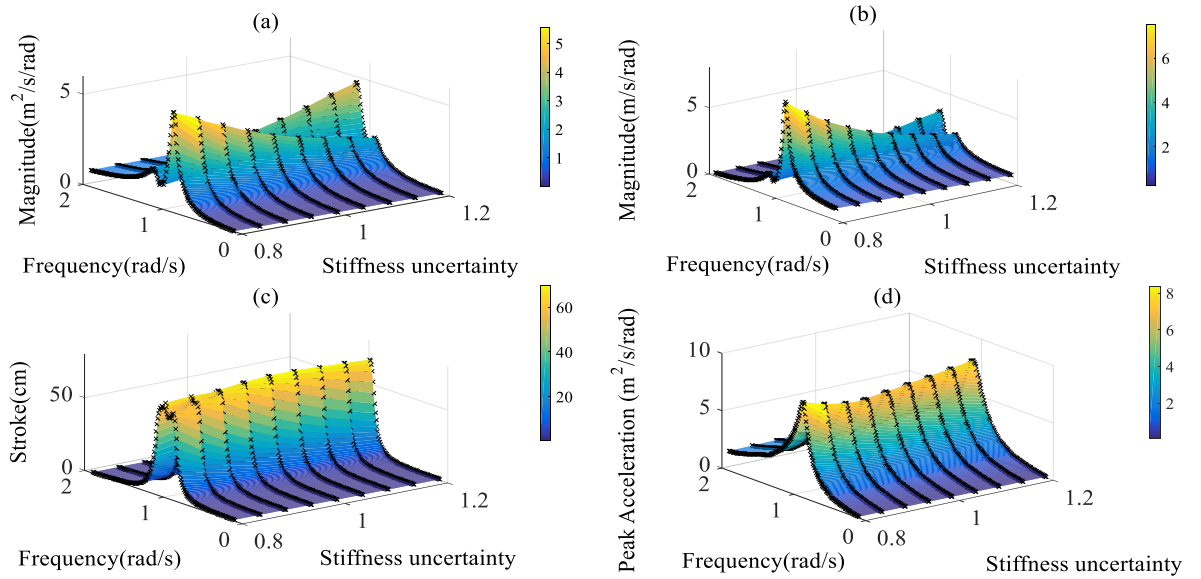


Figure A6.(a) Acceleration response, (b) Displacement response, (c) Maximum stroke, (d) Peak acceleration as a function of the stiffness uncertainty for the PID case

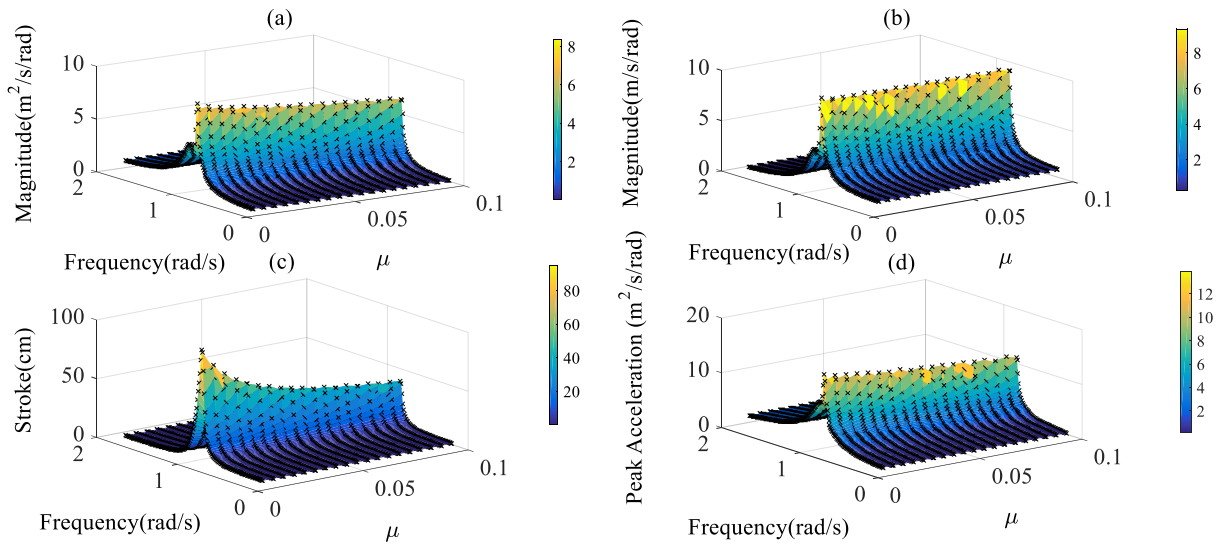


Figure A7.(a) Acceleration response, (b) Displacement response, (c) Maximum stroke, (d) Peak acceleration as a function of the mass ratio for the VBG case

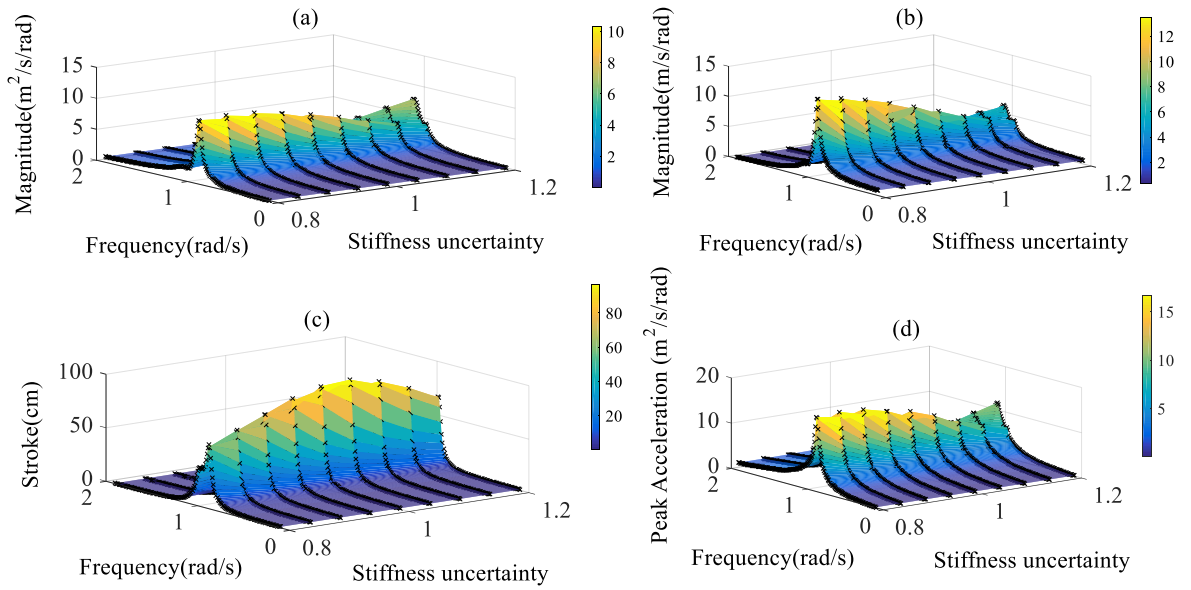


Figure A8.(a) Acceleration response, (b) Displacement response, (c) Maximum stroke, (d) Peak acceleration as a function of the stiffness uncertainty for the VBG case

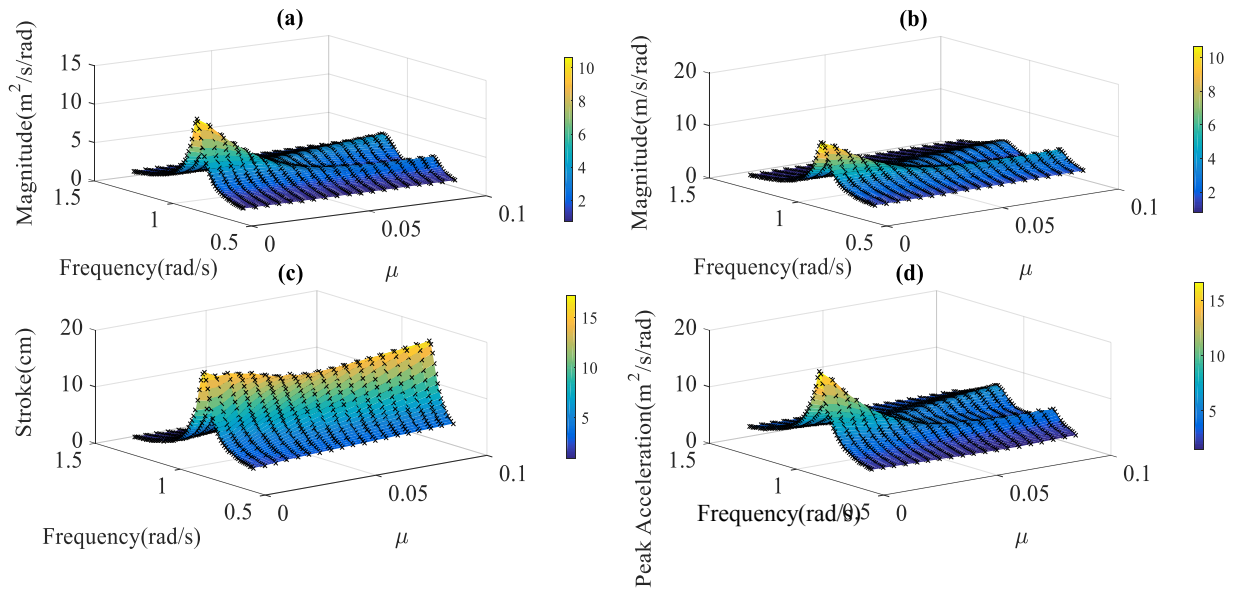


Figure A9.(a) Acceleration response, (b) Displacement response, (c) Maximum stroke, (d) Peak acceleration as a function of the mass ratio for the BANG case

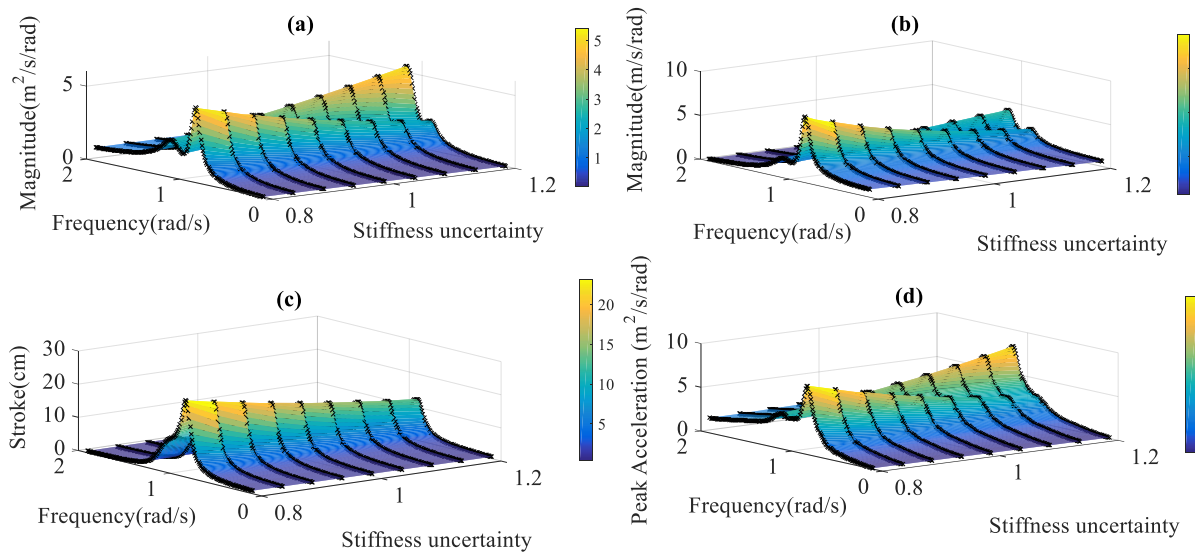


Figure A10.(a) Acceleration response, (b) Displacement response, (c) Maximum stroke, (d) Peak acceleration as a function of the stiffness uncertainty for the BANG case

Table A1. PID Controller Coefficients

Controller ID	P	I	D
PID₁	1.99 e8	4.23 e5	5.34 e6
PID₂	2.19 e8	5.51 e5	8.04 e6
PID₃	3.25 e8	6.22 e5	3.76 e6
PID₄	4.53 e8	8.01 e5	5.44 e6
PID₅	5.12 e8	4.01 e6	6.34 e6
PID_{opt}	5.07 e8	3.01 e6	6.04 e6
PD₁	7.14 e8	N/a	4.13 e6
PD₂	8.00 e8	N/a	4.2 e6
PD₃	6.33 e9	N/a	5.55 e6
PD₄	7.87 e9	N/a	6.12 e6
PD₅	8.32 e9	N/a	7.25 e6

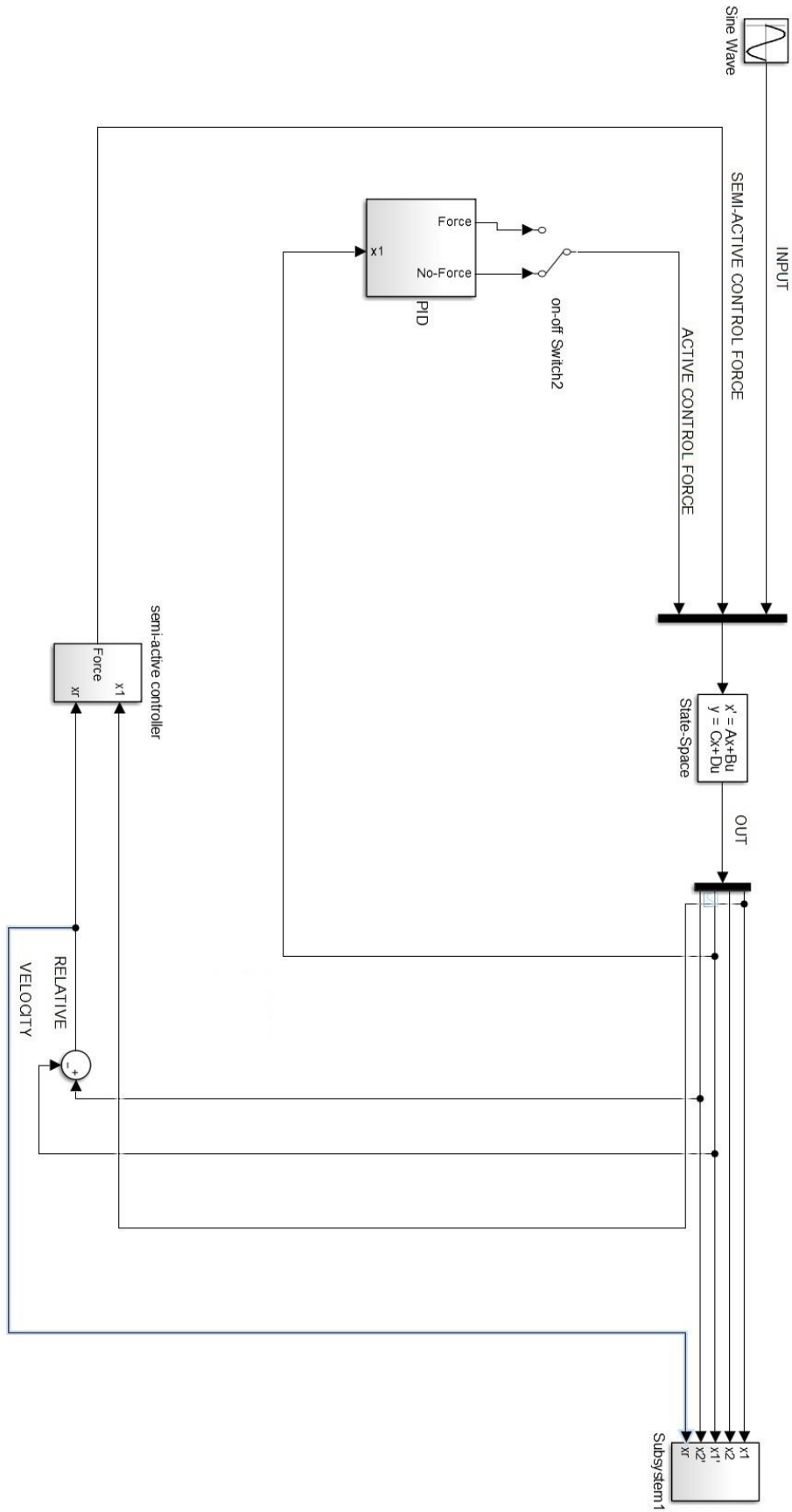


Figure A11. Simulink block diagram associated with the control architecture considered for the robust control of SHMD devices.

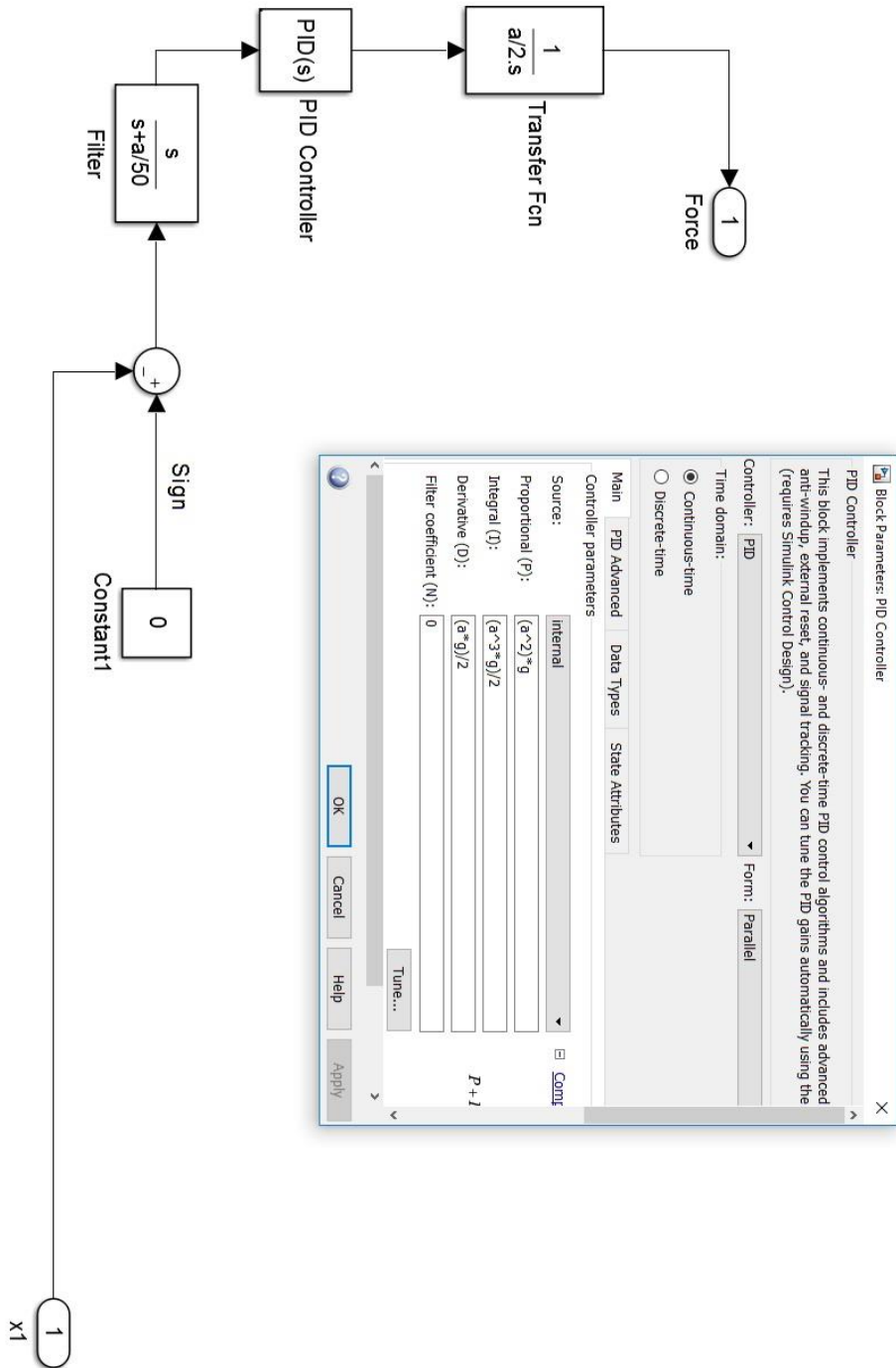


Figure A12. Simulink block diagram associated with PID Controller and the control architecture described in figure 62